THE BEHAVIOUR OF OPEN SPANDREL BRICKWORK MASONRY ARCH BRIDGES

H. TAO

Submitted In partial fulfilment of the requirements of the degree of Doctor of Philosophy.

April 2003.

Table Of Contents

List of Figures

List of Table

ACKNOWLEDGEMENTS

I owe a debt of gratitude to Professor Clive Melbourne, my teacher and advisor, who introduced me to the world of masonry arches; gave me an opportunity to experience the Western cultures and philosophies. The beginning and the completion of this thesis was possible only through his academic and moral support.

The institutional and financial support has made it possible to carry out the research. I would like to give my sincere thanks to University of Salford and Bolton Institute. The librarians, especially those in the interlibrary loan department of both universities have been very helpful.

Many colleagues have aided me in different ways. I would particularly like to thank Dr. John Hodgson, whose comprehensive knowledge of arch bridge tests speeded up the test programme, especially at the early stage of the research; Dr. Lawrence Weeks, whose 'trouble-shooting' skills ensured the computers, either hardware or software, always in the excellent working conditions.

I owe many thanks to the technical staff, B. Porter, A. Dale, Philip, Jeffery and Phil, in particular the assistance provided by Lionel, the chief technician at Salford civil engineering laboratory, whose attitude to work deserved all respects, and to C Tivey, who spent 'dozens' of hours to edit and proceed the images of the model arch tests.

Thanks go also to the bricklayer, Len, his high standards of the work made it possible to maintain the consistent high quality of the model arches.

Last but not least, to Yan, my wife, goes my heartfelt appreciation for her support through the years.

ABBREVIATIONS

SA	–	Spandrel Arch (SA1, SA2, and SA3, Etc., Refer To The Spandrel Arches From Left To Right)
MA	–	Main Arch
OSMA	–	Open Spandrel Masonry Arch
OSBMA	–	Open Spandrel Brickwork Masonry Arch
OSMAB	–	Open Spandrel Masonry Arch Bridge
OSBMAB	–	Open Spandrel Brickwork Masonry Arch Bridge
MSNF	–	Open Spandrel Arch Without Fill
MSWF	–	Open Spandrel Arch With Fill
CTAT	–	Convergence Tool Of Automatic Timimg
CTLS	–	Convergence Tool Of Line Search
CTP	–	Convergence Tool Of Predictor
NRF	–	Full Newton-Raphson Iteration Method
NRM	–	Modified Newton-Raphson Iteration Method
SPMA	–	Span Of Main Arch
TKMA	–	Thickness Of Main Arch
RSMA		Rise Of Main Arch
SPSA	–	Span Of Spandrel Arches
TKSA	–	Thickness Of Spandrel Arches
RSSA	–	Rise Spandrel Arches
WTSP	–	Width Of Spandrel Piers
WTAB	–	Width Of Model Arch
NPI	–	Number Of Pre-Defined Interfaces Along Arch Ring
β_1	–	Shear Transfer Coefficient For Open Crack
β_2	–	Shear Transfer Coefficient For Close Crack
σ_t	–	Uniaxial Tensile Cracking Stress
σ_c	–	Uniaxial Crushing Stress
$\sigma_{cm}/\sigma_{cb}/\sigma_{cbw}$	–	Compressive Strength Of Mortar/Bricks/Brickwork
$E_m/E_b/E_{bw}$	–	Young's Modulus Of Mortar/Bricks/Brickwork
μ	–	Coefficient Of Friction
kn	–	Normal Contact Stiffness
ks	–	Tangential Contact Stiffness

Fn	–	Normal Force Of Contact Element
Fs	–	Tangential Force Of Contact Element
H	–	Horizontal Force
V	–	Vertical Force

Abstract

The behaviour of open spandrel brickwork masonry arch bridges (OSBMAB) was studied through model tests and finite element simulations. One three-metre and two five-metre span full scale OSBMAB were constructed and tested to destruction. Two 'partial' models including a combination of spandrel arches and piers, and a five-metre span single arch were also tested with intention of studying the functions of the components of the OSBMAB. To simulate the behaviour of the brickwork masonry arches, three finite element modelling techniques were developed: - (a) smeared modelling method (SMM), in which the failure of brickwork masonry caused by tensile cracking, compressive crushing or sliding is simulated as "loss of stiffness" in the corresponding directions within the domain of the geometry of the arch structure; and (b) discrete modelling method (DMM), in which the failure of brickwork masonry caused by tensile cracking or sliding is simulated as the change in the geometry of the arch structure, i.e., the geometrical discontinuity at prescribed locations; and (c) the mixed modelling method (MMM), in which the main arch, spandrel arches/piers are modelled using the SMM, and the interfaces between the fill and arch are modelled using the DMM. Parametric studies were carried out to investigate the effects of changes in material properties and finite element model related parameters on the behaviour of the OSBMAB, and to justify the values of those parameters adopted in the finite element models using the FE Package ANSYS 5.3. The comparisons were made between the finite element results and those obtained from the model tests. It has been demonstrated in terms of the ultimate loads, the modes of failure and the responses of loads vs. displacements that FE modeling can give good correlation.

CHAPTER 1 MASONRY ARCH BRIDGES

1.1 General

An open spandrel masonry arch bridge is one of the most sophisticated forms of arched bridges. It was largely developed in the middle of the first century in China (Luo, 1959; Knapp, 1992; Brwon 1993), and it was used regularly in the nineteenth century Europe (ICE, 1828; Tellett, 1983; Ruddock 1974a). This form of arch is still preferred in certain parts of China (Xiang, 1993; Hu, 1995). Fig. 1.1 shows a typical open spandrel masonry arch bridge.

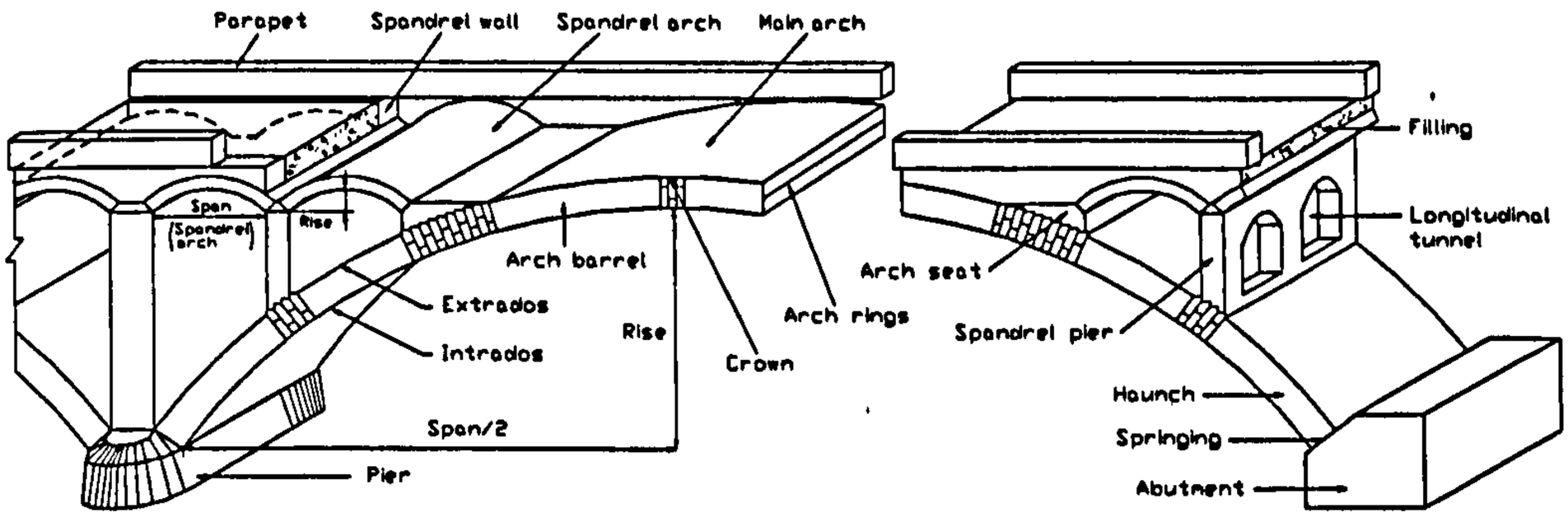

Fig. 1.1 Open Spandrel Arch Bridge And Relevant Terms

It is believed that open spandrel masonry arch bridges (OSMAB) evolved from multi-span masonry arch bridges with the voids through each spandrel over the middle of the intermediate piers; to the filled arch bridges with cylindrical tunnels through each spandrel above the haunches; to the real open spandrel arch bridges where a series of spandrel arches were built on the extrados of the main arches. The original purposes of building the 'openings' might be for the flow of floodwater and savings of masonry materials (Gautier, 1717; Mao et al., 1986).

To understand the behaviour of OSMAB, the functions and the behaviour of their components such as single arches and spandrel piers need to be first studied. In the following section, the development of both filled and open spandrel arch bridges will be briefly reviewed. The detailed review of masonry arch bridges in different parts of the world at various stages of the development may be found elsewhere (Howe, 1897;

Pippard and Chitty, 1951; Luo, 1959; Heyman, 1982; Tellett, 1983; and Mao et al., 1986).

1.2. Development Of Masonry Arch Bridges

Masonry arch bridges have existed for thousands of years. Their ancient forms are generally studied through archeological evidence (EB, 1984a). Although their surviving structures may show that the knowledge of such bridges had been grasped in the early times, the recorded attempts to understand the structural performances might be considered to start from Hooke's work in 1675. The Appendix I lists selected achievements on the understanding of arches at different stages, from which, the following four stages may be identified: prehistoric stage; development stage; introspective stage and modern stage. It may be seen from the Appendix I that many problems associated with masonry arches were independently studied by different investigators at various stages of the development.

1.2.1 Prehistoric Stage: Empirical Knowledge

The prototypes of arch bridges may have been created by nature, of which either the overhanging stratifications of stone (Mare, 1975), or the rock from beneath which the soft strata or shale had been eaten away by running water (Brown, 1993), or, more likely, arches which were formed by the stones from mountains scoured by running water in rivers (Luo and Tang, 1993), gave men their first inspiration to build arches.

True arches were believed to evolve from corbelled arches (EB, 1984b). The corbelling was considered as intermediate stages between a simple cantilever and a true arch, which consists of successive courses of masonry placed on either side of an opening and projecting inwards closer and closer to each other until they meet as shown in Fig. 1.2.

(a) Corbelled Arch **(b) True Arch**

Fig. 1.2 Evolution of Arch: Corbelling to Arch

The tomb structures found in China around 250BC presented another story of the development of true arch forms. As Fig. 1.3 shows, as number of inclined stone beam segments increases from three to five to as many as seven, multi-sided polygonal bridges begin to approximate true arches.

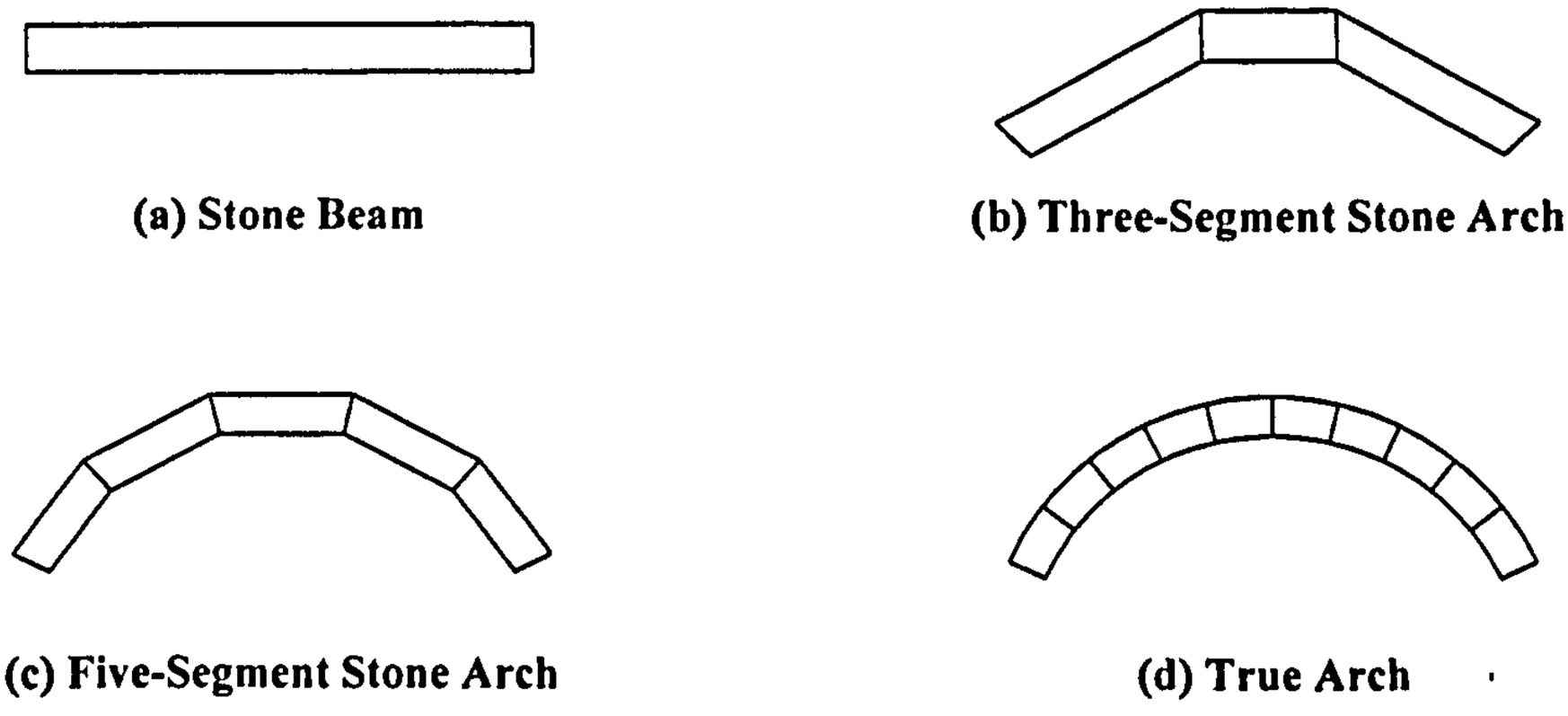

(a) Stone Beam

(b) Three-Segment Stone Arch

(c) Five-Segment Stone Arch

(d) True Arch

Fig. 1.3 Evolution of Arch: Segmenting to Arch

It was recorded that Bing Li, an ancient Chinese hydraulic specialists, built *Seven Star* Bridge when he built the *Du Jiang* Weir in the southwest of China 251BC. The bridge was composed of a series of seven small stone arches of the total length about 35m; the height 10m; and the width 5m (Mao et al., 1986).

One of the features of Roman arch bridges may indicate a concern about waterflows (EB, 1984a): it was the provision of tunnels in the spandrels, which were placed on the top of intermediate piers as shown in Fig. 1.4. Conceivably, this was a device to balance the consequences of the Roman massive piers. But equally, these tunnels would have acted as flood arches and such may have been the intention.

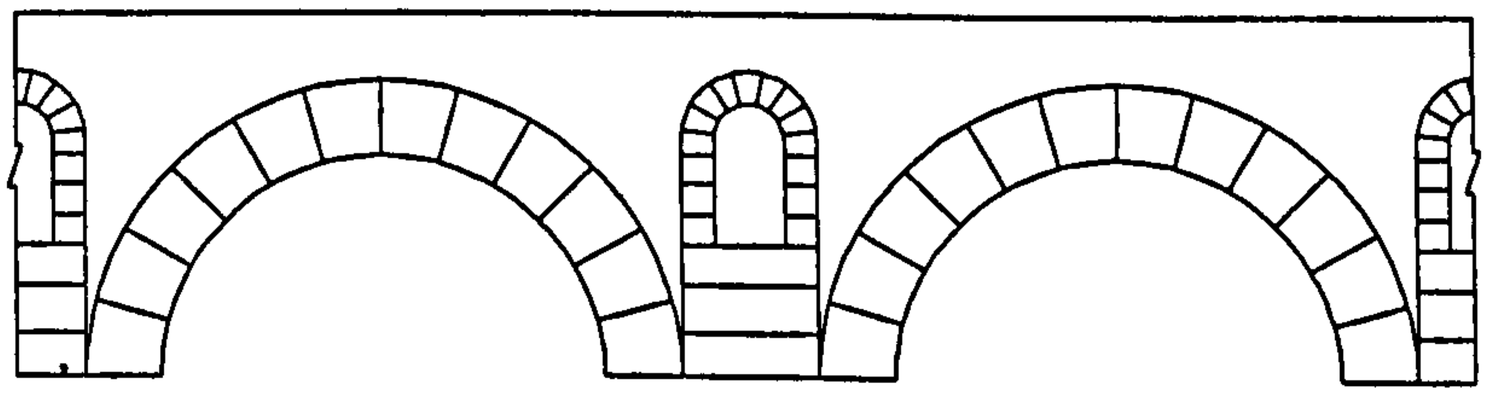

Fig. 1.4 Ancient Roman Multi-Span Arch Bridges

It should be noted that the spandrel openings were only provided on the top of the intermediate piers of multi-span arch bridges, and may not be considered as open spandrel arch bridges.

1.2.2 Development Stage: Fundamental Understanding

1.2.2.1 Construction

When the Roman Empire fell the building of masonry arch bridges stagnated in Europe, and many of the old skills were lost (EB, 1984c; Smith, 1993; Brown, 1993).

It was during this period that the building of masonry arch bridges reached its zenith in China. Among them, the most distinctive one must be credited to *Zhao Zhou* Bridge (Fig. 1.5), an open spandrel stone arch bridge built between 595 AD and 606 AD in Shijiazhuang some 250 miles away from Beijing.

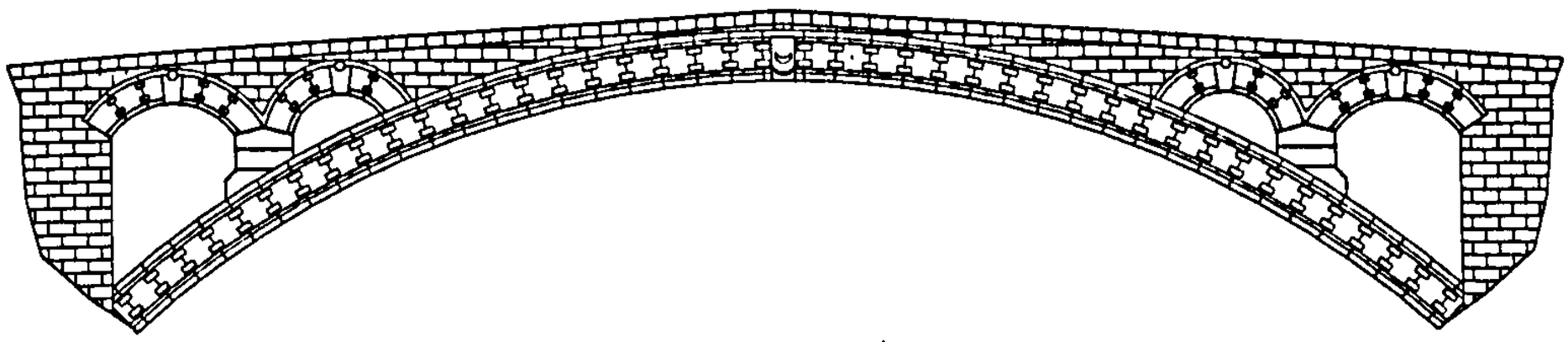

Fig. 1.5 *Zhao Zhou* Bridge (Li, 595-606 AD)

This bridge broke the convention of a semi-circular arch advancing with a segmental one. Most remarkably, the haunches on both sides of the bridge were pieced by pairs of smaller arches. The inspiration for the segmental and open spandrel forms may be inferred from the actual circumstances encountered by its builders at the time. This bridge was built to cross the *Xiao River* in the North China Plain. Although both multi-span and semi-circular single-span arch bridges had been built in Sui dynasty in 581 AD, neither was appropriate on the flat plain where mule, horse, and human drawn cart traffic required a fairly level approach. A series of arches each with a small diameter was not the answer because of the difficulty of sinking stone piers within the course of the river itself. A single semi-circular arch reaching from bank to bank that would be of sufficient height to permit boat traffic not only would have had to exceed a rise of almost twenty metres, its weight would have been excessive for the soil and rock supporting the abutment at either side (Mao et al., 1986; Knapp, 1988).

Confronted with the need to span nearly forty metres with a stone bridge light enough not to overwhelm its supporting abutments, Chun Li, a bridge architect, recognized that it was possible to flatten the curve of the arch if one viewed the arc as but a segment of a larger semi-circle. This observation was revolutionary, making it possible for the segment to spring from its abutments in a gentle arc that tended towards a greater horizontality than was possible with a semi-circular arch. The completed main arch has a span of 37.02m; rise of 7.23m and thickness of barrel of 1.03m.

Further, Chun Li suggested a novel innovation for the spandrels, where, unlike traditional filled arches, two small arches pierced the spandrel of the *Zhao Zhou* Bridge. The outcome of his innovation was not only the reduction of the self-weight of each of the two bridge spandrels and provision of larger openings to " sweep away the clashing onrush of angry water ", but also the reduction of the sizes of the abutments.

Several measures were taken to stabilize the rows of wedge-shaped voussoirs making up the underlying parallel arches. Nine reinforcing stone rods, each with a cap to pull in the stones, were thrust through the twenty-eight arches. The voussoirs themselves were joined to one another by double dovetail-shaped iron keys sunk into chiselled indentations in the limestone along the outward facing surfaces of each arch. A supplementary device to secure the arches beneath was a course of 0.33 metres thick stone slabs. Along each of the outer arches, six of the exterior stone slabs were cut so as to overhang, forming stone hooks to prevent the voussoirs from falling outwards. Except for the loss of some outer voussoirs, the bridge remained intact down to the present in spite of flood, earthquakes, and long-term traffic (Mao et al., 1986; Coyne, 1989; Knapp, 1992; Luo and Tang, 1993).

The Architecture of Bridges published by the Museum of Modern Art, New York described *Zhao Zhou* Bridge: " This is the oldest open spandrel bridge in the world. The low rising arch ring, a segment of a circle, brought into sharp relief by the introduction of arched openings in the spandrel walls. These serve not only to lighten the bridge but to differentiate cause from effect, i.e., supporting arch from supported roadway ", and, "The structure is phrased with such logic and grace, such acute awareness of its own nature, that it makes most Western bridges seem heavy and inarticulate by contrast " (Mao, 1978). In 1989, the *Zhao Zhou* Bridge was designated an International Historic

Civil Engineering Landmarks by the American Society of Civil Engineers (Knapp, 1992).

Open spandrel arch bridges started to be built in Europe in the twelfth century. However, later bridges such as *Westminster* Bridge (1736-49) and William Edwards' bridges at Pontypridd (1746-1756), could well solve the puzzle: why and how an OSMAB was developed both formally and structurally.

In 1746 William Edwards contracted to build a bridge over the Taff at Pontypridd. His first bridge was multi-span arch bridge, and stood for about two years. One (at least) of the piers was in the river, and a flood brought the bridge down, presumably as a result of scour of the foundations. William Edwards, who was required by his contract to provide a bridge that would stand for seven years, then determined to span the river with a single arch. When the second arch was almost complete, the timber centering collapsed, because of the great weight of the spandrels at both haunches and the weakness of the centerings. The third bridge was a single arch of 42.8m span and 10.7m rise of light masonry built on stronger centering. The arch ring was completed in September and the centering removed; work continued on building up the spandrel walls and filling the haunches to provide the roadway. While this work was going on, on 7 November 1754, the arch collapsed. The cause and mode of failure were described by Morgan (1754) as follows: ' The quantity of matter in the crown of the arch was but little in proportion to that which was necessary to be laid on the abutments in order to make the ascent ease the weight of this matter caused such an inequality of pressure on the arch, that in about a year's time, it crushed that stupendous pile, and it fell again to the bottom ', and by Malkin (1804) ' The arch was finished, but the parapets not yet erected, when such was the pressure of the unavoidably ponderous work over the haunches, that it sprung up in the middle, and the keystones were forced out '. The arch was apparently of the wrong shape to carry its own weight (Smeaton, 1760; Ruddock, 1974a; Heyman, 1982).

William Edwards evidently had warning of the collapse, and he was able to modify the design of his fourth and final bridge, which was a segment arc of 106° with a span-rise ratio of 4 and the thickness of arch barrel 0.76m. In each side of the bridge three open cylindrical openings of 2.75m, 1.83m and 1.22m diameter were made, and a further hidden semi-circular void, through each spandrel as shown in Fig. 1.6. The load at the

crown was increased, and that at the haunches lightened by the provision of the cylindrical openings. The bridge still stands.

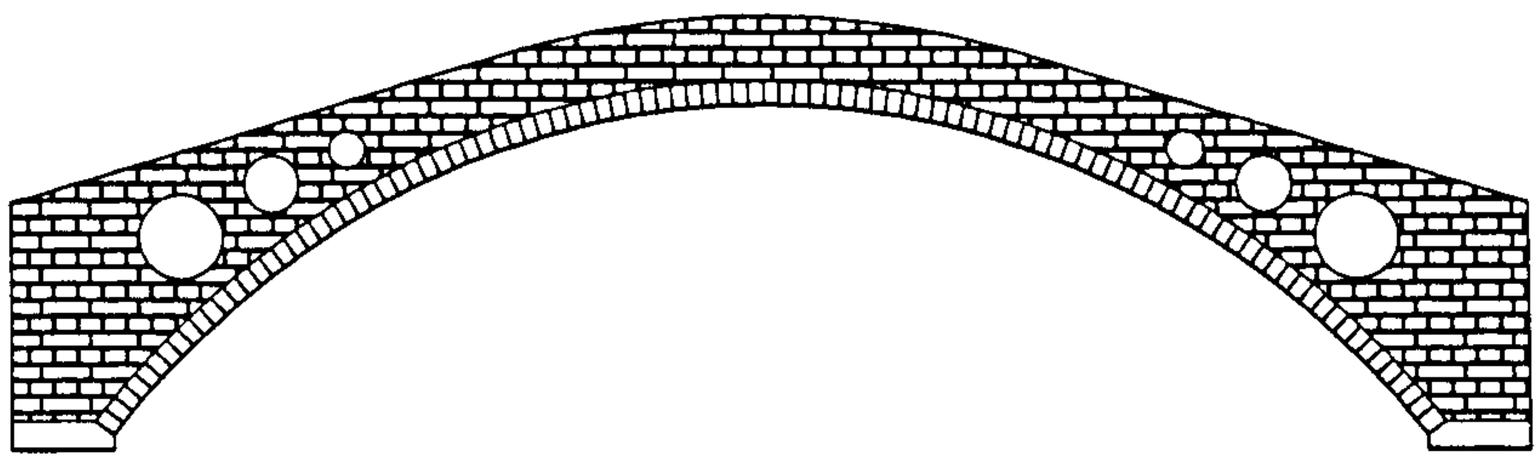

Fig. 1.6 William Edwards' Fourth Bridge At Pontypridd (1756)

It has probably never been subjected to even moderate traffic loads because the steepness of the approaches made it impractical in use (about 29%, measured from the drawing of Ruddock (1974b)). Without the judgment of the success of William Edwards's final bridge itself, one may be convinced that an open spandrel arch bridge is probably the best (and in some cases the only) alternative for large span masonry arch bridges.

The distributions of the types and styles of ancient masonry arch bridges might indicate the concerns of practice and suitability. In Roman, masonry-pierced bridges were adapted to suit valley profiles, as one would expect, while wide and flat river valleys were crossed with long multi-spanned structures using semicircular arches (Smith, 1993). In northern China, where waterflow varies, and may become very strong at flood seasons but it may be iced during winters, either thick pier multi-span arch bridges or open spandrel arch bridges without intermediate piers were commonly used; In southern China, multi-span arch bridges with slender piers were adapted to meet the requirements of the soft foundations (Mao et al., 1986; Luo and Tang, 1993).

1.2.2.2 Understanding of The Performances

The success of the *Zhao Zhou* Bridge (595AD) is a mystery. Apart from those mentioned above, the modern surveys also show that there may have been some consideration of the 'middle-third rule' (Qian, 1987), the proportional arch (Mao, 1978), economy of materials and aesthetics of masonry arches (Mao et al., 1986; Knapp, 1992) involved in this bridge. Perhaps more remarkably, the field and laboratory works

confirmed that the compressive stress of the foundation base is 0.30 N/mm^2, maximum 0.43 N/mm^2 that is approximately the allowable stress of the foundation soil. On the other hand, the sliding resistance of the foundation would not be sufficient if the contribution of the soil pressure behind the abutments were not be accounted for (Luo and Tang, 1993). The bridge itself tells the measures to prevent the possibly weak transverse-integrity (using 'stone hooks'), to prevent the possible hinges and sliding (using 'iron keys') and to prevent the possible instability of the stones (the width of arch at the crown is 60 cm less than that at the springings, and a slight camber was built so that the bridge would slightly fall in on itself to increase its stability).

The achievements of this bridge can only be judged from the brief notes in later chronicles, the bridge itself and recent survey works since no contemporaneous materials record either the background of adopting this arch form or the measures or the construction process. However, it is not unfair to say that the accumulated experience of the previous masonry arch bridges constructed before it made it possible. In fact, Chun Li had made himself advanced so far as the surviving *Xiao Shang* bridge is concerned (*Xiao Shang* bridge, an open spandrel stone arch bridge, built in Henan province, China, eleven years before the *Zhao Zhou* Bridge. It was said that the bridge was built by the same masons headed by Chun Li, but not as elegant.) (Luo, 1959; Mao et al., 1986).

During this development stage masonry arches were investigated both theoretically and by model tests. On the one hand, Hooke's Anagram (1675) and De La Hire's Statics of Arch theory (1695) made it possible to understand basic behaviour of single arches. On the other hand, some aspects of masonry arches, which still appear not to be fully understood nowadays, were observed and investigated. Some of these aspects are given below.

(a) Stability of Arches

In 1729, Couplet recognized that the line of thrust in an arch, consisting solely of a semicircular ring of voussoirs, is not itself a semicircular, he was then able to approximately determine the minimum voussoir depth necessary for the line of thrust to lie just within the arch ring (Heyman, 1969).

In Great Britain, the idea of the line of pressure was presented by Moseley, who showed in 1835 that for the stability of an arch in which the mortar cannot transmit tension the line of pressure must lie everywhere within the arch. In 1846, Barlow pointed out that 'If the thickness of an arch is more than sufficient to contain this (Moseley's limiting curve) it is obvious that more than one such curve would be contained in it and that if the theory advanced is correct the arch ought to be capable of being supported in any one of the curves'. In a sense this marks a new approach to the problem. From this time onwards interests focused on the correct choice of the line of the centre of pressure. The prevailing view seems to have been that since any line of pressure, which could be drawn within the prescribed limits, was a possible one; the matter of selection was simply one of convenience.

(b) Effects of Friction

The effects of friction between masonry units were studied as early as 1695 by La Hire. He proposed to make the joints of the voussoirs perpendicular to the line of thrust to ensure no sliding occurred, and to build arches with variable thicknesses.

Barlow (1846) argued that, in La Hire's arch, each voussoir was supposed to act as a wedge, it was considered necessary that the pressure should be transmitted, so that the direction in which it acted at each joint, should be at right angles to the surface of contact. This condition was only necessary for stability when no friction existed between the surfaces of contact of the voussoirs. But when the thickness of the arch and the friction at the surfaces of the contact between the voussoirs, were both included in the investigation, it was shown by Moseley, who argued that, firstly, the line of resistance in which the pressure was transmitted should fall within the thickness of the arch at every joint, and secondly, the direction of the pressure, at each joint, should be within certain limits, depending on the friction of the materials employed.

Barlow further believed that the pressure must be transmitted through the points of contact. In an arch composed of numerous voussoirs, it was assumed that the voussoirs were contacted at the points rather then along the adjacent surfaces. If the original form of the arch was such that the line of resistance passed through the points of contact, no motion would arise among the voussoirs, on removing the centering; but if the arch was

a segment of a circle, or any other form which did not coincide with the line of resistance, the voussoirs would take up a new position.

(c) Modes of Collapse

It was believed that the seeds of the idea of the collapse mechanism were sown by Couplet in 1730, who argued that the voussoirs were infinitely rough and interlock with each other, thereby prevented any failure due to sliding, but had no resistance to separation between voussoirs, thus the arch must fail by the rotation of some of the voussoirs about their edges. Coulomb (1733-1802) also independently investigated the collapse modes of arches, and concluded that there were two causes of 'rupture': the first arising from the turning over of certain parts of one voussoir on the wedge of another; and the second, from the sliding of the voussoirs on each other. Other investigations were carried out by Boistard (1810), and Moseley (1835). It was Barlow who first placed the concept of the collapse modes of arches in a solid engineering context in 1846. In the same year, Snell pointed out the possible failure of masonry materials, and its effects on the modification of the position of the line of thrust.

(d) Open Spandrels

Though the "eyes" bridges were used by the Romans as early as 109BC, the first record about these types of bridges appeared to be given by Gautier (1714). He described: voids or tunnels through the spandrels over the middle of the intermediate piers. The advantages of the eyes were stated: ' they relieve the structure of much of its weight, save masonry, and make passages for floodwater '. It appeared that, until 1736 when the Westminster Bridge was designed and built, Langley first attempted to explore the structural performances of such type of bridges: ' ... by making the cylinders in the upper spandrels, proportionally larger than the cylinders in the lower spandrels, their pressures will be equal, and therefore free from the danger of unequal pressure.' The cylinders were believed to effectively reduce weight, as well to relieve the piers with their foundations, to prevent the lateral pressure of the earth against the spandrel walls. The detailed development of OSMAB in Great Britain was given by Ruddock (1974a).

The effects of the 'open spandrels' may be achieved by the means of building cylinders, spandrel arches or parallel-wall through the spandrels. Compared with spandrel arches,

cylindrical voids might not be built too large to avoid a steep road surface such as Edwards' fourth bridge.

By the early nineteenth century, the parallel-wall method was described as ' the customary practice of the most experienced bridge builders' (EE, 1804). However, such practice might only be either for pure decoration or fashion without a single application of mathematical calculations (Ruddock, 1974a).

In 1897, Howe described an open spandrel masonry arch bridge as an arch bridge that " consists of an arch-rib of masonry, with joints carefully made and as thin as practicable. At regular intervals this arch supports thin lateral walls, which in turn carry small arches or slabs which support the roadway ". He proposed a graphical method to design such types of arch bridges (Howe, 1897).

By the late nineteenth century, there was a body of fundamental understanding of the behaviour of masonry arch bridges. Especially in 1879, Castigliano's strain energy theory made it possible for the first time to accurately calculate the line of the thrust for a complete arch within the limits of his assumptions. It may be noted that although weak arch bridges had been found, under the British Rail Traffic Act (RTA) 1845, the railway companies were only liable, as regards sufficiency of structure, to maintain the bridges to carry the weight of traffic as existing at the time when the bridges were built, that is, no attempts had been made to increase the load capacities of the weak bridges. It was only since the early twentieth century that to repair and to strengthen the old weak bridges became more and more important.

1.2.3 Introspective Stage: Elastic Arch

The introspective stage may be defined from the beginning of the twentieth century to the nineteen seventies when plastic arch theory was explicitly introduced. Typical work during this stage was by Fordham (1929); Pippard and his colleagues (1937-1962); Davey (1953) and Chettoe (1957), and also included the load capacity assessment of old masonry arch bridges by British and Chinese roadway/railway authorities.

Fordham (1929) argued that small span filled arch bridges might safely be designed following empirical rules. In the case of large span arches, the spandrel space should be left hollow, and a series of arches resting on piers standing on the back of the main arch were proposed. Fordham essentially restated the lessons from the Williams Edwards' work.

Having reviewed the early findings and their own comprehensive work from 1936 to 1962, Pippard et al. argued that a voussoir arch might fail in any of four ways: (a) by the development of excessive tensile stress in the joint material; (b) by the development of excessive compressive stress in the material; (c) by the sliding of one voussoir over another; and (d) by spreading of the abutments.

Pippard et al. also investigated the effects of mortar strength on the arches, and argued that, for weak mortars, "it did in fact develop sufficient tensile strength to prevent joint-failure until the linear arch was well outside the middle-third core"; for relatively strong mortars, "...joints developed sufficient tensile strength to prevent joint-cracking until the linear arch was well outside the arch ring". The tensile strength of the mortar was believed not only to delay the appearance of the first crack, but also to raise the ultimate loads to values considerably higher than those calculated for the unmortared arches. "After the appearance of the first crack, it was usual for no other crack to appear until the arch suddenly failed by instability; that is, the last three cracks developed practically simultaneously". Pippard et al. also pointed out that the crushed joint material caused the hinges to form at short distances from the edges of the arch ring. It should be noted that all the experiments were conducted on the small arch rib models, and neither fill nor spandrel walls were considered.

The assessment of old masonry arch bridges was first undertaken in Great Britain when the Road and Rail Traffic Act 1933 was issued (Hayes, 1938; Das, 1995). Arch bridges were usually assessed by graphical or semi-graphical methods. A purely analytical method was rarely used, owing to the tedious computations involved. A fully graphical method was susceptible to considerable inaccuracies, and a large-scale diagram had to be adopted. Compared with the tested results, the ultimate strength of an arch was generally underestimated. This was partly because of the assessment methods used, and partly because of the unknown backing states, the interactions between arches and fill,

and the live load distribution patterns from the roadway to the fill, and further to the arch ring through the fill. It had been found that it was more accurate to assess an open spandrel arch, in which loads being transmitted by vertical spandrel piers to the main arch was fairly definitely vertical (Hayes, 1938). This was also pointed by Morley (1912) and Williams (1927).

In 1953, Selberg proposed an " Interactive Slices " method, and used it to effectively investigate the contribution of the superstructure (fill) to the bearing capacity of old masonry arch bridges.

In China, the repairing, strengthening and assessment work of old masonry arch bridges largely took place after 1949 when the People's Republic of China was founded. Many arch bridges that were damaged during the civil wars needed to be repaired and assessed/strengthened (MoR, 1964). Since there was shortage of steel and cement at that time, many new masonry arch bridges were constructed in both national highway and railway networks (Luo, 1959). Particularly, in 1957 *Song Shu Po* Railway Bridge with span 38m first broke the record of 37.02m of *Zhao Zhou* Bridge, which had kept over 1,350 years. In the same year, *Huang Hu Gang* Highway Bridge with main span 60m was built. By the end of sixties, the construction of masonry arch bridges reached its second zenith in China. In 1961, an open spandrel stone arch bridge with span 112.5m was built in Yunnan Province. In 1966, *Yi Xian Tian* arch bridge with span 54m was constructed in Chengdu-Kunming railway lines, which was the longest single span stone arch bridge in Chinese railways at the time. During this period, many open spandrel masonry arch bridges with spans between 50m and 80m were built (MoT, 1978). It may be noted that the masonry arch bridges built during this stage were designed based on conventional elastic arch theory.

1.2.4 Modern Stage: Ultimate Limit States

The modern stage was marked by the introduction of ultimate analysis and design philosophies in masonry arch bridges. The work being carried out during this stage largely remained similar to those many years ago. However, the tools with which masonry arch bridges were analyzed, designed and built, were radically different. Various analysis and assessment approaches were developed, and a great deal of

masonry arch bridges was systematically tested both in laboratories and fields; and large span masonry arch bridges were built with more confidence than before.

1.2.4.1 Design

One of the key activities in the design of masonry arch bridges is to determine the superstructure of the main arch that will ensure that the line of pressure or thrust is sufficiently close to the axis of the main arch under the dead loads (here, the dead loads are assumed to be much greater than the live loads). To this end, various profiles of axis of arch such as circular, elliptic, parabolic, and inverted catenary, etc., have been used. The line of pressure may be located in line with the axis of the main arch by trial and error methods using the formulas developed in the early of 20th century. For the design of open spandrel arches, inverted catenary profile of axis of arch is generally adopted, and, due to the discontinuity of the dead loads of the superstructures, the line of pressure is normally chosen to be coincident with the axis of main arch at five locations, i.e., crown, quarters of span, and springings also by trial and error methods.

In the design of both filled and open spandrel arches, dead loads from the top of the extrados of main arch, i.e., roadway, fill, spandrel arches/piers, etc., were traditionally simplified as vertical point or distributed loads. That is, the interactions between the main arch and the superstructures were ignored. In China, however, it was found that a large amount of old masonry arch bridges that carried modern vehicles would be classified as the " weak " if they were checked against the modern traffic loads based on the above design assumptions. Since the Sixties, much research has been done, and various design assumptions and theories have been developed to explain the "dilemma". These new theories such as Shell Theory (Yu, 1961), Elastic Foundation Arch Theory (SRAT, 1963), Plane-hinged Arch Theory (MoT, 1980), Granular Theory (Luo, 1993), etc., were all attempted to take the interactions between the main arch and the superstructure into account based on various assumptions.

(a) Shell Theory

The axis of an arch was derived using thin shell theory on the assumptions that the arch ring only carries the loads in the radial directions, and linear distribution loads were then determined. This theory was used to analyze the old masonry arch bridges with thin rings, and the load capacities of these bridges were determined. However, the

application of this theory was limited due to relatively small number of "thin" arches remained.

(b) Elastic Foundation Arch Theory

The treatment of the dead loads of the superstructures was the same as the traditional methods. Under live loads, the arch would deform inwards and outwards. The outwards deformation was assumed being constrained by the superstructures, and elastic resistance was thus induced, which was similar to curved beam on elastic Foundation. The radial resistance was assumed to be proportional to the outwards displacements of the arch. The inwards deformation was assumed as free curved beams. Based on this theory, the deformations and forces calculated were smaller than those using the traditional methods, which do not take into account of the interaction between the main arch and the spandrel structures. Consequently, a higher load capacity of an arch would be predicted. However, this theory ignored the interactions between the main arches and the superstructures under dead loads. The results predicted using this theory might still be conservative.

(c) Granular Theory

This theory was proposed to analyze masonry arches with fill. Since granular materials such as sands and limestone, etc., were generally used as fill materials, the fill would tend to slide towards the springings along the extrados of the arch as the slopes increase. Active pressure against the fill above the springings (or side walls) would be thus generated, i.e., the fill actually acts as " arch ". To analyze arches using this theory, the axis of arch was assumed as circular or combination of circular segments, and N blocks of fill and arch were divided into with each block of the equal angle along the axis of the arch. The tangential forces, which were generated due to the weight of the blocks, were assumed to be partly taken by the arch, and partly transferred to the side walls (Fig. 1.7). The tangential forces that the arch could take were assumed as the cohesion plus the friction between the arch and the fill. The unbalanced tangential forces would be minimum (or zero) at the crown, and maximum at the blocks adjacent to the springings. The required distribution of fill loads could be derived based on the assumption that the line of pressure coincides with the axis of the main arch.

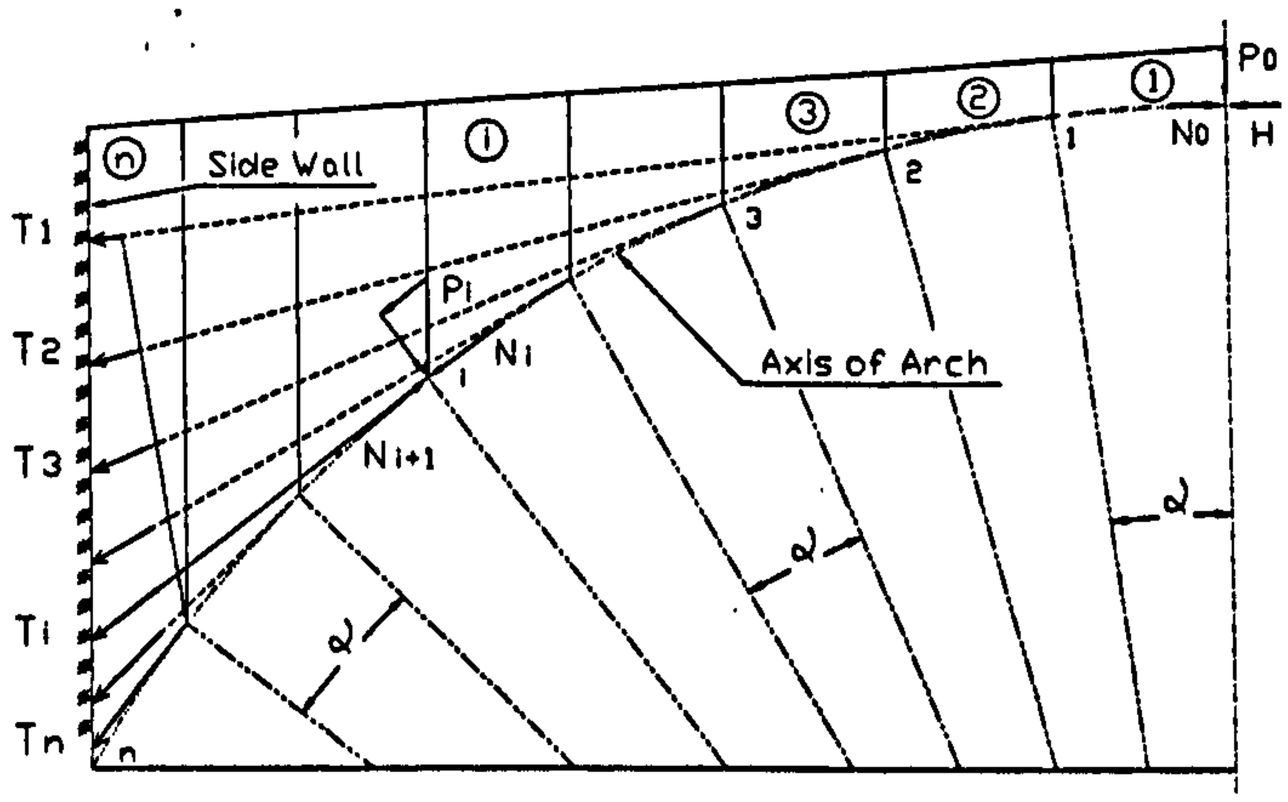

Fig. 1.7 Model of Arch With Fill Based on Granular Theory

It is interesting to note that the traditional arch analysis method could be derived from the granular theory by assuming infinite cohesion and friction, and the shell theory could also be derived by assuming zero cohesion and friction between the arch and the fill. Also, half circular masonry arches, which were considered impossible according to the traditional method, would become possible to be built based on this theory.

For the derivation of the above theory, the main arch was considered as part of the blocks. Thus, the unbalanced tangential forces would be greater than that in reality, and the resulting load capacities of masonry arch bridges would be overestimated. The theory assumed granular fill materials, and it might not be suitable for the analysis of arches with others fill such as mortar, etc. The accurate coefficients of cohesion and friction might not be easily obtained.

(d) Plane - Hinge Theory

It was found that masonry arch bridges could safely carry traffic loads even when some cracks occurred within the springings. This phenomenon was then considered as the natural characteristics of masonry arches, which were " weak " in tension. To reflect this nature in design or analysis of masonry arch bridges, plane - hinge was introduced. The difference between the plane - hinged and fixed boundary conditions was that the former allowed masonry arch to crack to certain extent at the springings, which further led to the redistribution of the internal forces within the arch. The plane - hinge was also different from real hinge due to its capacity to carry bending moments. A plane - hinged arch model was represented as shown in Fig. 1.8.

For a plane - hinged arch, the bending moments at springings were assumed as those calculated from the corresponding fixed arch multiplied by a factor of modification.

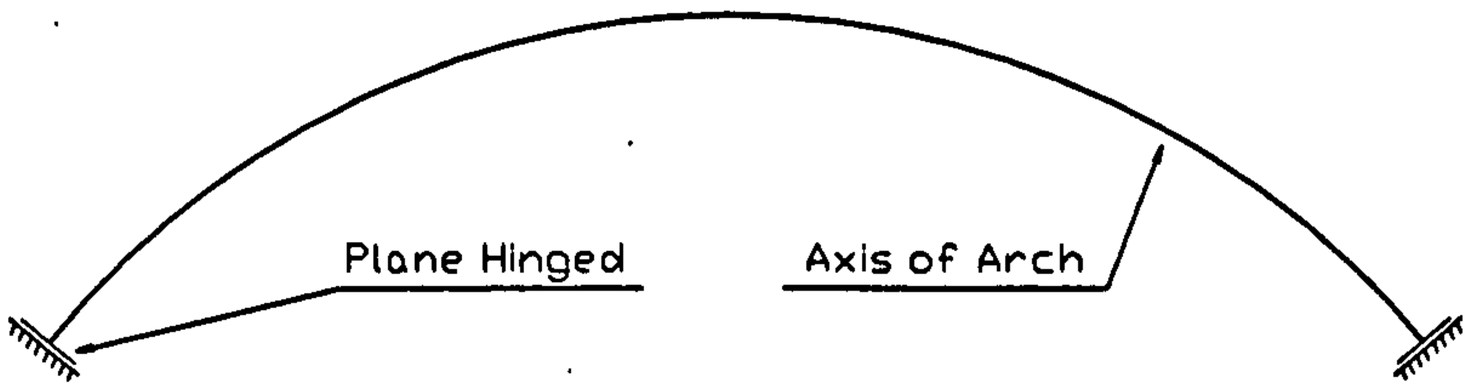

Fig. 1.8 Plane - Hinged Boundary Conditions

For a plane - hinged arch, the procedures of the analysis of the forces at the springings are:-

(1) Calculate the bending moments and the axial forces for a corresponding fixed arch under dead, live and other loads;

(2) Calculate the eccentric values at both ends (the bending moments divided by the axial forces);

(3) Find the factors of modification to bending moments for both ends according to the calculated eccentric values from the design table;

(4) Calculate the "real " bending moments, the axial forces and the eccentric values;

(5) Check the sections under the eccentric loads at the springings. The sections would be passed if the eccentric values and the maximum compressive stress are within the specifications.

For the step 3, the relationship between eccentric values and factors of modification to bending moments were produced based on model arch tests, and documented as table formats.

The plane - hinge concept was proposed in the Sixties during the study of two-way curved arch bridges. The introduction of this theory enabled masonry arch bridges to be built with more confidence.

In the above theory, a representative factor of modification to bending moments is important to achieve " real " solutions for an arch. It may be noted that if the factor is

assumed as 1, which means no modification is applied, and the plane - hinged arch method is the same as traditional one; and if the factor is assumed as zero, the fixed arch would become a hinged one.

1.2.4.2 Analysis

Three methods are generally used to analyze masonry arch bridges, i.e., elastic methods; mechanism methods; and finite element methods. Derived from the classical Castigliano energy principles, the elastic cracking Castigliano method was developed for the analysis of masonry arch bridges (Hughes and Vilnay, 1988; Bridle and Hughes, 1990 and Roca. et al. 1998). Combined with a brittle material model in tension, the depth of arch was reduced at the sections in tension. Both the ultimate loads and the modes of failure of a masonry arch could be determined.

It appears that Koohariani first predicted the maximum load and the corresponding modes of collapse for a voussoir/concrete arch based on limit philosophy in 1952. Between 1966 and 1982, Heyman reviewed, discussed and evaluated the work related to masonry arches/arch bridges, especially those before the mid-nineteenth century. Based on the limit theorem, he first studied masonry arch bridges, and largely concerned with understanding the stability of such structures.

Both single- and multi-span arches were studied using mechanism method (Livesley, 1978 and 1992) and (Gilbert, 1993). "Encouraged by Tang, ... , and inspired by the meeting with Heyman in Cambridge in 1984", Prof. Lingxi Qian, based on the ultimate philosophy, analyzed the *Zhao Zhou* Bridge using mathematical programming methods (Qian, 1987), in which the spandrel piers and arches were simplified as static loads, and the main arch was studied under different loading cases. The analysis showed that the geometrical factor of safety of this bridge was 3.703, which was in accordance with the well-known 'middle-third rule' of traditional masonry arch design principle.

Since the pioneer work by Towler (Towler, 1981), a number of researchers have attempted to use the finite element methods to study the behaviour of masonry arches. Failure modes of masonry arches have been extensively studied, and other aspects such as the effects of geometric non-linearity (Crisfield, 1985b), strain softening (Loo et al,

1991) and ring separations (Hodgson, 1996), etc., have also been investigated. Most of the work was concentrated on the arch barrel while the other aspects such as fill and foundations were attempted. The modelling methods that were adopted previously and their findings are briefly reviewed.

(a) One-dimensional Models

One-dimensional curved beam finite element was adopted to model brickwork arch bridges (Towler, 1981). The material non-linearity was treated through a no-tension formulation, which was combined with a parabolic stress-strain relationship including strain softening for brickwork in the compressive regime. The potentials of the application of non-linear finite element methods were demonstrated in terms of the ability to trace the full behaviour of masonry arches up to collapse under various loading conditions. The material properties from brickwork prism tests were used in the model, and no lateral resistance of the fill was considered. A straight tapered beam element was developed to simulate the behaviour of masonry arch bridges (Choo et al, 1990 & 1991). No tension capacity and a linear stress-strain relationship for compression were assumed. Depending on the development of cracking and crushing portions of the arch barrel, an effective arch ring was introduced. The resulting effective depth of arch ring was computed at each nodal cross-section by satisfying the equilibrium between the axial force, the bending moment and the internal stress. Crisfield (1984 & 1985a) developed beam elements to model arch rings. The model could simulate the effects of strain-free rigid-body rotations and hinges associated with the formation of arch failure mechanism

One-dimensional modelling methods are normally ' simple ', and a converged solution could be achieved relatively easily and quickly. The limitations of the elements might not be able to model the phenomena such as inter-elements' sliding and ring separations, etc.

(b) Two-dimensional Models

A failure criterion that was generally used for modelling plain concrete was adopted by Loo (Loo et al, 1991 & 1995), in which the effects of cracking, crushing and strain softening of masonry materials were simulated. A single crack-surface interlock factor along cracking surfaces was used to take the reduction of shear transfer capacity due to

material cracking into account. One factor might be limited since the shear transfer capacity is different between open cracks and close cracks. Furthermore, the treatment of fill in the model might be less efficient. Two dimensional non-tension models, in which eight-node isoparametric elements with plane stress for arch ring and plane strain for fill, were developed (Crisfield, 1985b, 1988 and 1990). Free-slip was allowed between arch and fill by using special slip element. For the arch ring, the material properties were resolved into radial and tangential directions, and only the latter were degraded to account for tensile cracking or compressive yielding. Similar methods were also developed for the modelling of the effects of ring separations (Choo et al., 1992). In order to simulate cracking within arch rings, the model allowed the elements next to the cracks to disconnect when the nodal tension reached the material tensile capacity. Joint elements were adopted in both radial and tangential directions to simulate ring separations. The effects of friction were taken into account by applying a pair of equal and opposite frictional forces at the nodes.

(c) Three-dimensional Model

A three - dimensional model using eight-node curved quadrilateral shell elements was developed to model a skewed arch barrel (Choo et al., 1995). The treatment of non-linear effects such as cracking and crushing of the arch ring materials was similar to that used in the one-dimensional model (Choo et al, 1990). The main conclusion of the analysis was that the load carrying capacity increased as the skew angle of arch increased, and hardly affected by the variations in the ratios of span to width and ring thickness to span, which appeared in conflict with the other findings (Gu, et al., 1994). The author suspects that Choo's conclusion may be valid only in the special cases under his assumptions. Hodgson (1996) developed a sophisticated finite element model for brickwork masonry skew arch bridges. A combination of concrete type elements, non-linear spring elements and interface elements were used to capture the behaviour of the skew arches such as cracking, crushing, sliding and separation along axial, radial and circumferential directions.

Though considerable efforts have been made to investigate the behaviour of masonry arch bridges using finite element methods and many conclusions have been drawn regarding to the various aspects of the masonry arches, it appears that there are still many uncertainties which need further investigation:-

- The work so far has largely been concentrated on the computation and verification of collapse loads under a simple load regime applied at a fixed point or line. Few attempts using finite element methods have been made to investigate the behaviour of masonry arches under static or dynamic vehicle loads;
- To date, the finite element work has been only applied to a single span square or skewed masonry arch, and no evidences show its applications in curvic masonry arch bridges;
- No attention has been paid to the relationship between the finite element models and different characteristics of various fill materials.;
- The effects of the values of Young's modulus (E) in the finite element model were emphasized. But no consistent conclusions have been drawn. The true value of E from brickwork prism tests was suggested to be used in the finite element models (Towler, 1981) while a reduced value of E were believed to lead to a more realistic load-deflection responses for a masonry arch (Crisfield, 1985; Choo et al., 1991; and Hodgson, 1996), but few attempts were made to quantify it.

1.2.4.3 Assessment

The assessment of old masonry arch bridges is of worldwide interest (Melbourne 1995).

In the UK, a number of masonry arch bridge tests have been carried out both in the laboratories and the fields (Hendry et al., 1985 -1990; Melbourne et al., 1986-1997; Page, 1987-1989). For assessment methods, the MEXE method is easy to use and has served well, but it is now considered to be conservative, particularly for long spans. It also has an additional shortcoming in that only filled arches of spans up to 18 m were considered. For the purposes of the assessment of old masonry arch bridges, a number of computer programs, such as ARCHIE (Harvey et al., 1988), MARCH (Davies, 1989), MAFEA (Choo et al., 1990), CTAP (Hughes, 1990) and Crisfield's mechanism and finite element assessment programs (1984; 1985; 1987; and 1990), were developed. These programs certainly facilitate the procedures of assessment and help one understand the factors being concerned; but due to the variable conditions related to the old arches, the success of the assessment work not only depend on the programs themselves, but also on the users' understanding of individual masonry arches

The survey in 1979 shows that there were 4,085 two-way curved arch bridges in China, 6.6 per cent of which were evaluated as weak ones and repairs or strengthening were thus needed (MoT, 1980; Lou et al., 1993a). It was found that cracks occurred, i.e., within the main arches: circumferential cracking near the springings, circumferential cracking around the crown, radial cracking; within the spandrel arches, radial cracking of 'three sections' with the end spandrel arches, radial cracking between spandrel arches and spandrel walls, vertical cracking between spandrel arches; and within the spandrel piers, cracking at the top and/or bottom interfaces between the spandrel piers and main arch or the springings of spandrel arches. Four assessment methods, i.e., 'defect' method, 'cracking length of the main arch barrel' method, elastic analytical method, and test method, have been proposed and used (Lou et al., 1993b). It may be noted that the cracking patterns within the two-way curved arch bridges may differ from those to be discussed in this thesis since the reinforcements are generally added for the former structure. However, the similarity between the two types of arches undoubtedly exists.

1.2.4.4 Construction

Few masonry arch bridges have been built in the UK since before the Second World War, and "the first completely new" eight metre span brick arch highway bridge *Kimbolton Butts* Bridge, built in Cambridgeshire County in 1992, might mark the renewed interests of building such form of bridges (Cox and Halsall, 1996).

In certain parts of China, partly influenced by the prevailing geological formations and conditions, masonry arch bridges, especially open spandrel ones, have been widely built.

The Chinese state design codes for highway masonry arch bridges in 1985 which were based on the limit state design philosophy, replacing the old version (1974), facilitated the design and construction of such bridges. For various forms of masonry arch bridges and abutments/piers, the new code gave guidelines for the choices of construction materials, structural components, scope of analysis and the approaches as well as construction controls and checks. For the main arch, many forms such as two-way curved arch, rib-slab arch and ribbed arch, etc., have been developed.

Fig. 1.9 shows the cross sections of the corresponding forms of arches, and Table 1.1 lists a selection of some Chinese masonry arch bridges with spans over 100 metres.

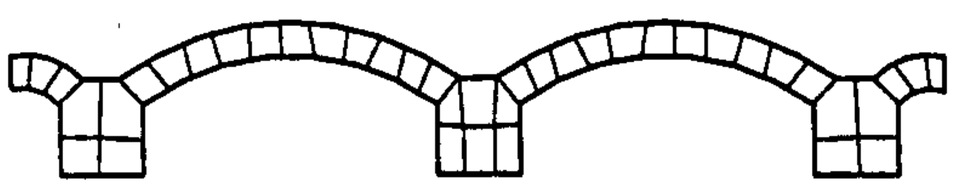

(a) Two-way Curved Arch

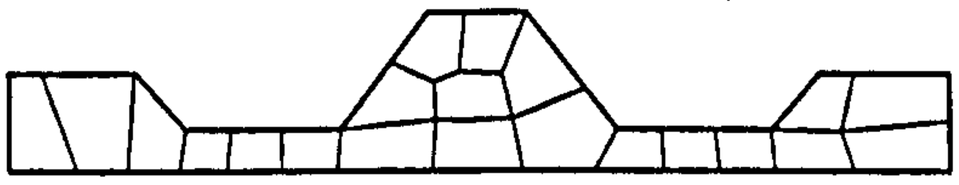

(b) Three-rib Slab Arch

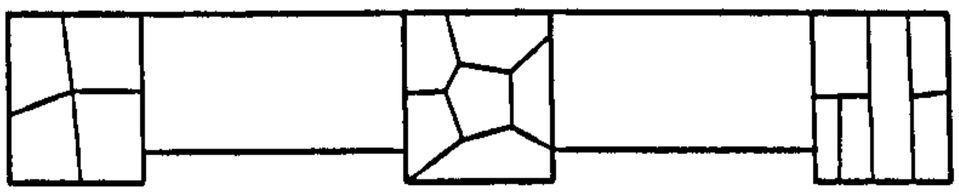

(c) Ribbed Arch (Transverse RC braces)

Fig. 1.9 Modern Types of Open Spandrel Arches

Chinese Masonry Arch Bridges With Main Span Over 100 m **Table 1.1**

No.	Name	Province	Main Span (m)	Width (m)	Cross Section	Year Completed
1	*Chang Hong*	Yunnan	112.5	7.0	Square	1961
2	*Hong Du*	Guangxi	100.0	7.0	Square	1966
3	*Hong Qi*	Sichuan	111.0	7.0	Square	1968
4	*Xiao Du huan*	Hubei	100.0	9.0	Square	1969
5	*Yu Gong*	Henan	102.0	9.0	Square	1969
6	*Hu Wan*	Henan	105.0	7.0	Rib, Π	1971
7	*Jiu Xi Gou*	Sichuan	116.0	8.0	Square	1972
8	*Jiang Jing*	Anhui	100.0	7.8	Rib, tw	1977
9	*Dan He*	Shanxi	105.0	7.0	Square	1983
10	*Wu Chao*	Hunan	120.0	8.0	Square	1990

Note: 'tw' means two-way curved.

1.3 Summary

To a certain extent, the history of masonry arches is the one of continual discovery and rediscovery, invention and reinvention.

The building of masonry arch bridges have experienced four great eras: (a) During Roman Empire (EB, 1984c); (b) During Sui Dynasty (581-618) in China (Luo, 1959); (c) During 1725-1850 in Europe (Smith, 1993; Heyman, 1982); and (d) Since 1950 in China (Luo and Tang, 1993). It may be noted that the Medieval Gothic arches, which replaced the heavy and restrictive round arches of the Romanesque style, might indicate that the workmanship at the time was at first not as good as that of the Romans, and the type of arches may have been preferred because it demands less precision than the circular one (EB, 1984a and c; Tellett, 1982; Brown, 1993).

The assessment of the existing masonry arch bridges have also been proposed and carried out four times in the history of masonry arches. (a) Around 1845 in Great Britain (Hayes, 1938); (b) After the Second World War in Great Britain (Pippard and Chitty, 1951); (c) During the fifties in China (Luo and Tang, 1993); and (d) Since the eighties worldwide (Melbourne, 1995). During the first great era of the assessment, under the British Rail Traffic Act 1845 the railway companies "are only liable, as regards sufficiency of structure, to maintain the bridges to carry the weight of traffic as existing at the time the bridge was built". Such assessment work may be called the 'defect assessment' rather than the 'prediction assessments' as have been practiced in the UK recent years.

Masonry arches were studied through tests on a large number of models made of various materials such as wooden voussoirs (Gautier, 1714), metal voussoirs (Atwood, 1801), stone voussoirs (ASE, 1890), chalk voussoirs (Williams, 1927), concrete voussoirs (Pippard et al., 1936; MoT, 1960), steel voussoirs (Pippard et al., 1951; MoT, 1962). Attempts were also made to localize the line of thrust at three sections by the insertion of blocks of lead near the curved axis between voussoirs (Howe, 1897). Brickwork masonry is mainly used more recently (Melbourne et al., 1986-1997; Smith and Harvey, 1989). In addition, the modern test techniques such as acoustic emission methods (Royles and Hendry, 1990), photoelastic method (Bron, 1991), and computer vision

method (Draper et al., 1995), etc., have also been adopted in either field or laboratory masonry arch tests.

By comparing open spandrel masonry arch bridges and filled ones, some of the advantages of the former over the later may be listed as follows:

- Saving of masonry;
- Reduction of self weight;
- Environmental attraction;
- Reduction of thickness of main arch;
- Increase in the openings for flood water;
- Reduction of water impact on bridge;
- Reduction of stresses within abutments/piers;
- Reduction of sizes of abutments/piers;
- Less strict requirements of foundations;
- Clear loading transfer patterns;
- Reduction of the possibilities of the spandrel wall failure;
- More reliable analysis results

1.4 Scope of Research

The previous investigators have concentrated on single- or multi-span filled masonry arch bridges, and the work related to open spandrel arch bridges is limited. Lou et al's one-dimensional method was limited to the two-way curved arch bridges, in which reinforcements were used. The literature survey shows that little research into open spandrel masonry arch bridges have been done so far.

Attempts have been made neither to fully investigate all the factors, which may have influences on the performances of the OSBMABs, especially those associated with their components, nor to develop a new finite element computer program for the analytical work.

The present research is dedicated to the understanding of the global behaviour of open spandrel brickwork masonry arch bridges. To this end, a series of full scale model tests

and nonlinear finite element simulations using ANSYS5.3 have been carried out. The aims of the research may be summarized as follows:

⇒ To investigate the failure modes of the OSBMA;

⇒ To investigate the load capacities of the OSBMA;

⇒ To examine the effects of a range of factors on the load capacities and on the failure modes of the OSBMA;

⇒ To evaluate the possibility and reliability of the application of the model tests and the finite element simulations in the analysis and assessment of the field masonry arch bridges.

CHAPTER 2 MATERIAL AND MODEL ARCH TESTS

2.1 Material Tests

The results of both model tests and finite element analyses of open spandrel brickwork masonry arches largely depend on the material properties of their components being used, i.e., bricks, mortar and brickwork masonry units. Therefore, it is necessary to study the characteristics and the behaviour of the components before the full model arches are investigated.

The properties of brickwork masonry arch components could be influenced by a large number of factors, such as bonding, anisotropy of bricks, dimension of bricks, joint thickness, material properties of bricks and mortar, the interaction of the constitutes and the quality of workmanship, etc. As far as the present research is concerned, the influences of some factors may be either minimized or ignored, but the influences of the others must be studied.

It may be noted that the standard test methods of brickwork masonry prisms only cover limited types of tests. It appears that little attention has been paid to some factors such as the angle of wedged mortar joints and the thickness of the mortar joints between bricks within brickwork masonry. A series of material tests that were conducted together with the model arches are given below, in which the standard tests methods were adopted where applicable.

2.1.1 Brick

Class A Engineering bricks (BS5628), and half scale Raewell bricks were used in the model arch tests.

Compressive tests were conducted for both types of bricks using the method described in BS 3921. The compressive strength was the stress measured normal to the bed face immediately prior to the crushing failure of the bricks. For each type of brick, a representative sample of ten bricks was directly chosen from the brick packs used for the

construction of the model arches. The set-up of the compressive tests of bricks is as shown in Fig. 2.1.

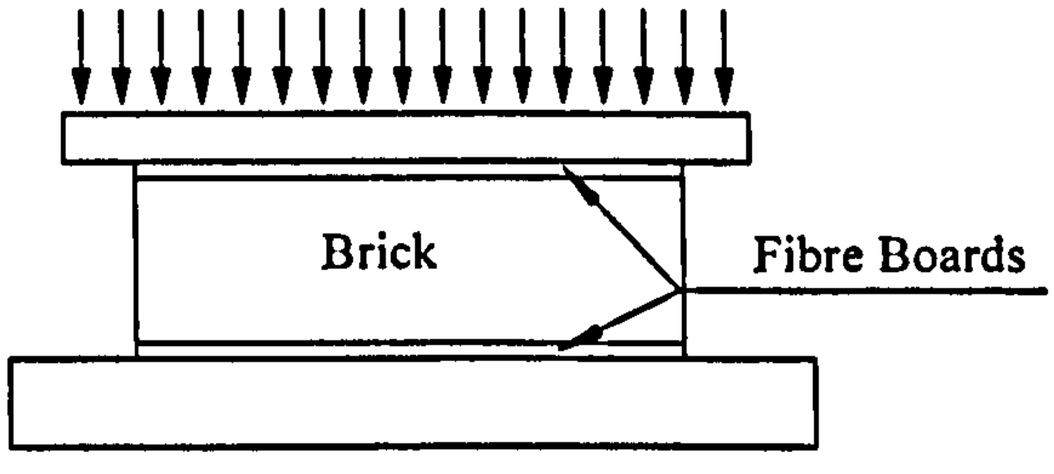

Fig. 2.1 Set-up of Compressive Test of Bricks

The average dimensions and the densities were measured, and the compressive strengths of the bricks were tested, as listed in Table 2.1.

Properties of Bricks **Table 2.1**

Brick Type	Compressive Strength (N/mm^2)	Nominal Dimension (mm)	Density (kg/m^3)
Class A Engineering	78.82	215×102×65	2420
Half Scale Raewell	19.23	114×54×38	1940

The typical mode of failure during the tests of both Class A Engineering bricks and Raewell bricks is as shown in Fig. 2.2.

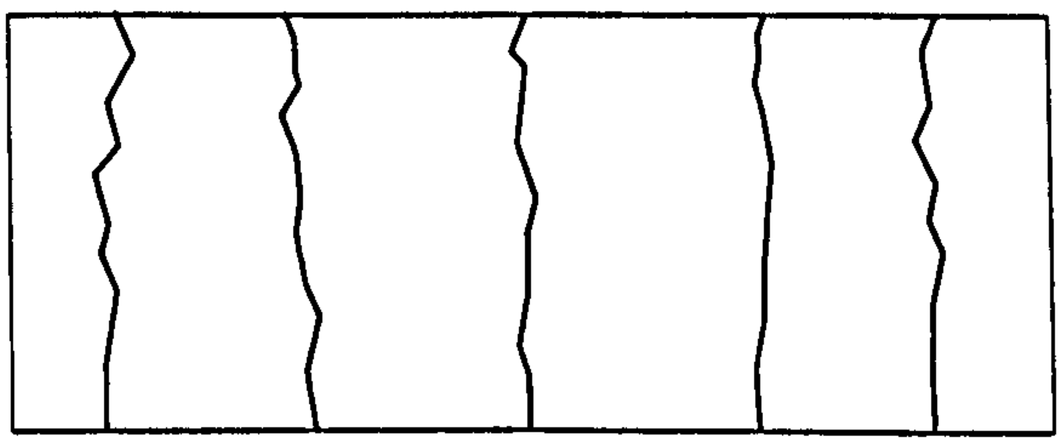

Fig. 2.2 Failure Mode of Brick in Compression

A relatively large variation of test data was found among individual bricks, especially for the half scale Raewell bricks. It was considered that the variation was mainly caused by the porous nature of the brick ceramic and irregular load bearing faces, and also by the confining effects of the loading platens of the test machine. In other words, under a

uniaxial compression load, the bricks tended to expand in the transverse directions due to the Poisson's effects. Where this expansion was restrained, transverse compressive confining stresses were built up, resulting in a triaxial compression stress state. As axial compressive stress increased, and axial compressive strain decreases as a result of such confinement. To minimize the effects of the confinement, fibre boards were attached to both the top and bottom of the specimen as soft cappings.

During the tests, sudden brittle failures were dominant.

2.1.2 Mortar

A weak mortar, 1:2:9 (cement:lime:sand) mix by volume, was used throughout the experimental test programme. The testing method (BS 4551) was used during the compressive tests of mortar cubes. A typical mortar cube sample and the strain gauge arrangement are as shown in Fig. 2.3.

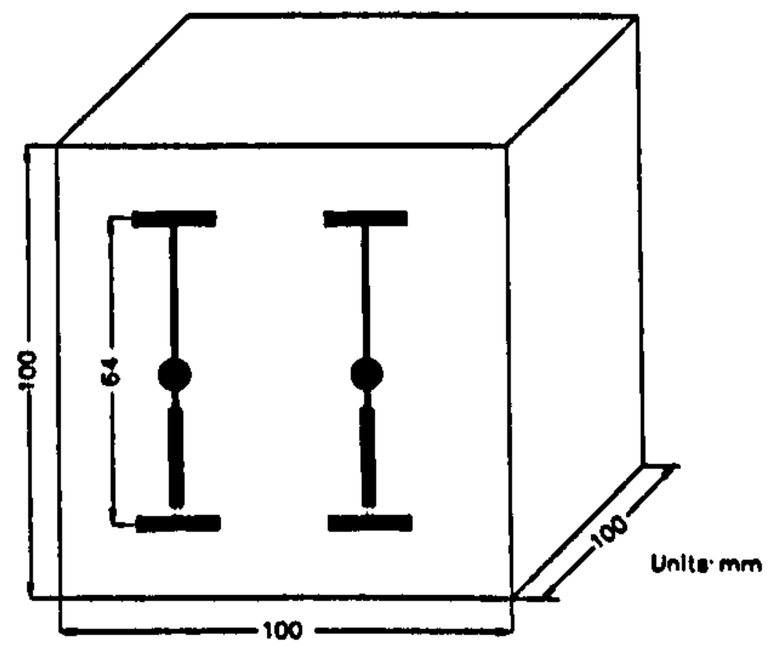

Fig. 2.3 Mortar Cube And Strain Gauges For Compressive Tests

The average density of the mortar cubes was 1540 kg/m^3. Despite the fact that the same workmanship and the mix were used, the results of the mortar tests were different from group to group. For the mortar used in models OSMA1 and OSMA2, the compressive strength (σ_{cm}) and the initial Young's Modulus (E_m) were 0.95 – 1.25 N/mm^2, and 1200 – 1500 N/mm^2, respectively. However, the σ_{cm} and E_m were 2.0 - 2.4 N/mm^2, and 2000 - 2500 N/mm^2 , respectively, for the mortar used in the models OSMA3, OSMA4, and OSMA5.

The typical strain – stress curves of the mortar under compression from the two groups of tests, OSMA1/2 and OSMA3/4/5, are as shown in Fig. 2.4.

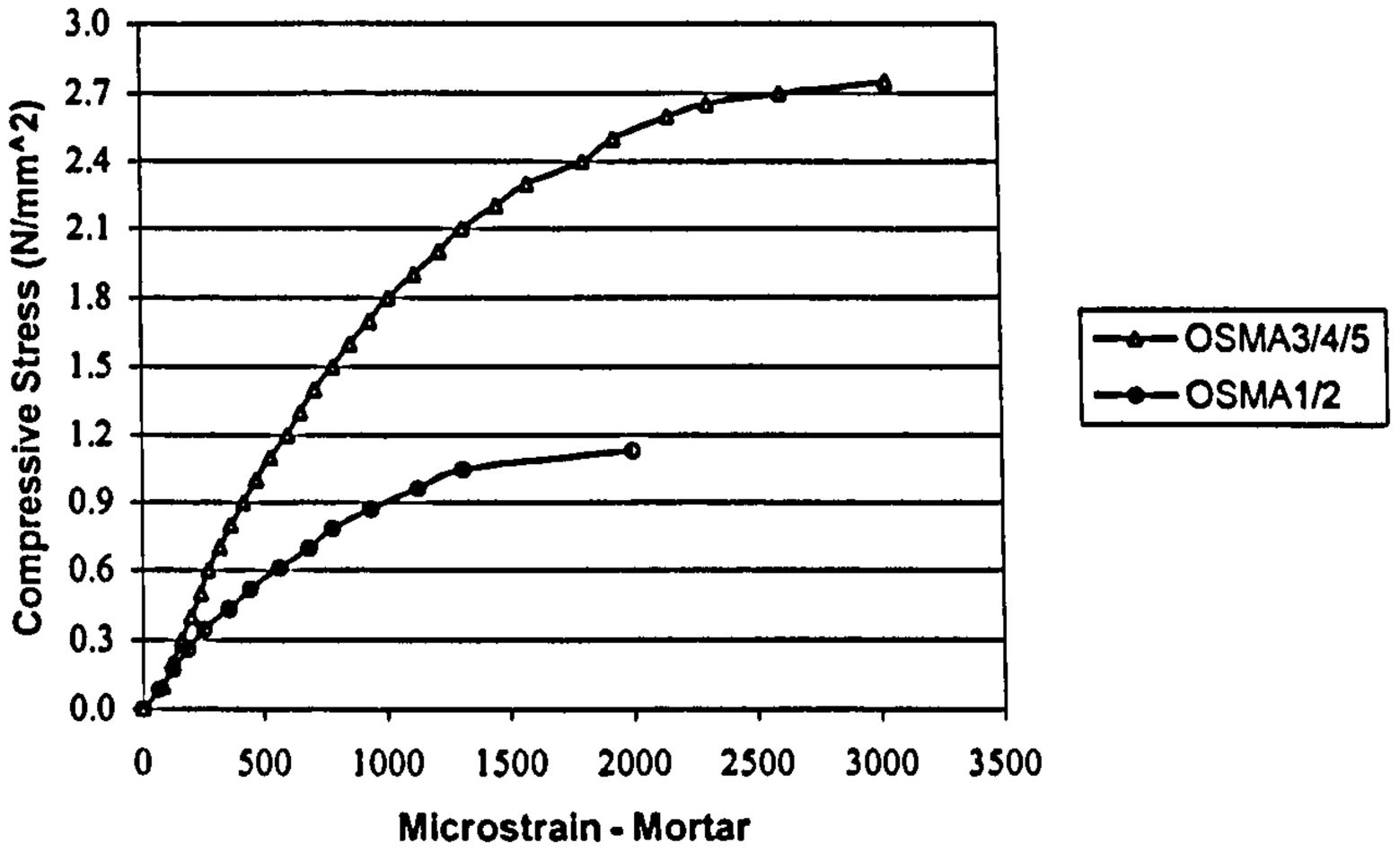

Fig. 2.4 Stress – Strain Relationship of Mortar Cubes Under Compression

Two failure modes were observed during the compressive tests of the mortar cubes, i.e., pyramidal shape crushing failure and shearing failure (Melbourne and Tao, 1997b).

It is known that mortar has several functions in addition to that of filling the gaps between bricks which result from their imperfect sizes and shapes. In the case of open spandrel brickwork masonry arches, the mortar, as a bedding agent, bonds individual masonry units into a composite assemblage to ensure the uniform transfer of various loads; it takes the curvature in the arch barrel (wedge) to facilitate ease of construction and allow for tolerances of brick units, and to achieve a desirable profile; the mortar of certain tensile strength may accommodate the small deformation associated with moisture and temperature changes.

It may be noted that the data obtained from the mortar cube tests may not directly apply to finite element modelling of the arches. In a brickwork masonry arch, brick units absorb the water from the joint mortar, and the water-cement ratio in the mortar would be reduced, which would result in a greater strength in the arch than that in the mortar cubes. The moisture content of the brick is therefore important as much as it affects the interface mortar strength and the interface bond. The wedged-shape joints and their restraint conditions in the arch were also different from those in the mortar cube tests.

2.1.3 Brickwork

2.1.3.1 Compressive Tests

Prior to the model arch tests, both five-course and four-course brickwork prisms were constructed using the materials and workmanship as those used in the model arches, and tested to determine the compressive strengths of the brickwork masonry of Raewell and Class A Engineering bricks, respectively. The set-up of the specimens is as shown in Fig. 2.5.

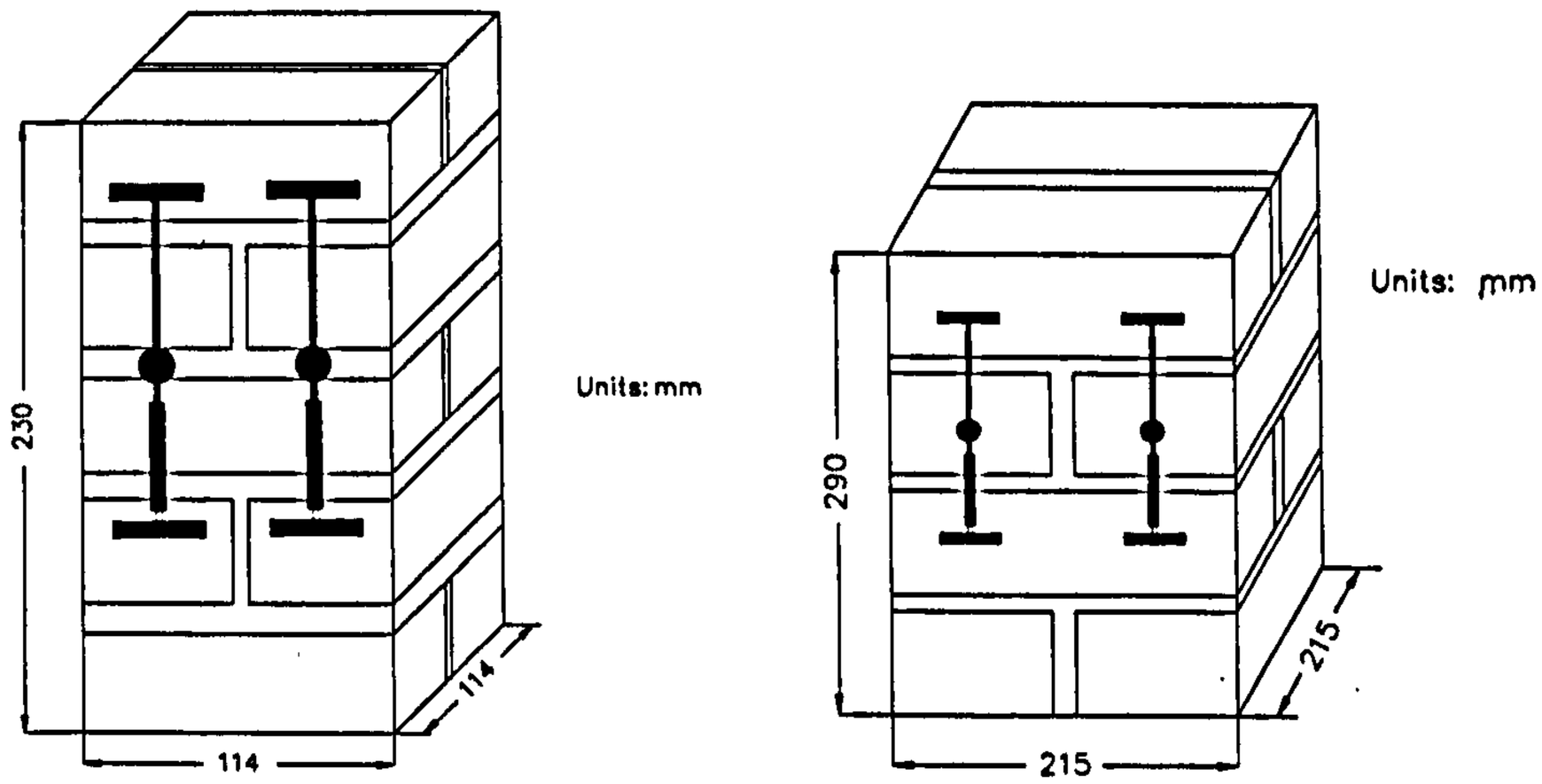

(a) Raewell Bricks **(b) Class A Engineering Bricks**

Fig. 2.5 Brickwork Prism And Strain Gauges For Compressive Tests

To reduce the effects of roughness and irregularity of surfaces on the load bearing faces of the bricks, and to reduce the restraint effects of the end platens of the test machine, soft capping (fibreboard) was used throughout all the prism tests.

For the Raewell brickwork prisms, the average density was 1800 kg/m^3, and the compressive strength (σ_{cbw}) and the initial Young's Modulus (E_{bw}) were 6.00 – 9.00 N/mm^2, and 3000 – 4000 N/mm^2, respectively; For the Class A Engineering brickwork prisms, the average density was 2300 kg/m^3, and the σ_{cbw} and E_{bw} were 16.00 – 20.00 N/mm^2, and 8000 – 12000 N/mm^2, respectively.

The typical strain – stress curves of the brickwork prisms under compression are as shown in Fig. 2.6.

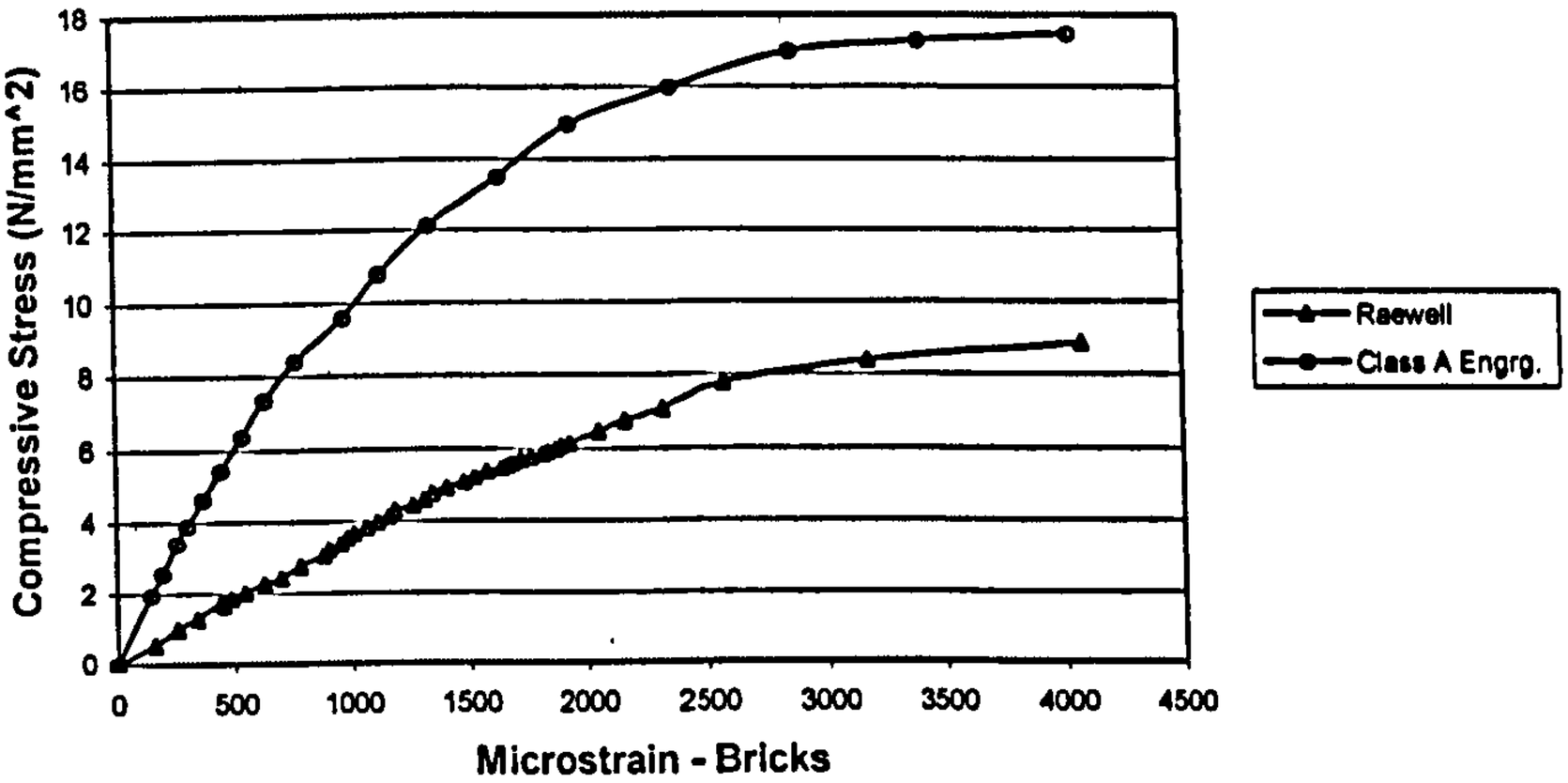

Fig. 2.6 Stress – Strain Relationship of Brickwork Prisms Under Compression

During the tests, the brickwork prisms generally failed by the development of tensile cracks through the prisms parallel to the axis of loading. The reason for this type of failure was due to the different moduli of the bricks and mortar. The weaker mortar tended to expand laterally at a greater rate than the bricks under compression, and the bricks restricted the expansion of the mortar. In conjunction with the confinement of the mortar, to maintain equilibrium, lateral tensile stresses were introduced in the bricks on both sides of the bed joints.

When the combination of vertical axial compression and horizontal biaxial tension were high enough, the mortar along the edges of joints were pushed out and vertical cracking through the prisms occurred, and eventually resulted in the failure of brickwork prisms. The load capacity of brickwork was higher than that of the mortar cubes and lower than that of the bricks.

The test results could be influenced by various factors, such as the loading set-up, instrumentation (gauge sensitivity and range setting), prism configuration and workmanship, etc. When cracks were about to occur, the loading speed could have significant effects on the compressive strength. In most cases, a quicker loading would lead to a higher strength.

The compressive tests were also conducted on five-course and two-course Class A Engineering brickwork prisms of section area 215 × 102 mm^2, and relatively higher compressive strength and the initial Young's Modulus were measured. For the two-

course brickwork prisms, as compressive loading increased, due to the more significant effects of the end confinement at the bearing plates, several vertical cracks occurred on both side of the brickwork units as shown in Fig. 2.7, and consequently resulted in conical type shear-compression failure modes.

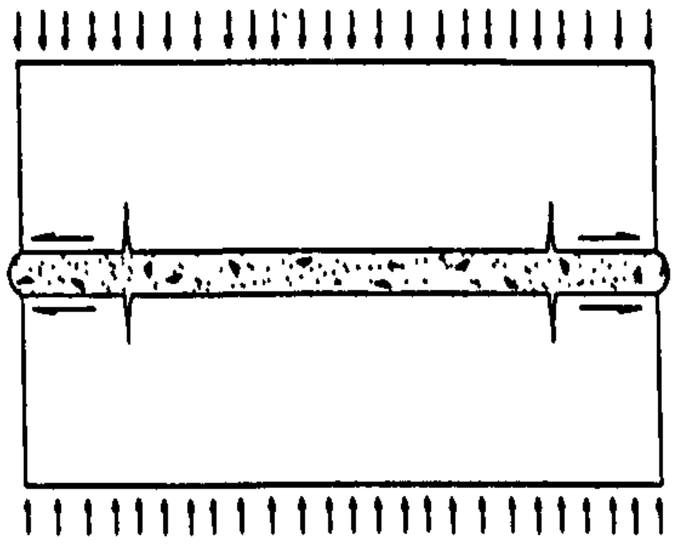

Fig. 2.7 Tensile failure of Two-Course brickwork Prism Under compression

2.1.3.2 Tensile Test

Three methods may be employed for the tensile tests of brickwork masonry, namely, direct pull test, wrench tests and bending tests (BRE, 1991; ASTM, 1986 and 1987) as shown in Fig. 2.8.

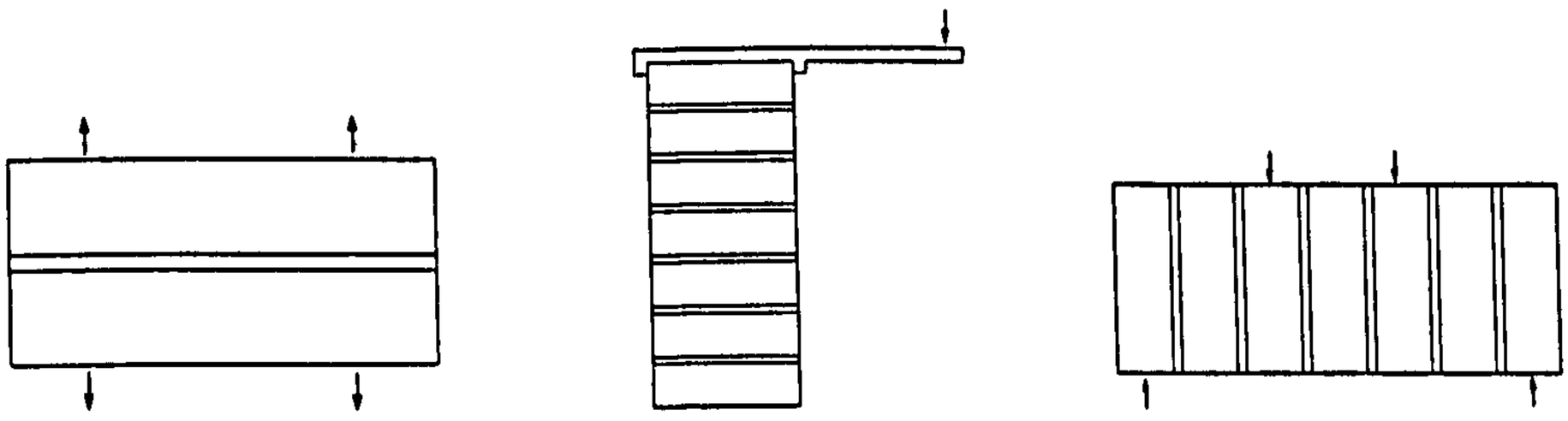

(a) Direct tension test **(b) Bond wrench test** **(c) Stack bending test**

Fig. 2.8 Tensile Test Methods For Brickwork Masonry

The wrench and the stack bending tests are similar in that both apply bending to the joint, and consequently results in the peak tensile stress being at the edge of the joint. A value for bond tensile strength is obtained by calculating the maximum tensile stress in the joint at the failure load using elastic bending theory. However, bond tensile strength at the edge of the joint can be significantly different from that of the remainder of the area of the joint. The difference may result from a number of factors, which include the loss of water from the mortar to the air at the edge of the joint and variation in water

absorption characteristic of the bricks between the edges and inner areas at the time of construction.

Alternatively, direct tension tests may be used. The disadvantage of using this method is that a uniform tensile stress distribution across the joint may not be readily ensured. Consequently bond tensile strength value calculated assuming a uniform stress distribution may tend to underestimate the real bond tensile strength. Also, bond condition of brickwork prisms may not be as strong as that of brickwork masonry units of a real arch as the initial pressure that is applied to construct prisms is generally lower than that within a real arch. To account for the uneven stress distribution across joints and other factors, a multiplication factor may be used.

Direct tensile tests were adopted for the tests of both Raewell brickwork and Class A Engineering brickwork prisms. Timber plates were first glued on the faces of bricks using Flexon®, and then steel plates were used with one face screwed together with the timber plate and the other gripping rods as shown in Fig. 2.9. The specimens were gradually pulled apart using a tensile testing machine.

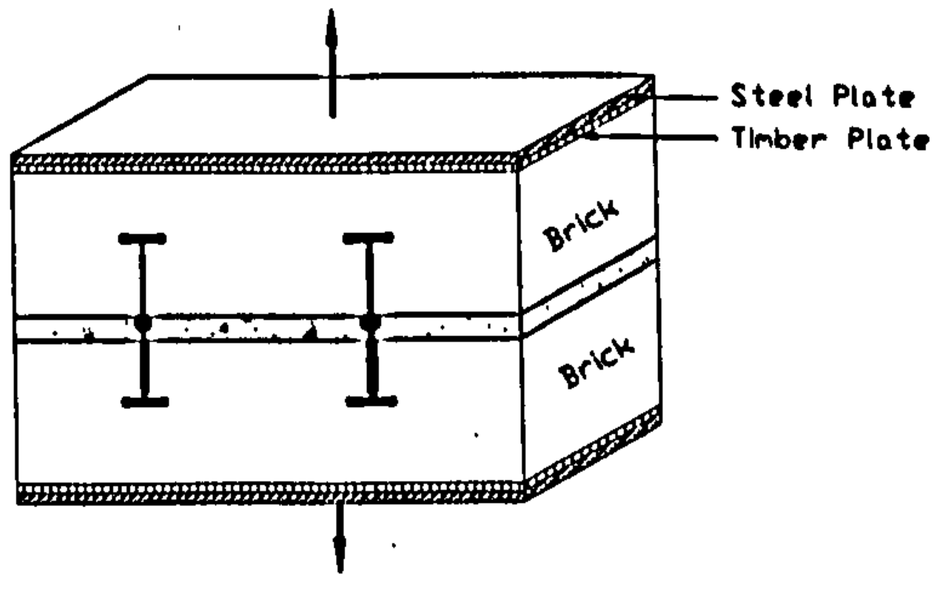

Fig. 2.9 Brickwork Prism For Tensile Test

For the Raewell brickwork prisms, the tensile strength measured varied between 0 and 0.015 N/mm^2. Difficulties were encountered in the application of sufficient small increments of loading due to the test facility used, and the test data were largely inconsistent. It was also noted that the bonding conditions between Raewell bricks and mortar were generally poor, and it was believed that such conditions might be created by the irregular surfaces of the bricks and the way that the two-course prism samples were constructed:- a light brick was simply laid on top of the other. As a result, the bonding strength between bricks could not be fully developed. In other words, such low tensile

strength from the tests might not represent the true tensile strength of brickwork units within the model arch, where relatively large compressive forces could be generated during the curing period. These compressive forces not only helped to accommodate the irregular surfaces of bricks via mortar, but also to develop bonding strength between within brickwork prisms.

The ultimate tensile strength for the Engineering brickwork used was largely between 0.20 and 0.35 N/mm^2 though the mean value of the sample of the model OSMA3 was higher than that of the models OSMA4 and OSMA5. The typical strain – stress curves of the Engineering brickwork prisms under tension are as shown in Fig. 2.10.

Similar to the brickwork masonry in compression, nonlinear stress-strain relationship appears when stress is about 85% of the ultimate stress.

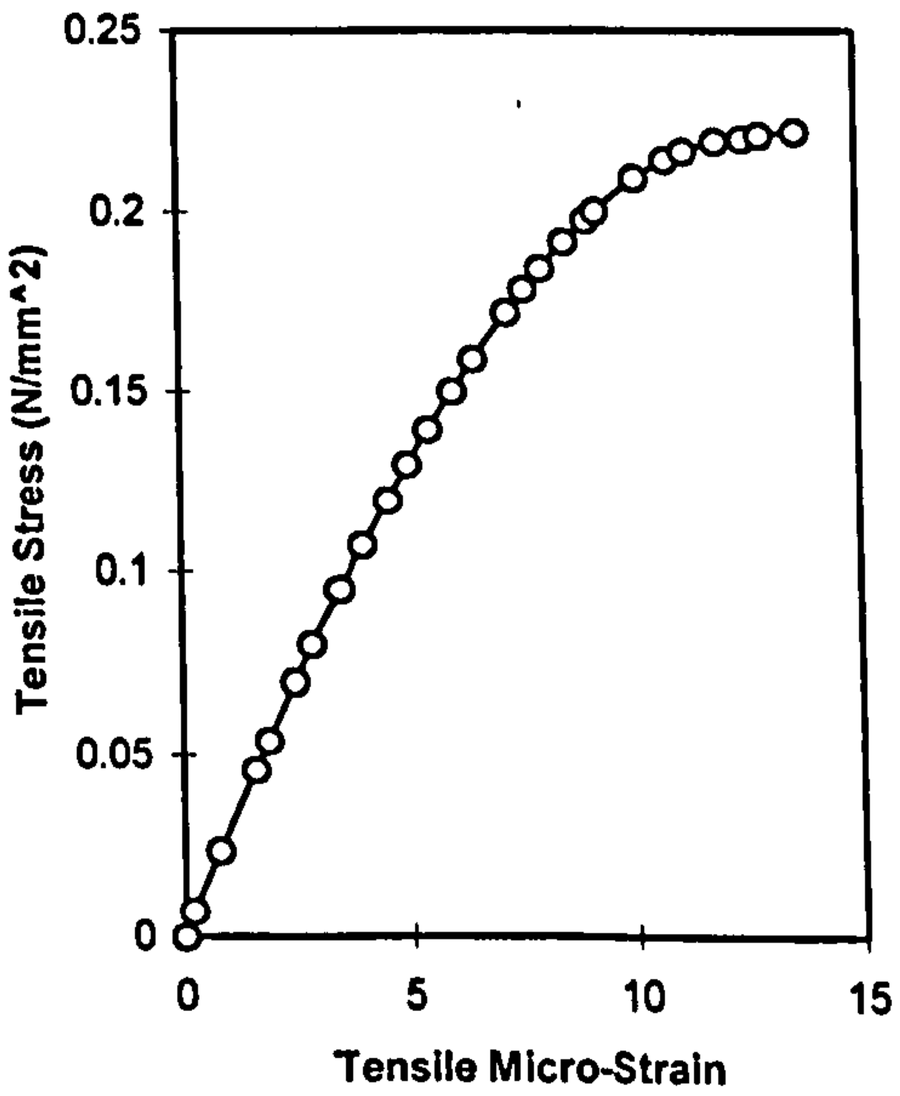

Fig. 2.10 Stress-Strain Relationship of Brickwork Masonry in Tension

It should be noted that tensile tests of brickwork masonry should be conducted slowly; otherwise a ' truly ' brittle failure modes could be dominated. Additionally, the conditions of the glue-bonds between bricks and timber plates must be ensured, and the tensile strength of the glue itself should be much higher than the strength to be tested. Therefore, the quality of glue and its spread within the connecting faces become important in the tensile test of brickwork prisms.

It was noted that the actual bond surfaces were smaller than the gross cross-sectional area of the prism specimen. It may be necessary to introduce the " effective bond area " if detailed theoretical modelling of brickwork prisms are required.

Due to the relatively low and variable tensile strength in masonry, the tensile strength may be ignored in masonry arch analysis (Crisfield, 1985, Choo, 1991) although tensile cracking has been accepted as a main cause of most masonry failures (Drysdale et al., 1994).

2.1.3.3 Shear Test

There are normally three methods for the shear tests of brickwork prisms as shown in Fig. 2.11.

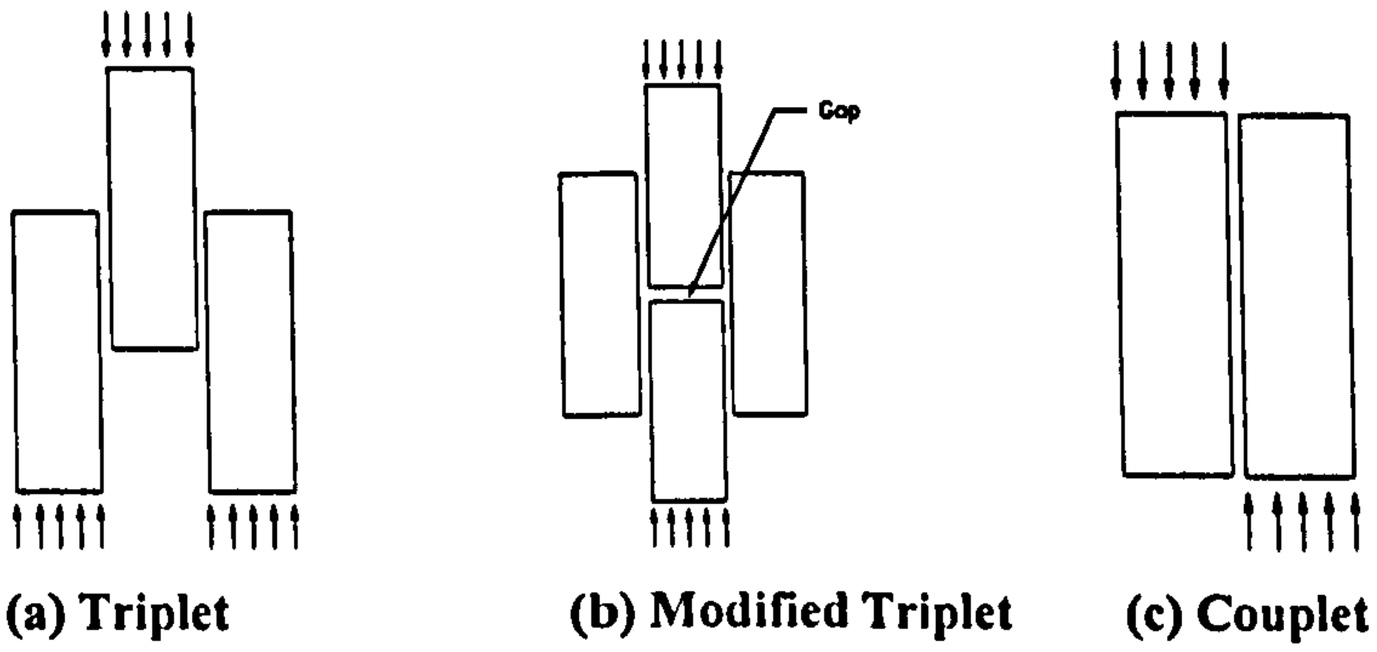

Fig. 2.11 Shear Test Methods For Brickwork Masonry

For simplicity, the Couplet test approach was employed in the present research as shown in Fig. 2.12.

One horizontal and one vertical hydraulic jacks were used to apply forces onto the top bricks through two steel plates, which were attached to the loading surfaces of brickwork prism. For pure shear test, only the jack2 was used, and the shear forces increased until the shear failure occurred. For the shear test under pre-compression, a prescribed compressive load was set by jack1, and the shear forces by jack2 increased until slip occurred.

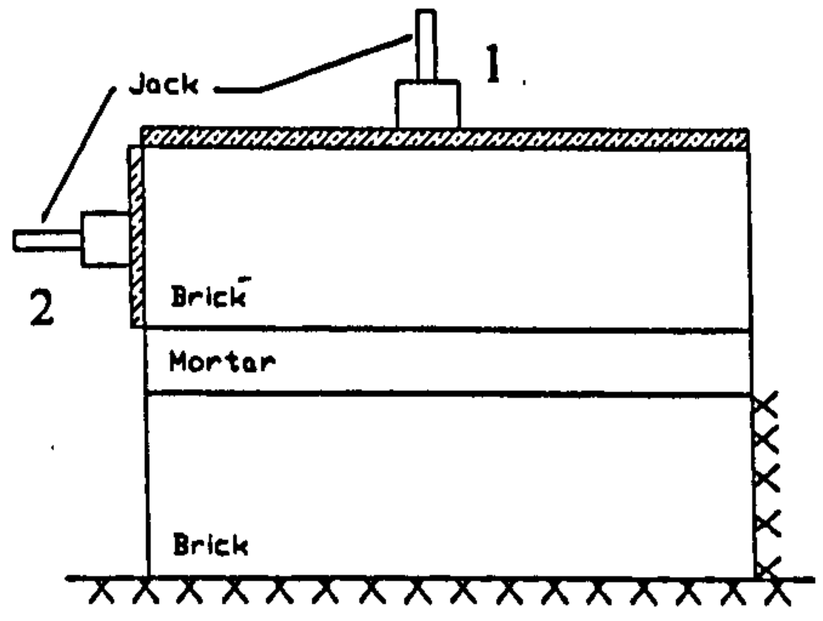

Fig. 2.12 Brickwork Prism For Shear Test

During the shear tests of brickwork prism, it was found that a steady vertical compressive load was not readily controlled since the top brick tended to move upwards as the horizontal loads increased, which could be one of causes to lead variable test results. As adopted by Hendry (1987), a " Coulomb friction" type linear-fit formula was used to model the relationship between the shear strength and the vertical pre-stress:-

$$\tau = 0.08 + 0.4\,\sigma_n \qquad \text{For Raewell Bricks;}$$

$$\tau = 0.15 + 0.8\,\sigma_n \qquad \text{For Class A Engineering Bricks.}$$

In which, the units are N/mm^2 for both τ and σ_n .

The test results are plotted in Fig. 2.13.

The initial shear bond strength (when vertical compression was zero) τ_0 was about 0.08 N/mm^2 for the Raewell brickwork prisms, and 0.15 N/mm^2 for the Engineering brickwork prisms. The friction coefficient was 0.4 for the former and 0.8 for the latter. It may be noted that the above parameters could be influenced by a number of factors, such as different shrinkage of mortar, surface roughness, quality of the mortar joints, nature of brick, and loading conditions, etc.

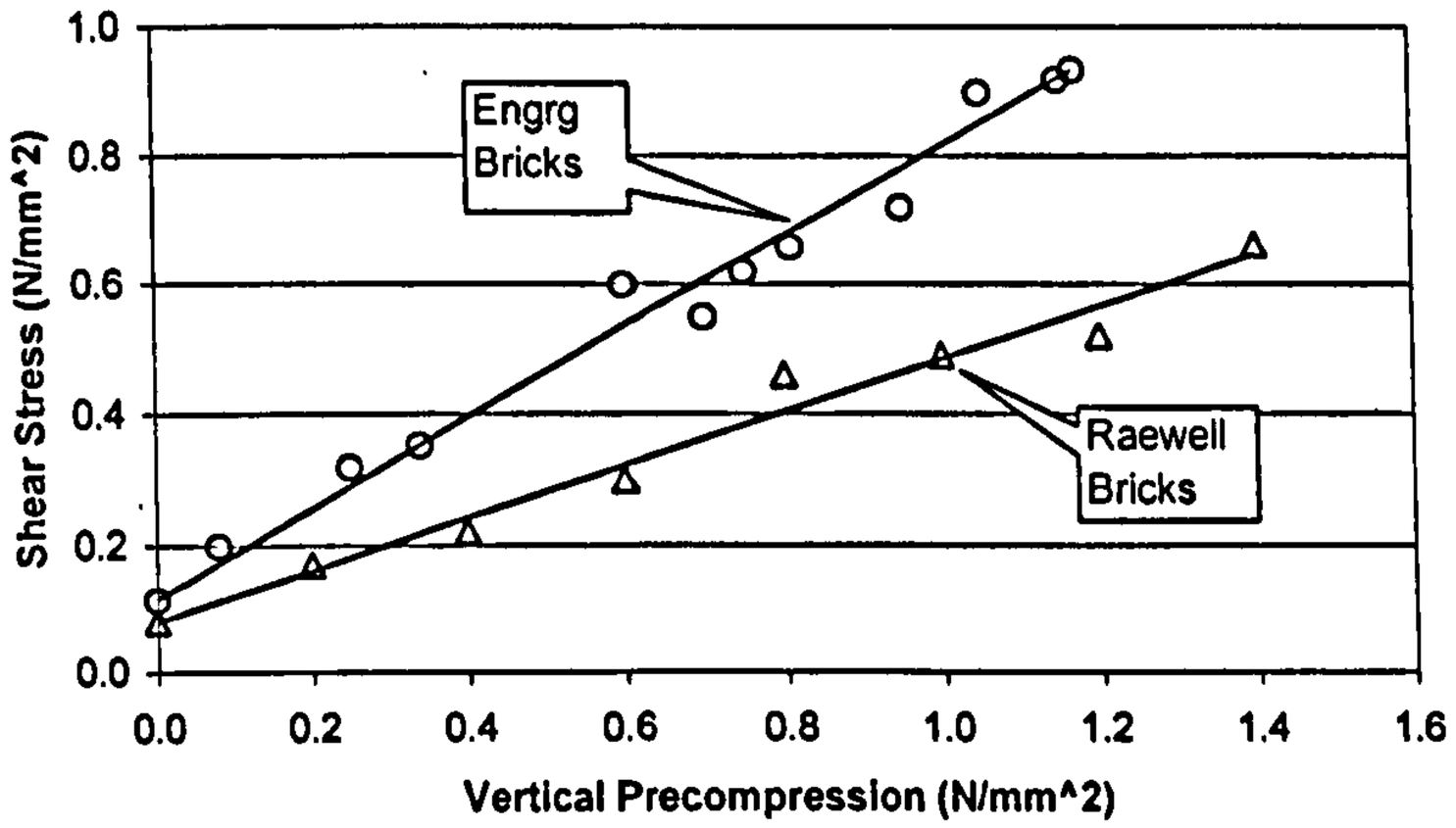

Fig. 2.13 Shear Strength – Precompression of Brickwork Masonry

Three failure modes of two-course brickwork prisms under shear force were observed in the tests, i.e., (a) uniform failure; (b) ' defect ' failure; and (c) ' cut off ' failure as shown in Fig. 2.14. It was noted that the uniform failure modes occurred only when the bond strength was small. The ' Defect ' failure modes might be caused by the effects of the quality of the mortar and of workmanship. Holes (up to ϕ40 mm) were found on the failure interfaces, which normally also resulted in low shear bond strength.

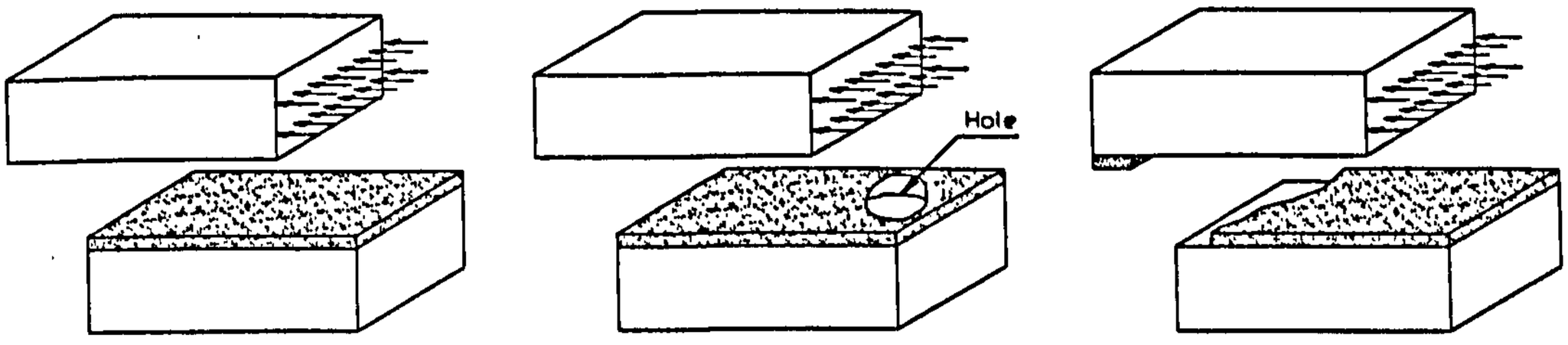

(a) Uniform failure **(b) ' Defect ' Failure** **(c) ' Cut off ' failure**

Fig. 2.14 Typical Failure Modes of Brickwork Prism Under Shearing

The ' cut off ' failure modes were also observed during the tests, where shear failures of brickwork prisms occurred because the joint mortar was cut off, or because the combination of the interface separation and mortar slipped, which normally occurred under relative high vertical compressive loads. This type of failure could be affected by the method of the test. It may be noted that a moment of $F \times t/2$ (Note: F is the load applied through the horizontal jack, and t is the thickness of brick) was introduced. The moment becomes greater as the t increases.

It should be noted that the test results indicate the validity of this concept only at low levels of compression, and the formulation does not apply to failure modes other than slip along the mortar joints, i.e., mode 1 or 2. For a higher compression (for failure mode 3), shear friction model may be used, in which the sliding force also depends on the shear strength and the influence of non-linear material behaviour of the mortar. An empirical friction law for either direct or indirect shearing was proposed, in which the ultimate shear strengths under different levels of normal stresses may be calculated (Mounajed et al., 1995).

2.2 Model Arch Tests

2.2.1 Description of Model Tests

2.2.1.1 Model Arches

A total of five model tests on brickwork masonry arches were conducted as the parts of the research programme between 1995 and 1997. The first two model arch tests were carried out at the Bolton Institute of Higher Education, and the rest were undertaken at University of Salford.

The first model (OSMA1) was of spandrel arches and piers only (Fig. 2.15a); the second (OSMA2) was of an OSBMAB with 3 metre span and three spandrel arches placed on each side of the main arch without fill (Fig. 2.15b); the third (OSMA3) was of an OSBMAB with 5 metre span and two spandrel arches placed on each side of the main arch without fill (Fig. 2.15c); the fourth (OSMA4) was of a 5 metre single-span arch only (Fig. 2.15d); and the fifth (OSMA5) was a 5 metre OSBMAB with two spandrel arches placed on each side of the main arch with mortar fill (as shown in Fig. 2.15e).

The dimensions and the configurations of the spandrel arches and piers of OSMA1 were identical to those of OSMA2. The purpose of conducting OSMA1 was to observe and study the response of spandrel arches and piers in an isolated condition under different loading locations. Its results were compared with those obtained during the model test OSMA2, from which the behaviour of the superstructures (i.e., spandrel arches and piers) and full open spandrel arch structures were studied. Both OSMA1 and OSMA2 were of 500 mm in width, and built using half-scale Raewell firebricks.

In order to further study the behaviour of open spandrel brickwork masonry arches, the model OSMA3 of 1000 mm in width was built mainly using Class A Engineering bricks (except the spandrel piers using half-scale Raewell firebricks). The main arch of OSMA3 was similar to those of OSMA4 and OSMA5; and its superstructure was identical to those of OSMA5. The model OSMA5 was created by casting mortar "fill" on the top of the tested main arch of OSMA4. With test results obtained from the models OSMA3, OSMA4 and OSMA5, the functions of spandrel structures and fill, and the effects of the interaction between the main arch and spandrel arches, piers and fill on the behaviour of the main arch were studied. Different load capacities and the modes of failure were compared among the models of main arch itself, and open spandrel arch with or without fill.

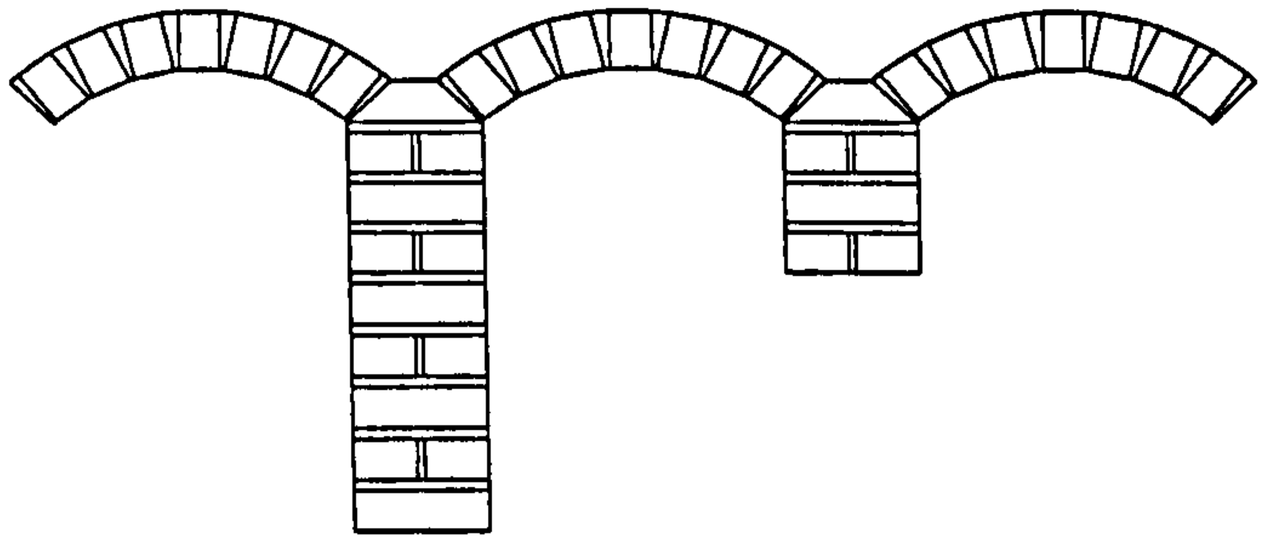

(a) The Isolated Spandrel Arches And Piers - OSMA1

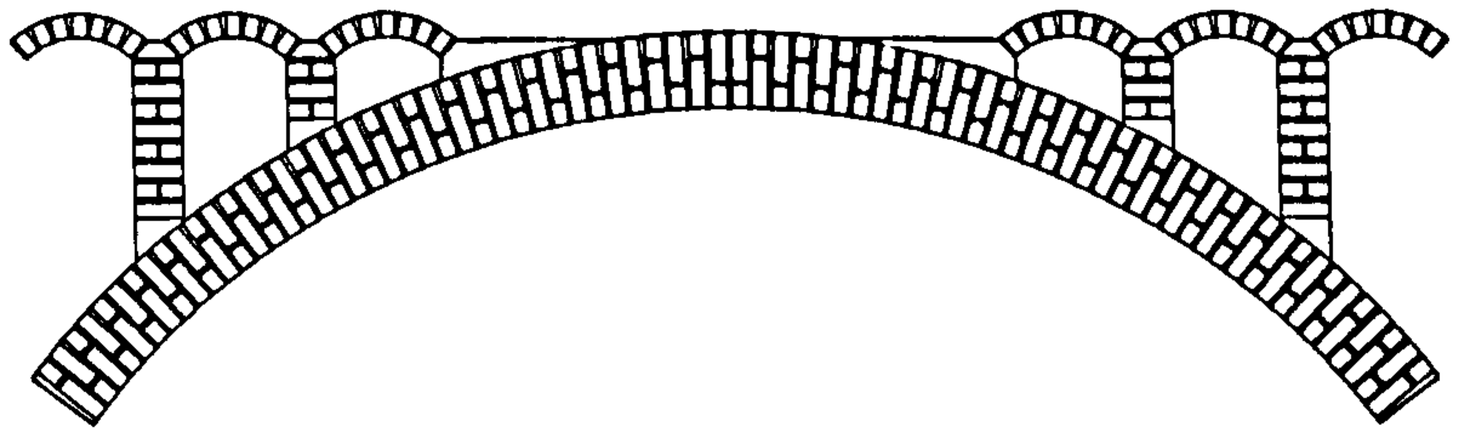

(b) Three Metre Span OSBMAB - OSMA2 *(Without Fill)*

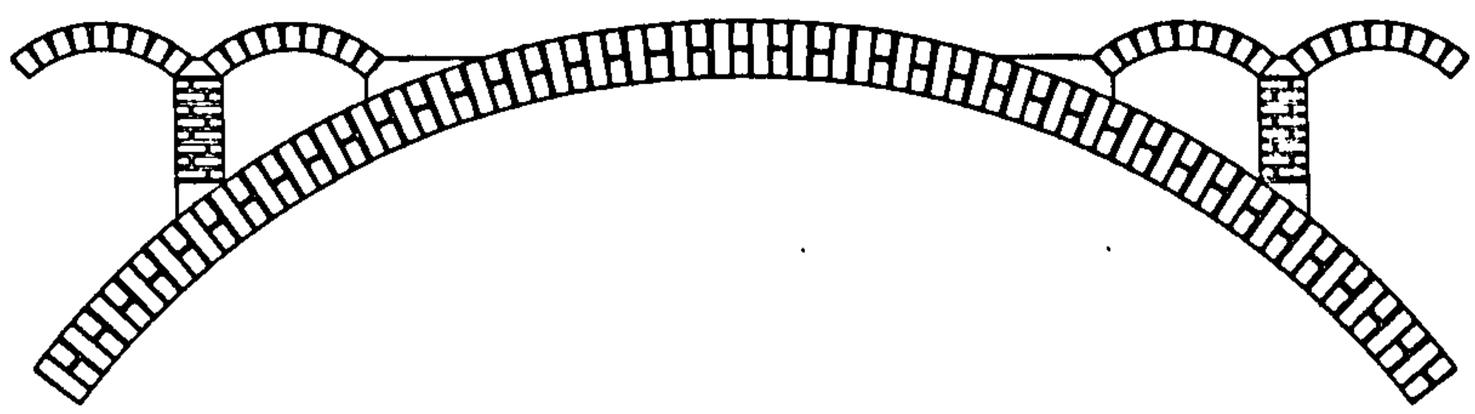

(c) Five Metre Span OSBMAB - OSMA3) *(Without Fill)*

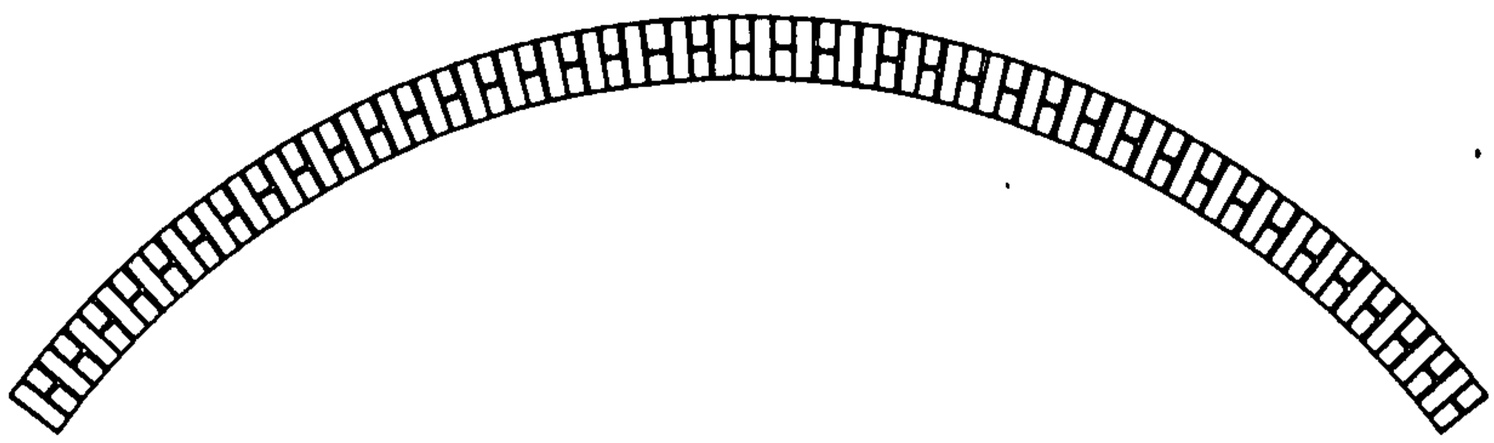

(d) The Isolated Main Arch - OSMA4

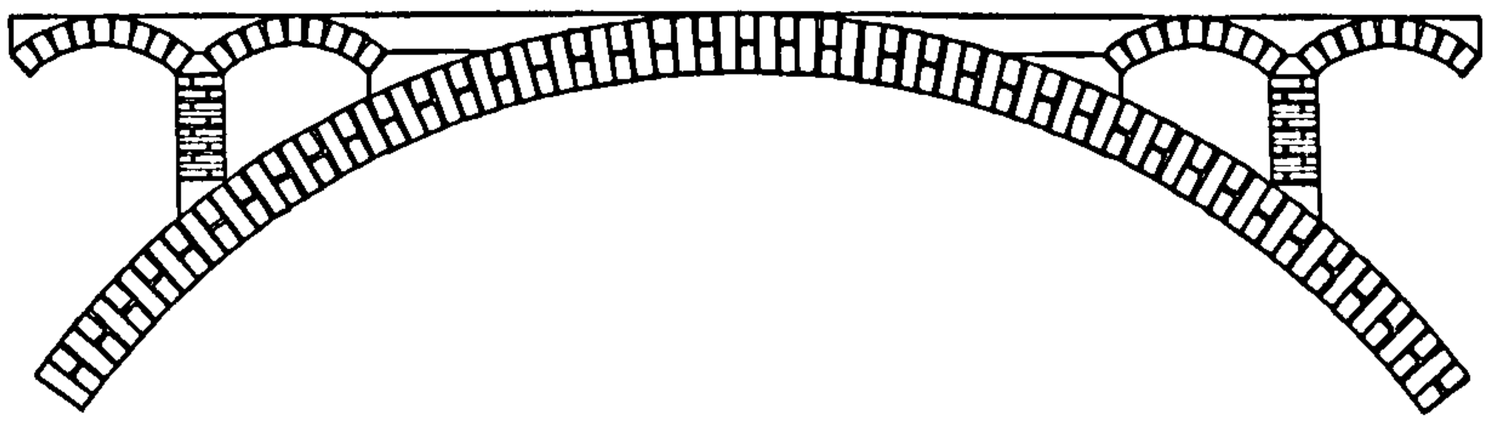

(e) Five Metre Span OSBMAB - OSMA5 *(With Fill)*

Fig. 2.15 Five Brickwork Masonry Model Arches

Fig. 2.16 illustrates the set-up of the fifth model arch (OSMA5).

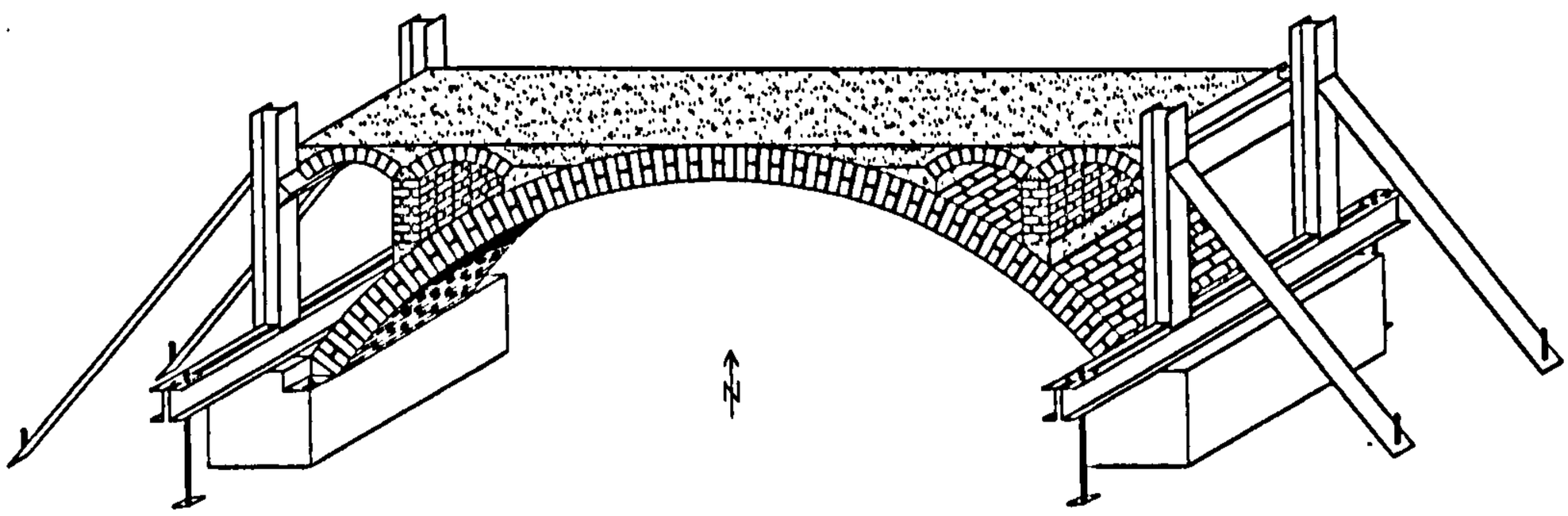

Fig. 2.16 Open Spandrel Brickwork Model Arch Bridge

For all model arches, the main arches and spandrel arches were segmental with squared cross sections of arch barrel. Header bond was used in all the tests, and the possible effects of the ring separation of the brickwork arches were therefore minimized.

It may be noted that the same bricklayer was employed for the construction of the model arches and brickwork prisms to maintain the consistent quality of the building.

The leading dimensions of the model arches and the selected test results are given in Table 2.2.

The detailed description for the five model arches was given elsewhere (Melbourne and Tao, 1995, 1996, 1997a and 1997b). The following will briefly introduce the construction procedures and the instrumentation, etc., with the emphasis on OSMA3, OSMA4 AND OSMA5.

2.2.1.2 Construction

(a) Abutments

The abutments of the main arches were designed and built as shown in Fig. 2.17 (Note that three vertical holes were incorporated to anchor the abutments to the floor while two horizontal ones were incorporated for lifting purpose). The end spandrel arches were supported upon the steel frames.

Dimensions of the model arches And Loading Capacities Table 2. 2

	OSMA1	OSMA2	OSMA3	OSMA4	OSMA5
M. A.					
Span (mm)	-	3,000	5,000	5,000	5,000
Rise (mm)	-	750	1,250	1,250	1,250
γ	-	4	4	4	4
Thickness (mm)	-	178	215	215	215
Bricks	-	H. S. R	E. C. A	E. C. A	E. C. A
S. A.					
Span (mm)	250	250	550	-	550
Rise (mm)	50	50	110	-	110
γ	5	5	5	-	5
Thickness (mm)	54	54	100	-	100
Bricks	H. S. R	H. S. R	E. C. A	-	E. C. A
S. P.					
Width (mm)	114	114	178	-	178
Height (mm)	393, 162	393, 162	550	-	550
Bricks	H. S. R	H. S. R	H. S. R	-	H. S. R
Arch Width (mm)	500	500	1,000	1,000	1,000
Fill	-	-	-	-	Mortar
Self Weight (kg)	100	700	4,500	2,950	5,300
Max. Load (kN)	13.00	13.50	23.50	12.50	32.50
Loading Position When Collapse	1/4L of End S.A. On LHS	Top of The Short Pier	Top of The Arch Seat	Quarter-Span	Top of The Arch Seat

Note:
(1) M. A. - main arch; S. A. - spandrel arch; and S. P. - spandrel pier; γ - Span/Rise
(2) E. C. A - Class A Engineering Brick; H. S. R - half scale Raewell brick;
(3) Density: - 2.30 t/m^3 for E. C. Brickwork; 1.80 t/m^3 for H. S. R. brickwork; 1.54 t/m^3 for mortar.

During the model tests, no movement of the abutments of the main arches was recorded while both the displacements and rotations of the steel frames were monitored using instruments (LVDTs).

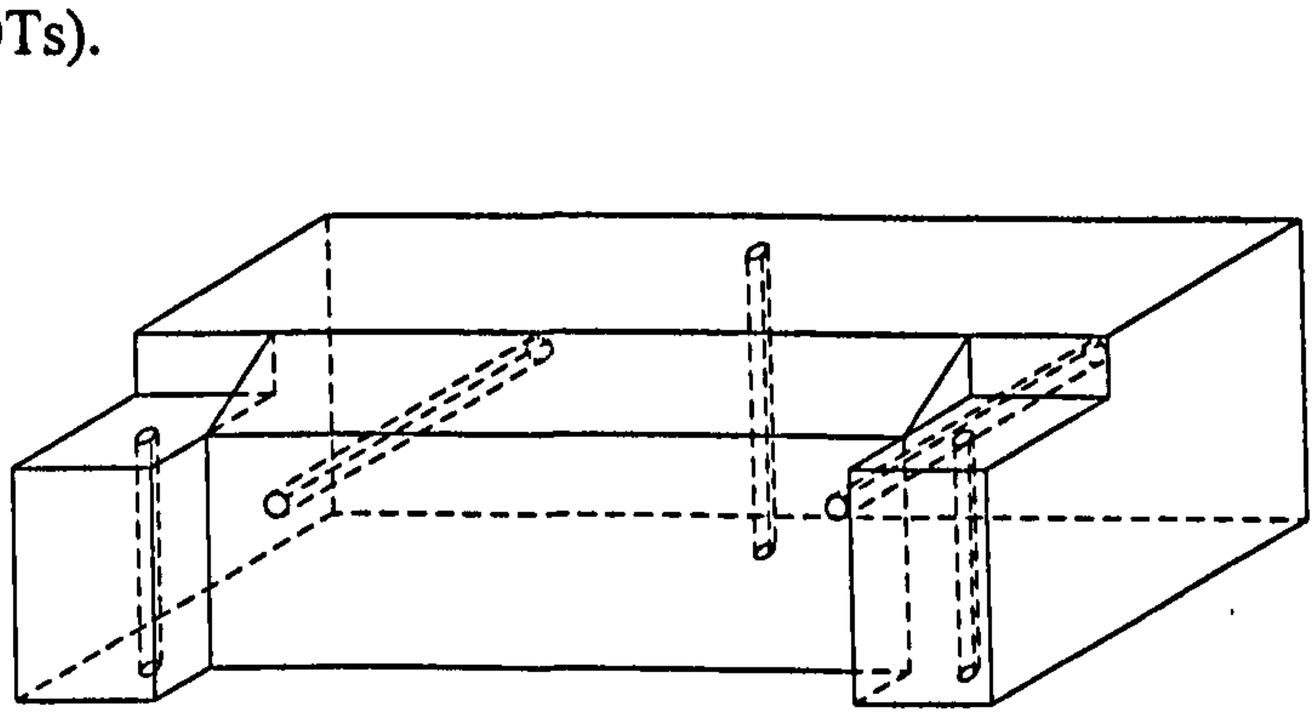

Fig. 2.17 Reinforced Concrete Abutment

(b) Centering

The sections of the main arches were assembled mainly using segmental steel sections. Three sections were linked together using five transverse steel scaffold tubes equally spaced along the circumferences of the sections. To form a uniform circular shape of construction base, two pieces of plywood board were nailed to the timber transverse joists which were secured to the curved steelwork using screw rods. Bricks were placed at the bottoms of both ends of the sections to achieve the designed rise of the main arches. Steel packs and timber wedges were also used to level and facilitate the removal of the sections. The general arrangement of the centering is as shown in Fig. 2.18. For the spandrel arches, timber frames were used and plywood boards were nailed on the top of the frames to form the designed profile.

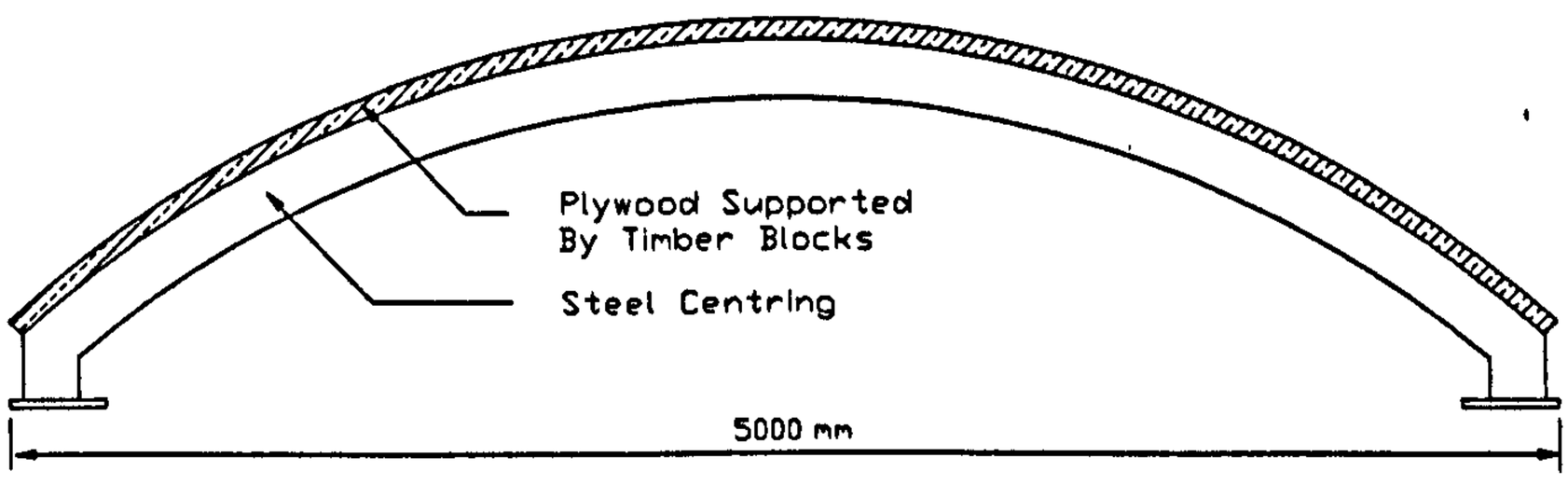

Fig. 2.18 Centering For The Main Arch Construction of The OSBMAB

A release agent was applied on the top of the plywood boards prior to laying bricks to avoid bonding of the bricks to the centering.

(c) Arches

The model arches were constructed symmetrically and segmentally, in the cases of the models OSMA2, OSMA3, OSMA4 and OSMA5.

Typical sequences of constructing an open spandrel masonry model arch during the tests are as shown in Fig. 2.19.

The main arch was constructed starting from the springings towards its crown using Class A Engineering bricks, followed by the spandrel piers. Finally the spandrel arches were built.

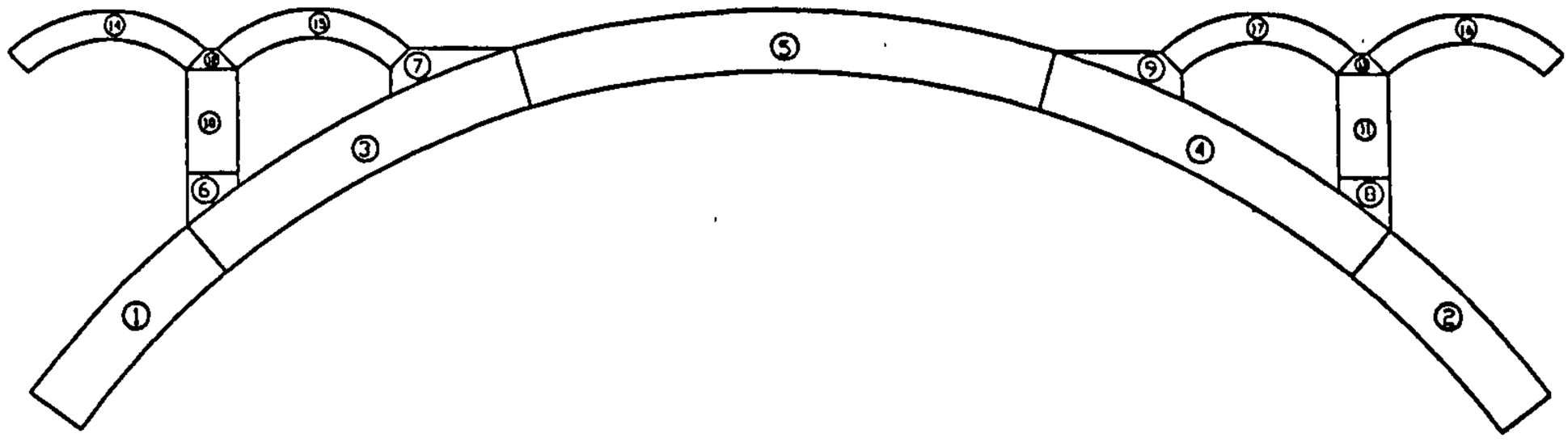

Fig. 2.19 Construction Procedures of The OSBMAB

The pre-cast reinforced concrete blocks were used for the top of the piers, and the cast in-situ concrete blocks were used to form the seatings for the spandrel piers and the spandrel arches adjacent to the crown of the main arch. Two different timber frameworks were made and clamped onto the main arch to form the moulds for casting concrete elements 6 & 7 and 8 &9 (Figs. 2.19). For the bottom parts of the spandrel piers, concrete pier base that was 10 mm wider than the width of the pier was cast to allow the construction tolerance; and for the arch seats, the bearing faces were built slightly larger than the depth of the springing of the internal spandrel arches. Fig. 2.20 shows the completed model arch and the materials used.

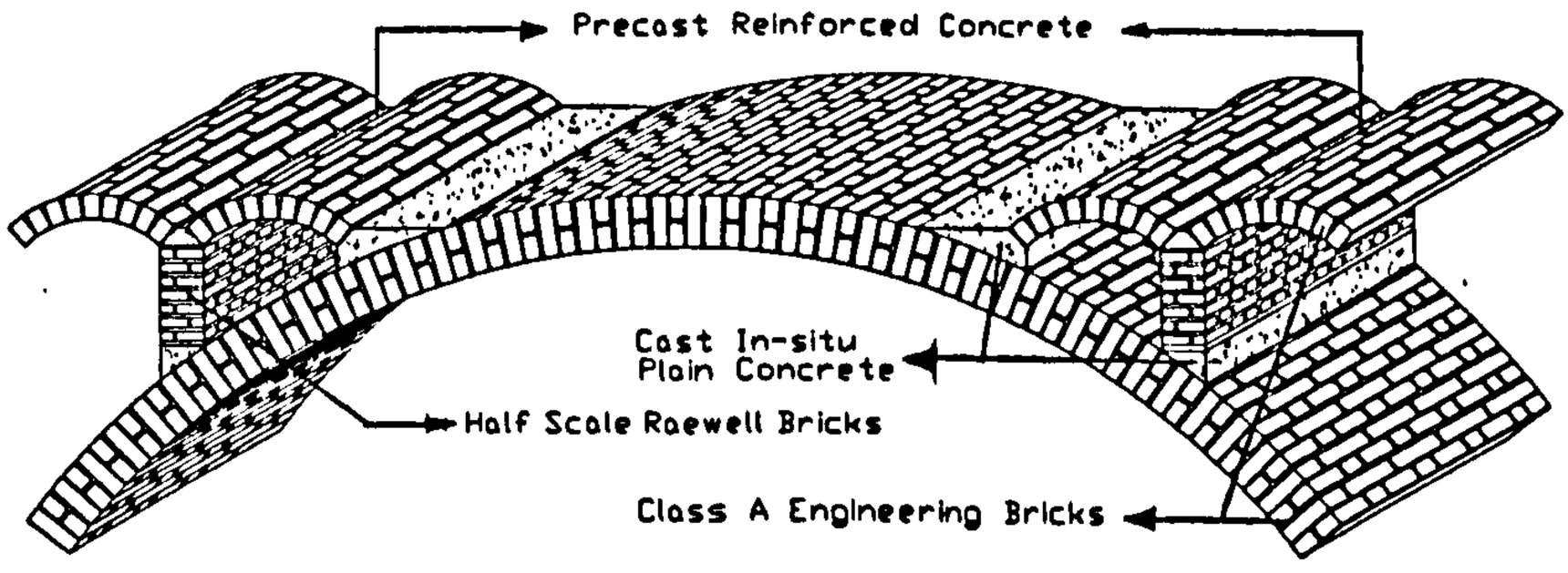

Fig. 2.20 Isometric View of The Open Spandrel Model Arch

It should be noted that the pier seatings were directly cast onto the extrados of the main arch in the cases of the OSMA2 and OSMA3 as shown in Fig. 2.21a. For the OSMA5, rebates were created within the extrados of the main arch, and the pier seatings were then cast as shown in Fig. 2.21b. This was mainly for the study of the load transferring mechanisms from the superstructure and to the main arch.

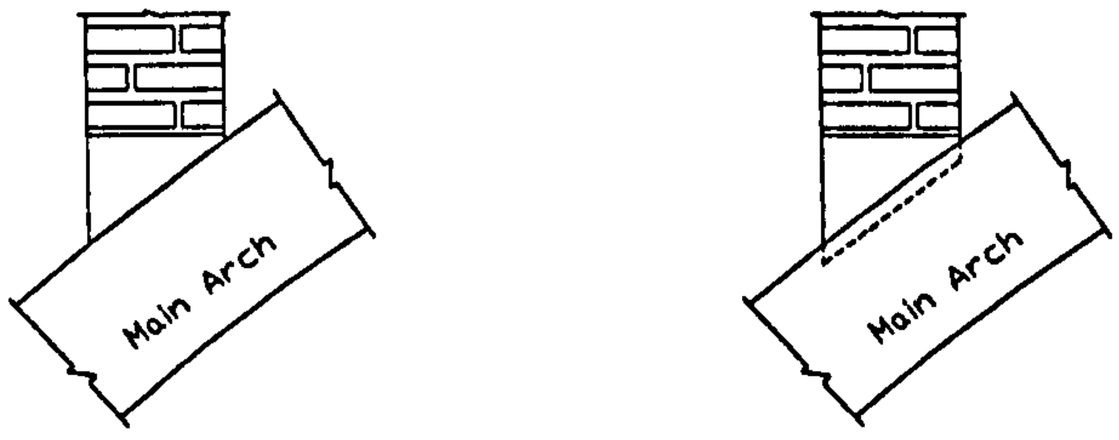

(a) OSMA2 and OSMA3 (b) OSMA5

Fig. 2.21 Cast Blocks For Spandrel Pier Seatings

The centering of the main arch was removed about two weeks after the removal of the centering of the spandrel arches.

2.2.1.3 Instrumentation

(a) Deflection Gauges

Deflection gauges (LVDTs) were used to measure the movements of the model arches at various locations (Figs. 2.22): -

i) The radial displacements of the intrados of both the main arch and the spandrel arches;

ii) The horizontal displacements of the spandrel piers;

iii) The vertical displacements at a series of loading positions; and

iv) The horizontal displacements of the steel frames at the levels of the springings of the end spandrel arches.

Deflection gauges were also attached to both far and near sides of the main arch and spandrel piers to measure the symmetrical behaviour of the model arches.

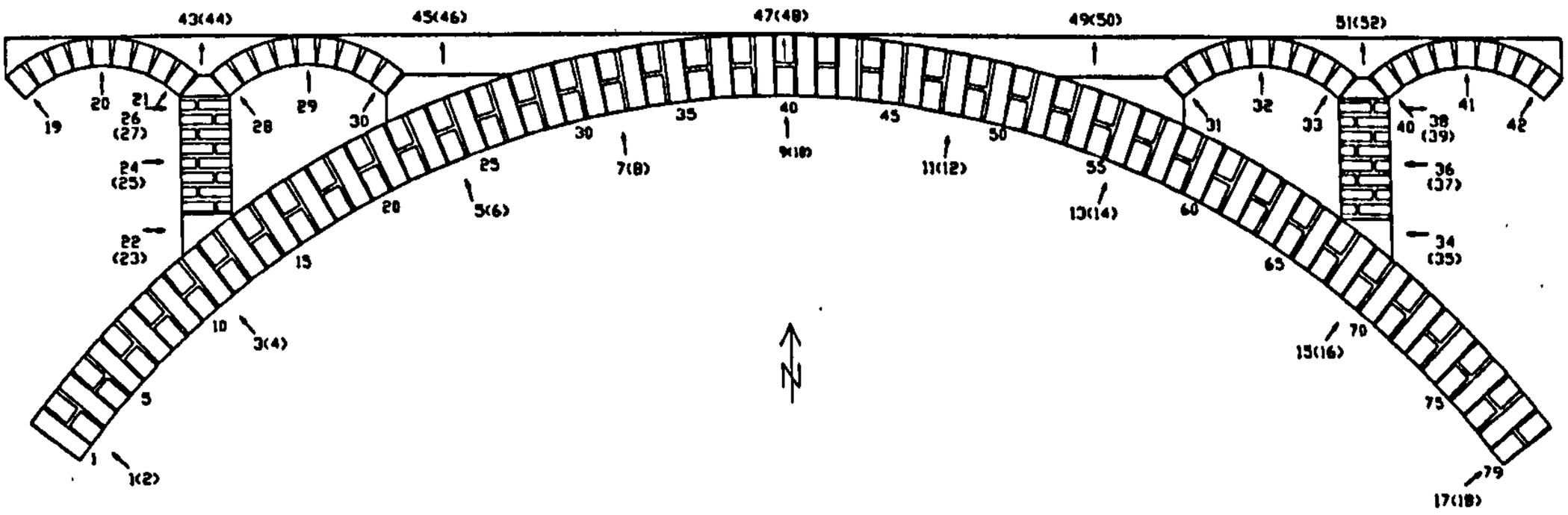

Fig. 2.22 Arrangement of Defection Gauges

(b) Strain Gauges

The vibrating wire surface strain gauges were used to monitor the surface strains of the model arches. The gauges were attached to the faces of the main arches and the spandrel arches/piers symmetrically as shown in Figs. 2.23. For the main arches, additional gauges were placed on the intrados and extrados around the springings and the crowns. The locations of placing the strain gauges were determined largely based on the results of the previous model tests and the theoretical predictions where cracks/hinges would likely occur.

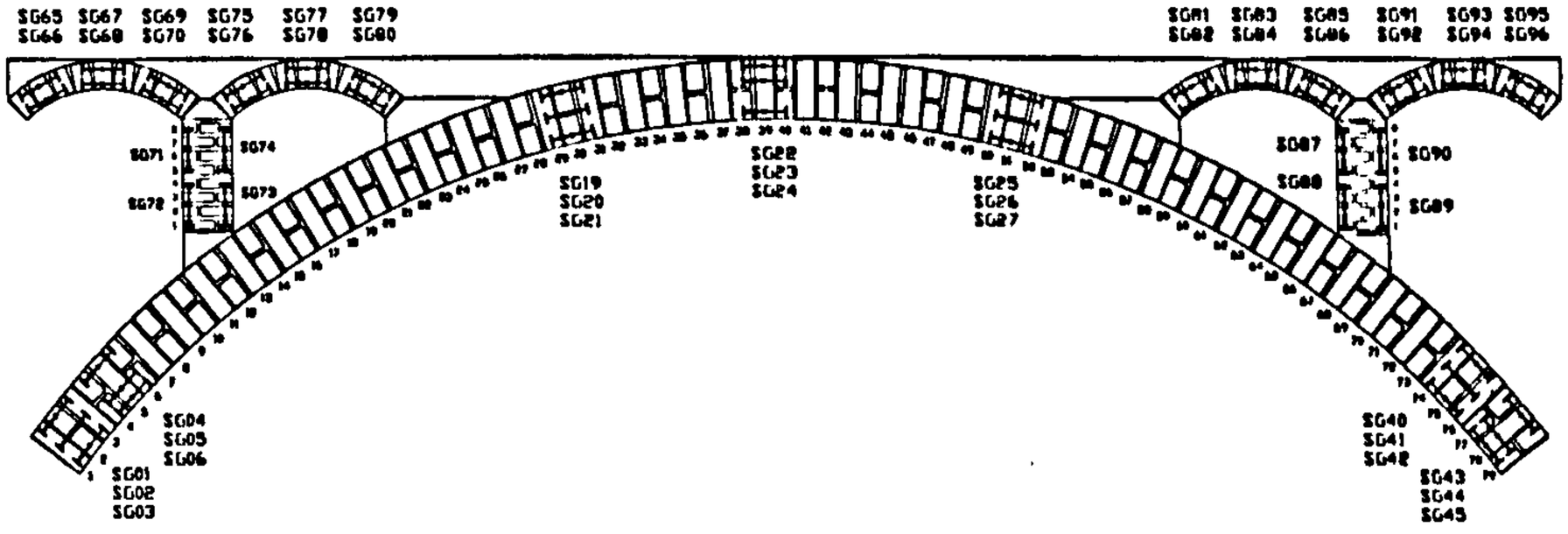

Fig. 2.23 Surface Strain Gauges Attached to Southern Elevation

The ambient temperatures were recorded using thermometers. In the cases of OSMA3 and OSMA5, angle meters were used to monitor the rotations of the steel frames that supported the end spandrel arches.

(c) Data Loggers

Two data loggers were used to acquire the test data during the tests. A Strain Manager data logger was used to acquire the surface strains, and a Solartron 'Orion' data logger was used to record the applied loads and the displacements.

Apart from the instruments used, the models were visually inspected prior to each increment of the load, and any cracks were recorded. During the destructive tests, especially during the second phase of the collapse tests, a high resolution video camera was set up in front of the models at a safe distance, and constantly recorded the movements of the model. The video images were then transferred into AVI formats, and the detailed behaviour of the model during the tests could be analyzed, and a full history of the failure modes could be retrieved.

2.2.1.4 Application of Loads

For the five model arch tests, the Knife Edge Load (KEL) was applied. The loads were applied by hydraulic jacks through a 20 kN load cell to a spreader beam across the full width of the model arches. Sand was placed on the top of the spandrel piers when fill was not applied to enhance uniform loading when loads were applied at those locations. Plywood boards were attached to the bottom of the spreader beam to take up any irregularities of the model arch surfaces at loaded areas, which effectively resulted in the changes of the KEL into patch loads as shown in Fig. 2.24.

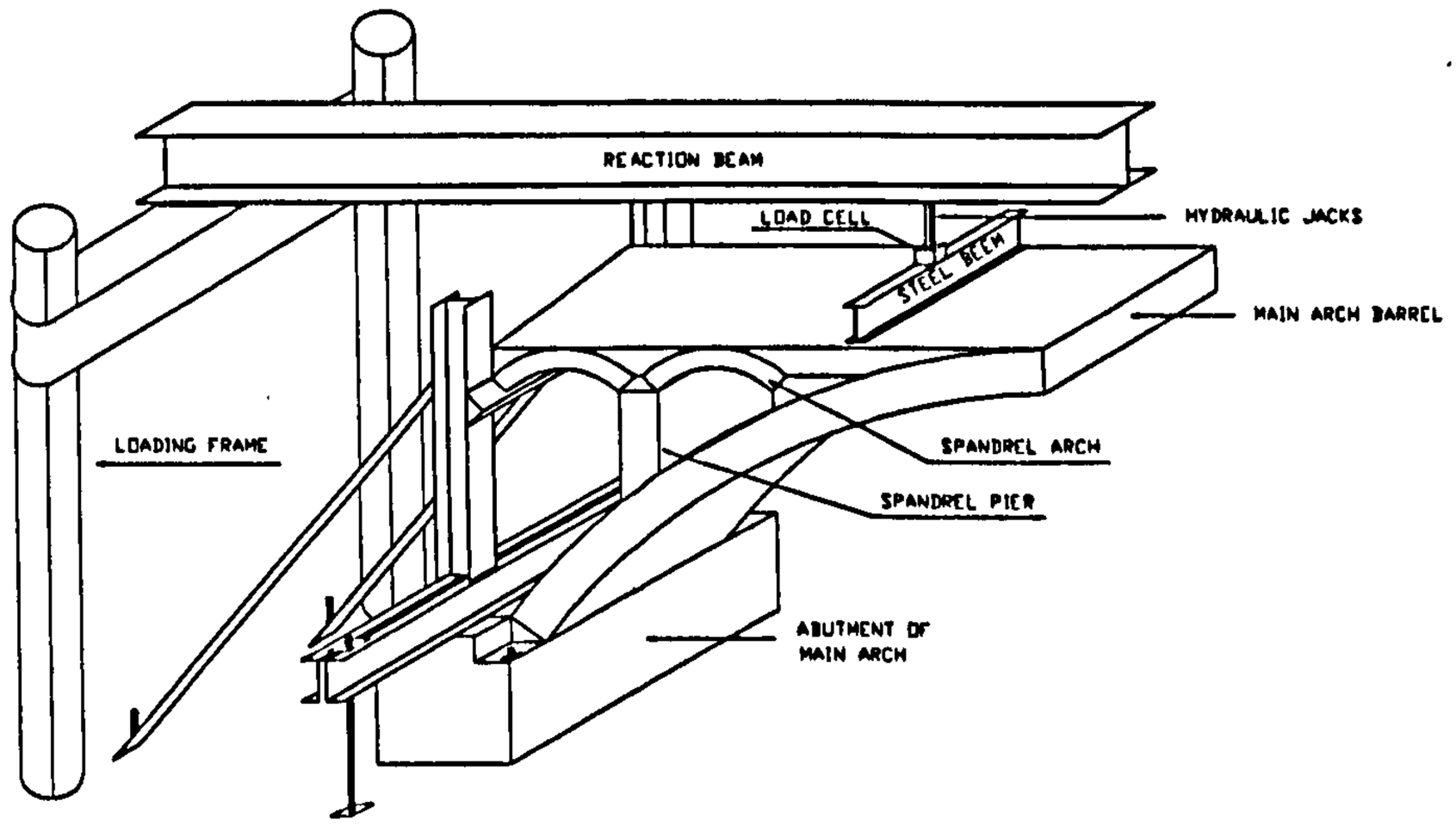

Fig. 2.24 Application of Loads

2.2.1.5 Test Procedures

The model arch tests were generally carried out in two stages, i.e., elastic stage and destructive stage. During the elastic stage, loads were successively applied at a series of locations. At each location, the test was stopped when the prescribed criteria were met. The destructive stage tests were further divided into failure tests and collapse tests. The failure tests were stopped when the maximum load was reached. Upon the removal of most instruments, the collapse tests were carried out until the model arches collapsed.

During each test, loads were gradually increased. The measurements of the displacements and strains, etc., were recorded after each increment of the load. Visual checks were carried out to record any cracks being developed. Small increments of loading were applied (about 0.2 – 1.0 kN) at the initial stages and the final stage when

the applied loads were close to the load capacity of the model arch predicted. Relatively large increments of loading were applied (about 1.0 - 2.0 kN) at other stages.

2.2.1.6 Control of Test Progress

Since a series of elastic tests were planned before the final destructive tests were undertaken for each model tests, it was important to control the progress of the elastic tests to avoid unexpected collapse of the model arches as it happened during the first test, where an increment of the applied load was too large.

The test progress was mainly controlled by three factors: occurrence of cracks; prescribed limits of displacements and surface strains. It was found that some fine cracks within the superstructures, especially around the end spandrel arches, which occurred prior to the application of test loads (due to the effects of self-weight and shrinkage of mortar, etc., to be discussed in Section 2.5) might be further opened or closed as the applied loads increased, therefore, visual inspection on cracks was mainly focused on the main arches unless significant cracks were found around the superstructures.

In addition, whether or not a elastic test was stopped was also determined by the results from the previous tests. In particular, since the loads were applied symmetrically about the middle of the span of the model arch, the progress of the later test largely depended on the results from the corresponding test conducted on the other side of the model arch.

In general, elastic tests would be stopped when the following prescribed conditions were met:-

- ◊ Cracking occurs within the main arch;
- ◊ Deflection was up to 0.1-0.5 mm;
- ◊ Micro-strain was up to 50-100.

2.3 Load Tests

2.3.1 Spandrel Piers & Arch (OSMA1)

The model of OSMA1 was partly served as a trial of the series of model tests planned. During the test, load was first applied at the quarter span of the arch adjacent to the higher piers in an increment of 1 kN from 0 to 5 kN. Since no visual damage of the model was observed and the deflection gauges did not show any measurements either, an increment of loading was then changed to 5 kN. The model suddenly failed without any warning at the load of 13 kN.

Though the model was monitored using a total of 18 deflection gauges placed along the intrados of the model, and 24 strain gauges attached to the surfaces of the spandrel arches and piers, all the measurements recorded were small (less than 10 micro strains) when the load was at 10 kN.

The failure mode of the model is as shown in Fig. 2.25.

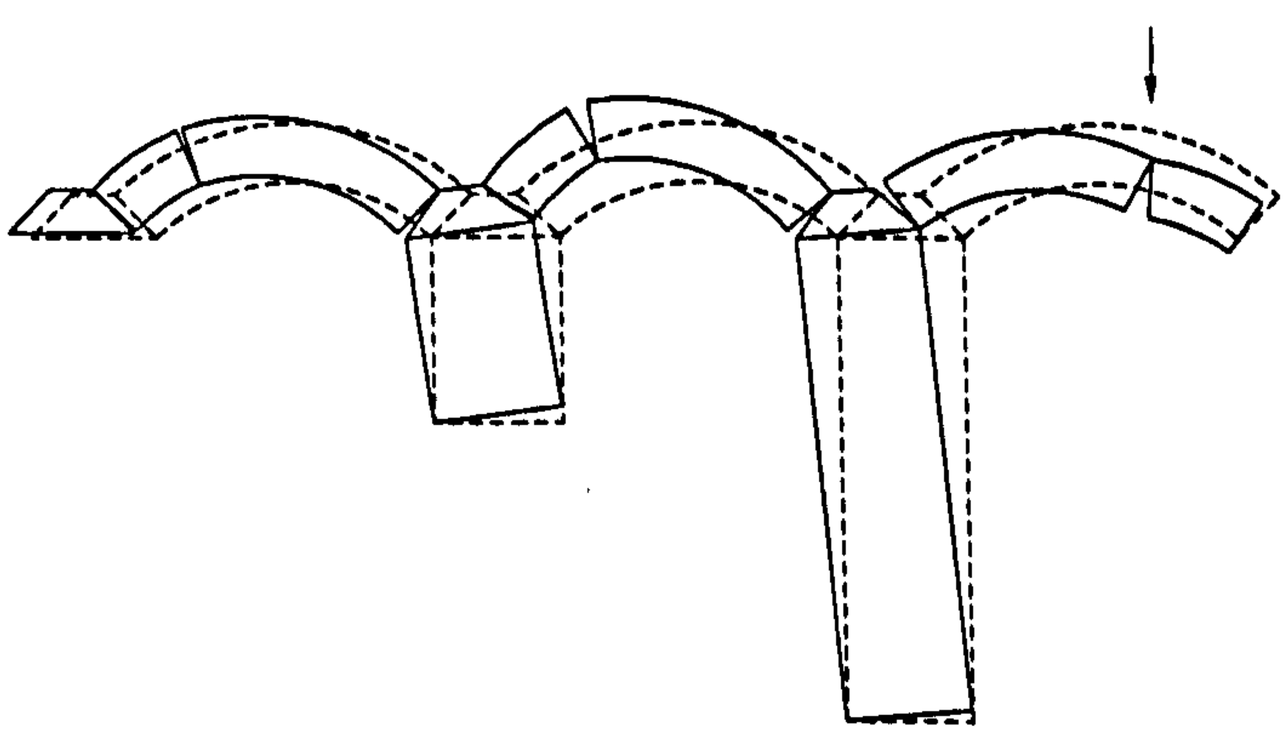

Fig. 2.25 Global and Local Failure Modes of OSMA1

This " brittle " type of failure was believed to be caused mainly by the movement of the support at the unloaded side of the arch (brickwork wall backed by concrete blocks was used as the supports on the left hand side of the model while the arch on the right hand side was built directly on a large solid reinforced concrete foundation). The movement of the support was caused by the forces at the springing of the left most spandrel arch, which was transferred through the middle arch and the spandrel piers.

As far as the spandrel arches are concerned, each might fail only by either crushing of the materials or sliding between individual bricks or between the bricks and their supports due to the geometrical constraints, i.e., a hinge cannot be formed if the supports were fixed (Melbourne and Tao, 1995).

2.3.2 Three Metre Span OSBMAB Without Fill (OSMA2)

Prior to the model test of OSMA2, fine cracks were found at the extrados along the interfaces between the supports and the end spandrel arches. It was considered that the fine cracks might have been caused by the shrinkage of the mortar. The average thickness of the mortar joints was 10 mm, and thickness of the half scale Raewell bricks was 38 mm, i.e., the mortar took up about 20 percent in the barrel of the main arch. If the shrinkage of the mortar was assumed to be 500 micro strains, the effect of the mortar shrinkage was equivalent to 9 °C drop in temperature (note: the thermal expansion coefficient of mortar was assumed as 11.5×10^{-6} per °C). In addition, the downwards displacements of the main arch under self weight (0.5 ton) upon the removal of the centering of the main arch resulted in the tensile stresses at the extrados of the end spandrel arches, which also could lead to the occurrence of the above cracks.

A total of eleven 'elastic' tests (ET) were carried out on the model. The loading locations and the loads applied are shown as in Fig. 2.26 and Table 2.3. Considering the unexpected failure of the first model OSMA1, only 0.5 kN increments in load up to 5 kN was applied when the loading was on the spandrel arches.

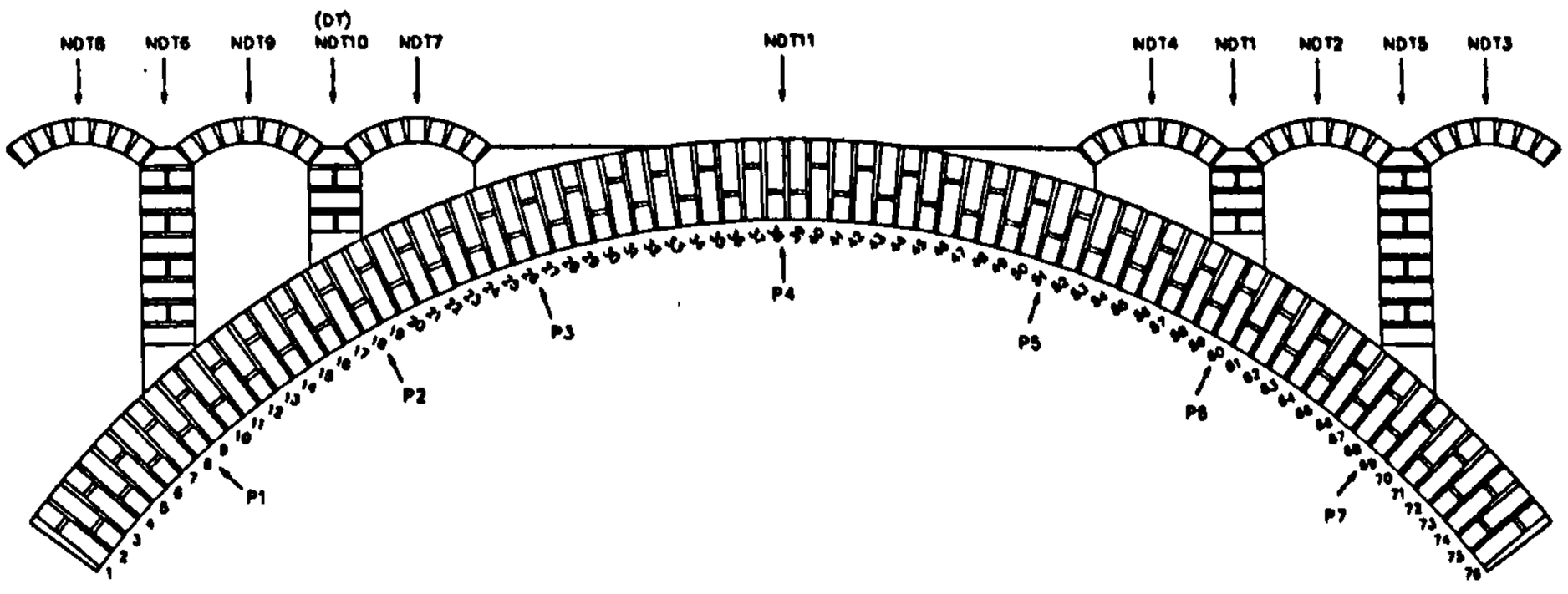

Fig. 2.26 Model Tests of OSMA2

Summary of ET and DT Tests of OSMA2 **Table 2. 3**

ET	1	2	3	4	5	6	7	8	9	10	11	DT
Max Load (kN)	9.0	3.5	4.5	5.0	10.0	10.0	5.0	3.5	3.5	10.0	12.0	13.5

When about 4 kN of loading was applied at the crowns of SA1 and SA6, fine cracks were found at the loaded side along the interfaces with the supports (either previously existed or newly developed), and between the spandrel arches and the top of the higher

spandrel piers. The fine cracks were observed between the spandrel arches and the top of the higher spandrel piers at the loaded sides when 3.5 kN of loading was applied at the crowns of either SA2 or SA4. When loads were applied at other locations during the initial stage of the tests, no cracks were noticed, and a maximum deflection of 0.5 mm was recorded at the intrados of the middle of the main arch with loading at the crown.

The fine cracks that occurred between the spandrel arches and the piers at the loaded sides when the loads were applied at SA1, SA2, SA5 or SA6 were believed to be caused by the displacements/rotations of the taller spandrel.

At the end of the eleven ET tests, a total of 7 fine cracks remained within the spandrel arches, i.e., 3 at the crowns of SA1, SA2 and SA5; 2 at the interfaces with the supports of SA1 and SA6; and 2 at the interfaces between SA5 & SA6 and with the top of the taller spandrel piers.

The model failed when up to 13.5 kN of loading was applied at the top of the taller spandrel pier on the left hand side. All the cracks/hinges occurred almost simultaneously, and it was unlikely to determine the progress of failure. Figs. 2.27 and 2.28 show the typical relationships between the radial deflections along the intrados of the main arch and the applied loads with loading at the crown of the main arch (ET) and the top of the higher spandrel pier (DT).

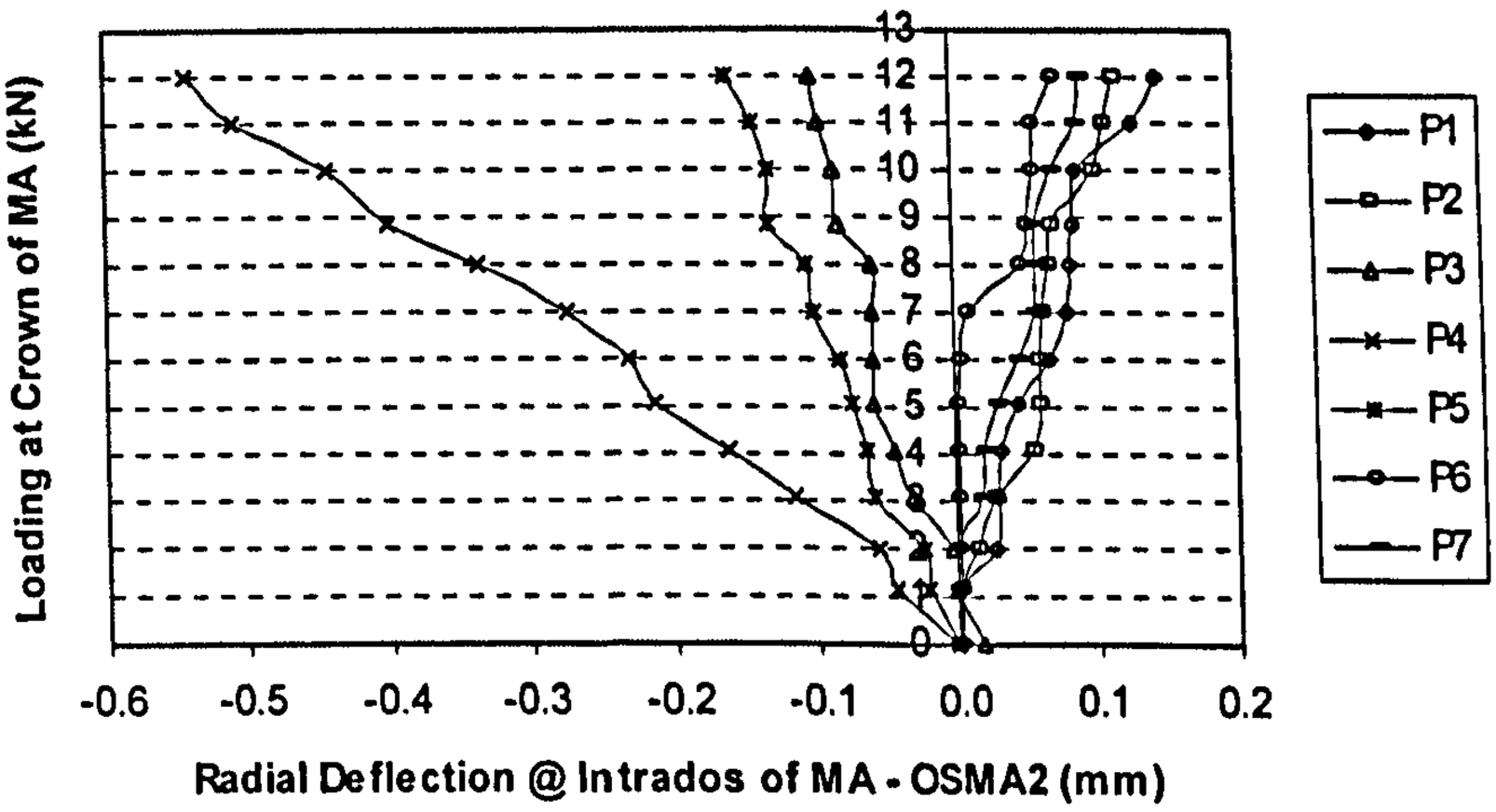

Fig. 2.27 Load-Deflection Curves of OSMA2 With Loading at Crown of MA

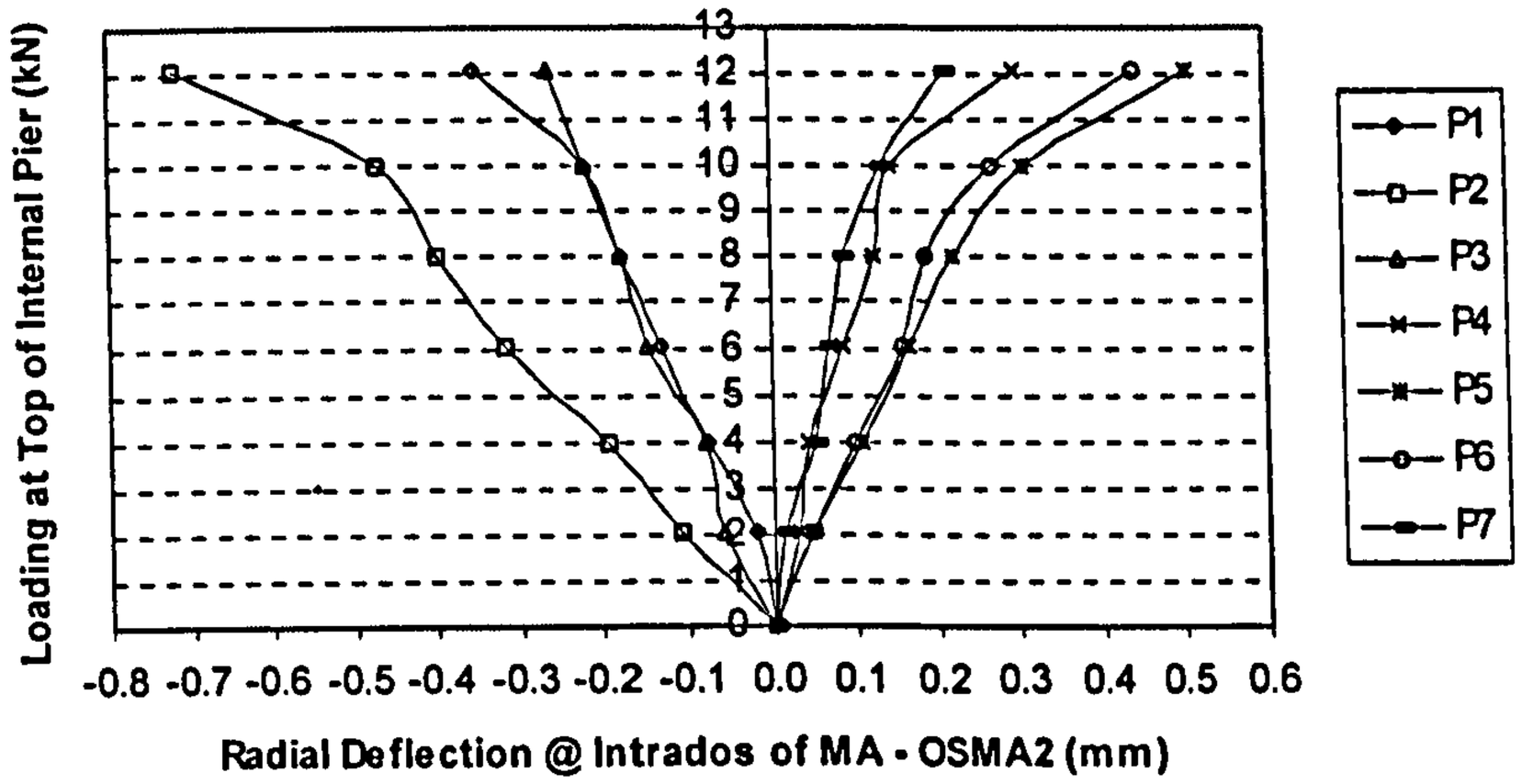

Fig. 2.28 Load-Deflection Curves of OSMA2 With Loading at Top of Pier 2

The failure mode of the model is as shown in Fig. 2.29.

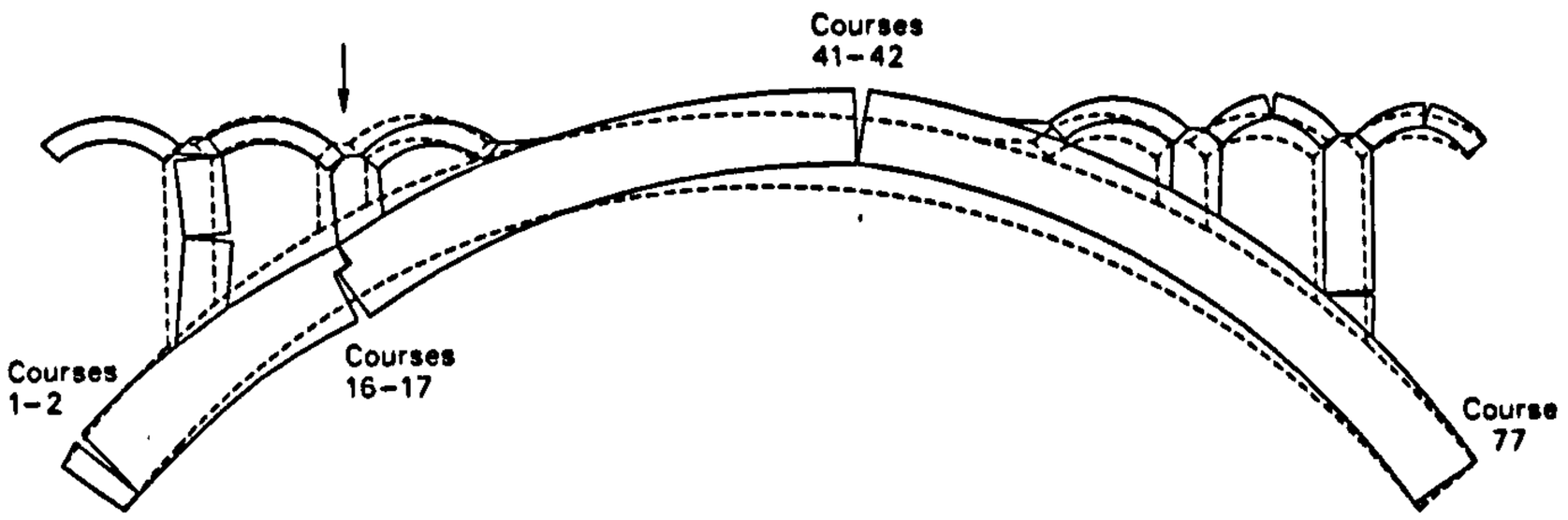

Fig. 2.29 Global and Local Failure Modes of OSMA2

Both global and local mechanisms appeared when the model failed.

For the main arch, it failed by forming four hinges located at both the springings, the extrados under the loaded pier, and the intrados near the crown at the unloaded side. The fourth hinge that appeared near the crown would indicate that the spandrel structures might provide horizontal stiffness towards the main arch. Depending on the value of the stiffness provided, the location of the fourth hinge could vary at the unloaded side of the model.

As discussed in Section 2.3.1, the spandrel arches were only likely to fail due to either abutment/pier movements or sliding. As shown in Fig.2.29, SA1 failed due to the sliding between the end and the top of the pier, and/or the movement of the pier. SA2

and SA5 failed due to the movements and the rotations of the corresponding two supporting piers; SA6 failed due to the movement of the supporting pier.

For the higher spandrel pier, one hinge was formed at the weakest location within its length when the model failed as shown in Figure 2.29.

2.3.3 Five Metre Span OSBMAB Without Fill (OSMA3)

As with the model OSMA2, fine cracks were found at the extrados along the interfaces between the end spandrel arches and the supports of the steel frame prior to the model test of OSMA3. The reasons were as described in Section 2.3.2 except that the self-weight of the model was about 4.5 t and the effect of the mortar shrinkage was equivalent to 7 °C drop in temperature due to the 65 mm thick bricks used if other parameters were assumed same.

A total of seven ET tests were carried out for the model. The loading locations and the loads applied are shown as in Fig. 2.30 and Table 2.4. Fine cracks were developed within the end spandrel arches in the vicinity of the loads when they were applied at the crowns of SA1 and SA4.

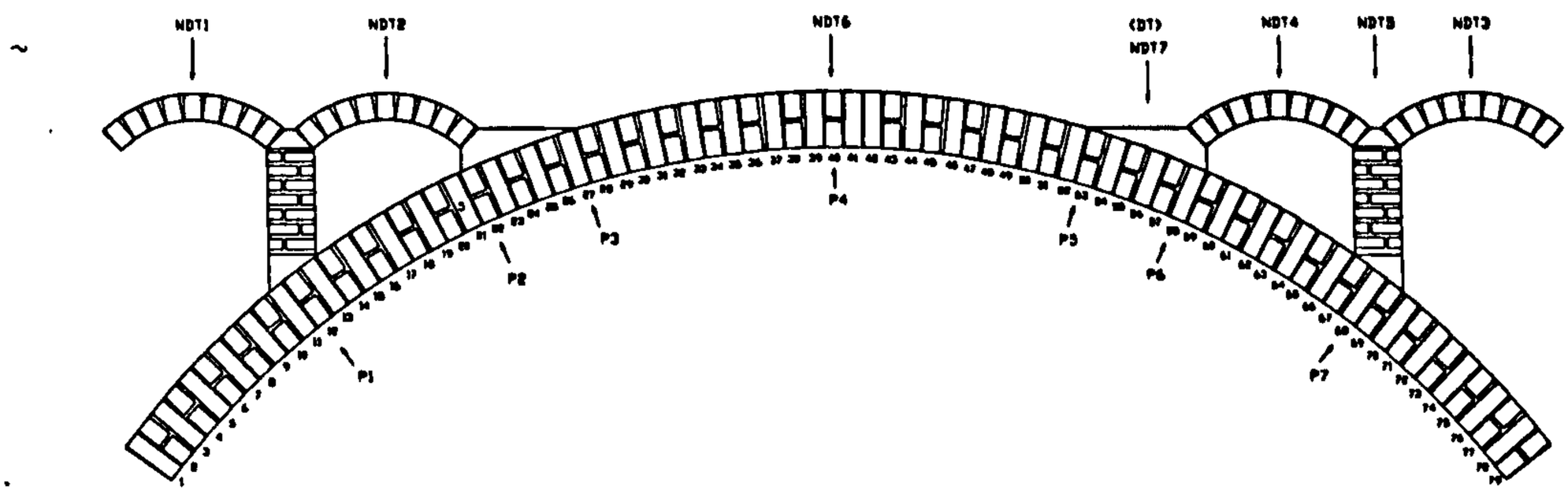

Fig. 2.30 Model Tests of OSMA3

Summary of ET and DT Tests of OSMA3 **Table 2. 4**

ET	1	2	3	4	5	6	7	DT
Max Load (kN)	5.0	18.0	5.0	9.0	10.0	20.0	18.0	23.5

A local failure suddenly occurred unexpectedly during the second elastic test with a load of 18 kN applied at the crown of the internal spandrel arch (SA2) as shown in Fig 2.31.

It was believed that the failure was partly initiated by the sliding of the arch seat, where the internal forces generated by the applied load were greater than the combination of the cohesion and the friction between the arch seat and the main arch. Though the sliding was involved, the local failure mode was a seven-hinge mechanism. Prior to the occurrence of the local failure, the load increment was 1 kN.

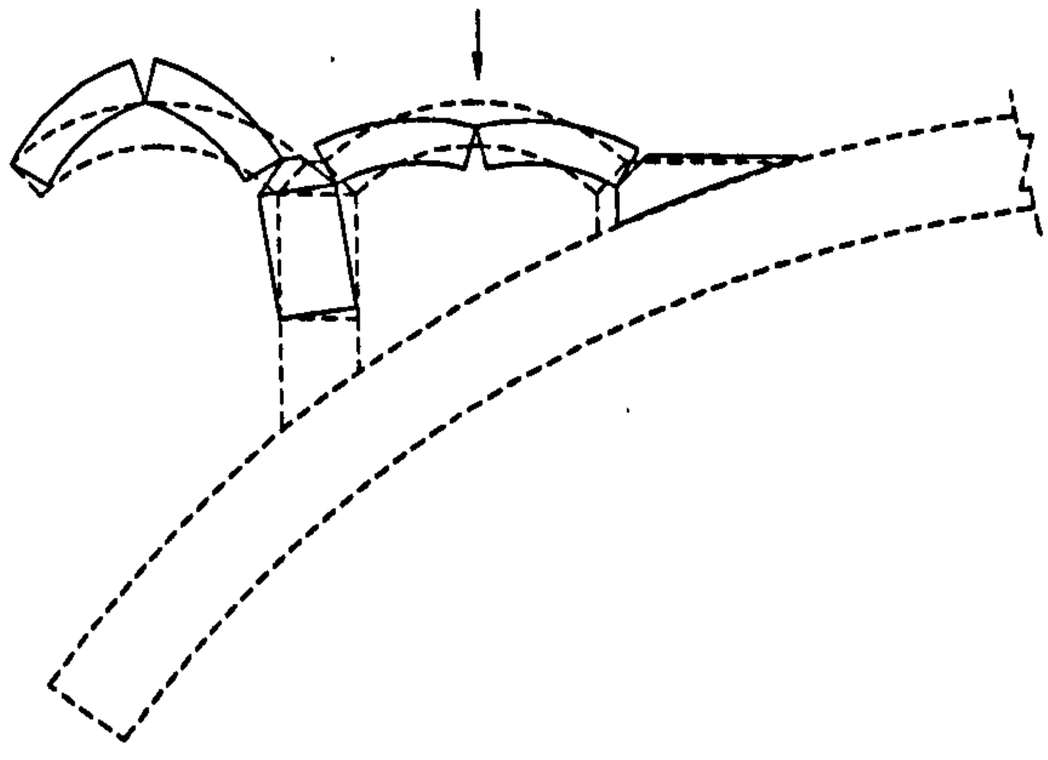

Fig. 2.31 The Local Failure Mode of OSMA3

Upon the removal of the loads, the local mechanism disappeared, and any cracking could hardly be seen.

The rest of the elastic tests continued after the " recovery " of the arch from the ET 2.

The model failed when monotonic loading to 23.5 kN was applied at the arch seat on the right hand side. Figs. 2.32 - 2.34 show the typical relationships between the radial deflections along the intrados of the main arch and the applied loads with loading at the crown of SA2 (ET), the crown of the main arch (ET) and the top of the arch seat (DT).

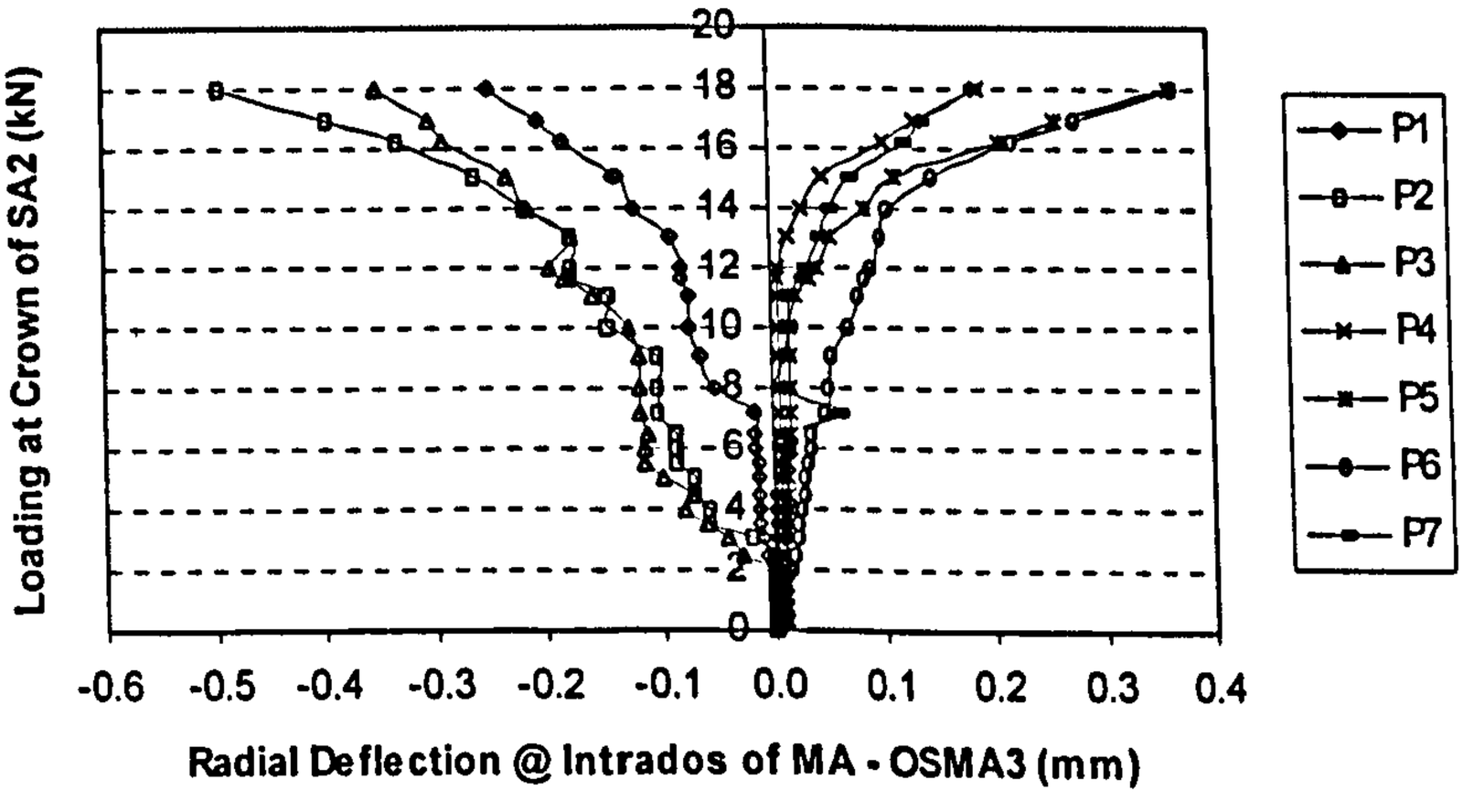

Fig. 2.32 Load-Deflection Curves of OSMA3 With Loading at Crown of SA2

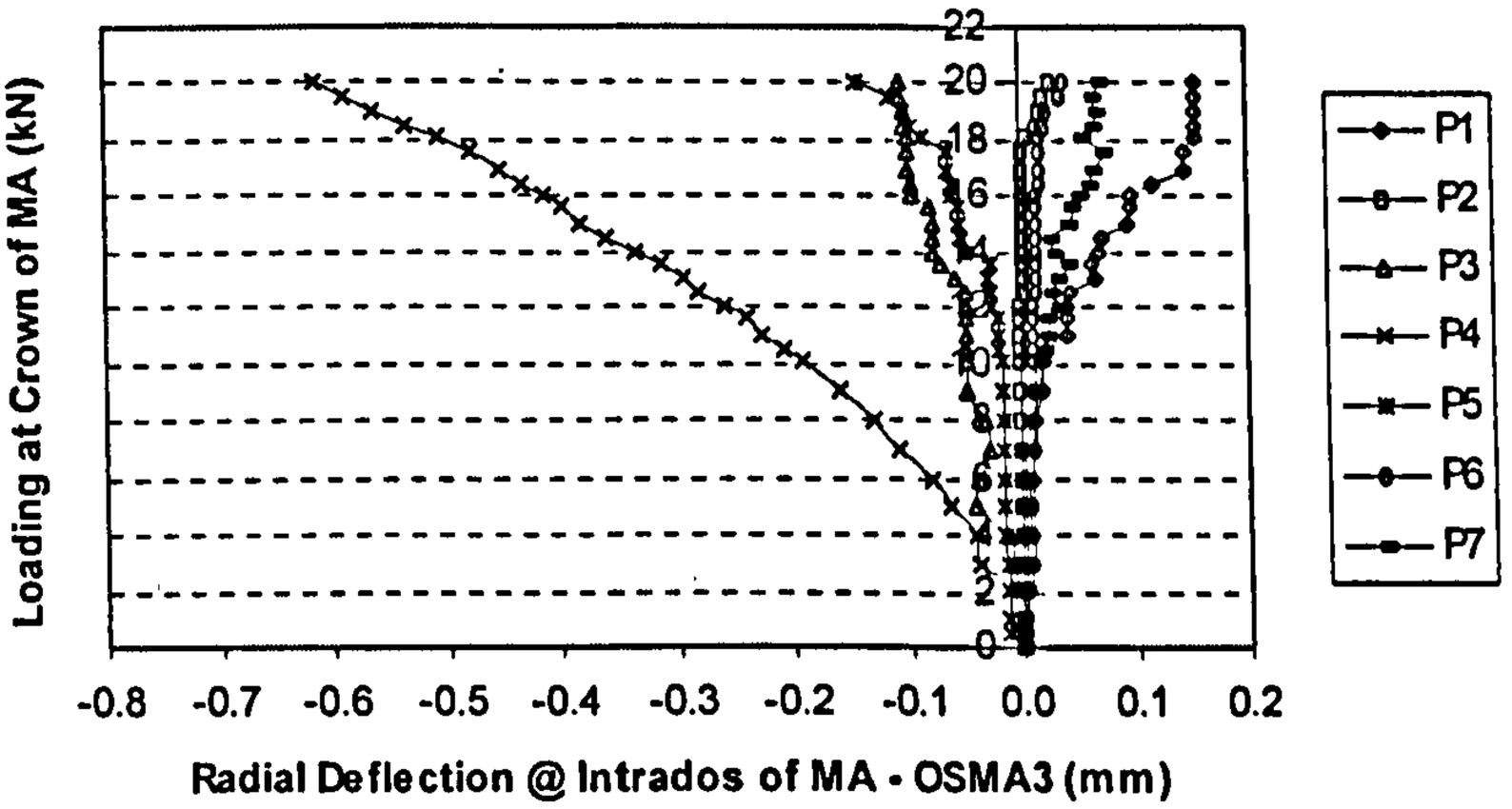

Fig. 2.33 Load-Deflection Curves of OSMA3 With Loading at Crown of MA

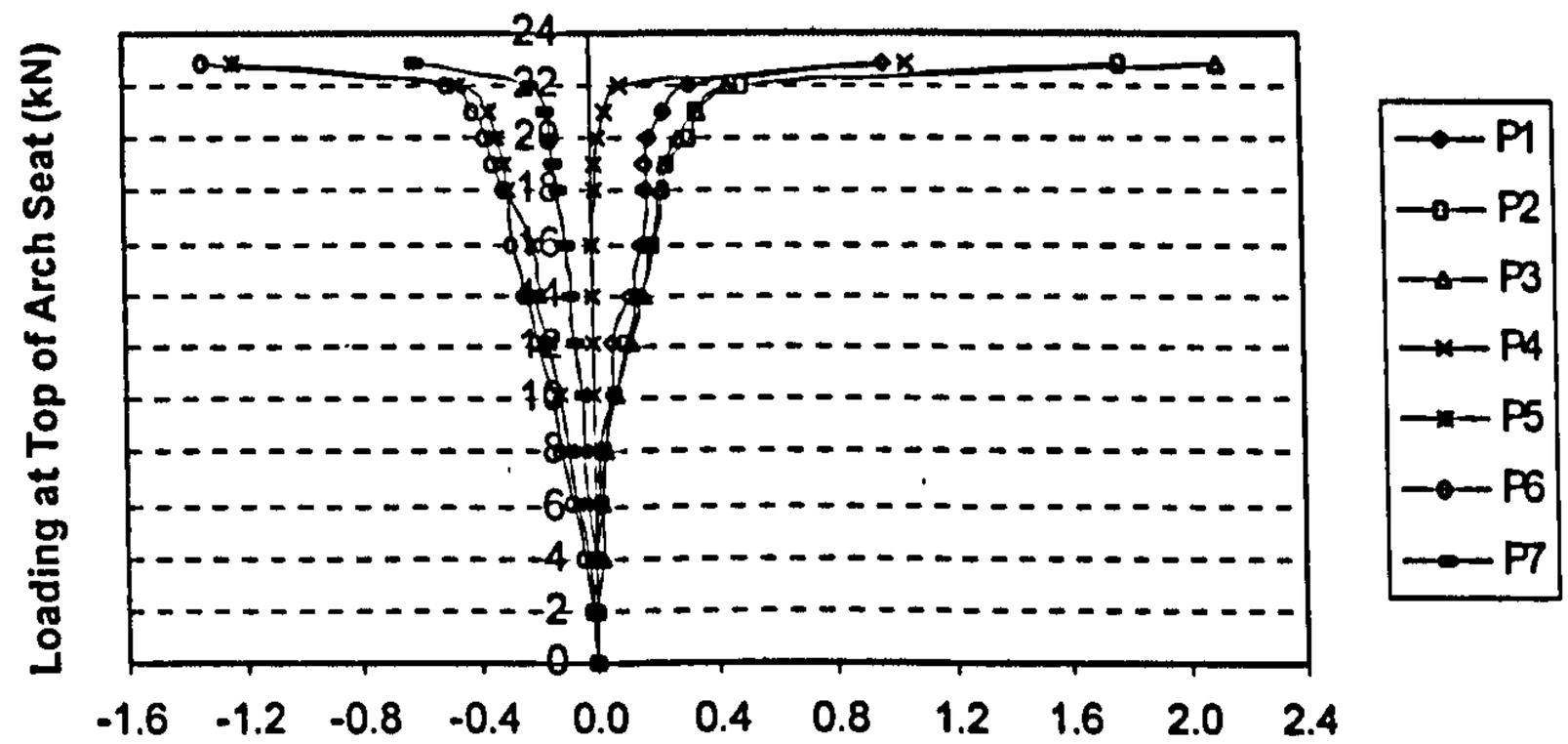

Fig. 2.34 Load-Deflection Curves of OSMA3 With Loading at ¼ Span of MA

The failure mode of the model during the failure test is as shown in Fig. 2.35.

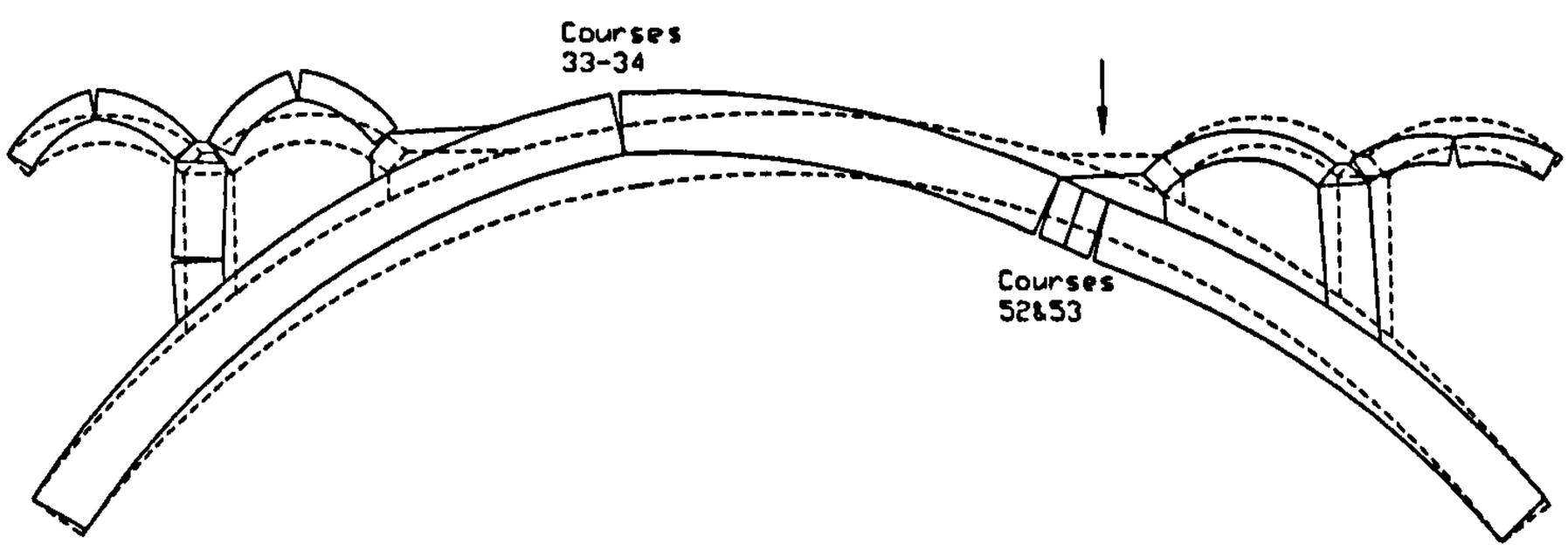

Fig. 2.35 Global and Local Failure Modes of OSMA3

As occurred during the model tests of OSMA2, global and local failure modes of the model were observed. For the main arch, the failure was due to the formation of four hinges. The first set of obvious cracks occurred between the brick courses 51 & 52 and between 53 & 54. The piers failed at the sections when their flexural tensile strengths were exceeded. For the spandrel piers, the local failure mechanisms were similarly to those described in Section 2.3.2. The failure was due to the movement/rotation of the abutments/ supports. The movement of the supports of the spandrel arches could be caused by: -

- The shear failure between the arch seats and the main arch;
- The shear failure between the spandrel piers and their top parts;
- The displacement/rotation of the supports of the end arches;

The abutments of the main arch might be assumed rigid since four vertical macalloy bars were used to anchor the reinforced concrete block abutments onto the test base. About 0.4 mm outwards movement of the steel frame on the unloaded side was measured at the level of the supports of the end spandrel arches. The movement could slightly reduce the load capacity of the tested arch as it released the stiffening effects on the main arch at the unloaded side. It might be assumed that such movement had taken place before the hinges were formed within the SA1, i.e., before the maximum load reached due to the fact that the loads upon the frame remained nearly constant once the hinges were fully formed. This may be verified in Section 4.4.2.

2.3.4 Five Metre Span Main Arch Itself (OSMA4)

A total of five ET tests were carried out for the model. The loading locations and the loads applied are shown as in Fig. 2.36 and Table 2.5. The maximum loads applied at each of the testing locations were largely based on the predicted values from the corresponding FE analyses. The model failed when monotonic loading to 12.5 kN was applied around the bricks 56 & 57 (about at the location of the arch seat for the models OSMA3 & OSMA5).

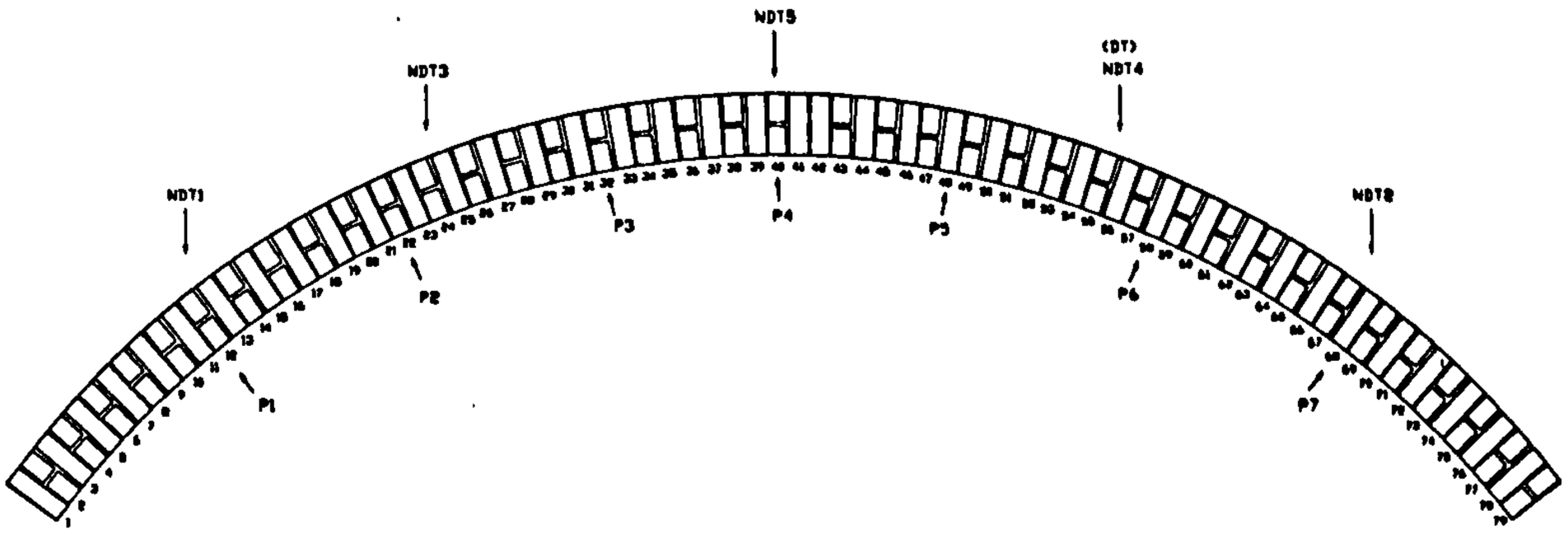

Fig. 2.36 Model Tests of OSMA4

Summary of ET and DT Tests of OSMA4 **Table 2. 5**

ET	1	2	3	4	5	DT
Max Load (kN)	15.0	15.0	11.0	9.6	13.0	12.5

Figs. 2.37 and 2.38 show the typical relationships between the radial deflections along the intrados of the main arch and the applied loads with loading at the crown (ET) and ¼ span of the main arch (DT), respectively.

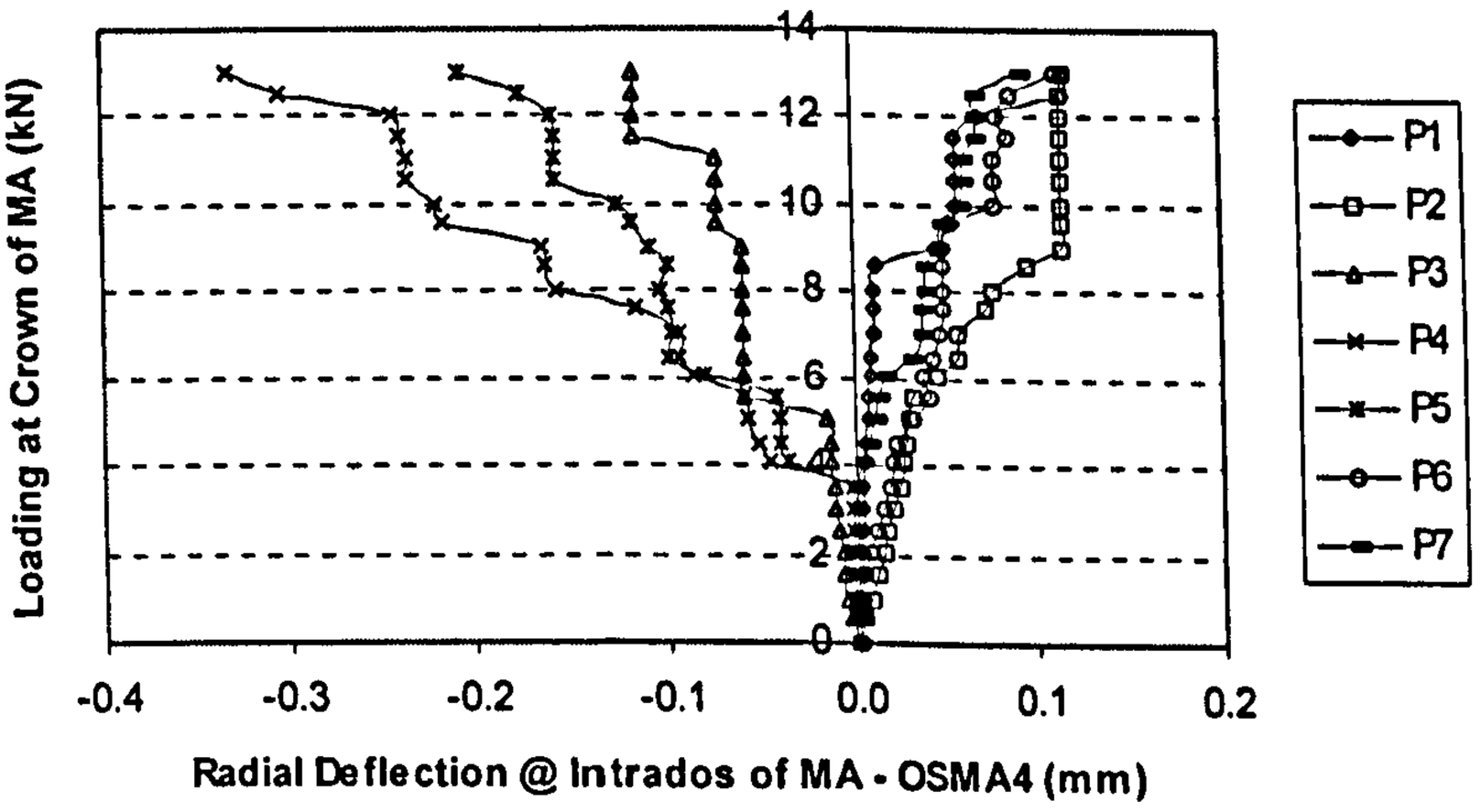

Fig. 2.37 Load-Deflection Curves of OSMA4 With Loading at Crown of MA

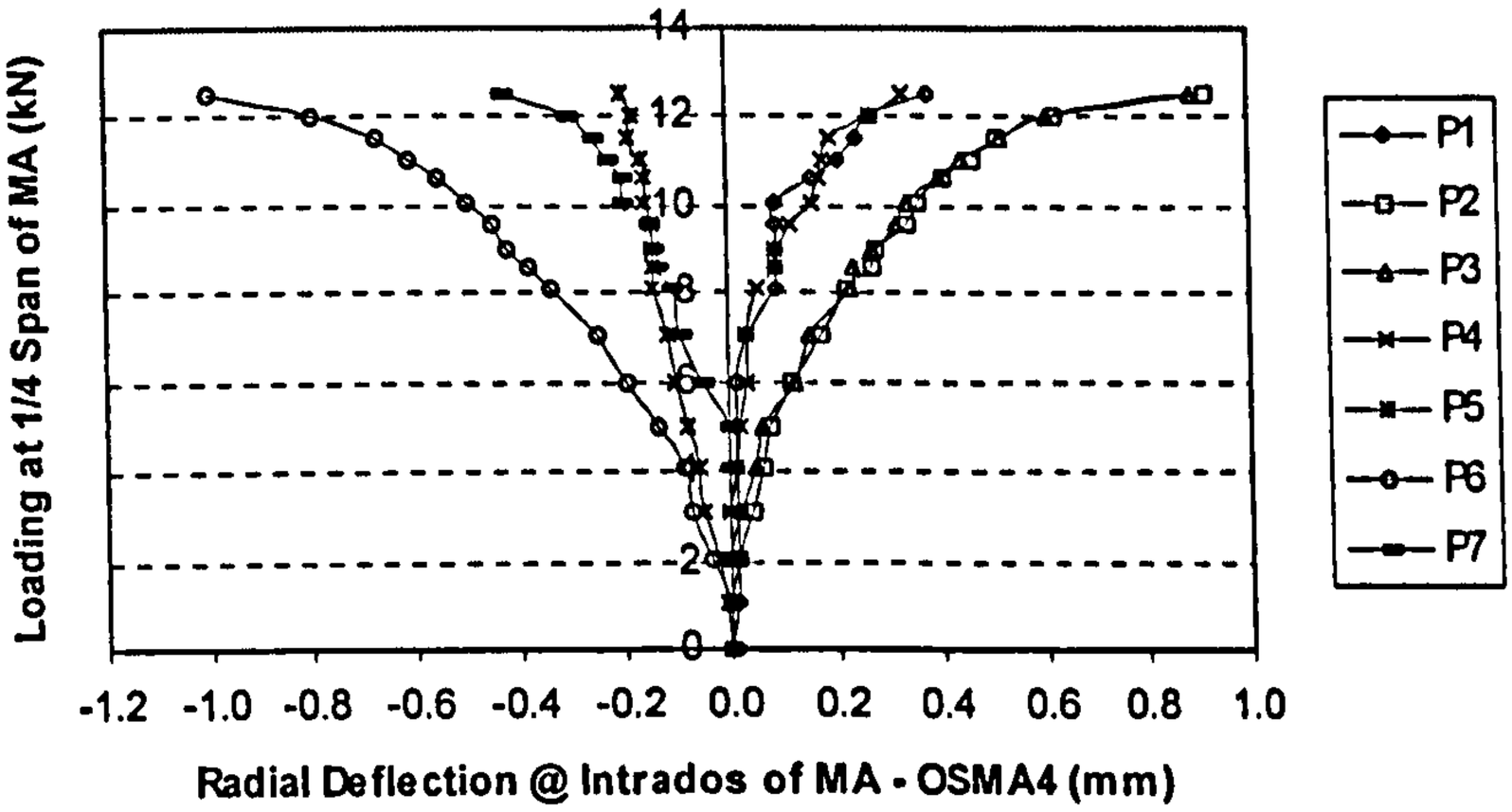

Fig. 2.38 Load-Deflection Curves of OSMA4 With Loading at ¼ Span of MA

The failure mode of the model during the failure test is as shown in Fig. 2.39.

As reported by numerous arch investigators, a clear four-hinge mechanism was developed as the applied load was increased.

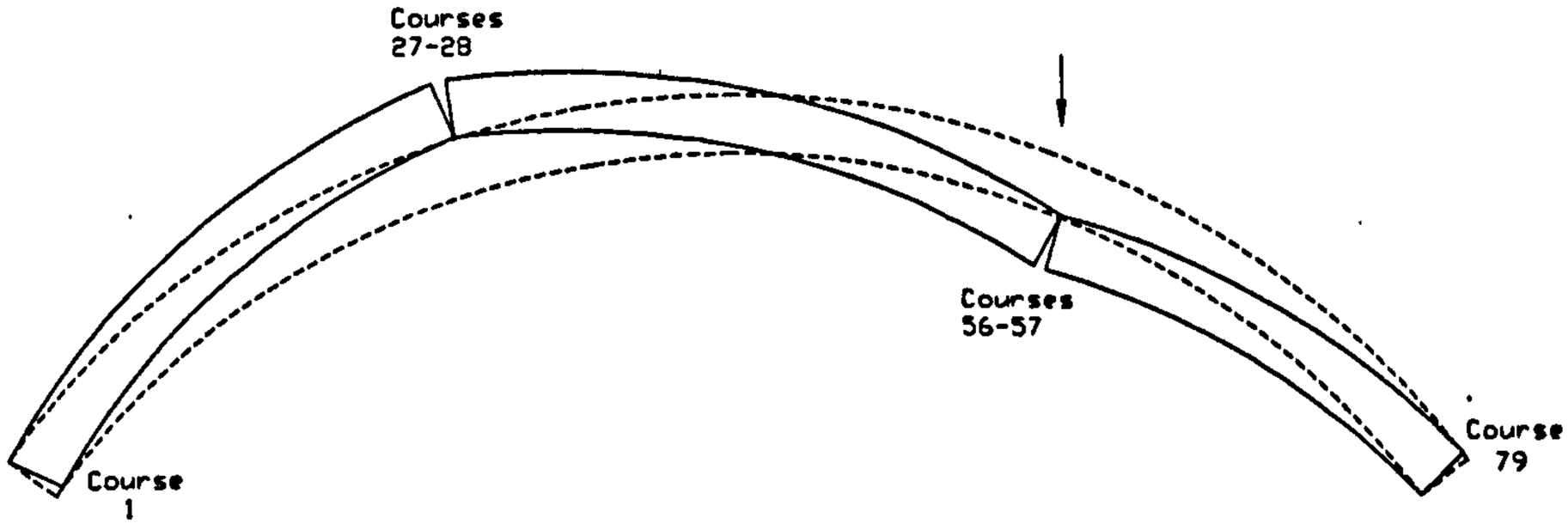

Fig. 2.39 Failure Mode of OSMA4

Since the tested model OSMA4 was planned to be used as the main arch of the model OSMA5, a small load increment (1 kN) was applied through the test. Upon the removal of the load, the model resumed to the initial profile prior to the tests since the final measurements of both deflections and strains were randomly small.

2.3.5 Five Metre Span OSBMAB With Fill (OSMA5)

Similarly to those reported during the model tests of OSMA2 and OSMA3, fine cracks were found at the interfaces between the mortar and the supports of the steel frames prior to the model test of OSMA5. It was believed that the effects of the mortar shrinkage were greater than those in OSMA2 and OSMA3, since weak mortar was used as fill material throughout the full space above the superstructures levelling up to 20 mm thick above the extrados of the crown.

A total of eight ET tests were carried out for the model. The loading locations and the loads applied are shown as in Fig. 2.40 and Table 2.6. The load capacity at each testing location was predicted using FE analyses, thus the test progress was under great control.

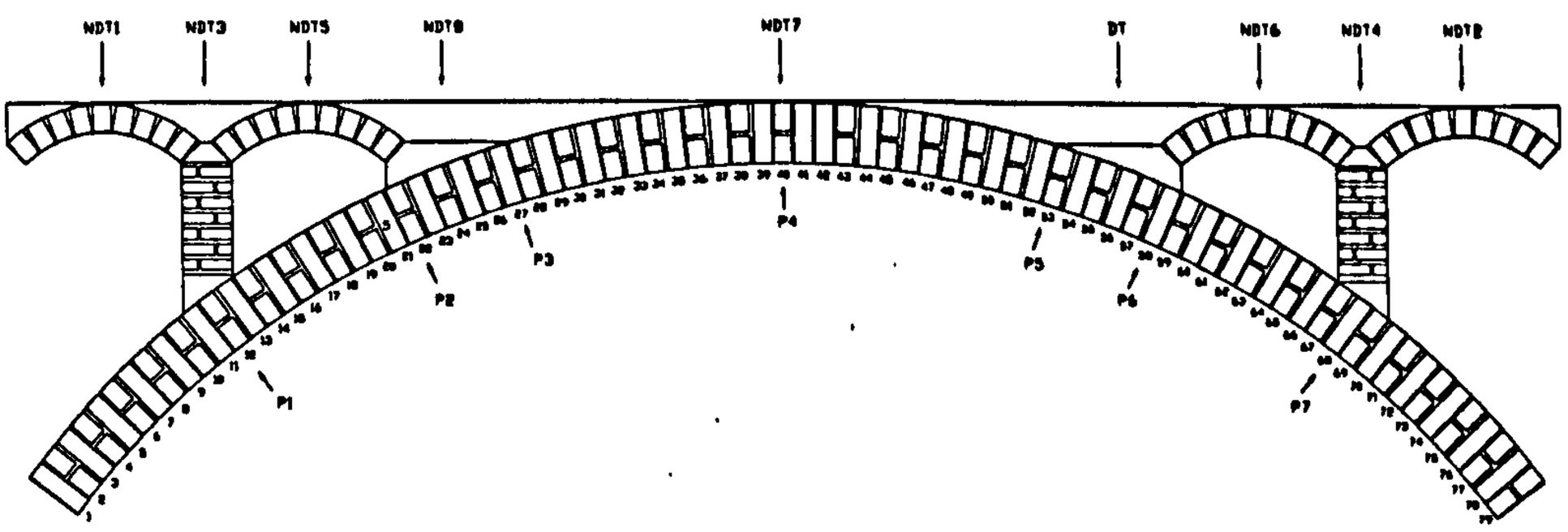

Fig. 2.40 Model Tests of OSMA5

Summary of ET and DT Tests of OSMA5 **Table 2. 6**

ET	1	2	3	4	5	6	7	8	DT
Max Load (kN)	7.0	7.0	14.0	14.0	16.0	14.0	20.0	20.0	32.5

The model failed when monotonic loading to 32.5 kN was applied around the arch seat on the right hand side.

Figs. 2.41 - 2.43 show the typical relationships between the radial deflections along the intrados of the main arch and the applied loads with loading at the crown of SA2 (ET), the crown of the main arch (ET) and the top of the arch seat (DT).

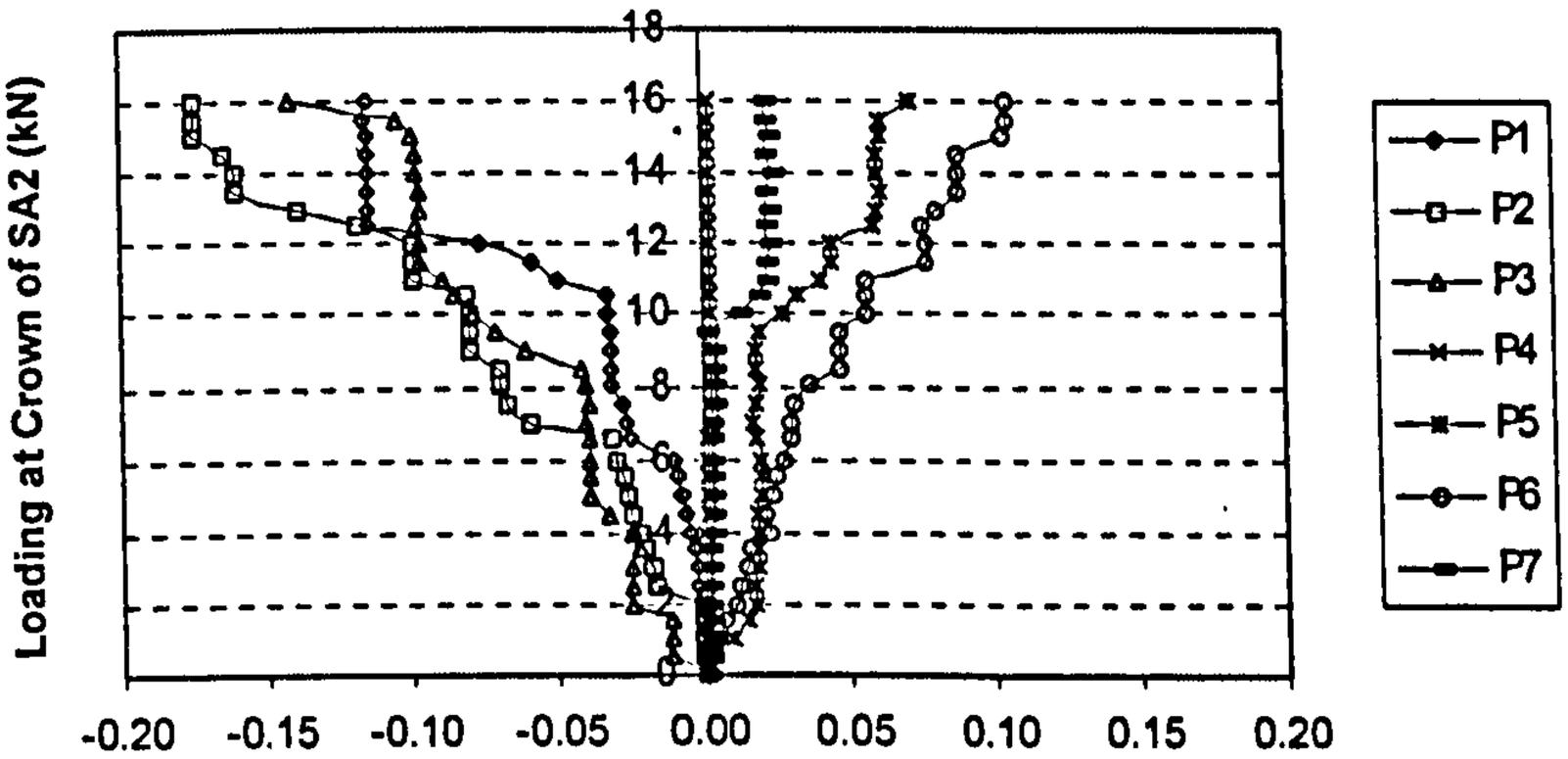

Fig. 2.41 Load-Deflection Curves of OSMA5 With Loading at Crown of SA2

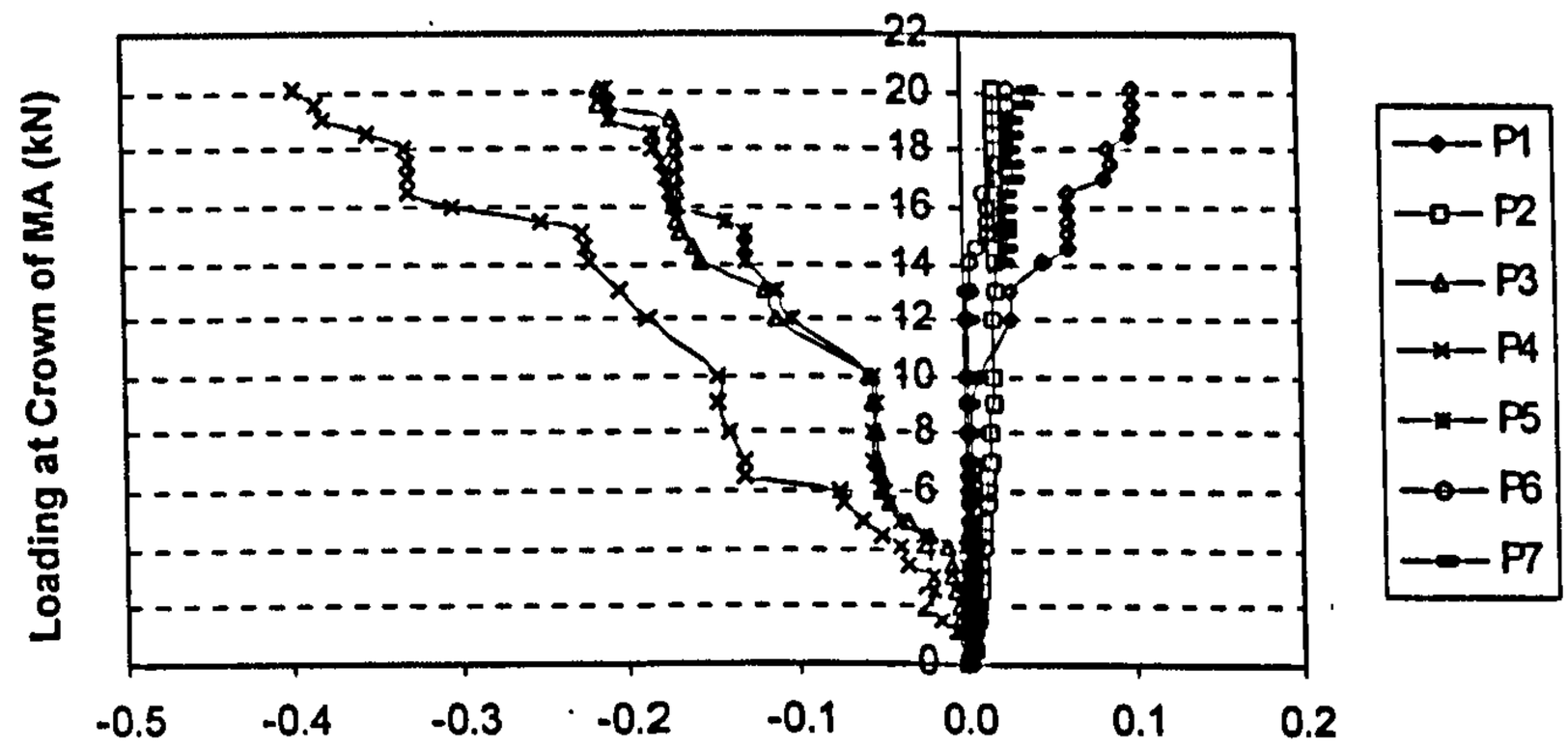

Fig. 2.42 Load-Deflection Curves of OSMA5 With Loading at Crown of MA

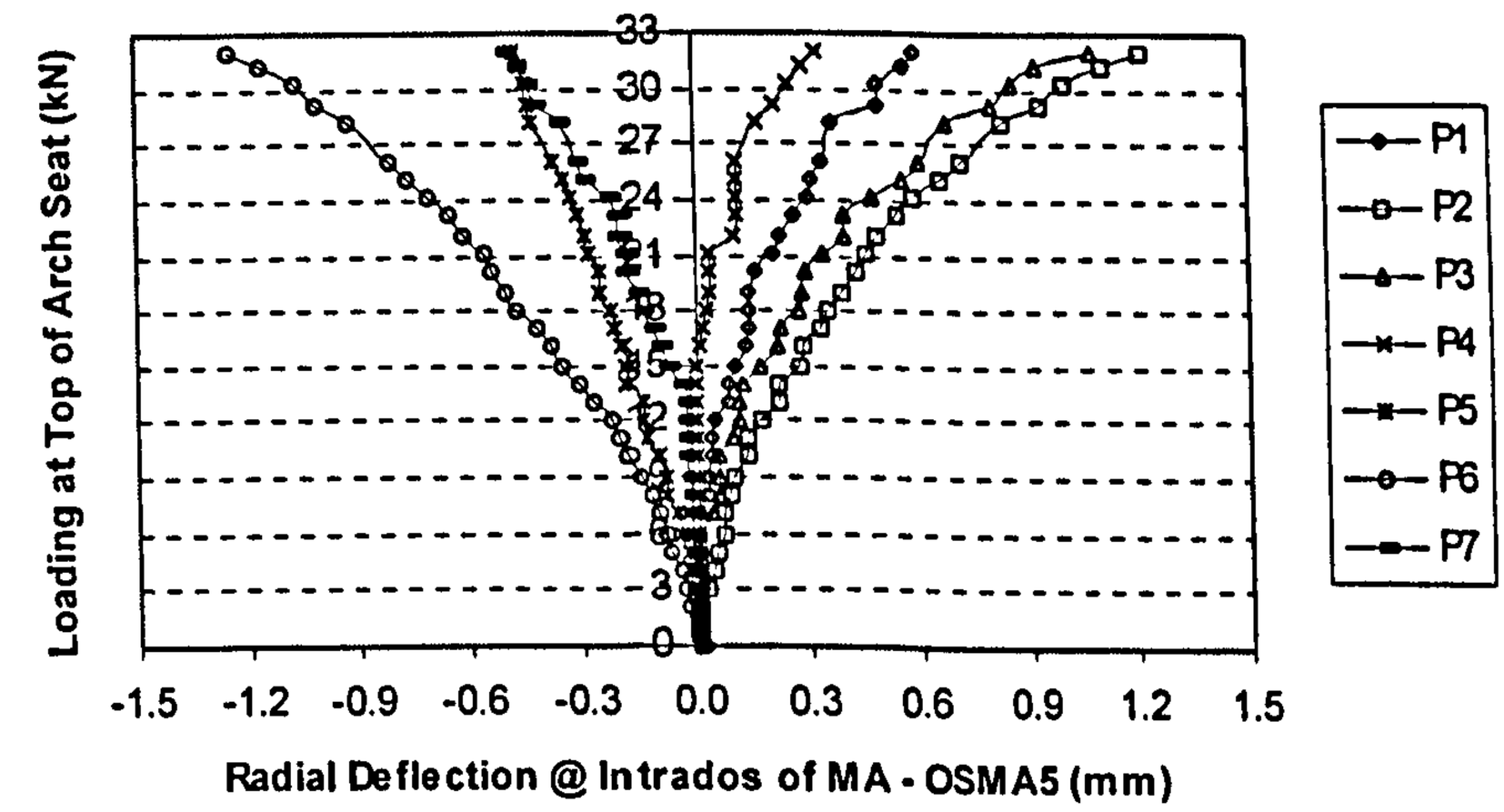

Fig. 2.43 Load-Deflection Curves of OSMA5 With Loading at ¼ Span of MA

When the load reached 31 kN, a global mode of failure was initiated with the pattern of the " hinges " shown in Fig. 2.44. It was noted that one of the hinges was recorded between the courses 30-31. The test was then stopped. After removal of most of the deflection and strain transducers, the jack was re-set, and the collapse tests continued.

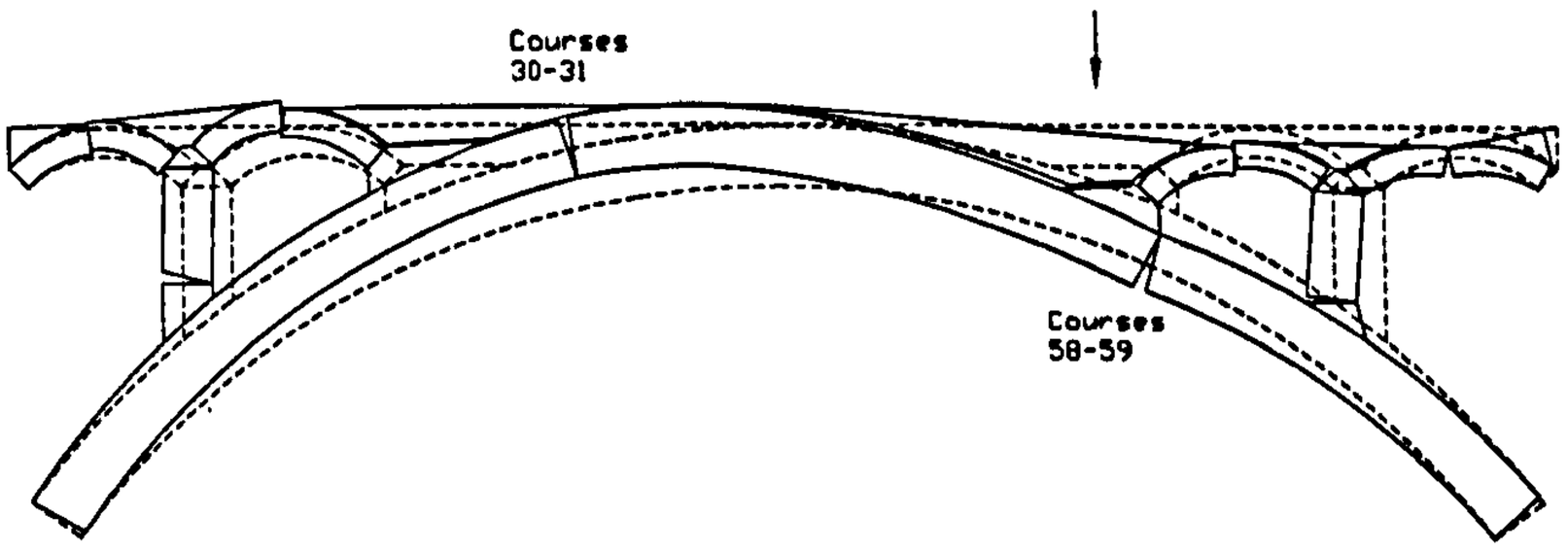

Fig. 2.44 Global and Local Failure Modes of OSMA5 (1)

The applied load was first resumed to its previous value of 31 kN. When the load reached 32.5 kN, the model arch collapsed. It was interesting to notice that the previous 'hinge' between the courses 30-31 was running through the region of the arch seat and finally settled down adjacent to the arch seat between the courses 21-22 as shown in Fig. 2.45.

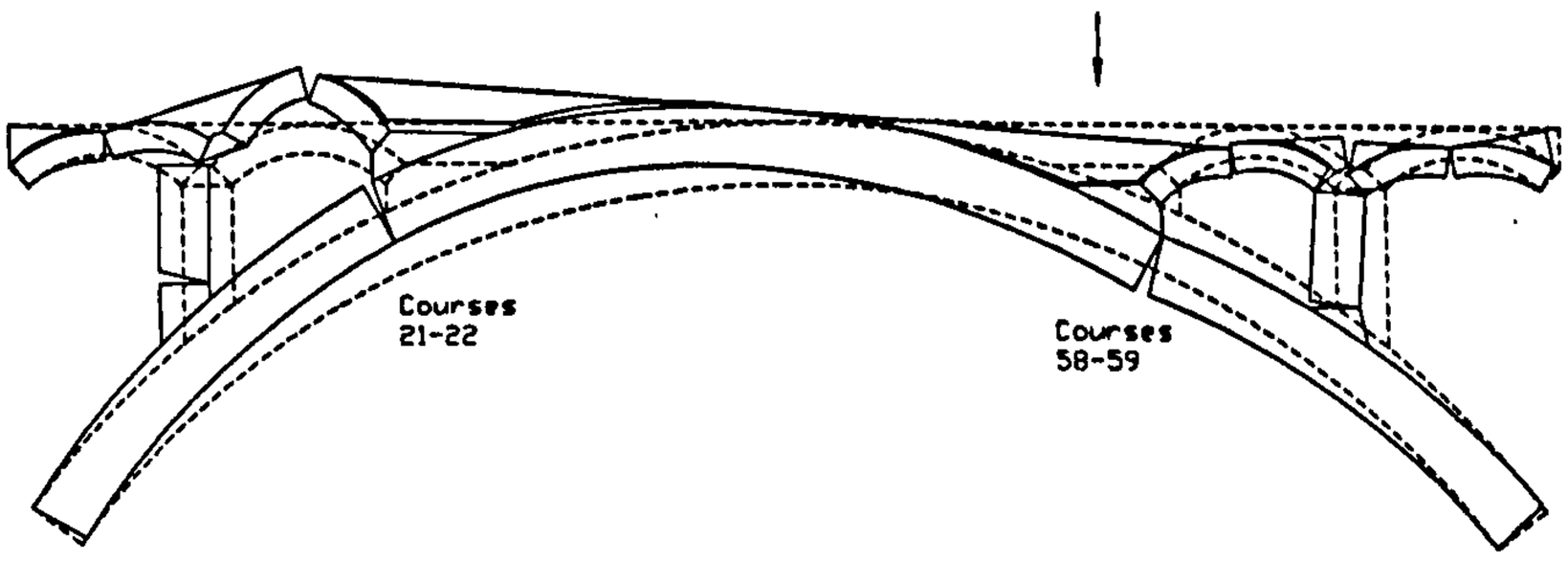

Fig. 2.45 Global and Local Failure Modes of OSMA5 (2)

No shear failure between the arch seats and the main arches were observed during the model test, which might be prevented by the " shear studs " provided at the bottoms of both the spandrel piers and the arch seats as described in Section 2.2.1.

2.4 Comparisons of Test Results

It was intended to study the load – displacement responses of the main arches of the three models OSMA3, OSMA4 and OSMA5 under similar loading conditions. Having reviewed the test data, however, it was found that the results of the OSMA3, especially those within linear stages, did not appear to share similar patterns as those of the others in most of the load cases. It was considered that the phenomenon was mainly caused by the different characteristics of the model OSMA3. The excessive loading during the second elastic test might also affect the measurements at initial stage since the model arch was relatively of small scale and deflections were generally small and sensitive to the initial conditions of the model. If the integrity of the main arch was slightly damaged, it could be reflected by the initial measurements. It was shown that the results of the models OSMA4 and OSMA5 could be compared through the entire loading history.

It was evident that an open spandrel brickwork masonry arch was of higher load capacity compared with the main arch itself. As described in Section 2.3, the load capacities of the model arches were 12.50 kN for main arch itself (OSMA4), 23.50 kN for the main arch without fill (OSMA3) and 32.5.00 kN for the main arch with fill (OSMA5). For the models OSMA4, OSMA3 and OSMA5, the ratios of the load capacities were 1.00 : 1.88 : 2.60 , and the ratios of self-weights were 1.00 : 1.53 : 1.80 (see Section 2.2.1.1). When the main arch deformed, the superstructure provided horizontal stiffness, and restrained the upward movement at the unloaded side around quarter span regions. Thus, the occurrence of the cracks (hinges) was delayed, and the load capacity was increased. Also, the superstructure changed the flow pattern of the applied loads, and transferred some of the loading to the supports of the spandrel structures.

It appeared that the presence of the open spandrel brickwork masonry arches stiffened the main arch.

When loads were applied at the crown of the main arches, as shown in Figs. 2.46 and 2.47, the radial deflections at the intrados of the main arch of the model OSMA5 were about 90% of those of the model OSMA3. That is, the contribution of the superstructure to the deduction of the deflections was less significant.

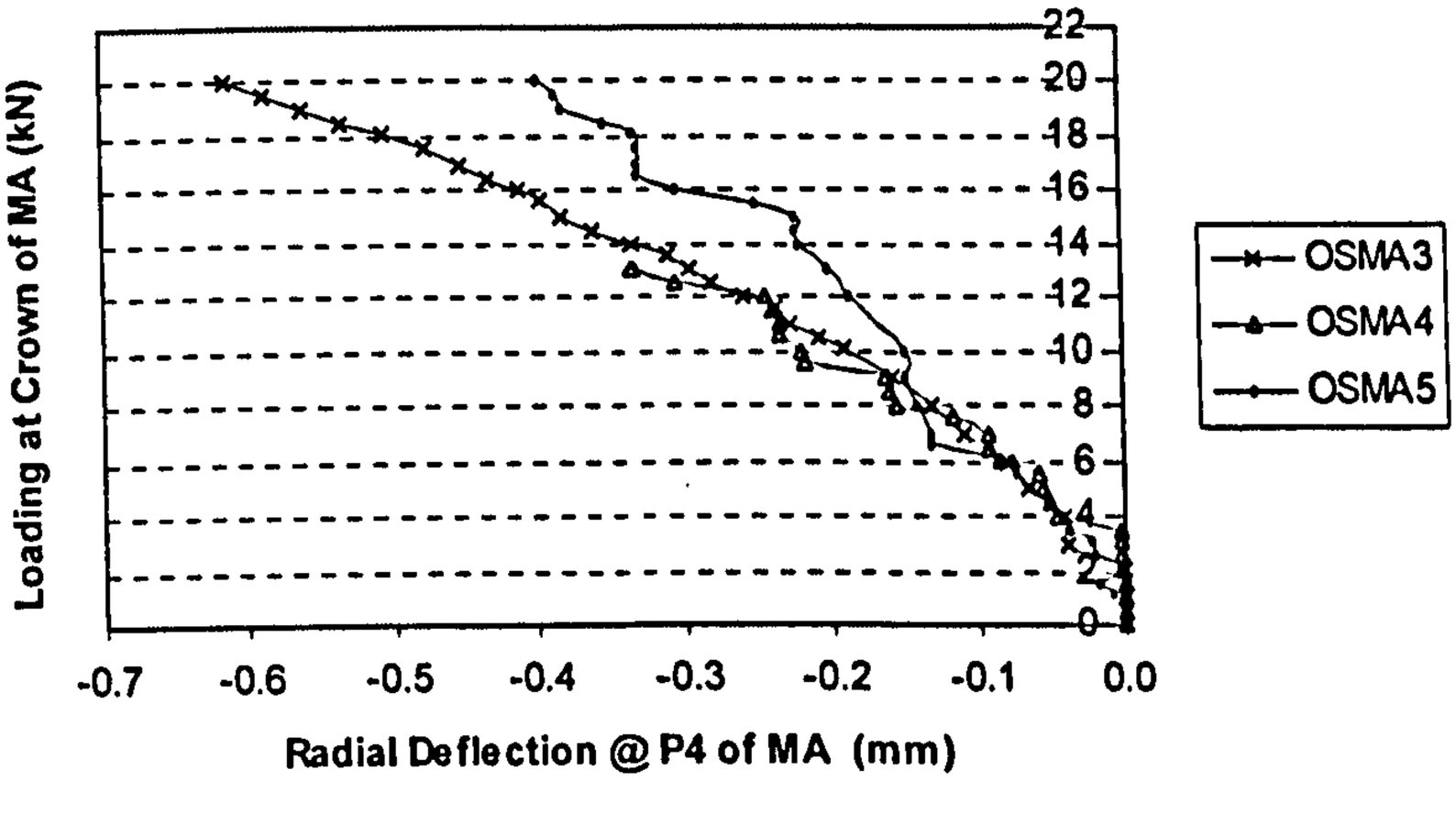

Fig. 2.46 Load-Deflection Curves @ P4 of OSMA3, OSMA4 & OSMA5 With Loading at Crown of MA

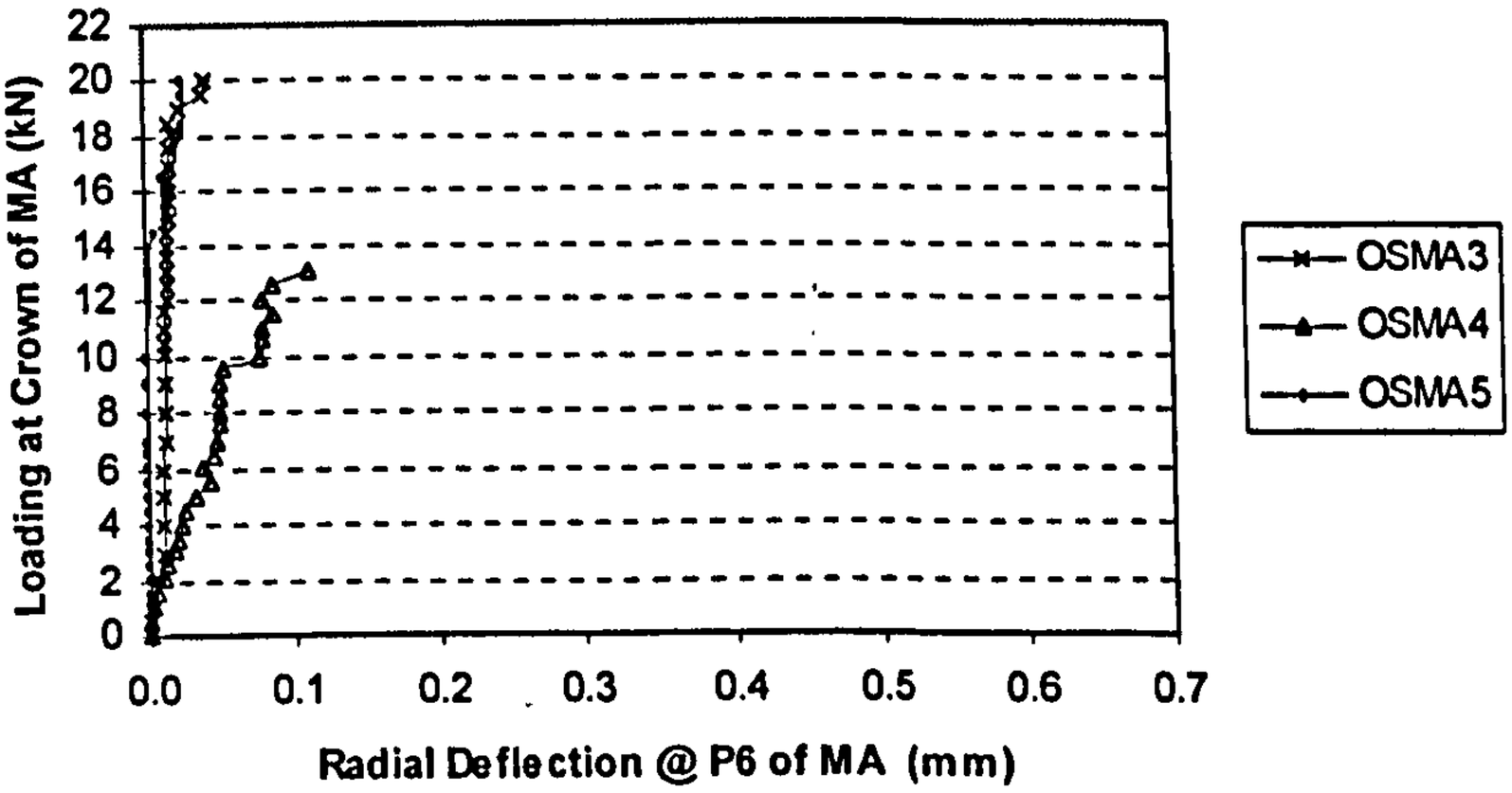

Fig. 2.47 Load-Deflection Curves @ P6 of OSMA3, OSMA4 & OSMA5 With Loading at Crown of MA

This was because the main arches moved downwards around the quarter - span regions (at P5, note that the upwards deflections at P5 were not plotted due to the unavailability of the measurements of the model OSMA3 at the corresponding locations of the models OSMA4 and OSMA5), and the constraints of the superstructures could not be effectively activated. Where the arch moved upwards, the effects of the superstructure became great as shown in Fig. 2.47, offering significant restraint or stiffening (reducing the deflections at 6 kN five fold for example).

When loads were applied at the quarter span of the main arches, as shown in Figs. 2.48 and 2.49, the radial deflections at the intrados of the main arch of the model OSMA5 were only 30% of those of the model OSMA3.

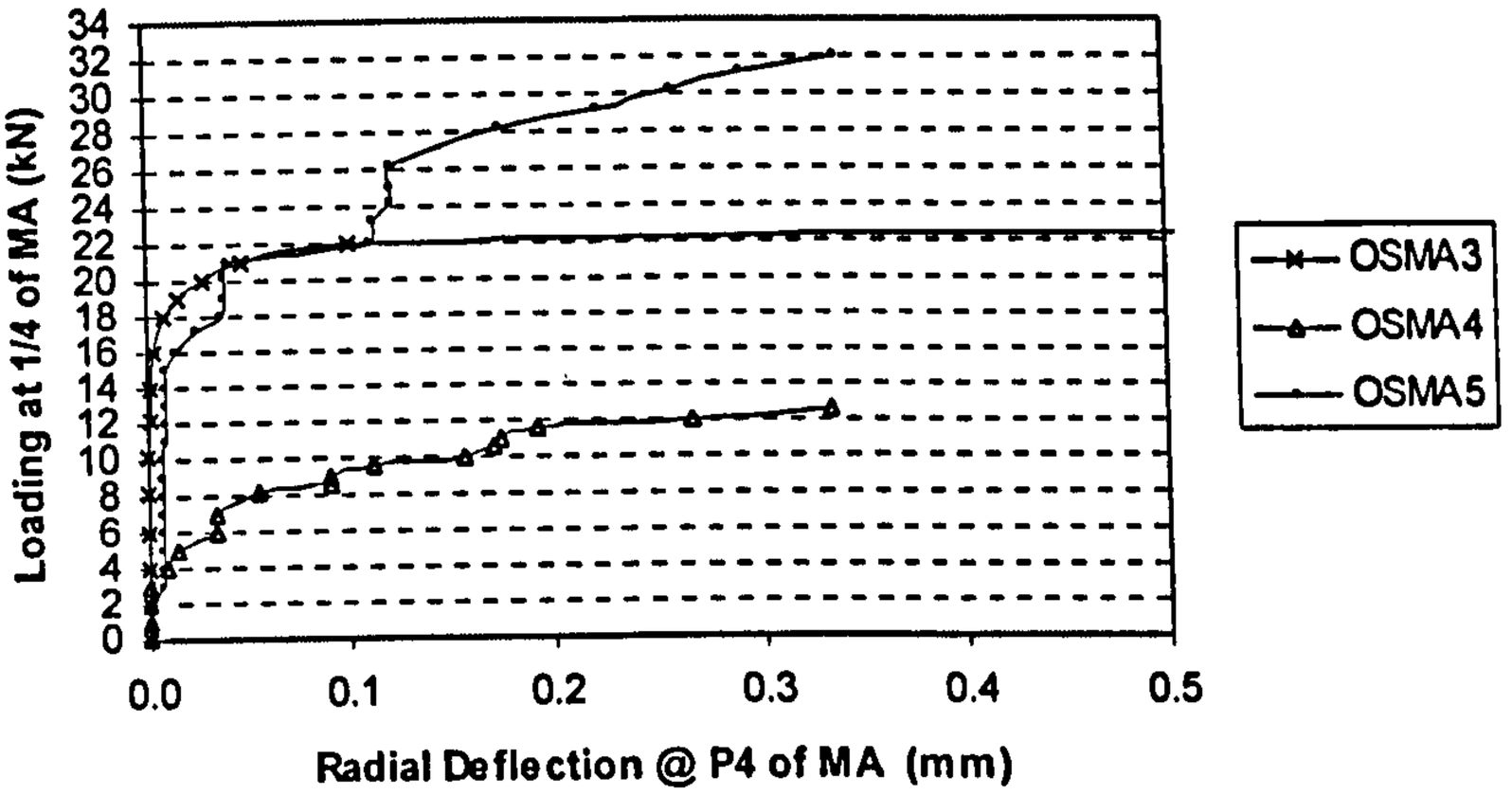

Fig. 2.48 Load-Deflection Curves @ P4 of OSMA3, OSMA4 & OSMA5 With Loading at ¼ Span of MA

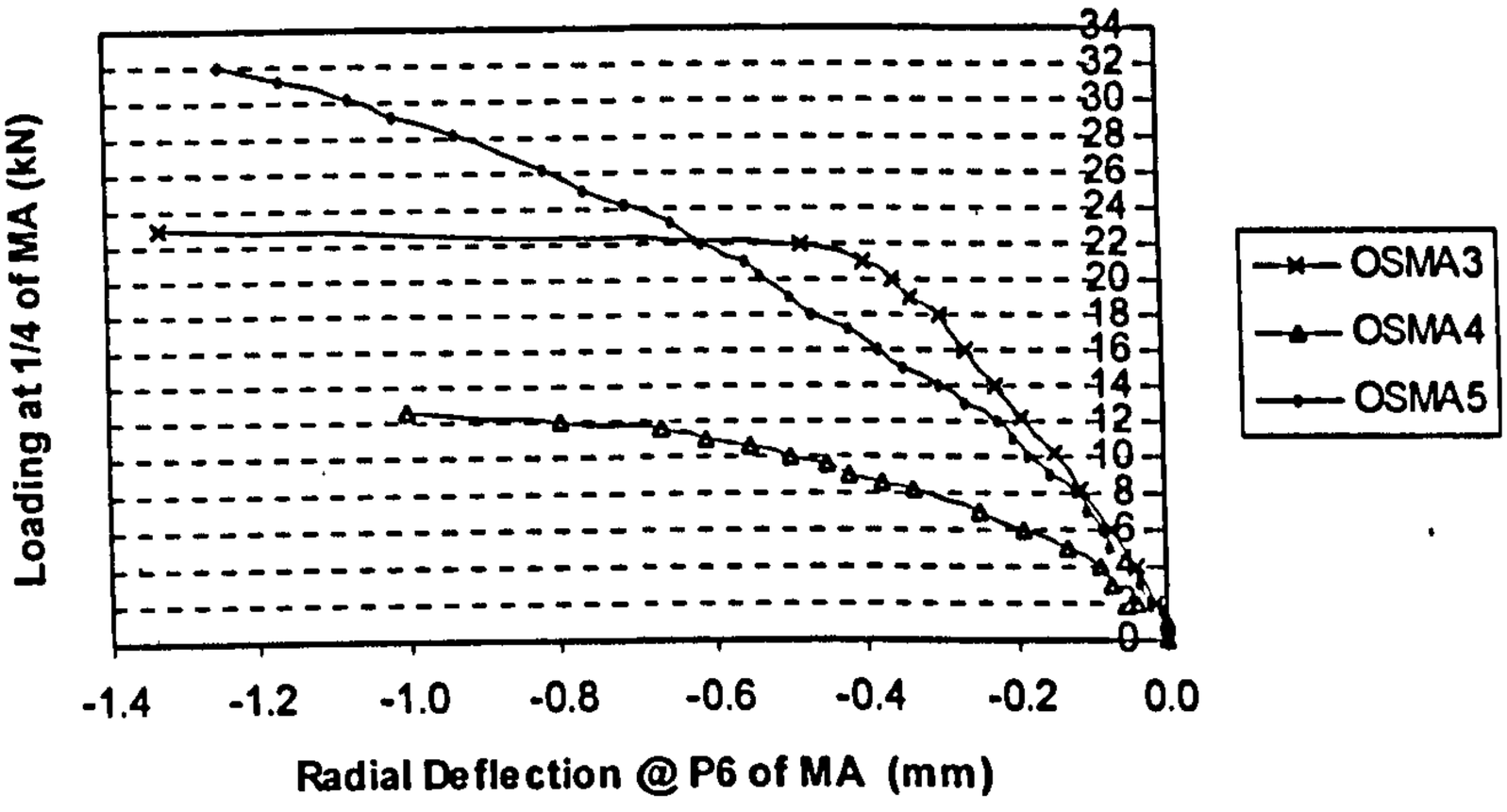

Fig. 2.49 Load-Deflection Curves @ P6 of OSMA3, OSMA4 & OSMA5 With Loading at ¼ Span of MA

That is, the interaction between the main arch and the superstructures was more significant when loads were applied at quarter span locations.

It was noted that that the model arches generally behaved linearly up to about 90 percent of the load capacities. In some cases of the model OSMA3, the arch behaved linearly up to failure.

The open spandrel arches (OSMA3 and OSMA5) were stiffer than the main arch itself (OSMA4). In most of the cases, the stiffness of the open spandrel arches with fill (OSMA5) was greater than that without fill (OSMA3).

Up to 90 percent of the load capacity, the arch behaved linearly overall. At this stage, the integrity of the arch might be affected by the development of micro cracks and the movement of the components, which were reflected by a series of small change in the stiffness along the curves. At later stage of the curve, any sudden change in the stiffness would indicate the development of the true cracks. From the above curves, it may be seen that the rate of increment of the deflections increases before a kink and decreases afterwards.

One of the explanations for the repeated change in stiffness (slope) along the curves might be that it was caused by the crushing failure of mortar. As a crack was developed at a mortar joint, the area in compression at the section of the joint would be reduced, and the compressive stress at the section would increase, which might result in the crushing of mortar due to its low compressive strength. Greater increment in deflection appeared under the same increment of the applied load. On the other hand, the crushing of the joint mortar would also lead to the reduction of the length of the axis of the arch, and the area in compression at the section would then be increased. The stiffness of the arch would also be increased. As the loading increased, the pattern of this change in slopes along the deflection – load curves would be remained until the arch failed.

Fill could not only increase the overall stiffness and load capacities of arches, but also adjust the flow pattern of applied loads. With loading at the crown of the internal spandrel arch, the deflections of the model OSMA5 were generally less than those of the model OSMA3, and more evenly along the intrados of the main arch (Figs. 2.50 – 2.52).

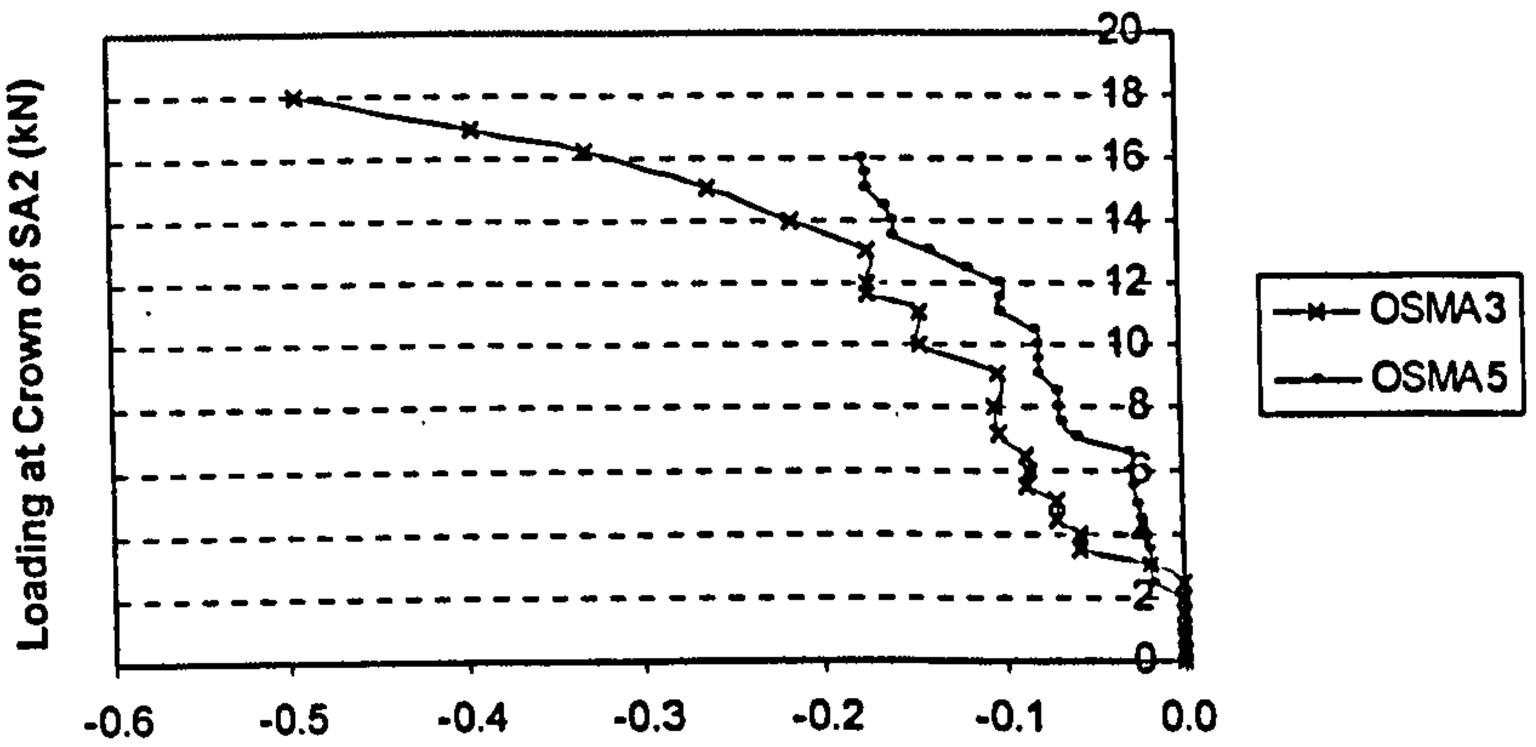

Fig. 2.50 Load-Deflection Curves @ P2 of OSMA3 & OSMA5 With Loading at Crown of SA2

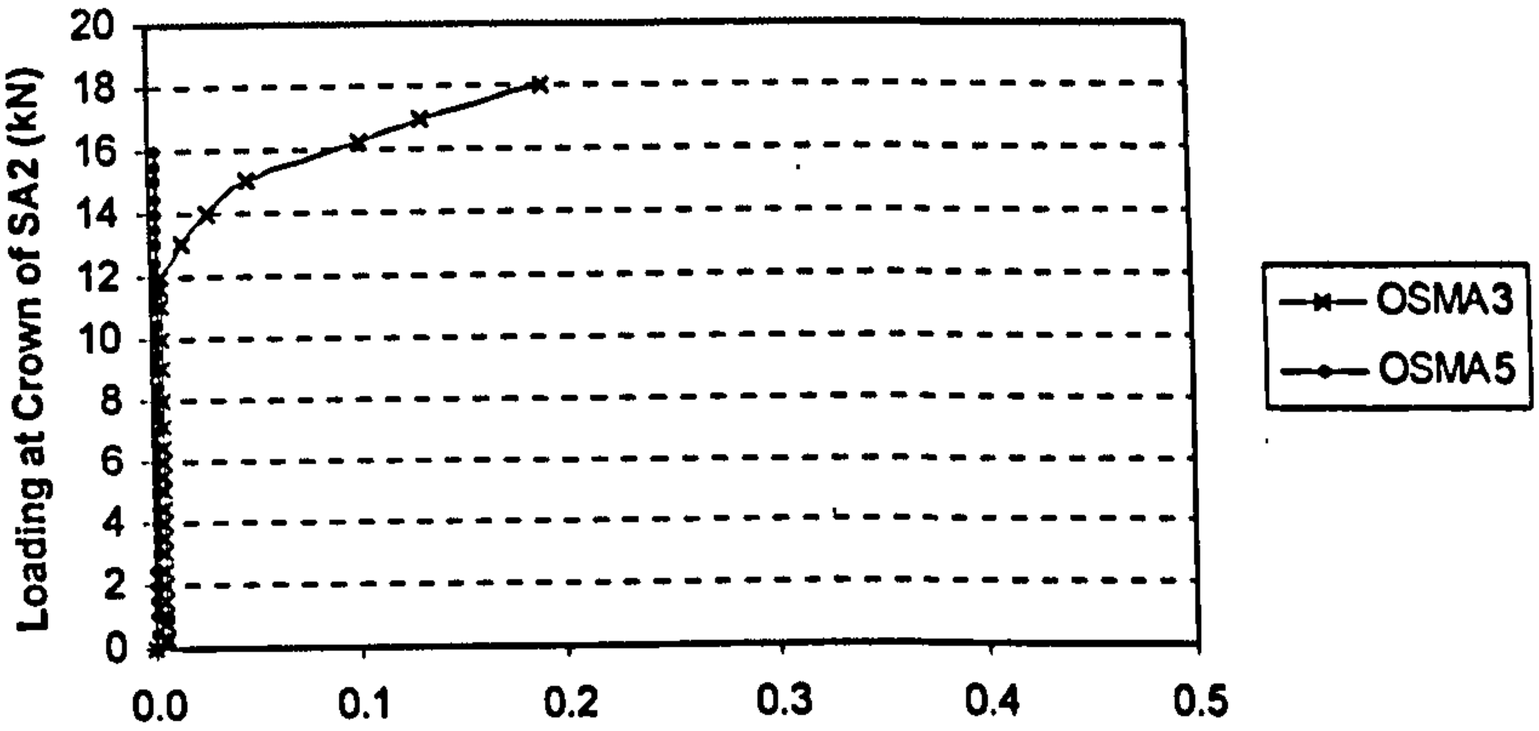

Fig. 2.51 Load-Deflection Curves @ P4 of OSMA3 & OSMA5 With Loading at Crown of SA2

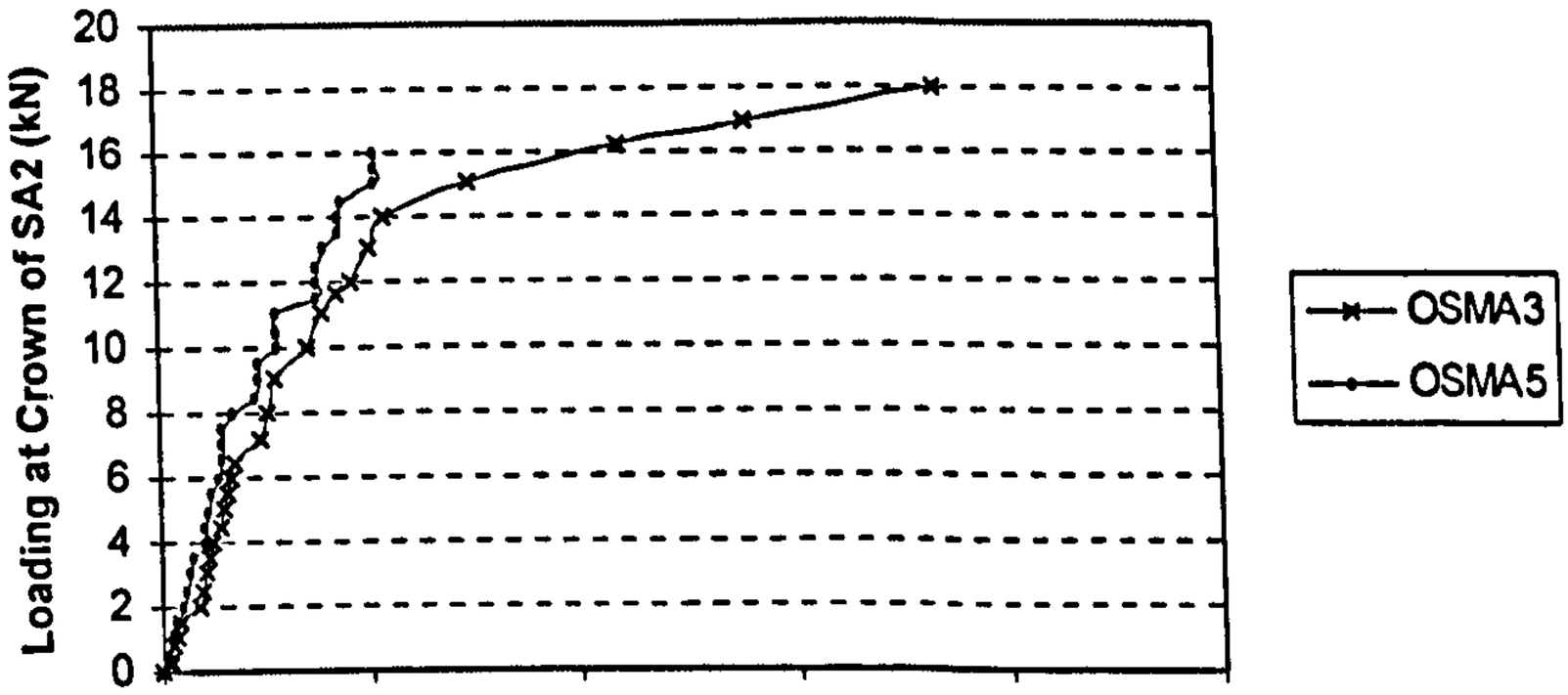

Fig. 2.52 Load-Deflection Curves @ P6 of OSMA3 & OSMA5 With Loading at Crown of SA2

2.5 Discussions And Summary

It should be noted that the results of the model tests might be influenced by various factors, such as the different characteristics of the bonds (brick-mortar, brick-concrete and brick-steel), the variable thickness of the mortar joints (especially within the top of the spandrel piers, where in order to achieve the desirable level, the thick or thin mortar joints were built), the variable sizes of mortar wedges, the removal of the centering of the main arch and the spandrel arches, the effects of irregularity of bricks.

It may be noted that one of the main features of arches built using standard size of bricks was that mortar wedge joints had to be constructed. The wedge effects would become more significant as the rise-span ratio is increased, particularly within the quarter-span regions. Also, the effects of irregularity become more significant when the half scale Raewell bricks are used as different sizes of mortar joints have to be used in both transverse and longitudinal directions.

In addition, the model arches could also be influenced by a number of other factors, such as workmanship, brickwork shrinkage and creep, changes in temperature, etc. The workmanship was believed to be an important factor, and it could affect the model arches in various ways. For instance, the time between spreading the mortar and placing the brick; the thickness of the spread mortar relative to the final joint thickness; the pressure applied when laying a brick; the thickness of mortar joints; the consistent shape of mortar wedges; and the quality of the filling of mortar joints, etc., would influence the finished model arch to different extents; The model arches were generally tested several weeks later after the completion of the constructions. During the interval period, the model arches might be influenced by changes in temperatures (or thermal cycle loading), which would generally lead to the main arch to move upwards or downwards. The upwards movement of the main arch might be restrained due to the interaction between the main arch and the superstructure, but the downwards movement would lead to adverse effects similar to that of the removal of the main arch centering. In either case, the end spandrel arches would be most affected. The effects caused by the shrinkage of brickwork masonry was similar to that induced by the drop of temperature.

The patterns of the hinges associated with the open spandrel arches were different from those of the single arches. That is, the hinge, which normally occurs with the region of

the quarter-span on the unloaded side for the single arch, moved upwards to the region of the crown. This was mainly caused by the existence of the superstructure on the unloaded side, which restrained the horizontal/upwards deformation of the main arch. However, this hinge may run down to the region of the quarter-span (normally stopping under the external side of the arch seats), if the superstructure failed first (a local mechanism). The superstructure was no long able to provide the resistance to the deformation of the main arch and failure occurs. In this case, the open spandrel arch effectively became a single-span arch with a mechanism superstructure.

For the model OSMA3, it may be noted that the true load capacity of the model with loading at similar locations could be greater than those recorded if the damage to the integrity caused by the effects of the local failure was taken into account.

The principal observations of the model arch tests may be summarized as follows:

- ◊ The OSBMA behaved elastically up to about.90 percent of the load capacity (see Fig. 2.34);
- ◊ The OSBMA generally experienced brittle types of failure once the load capacity was reached, which normally caused the difficulties in tracing the sequences of the cracks (see Figs. 2.28, 2.34 and 2.43);
- ◊ The OSBMA failed by the formation of both local and global mechanisms, but the patterns of the mechanisms considerably varied depending on a number of factors, such as loading locations, relative stiffness of the components and the bond strengths between the superstructures and the main arch, etc. (see Figs. 2.31 and 2.35);
- ◊ The main arch of the OSBMA failed as a result of the four-hinge mechanism, but the hinge on the unloaded side of the main arch occurred within the crown rather than around the quarter-span as appeared in the case of the main arch by itself (see Figs. 2.29, 2.35, 2.39 and 2.45);
- ◊ Local failure of the superstructure of the OSBMA could take place at the loaded side only. This would leave the rest of the structure intact if the stiffness of the rest of structure are considerably greater (see Fig. 2.31);

- ◊ The sliding failure of the OSBMA could occur along the interfaces between the superstructures and the main arch, and it might be prevented by building 'shear studs' within the contact areas of the main arch (see Fig. 2.21);
- ◊ Fine cracks developed during construction and in the time prior to the application of loading, especially those within the end spandrel arches of the OSBMA, might become closed as the loads increased;
- ◊ For the OSBMA, compared with the main arch itself, the load capacity could be increased up to 80% without fill, and 150% with fill when loading was applied at ¼ span point of the main arch;
- ◊ Compared with the main arch itself, the superstructures of the OSBMA could delay the occurrence of the cracks; reduce the deflections; increase the horizontal stiffness (especially at quarter-span regions) and the overall stiffness of the main arch (see Figs. 2.46 to 2.49);
- ◊ The superstructures of the OSBMA could transfer certain applied loads to the supports, and the loads that the main arch carried were effectively reduced;
- ◊ The radial deflections along the intrados of the main arch appeared more uniform compared with those of the main arch itself. This suggest that the fill of the OSBMA not only restrain the upward deformation of the main arch, but also effectively change the applied line loads into distributed loads.
- ◊ The overall stiffness of OSBMA could be different from one to another even if similar materials and workmanship were used, but the load capacities would be similar (see Figs. 2.48 and 2.49).

CHAPTER 3 FINITE ELEMENT MODELLING

3.1 Basic Modelling Approaches

As discussed in Chapter 2, brickwork masonry is a composite material made up of bricks bonded with mortar. The properties of the components, the conditions of the interface bonds and the patterns in which masonry units are assembled, can affect the behaviour of brickwork masonry arches. A detailed modelling of a brickwork masonry structure may need to take the above three factors into account. In the field of brickwork masonry walls, considerable efforts have been made to investigate and establish the constitutive models and the failure criteria of masonry units under various stress conditions at both macro and micro levels (Dhanasekar et al, 1985; Pande and Middleton, 1994; and Lourenco and Rots, 1997). In the field of brickwork masonry arches, however, it appears that the constitutive models have largely remains at a macro level.

Finite element models of brickwork masonry arches adopt either smeared modelling approach (continuum modelling approach) or discrete modelling approach. Using either approach, masonry arches are generally modelled at macro levels, i.e., the orientations of individual bricks and mortar joints are not considered. Due to relative simplicity and computational efficiency, the former has been largely used in recent years to model the cracking behaviour of masonry arches (Towler, 1981; Sawko et al., 1982, Choo et al., 1991 and 1995, Crisfield, 1984, 1985a, b and 1987, Loo et al., 1991 and 1995), while the discrete modelling approaches have also been attempted (Crisfield, 1985; Choo et al., 1992; Hodgson, 1996).

It may be noted that the concepts of both 'smeared' and 'discrete' approaches were originally developed through the modelling of structures made of brittle type materials, especially reinforced/plain concrete and rock structures (Willam and Warnke, 1975; Buyukozturk and Shareef, 1985; Goodman et al, 1968; Heuze and Barbour, 1982). The application of both approaches in the modelling of masonry structures is limited, either by using finite element packages such as DIANA (Rots and Lourenco, 1993; etc.) or ANSYS (Hodgson, 1996; etc.), or by developing relatively 'simple' but special models (Loo et al.; etc.).

In the present thesis, attempts have been made to model open spandrel brickwork masonry arches using both smeared and discrete modelling approaches.

For a basic brickwork masonry unit as shown in Fig. 3.1, depending on the treatments of the brick unit and mortar joint, four different finite element modelling methods may be used.

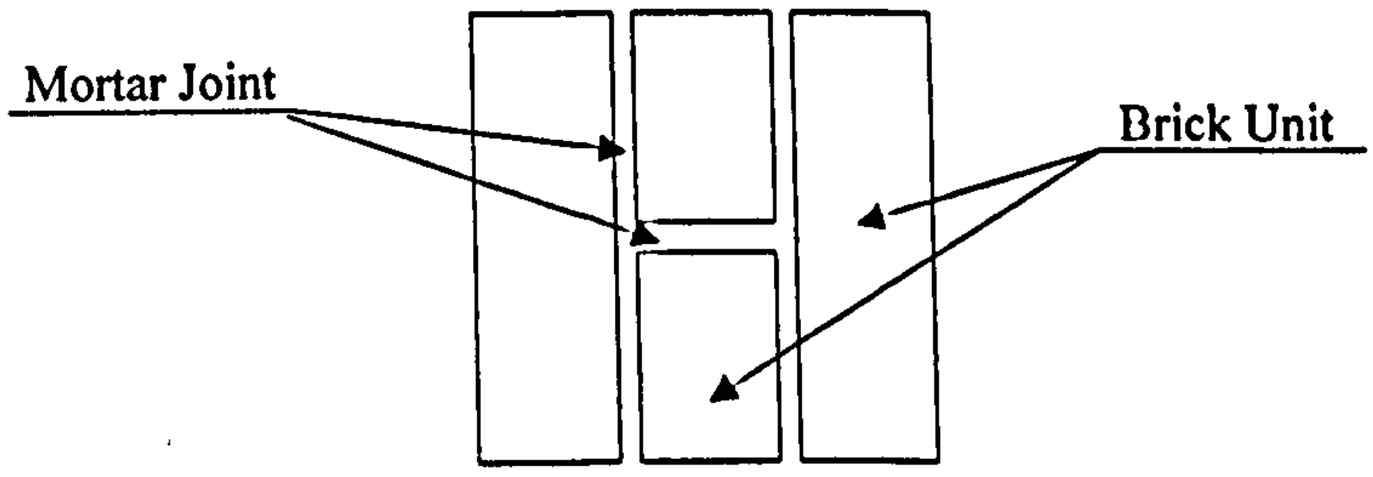

Fig. 3.1 Brickwork Masonry Unit

As shown Fig. 3.2a, the bricks and the mortar are considered as one continuum material. The material properties of the masonry unit may be obtained either by the corresponding brickwork prism tests or by applying the weighted average properties of the bricks and the mortar. The nonlinear behaviour of the masonry unit may be modelled by using such as the Drucker-Prager yield criteria.

In Fig. 3.2b, the bricks and mortar of the masonry unit are considered as two continuum materials. The true material properties of the bricks and the mortar are applied. Either similar or different failure criteria may be used to model the nonlinearities associated with the bricks and mortar.

In Fig. 3.2c, brick and mortar are considered as one material. The joint, whose thickness is assumed to be zero, is modelled by using interface elements (initially maybe coincident). The treatment of the nonlinearity of the material may be similar to that discussed for Fig. 3.2a. With this modelling method, average Poisson's ratio of brickwork prisms may be used to take account of the Poisson's effects. The mortar joints are explicitly ignored but implicitly taken account of in the "average" material properties.

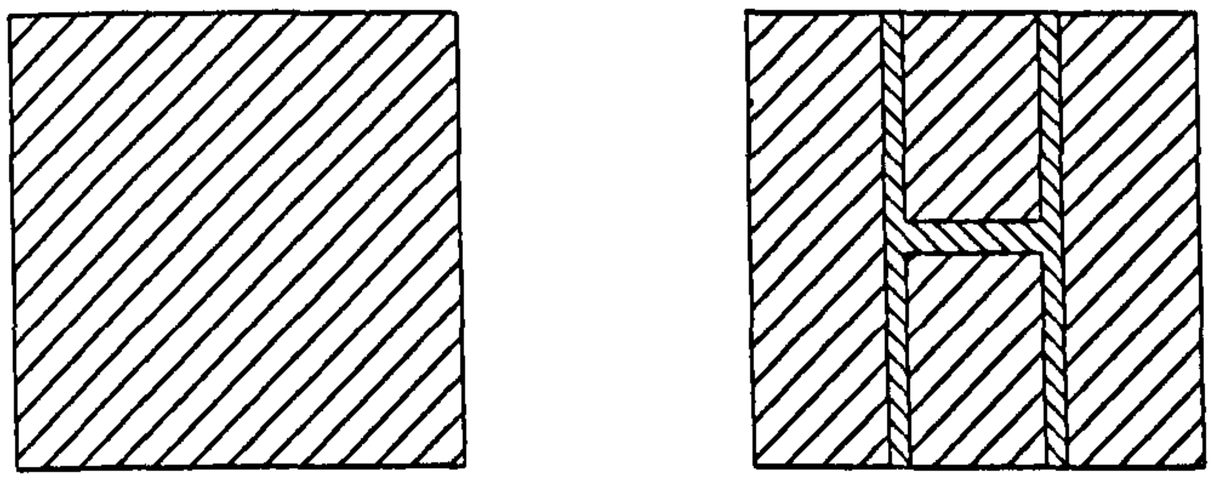

(a) Smeared Model 1 **(b) Smeared Model 2**

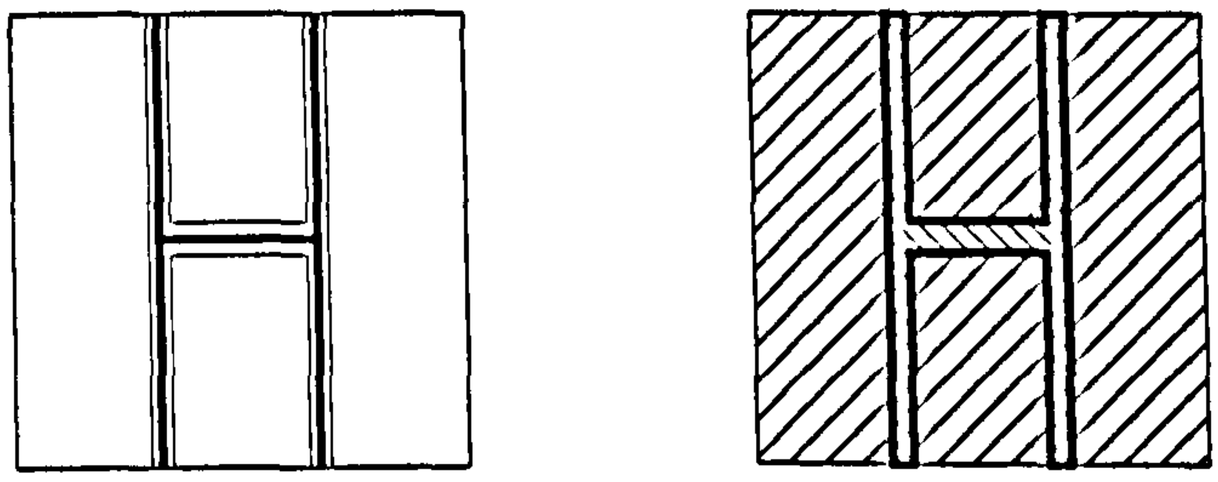

(c) Discrete Model 1 **(d) Discrete Model 2**

Fig. 3.2 Different Modelling Methods Of Brickwork Masonry Unit

In Fig. 3.2d, brick and mortar are considered as two different materials. The joints between the bricks and the mortar are modelled by using interface elements (initially maybe coincident). Such modelling method makes it possible to trace the composite behaviour of the masonry material, but, as a result, the number of the interface elements will be greatly increased. The treatment of the nonlinearity of the material may be similar to that discussed for Fig. 3.2a.

It may be noted that one of the economical approaches to model a brickwork masonry arch may be to treat the material nonlinearity through the application of the smeared modelling method while the discrete modelling approach may be adopted to take into account of the nonlinearity associated with the interfaces between mortar and bricks. For a large masonry arch bridge, special care should be taken if both nonlinearities of the material and the interfaces between mortar and bricks are modelled simultaneously since it greatly increases both human and computer resources required, and possibly create difficulties with convergence.

It should be noted that though the complexity and the difficulties associated with the different methods vary, it may not be necessary to suggest that one method is better or more accurate than another. The success of the modelling of masonry arches using either method largely depends on its application to individual problems; in other words, it depends on whether or not the true conditions and the possible behaviour of a masonry arch is well represented and modelled.

3.2 Smeared Modelling Approach

3.2.1 General

In the present thesis, the FE Package ANSYS was used for the modelling and analysis of the open spandrel brickwork masonry arches. ANSYS is a general-purpose finite element package, and it contains a large number of element types. For a particular problem, an ideal constitutive model or element may not be readily available within the Package. Thus, the challenge remains to choose the best possible element or combination of elements.

Through preliminary modelling and studies, it was concluded that the element (SOLID65), which ANSYS provides to model brittle type of materials such as concrete and rock etc., could be used to model brickwork masonry arches.

The element SOLID65 of ANSYS5.3 is designed to model cracking in tension, crushing in compression and other plastic behaviour of a brittle material. The material modelled is assumed to be a homogeneous continuum, and initially isotropic (ANSYS5.3 Element & Theory References and Willam et al., 1974). It is known that cracking and crushing are most common failure modes of brickwork masonry, and also considerable evidence in the literature could justify brickwork masonry being treated as a homogeneous, brittle and isotropic continuum (Dhanasekar et al., 1985; Pande and Middleton, 1994; Lourenco, and Rots, 1997). Thus, it may be logical to use the element SOLID65 to model the brickwork masonry.

Prior to the application of the SOLID65, it is necessary to introduce the theory that ANSYS 5.3 used for developing this element, and at the same time to study the suitability of adopting such an element to model brickwork masonry. It is not intended to compare the various modelling techniques and the constitutive relations for this element that ANSYS adopted with others, which are also widely used for the modelling of brittle type of materials.

3.2.2 Constitutive Relationships

The element SOLID65 considers a material to behave linearly in compression up to a yield surface. Beyond the yield surface the material is assumed to be either perfectly

plastic or present other material nonlinearities following isotropic hardening rule or Drucker-Prager criterion. In tension, the element behaves linearly up to a limiting tensile strength, at which stage the material cracks and cannot sustain any stress in the direction normal to the cracking plane.

Brickwork masonry presents different response under tension and compression. For uncracked brickwork masonry, several approaches have been used to represent the constitutive relationships, which may be classified into the following two groups: bilinear and parabolic stress-strain relationships. The material tests in the previous chapter shows that, under uniaxial compressive loads, the brickwork masonry largely exhibits linear response up to 85% of the ultimate load. The tests conducted by Page (1982) and Dhanasekar et al. (1985) showed that brickwork masonry exhibits elastic behaviour when it is subjected to either biaxial tension-tension or tension-compression stress state. In other words, the constitutive relationship of brickwork masonry, to some extent, is similar to the concrete stress-strain relationships proposed by Kupfer et al. (1969) and Launay et al. (1972), which were adopted by ANSYS.

The above constitutive relationships have been adopted in the previous analysis of masonry arches. For the material under compression, either bilinear (Choo et al., 1991, and 1995; Crisfield, 1984, 1985a, b, 1988, and 1990) or parabolic (Towler, 1981; Loo, 199; Loo et al., 1995; Choo et al., 1992) stress-strain relationship was used; for the material under tension, a bilinear stress-strain relationship was assumed by Crisfield (1984) and Loo (1991).

In the present analyses, brickwork masonry was assumed to be elastic perfectly plastic behaviour in compression and elastic perfectly brittle behaviour in tension. Therefore, only two elastic constants, Young's modulus E and Poisson's ratio ν are needed to define the material properties at the initial elastic stage.

3.2.3 Material Failure Envelopes

As discussed in Chapter 2, the failure modes of brickwork prisms and arches could be affected by a large number of factors such as variable sizes of bricks and conditions of mortar; loading locations, patterns, and rates, etc. The features common to the failure of

the masonry include tensile cracking and compressive crushing of the masonry material and the sliding between mortar and bricks.

The failure surface adopted by ANSYS for the element SOLID65 is largely based on the experimental results reported by Kupfer et al. (1969) and Launay et al. (1972). The failure criterion due to a multiaxial stress state can be expressed in the form:

$$\frac{F}{f_c} - S \geq 0$$

in which F is a function of principal stress states; S is failure surface expressed in terms of principal stresses and a further five parameters, i.e.

f_t Ultimate uniaxial tensile strength;

f_{cb} Ultimate biaxial compressive strength;

f_1 Ultimate compression strength for a state of biaxial compression superimposed on hydrostatic stress (σ_h) state;

f_2 Ultimate compression strength for a state of uniaxial compression superimposed on hydrostatic stress (σ_h) state; and

f_c Uniaxial crushing strength.

If a hydrostatic stress is low enough ($\leq \sqrt{3}\, f_c$), the above failure surface may be specified using only two constants uniaxial tensile strength and uniaxial crushing strength (ANSYS5.3 Theory References and Willam et al., 1974).

If the above equation is not satisfied, there is no attendant cracking or crushing of the material. Otherwise, the material will crack if any principal stress is tensile, while crushing will occur if all principal stresses are compressive.

The failure of the material is categorised into four domains:

- $0 \geq \sigma_1 \geq \sigma_2 \geq \sigma_3$ (compression - compression - compression)
- $\sigma_1 \geq 0 \geq \sigma_2 \geq \sigma_3$ (tensile - compression - compression)

- $\sigma_1 \geq \sigma_2 \geq 0 \geq \sigma_3$ (tensile - tensile - compression)
- $\sigma_1 \geq \sigma_2 \geq \sigma_3 \geq 0$ (tensile - tensile - tensile)

In each domain, independent functions describe F and the failure surface S. The details of the F and S functions for each domain may be found elsewhere (Willam and Warnke, 1975).

Fig. 3.3 shows the failure surface for tensile and compressive failures in biaxial or nearly biaxial failure envelopes. If the most significant non-zero principal stresses are in the σ_1 and σ_2 directions, the three surfaces presented are for σ_3 slightly greater than zero, σ_3 equal to zero, and σ_3 slightly less than zero. It may be seen that crushing failure of materials may occur when all principal stresses are compressive, and cracking failure of materials may occur if any principal stresses are tensile. Also, for the tensile failure, considering one principal stress direction the tensile strength of the material in this direction does not change with the introduction of a tensile stress in the other principal stress direction, but a compressive stress decreases this strength.

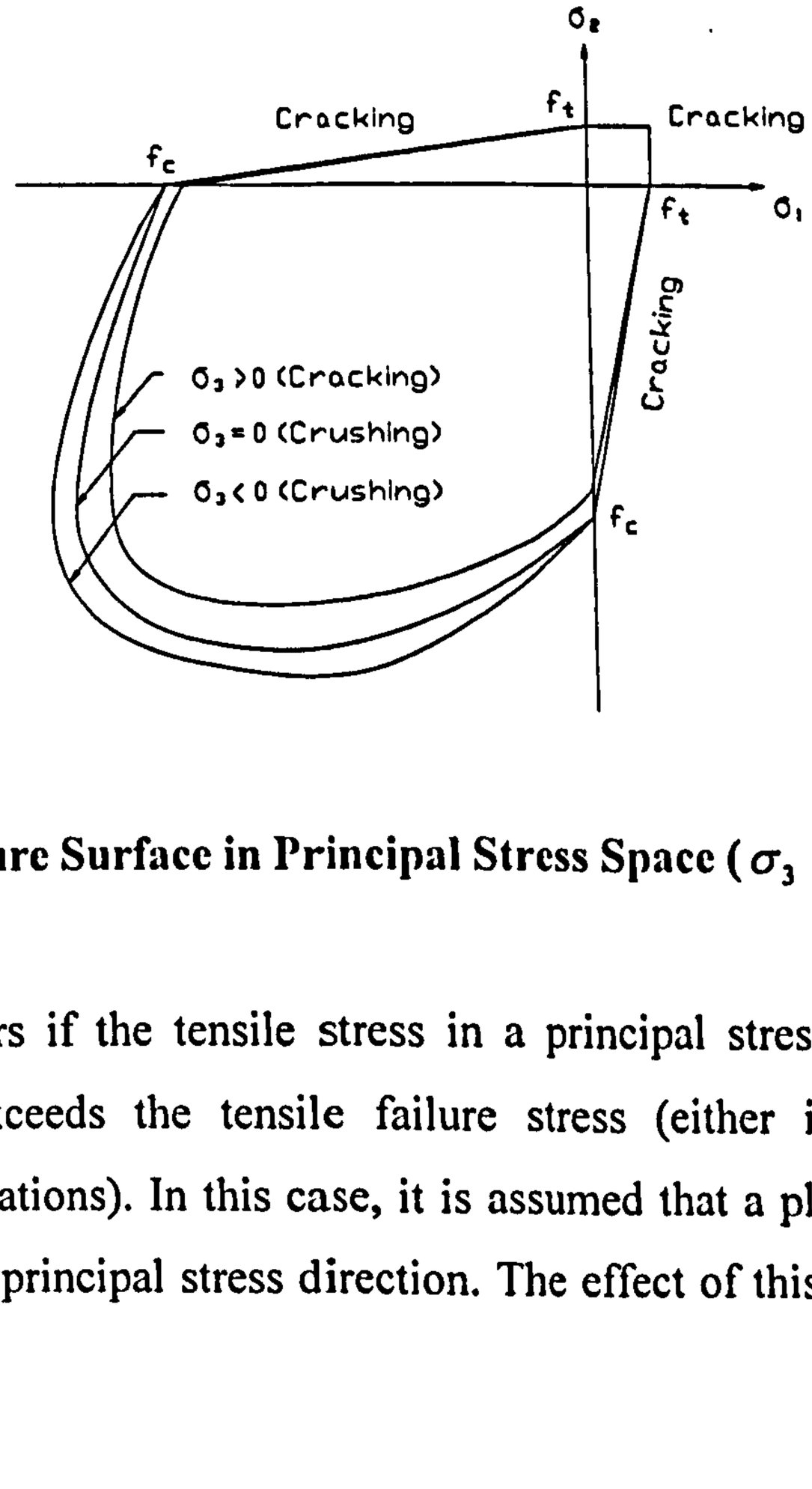

Fig. 3.3 Failure Surface in Principal Stress Space (σ_3 Close to Zero)

Tensile failure occurs if the tensile stress in a principal stress direction at a Gauss integration point exceeds the tensile failure stress (either in tension or tension-compression combinations). In this case, it is assumed that a plane of failure develops perpendicular to the principal stress direction. The effect of this material failure is that

the normal stiffness and the corresponding normal stress are reduced to be negligible, and the shear stiffness and the corresponding shear stress across the plane of failure are also reduced to be a level depending on shear transfer coefficient used. This is achieved by modifying the Young's modulus normal to the tensile failure plane and the shear modulus across the failure plane. The unbalanced forces are distributed throughout the surrounding zones.

3.2.4 Post-Tensile Cracking Behaviour

To simulate the post-failure behaviour caused by cracking, it is assumed that the masonry material may lose its stress components in the direction normal to the crack plane, but the stiffness and stress in other directions are still retained.

Once a tensile plane of failure has formed, it is checked in each subsequent solution step whether the failure is still active. The failure is considered to be inactive provided the normal strain across the plane becomes negative and less than the strain at which the ' last ' failure occurred, and otherwise it is active. Therefore, a tensile failure plane may repeatedly be active and inactive.

If a tensile failure plane has developed, which may or may not be active, the material stress-strain relationships are established corresponding to the principal stress directions in the failure plane and the direction perpendicular to this plane. Hence, instead of using the principal stresses and corresponding directions as done for the uncracked material, the stress conditions along and normal to the material tensile failure plane are used to evaluate the stress-strain matrix. Also, when a failure plane is or was active, a subsequent failure plane is assumed to form perpendicular to the direction of the one that developed first, once a normal stress along the original failure plane has reached the tensile failure stress. It follows that at any integration point, the direction of the third tensile failure plane is fixed once failure has occurred in two directions. After the solution converges to the cracked state, the modulus normal to the crack face is set to zero. Thus, the stiffness is zero normal to the crack face.

Since a smeared crack representation is employed to simulate brickwork masonry cracking, it is assumed that the crack effects is distributed within the domain of the

volume. The masonry becomes anisotropic, and the direction of the crack determines the main directions of anisotropy.

As discussed above, the presence of a crack at an integration point is represented through modification of the stress - strain relations by introducing a plane of weakness in a direction normal to the cracking face. Also, a shear transfer coefficient is introduced at the integration point across the failure plane to represents a shear reduction for subsequent loading. It should be noted this coefficient is clearly associated with the notion of 'aggregate interlock' for concrete material, and should be kept minimum for brickwork masonry.

If a crack closes, then all compressive stresses normal to the crack plane are transmitted across the crack and only a shear strength reduction factor for a closed crack is introduced. The total of six different stress - strain relations is applied for a material that had cracked in one direction only and where the cracks have re-closed, and in two directions and both cracks re-closed, and in all three directions and all three cracks re-closed. Sixteen possible combinations of crack arrangement and appropriate changes in stress - strain relationships are considered.

The open or closed status of integration point cracking is based on the value of the crack strain ε_{ck}^{ck}. For the case of a possible crack in the x direction, the strain ε_{ck}^{ck} is evaluated as:

$$\begin{cases} \varepsilon_x^{ck} + \dfrac{\nu}{1-\nu}(\varepsilon_y^{ck} + \varepsilon_z^{ck}) & \text{if no cracking has occurred;} \\ \varepsilon_x^{ck} + \nu\varepsilon_z^{ck} & \text{if y direction has cracked;} \\ \varepsilon_x^{ck} & \text{if y and z directions have cracked.} \end{cases}$$

In which ε_x^{ck}, ε_y^{ck}, and ε_z^{ck} = three normal component strains in crack orientation.

The vector $\{\varepsilon^{ck}\}$ is computed based on the modified total strain.

If ε_{ck}^{ck} is less than zero, the associated crack is assumed to be closed.

If ε_{ck}^{ck} is great than or equal to zero, the associated crack is assumed to be open for the next iteration.

When cracking first occurs at an integration point, the crack is assumed to be open for the next iteration.

The points of crack initiation will depend upon the relative strengths of the cohesive bonds and the local state of stress. The cracking may initiate within joint mortar or at the interfaces between the brick units and mortar. If the cracking initiates within the joint mortar, as the load is increased, the cracking propagates until it reaches the interface between the brick unit and mortar, and then it may extend along the interface until a hinge is formed. It may not be possible for the cracking to propagate within the mortar until a hinge is formed. As the cracking extends, the compressive area of the mortar decreases, which will eventually result in the crushing failure of the mortar due to its low compressive strength.

However, the cracking will normally be confined within the joint.

For visualization, the 'plane of tensile failure' is referred to 'crack', but one should interpret this terminology judiciously because a physical crack does not actually develop at the element integration point. Instead, the material has failed in one principal stress direction.

3.2.5 Post-Compression Crushing Behaviour

If the brickwork masonry at an integration point fails in uniaxial, biaxial, or triaxial compression, the material is assumed to crush at that point. Under conditions where crushing has occurred, material strength is assumed to have degraded to an extent such that the contribution to the stiffness of an element at the integration point in question can be ignored.

3.2.6 Smeared Modelling Of The OSBMAB

The element SOLID65 with $2 \times 2 \times 2$ Gauss integration points was adopted for the modelling of the three models arches OSMA2, OSMA3 and OSMA4. It may be noted that this type of element, rather than higher order elements (say, twenty-node), may be

sufficient in terms of both accuracy and flexibility, as pointed out by Zienkiewicz et al. (1971) "... 2 × 2 × 2 integration point mesh leads to displacements that are within a few percentage points of the theoretically derived displacements".

Typical finite element meshing of the three models is as shown in Figs. 3.4 – 3.6.

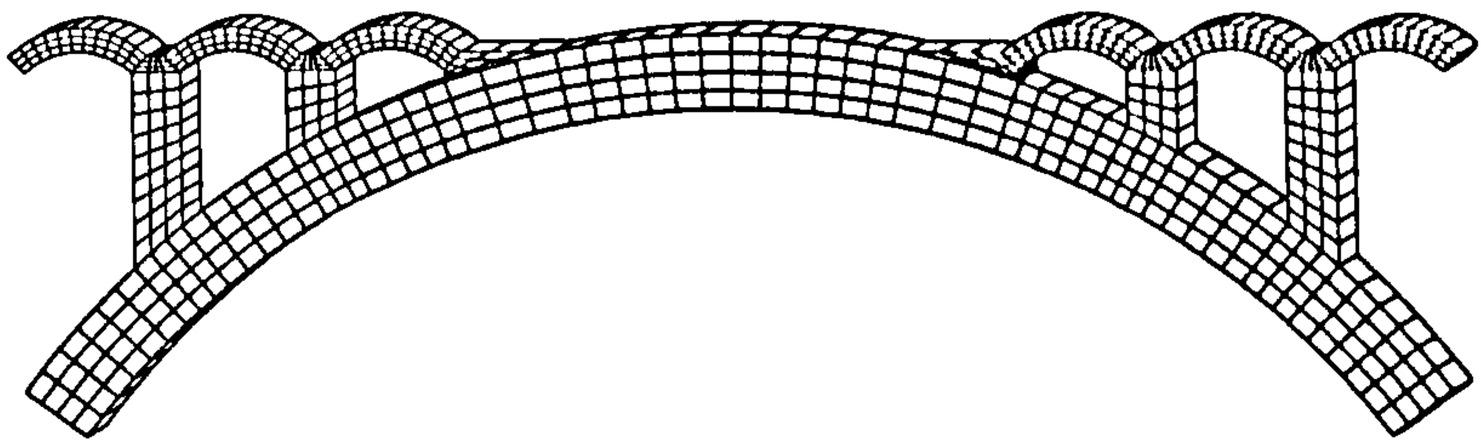

Fig. 3.4 Smeared FE Model of OSMA2

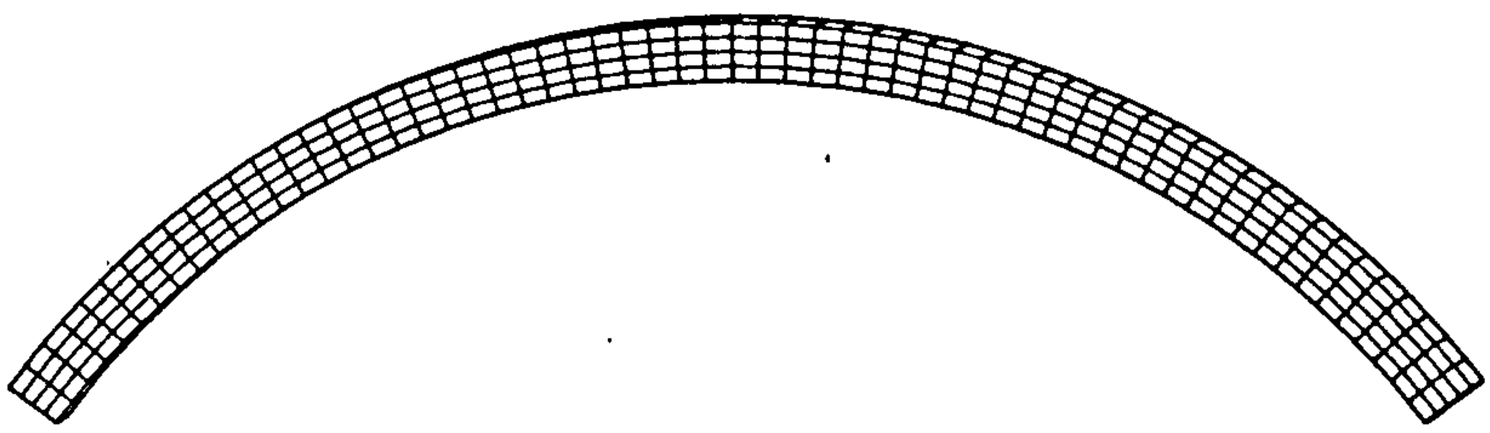

Fig. 3.5 Smeared FE Model of OSMA4

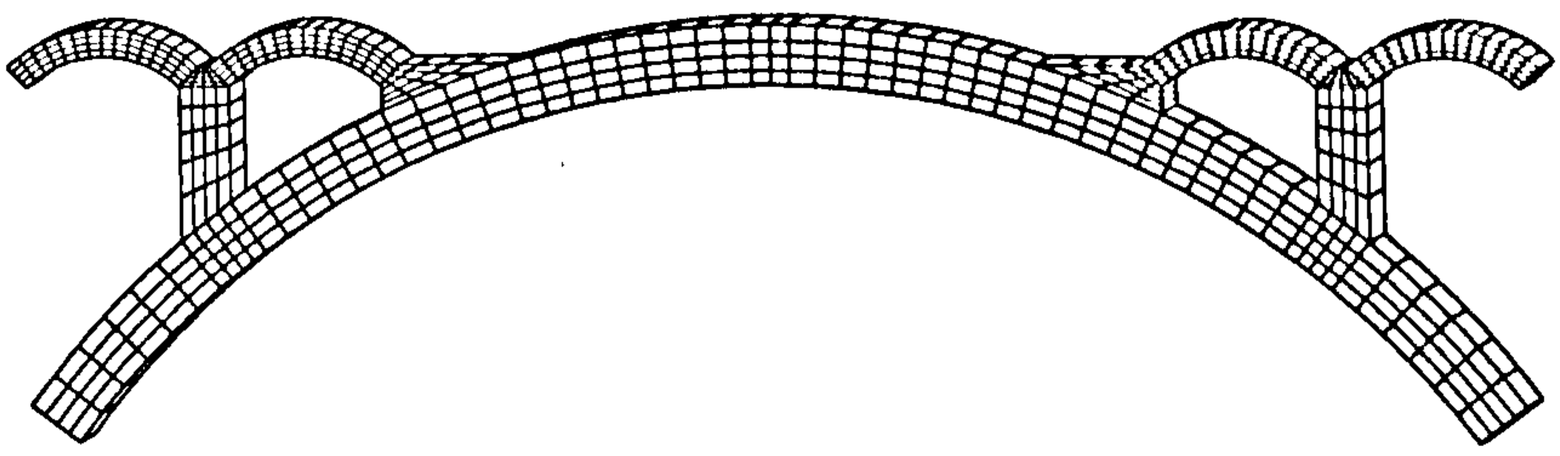

Fig. 3.6 Smeared FE Model of OSMA3

Due to the three-dimensional nature of the element SOLID65, three-dimensional models were created for the three arches. For simplicity and computing efficiency, only one layer of elements were generated along the width of the models considering that the models behaved largely in one plane. That is, "plane stress" condition was assumed. The effects of the numbers of the layers of the elements along the width of the model arches

were studied, and the results were presented in Chapter5. In order to study the mode of failure, a minimum three elements must be created along the thickness of main arch and spandrel arches, and along the width of spandrel piers. A large number of elements were generally created within the regions of loading and possible failure zones of either cracking or crushing.

As described above, the cracking and crushing conditions were checked at the integration points of elements at each increment of load. Thus, for the modelling of the model brickwork masonry arches tested, the boundary conditions of both main arch and spandrel arches may be simply assumed fixed provided that the sizes of elements are reasonably small. Cracks may occur with the elements adjacent to the boundaries if the failure criteria are satisfied. In this case, 'hinges' are assumed being developed at the springings of the arches associated with these boundaries.

As discussed in Chapter 2, a number of basic rules were followed to build the model arches: (a) both the main arch and the spandrel arches are segmental; (b) the sizes and the slopes of the top of the spandrel piers are just sufficient to accommodate the springings of the spandrel arches; and (c) the crowns of the main arch and the spandrel arches are in the same level. Therefore, once the dimensions of the main arch and the superstructures are defined, the geometry of the open spandrel model arches can be readily defined numerically.

Let spma be the span of main arch; let rsma be the rise; let tkma be the thickness. Let spsa be the span of spandrel arches (the same span is assumed for all spandrel arches); let rssa be the rise; let tksa be the thickness. Let wtsp be the width of spandrel piers; and let wtab be the width (or depth) of model arch. Thus,

The internal radius of main arch is:	rima=(spma**2+4*rsma**2)/(8*rsma);
The external radius of main arch is:	rema=rima+tkma);
The internal radius of spandrel arches is:	risa=(spsa**2+4*rssa**2)/(8*rssa);
Half of the central angle of main arch is:	$\tan^{-1}$ (0.5*spma/(rima-rsma));
Half of the central angle of spandrel arch is:	$\tan^{-1}$ (0.5*spsa/(risa-rssa)); etc.

The locations (or coordinates) of the intersection points, and the crowns of main arch and spandrel arches could then be determined based on the above primary and other derived parameters. In the case of the model OSMA3, one global Cartesian, and five local cylindrical coordinate systems, i.e., one for the main arch, and the rest for the four spandrel arches, respectively, were used for the calculation of the coordinates. The adoption of the local coordinate systems was not only for readily locating the coordinates, but also for facilitating the application of boundary conditions, and for efficiently reviewing the results during the post-processor session. Due to the symmetry of the model arch, only the coordinates of the points at one side of the arch were calculated, and those at the other side were mirrored.

This 'parametric' method of the creation of the finite element model in terms of both the geometry and the control of mesh sizes is efficient for a structure with relatively complex geometry like the one being discussed. The change in the values of any parameters will result in the change of the others accordingly, which makes it effective to carry out parametric studies relating to the geometry of the arch. Also, the model that is created parametrically may check its own feasibility as a structure. In other words, if 'incompatible' parameters of the geometry of the arch are given, the model (or the input codes) will immediately issue a warning that the input parameters are not compatible, and an open spandrel model arch cannot be built following the rules of the above (a), (b) or (c).

3.3 Discrete Modelling Approach

3.3.1 General

The nature of brickwork masonry and the failure modes observed during the model tests of open spandrel arches might indicate the potential applications of interface solutions of finite element methods. The masonry arches are made up of individual bodies (bricks or mortar) connected together. Failure of masonry arches may be caused by the separation or contact and/or relative movements of the connected bodies along the interfaces. In other words, the model arches may be assumed to be made up of discrete bodies, which are linked together at the interfaces. The individual bodies would be separated once the normal bond strength at the interfaces are exceeded, and they would slide in relative tangential directions once the shear bond strength and Coulomb friction at the interfaces are exceeded.

The formation of a discrete crack is a problem of changing geometry. Therefore it makes sense to change the geometry rather than the material properties as the cracking develops. As an interface forms, a graphical representation of the geometrical discontinuity represented by the interface is automatically obtained by the altered mesh.

Because mortar joints are weak in tension and shear, it is reasonable to assume that cracking will occur when the tensile stresses normal to the interfaces exceed the normal strength of bonds, and slip will occur when the shear stresses at the interfaces exceed the tangential strength of the bond plus the friction.

Prior to the application of the discrete modelling method, it is necessary to briefly discuss the formation of the interface problems and solving schemes using finite element methods.

The first interface element was formed in the analysis of rock joints (Goodman et al., 1968). Since then, a variety of interface elements have been developed, including node to node/segment and node to surface elements for one-, two- or three-dimensional analysis. The interfaces may be between flexible bodies or between rigid and flexible bodies.

The behaviour of a structure involving interfaces is generally non-linear. The nonlinearities occur when two or more components come into or out of contact with each other or slide relative to one another during the course of the deformation process. It is because one or both of the following are unknown: (a) the contacting (or separating) areas; and (b) the normal and tangential forces transmitted. The interface problems may also be a severe nonlinearity since the analysis may experience an abrupt change when areas make or break contact.

3.3.2 Formation of Interface problems

Consider two bodies A and B, as shown in Fig.3.7 (a), prior to contact. The two bodies are brought into contact by a combination of the forces applied on boundary Γ_t and the displacement prescribed on boundary Γ_u respectively.

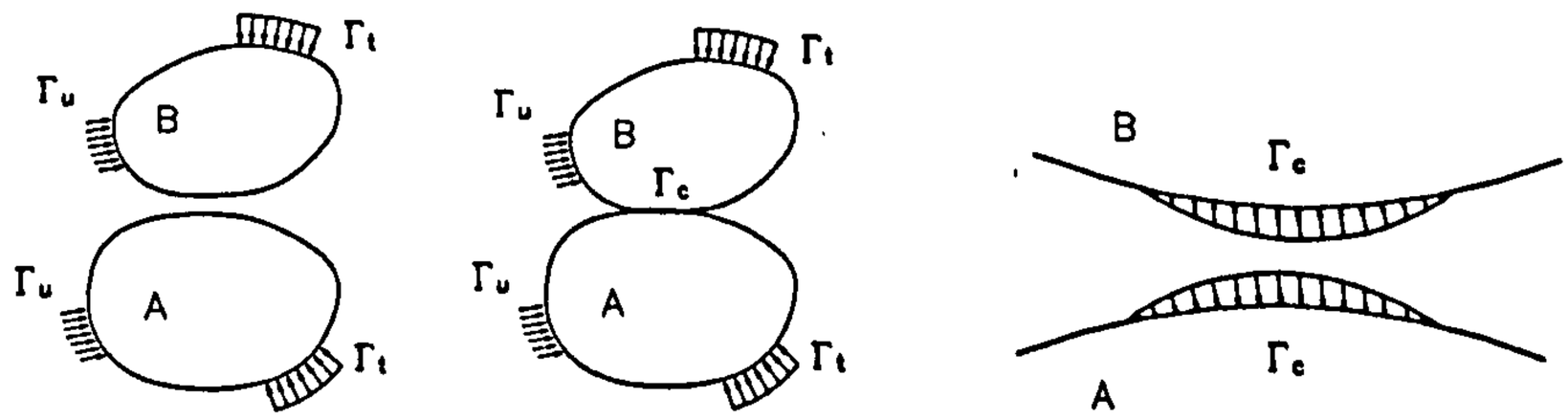

(a) Prior to Contact (b) Contact (c) Forces at The Region of Contact

Fig. 3.7 Formation of Interface Problems

It is assumed that A is called as target body, and B as contact body. On the application of loads (forces and/or displacements), the two bodies come into contact as shown in Fig. 3.7(b). Contact forces develop in the contact region Γ_c and as shown in Fig. 3.7(c).

On certain discretization through a finite element mesh, the contact conditions can be geometrically divided into two categories: node-to-node contact and node-to-segment contact as shown in Fig. 3.8 (a), (b) respectively.

(a) Contact conditions for node-to-node

Considering a generic pair of a contact (or slave) node *i* at the contact surface of the

contact body B and target (or master) node *k* at the target surface of target body A, a local coordinate system n, t along the normal direction and the tangential direction of the target surface at the node k is established. The contact forces and displacements at the nodes *i* and *k* as shown in Fig. 3.8a, where,

r_{ni}, r_{ti} = contact forces at the node *i* in the local coordinate system;

r_{nk}, r_{tk} = contact forces at the node *k* in the local coordinate system;

u_{ni}, u_{ti} = displacements at the node *i* in the local coordinate system;

u_{nk}, u_{tk} = at the node *k* in the local coordinate system.

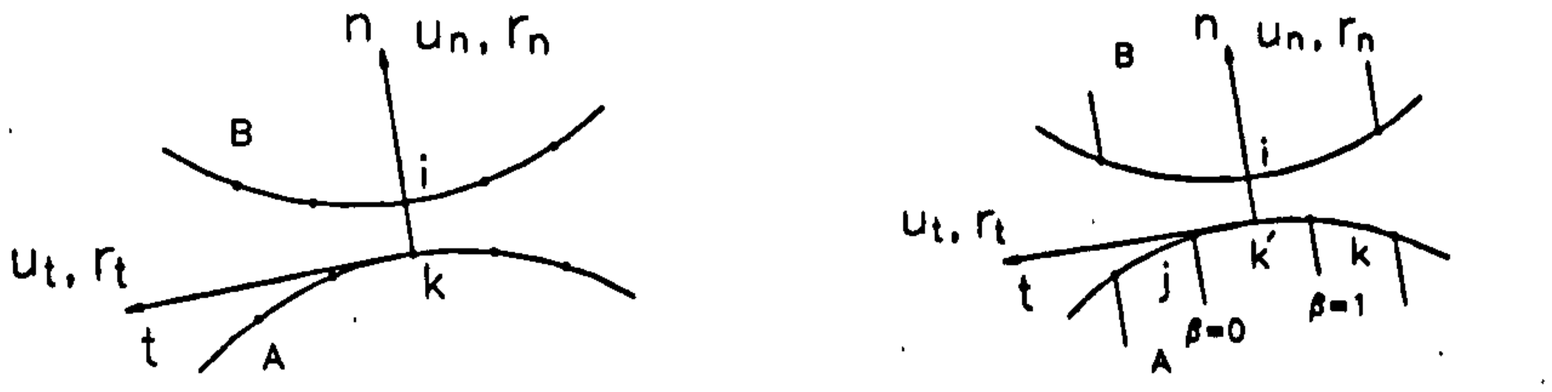

(a) Node-to-Node **(b) Node-to-Segment**

Fig. 3.8 two-dimensional Contact Elements

(b) Contact conditions for node-to- segment

In the node-to-segment contact condition, the node *i* at the contact surface will contact with an assumed node *k'* at the segment formed by the nodes *j* and *k* (for linear element). The contact forces and the displacements at the node *k'* can be obtained through interpolation.

In the present analysis, the behaviour at the interfaces of the model arch was modelled using the node-to- segment element CONTAC48 of ANSYS5.3.

3.3.3 Solution Methods For Interface Problems

It may be noted that the finite element modelling of interface problems has been a comparatively recent development, and a large number of papers have appeared offering a variety of numerical approaches. Essentially all the methods attempt to prevent overlapping of the finite element meshes and to give a satisfactory stress distribution over the contact regions.

In the context of finite element analysis, the methods of contact force calculation can be divided mainly into two categories: (a) penalty method (Stadter et al., 1979 and Ostachowicz, 1984); (b) Lagrange multiplier method (Hughes et al. 1976, Bathe et al. 1985 and Pascoe et al. 1988). Penalty method modifies the stiffness matrix by adding a large term (or large stiffness of spring) to prevent too much penetration (a "penalty"). Higher the stiffness ("penalty"), the less penetration becomes (or more realistic it will be), and more difficult to achieve a converged solution. Lagrangian multiplier method, on the other hand, augments the stiffness matrix by adding extra degree of freedom terms to reconcile the contact.

For either penalty method or Lagrange multiplier method, ANSYS5.3 adopts pinball and pseudo element algorithms to firstly detect whether the penetration has occurred; and if yes, to associate a single target to each contact node. The radius of the pinball is internally fixed to be 50% greater than the distance between the target nodes (in the case of two dimensional interface problems), and between the two target diagonals (in the case of three dimensional interface problems). If a contact node is inside the pinball, contact occurs; otherwise separation occurs irrespective of whether separation or over-penetration has occurred.

The pinball and pseudo element algorithms provide a one-to-one mapping between a contact node and a target. The penetration is represented by the magnitude of the gap (g) and is a violation of compatibility. In order to satisfy contact compatibility, forces are developed in a direction normal to the target that tend to reduce the penetration to an acceptable numerical level. In addition to compatibility forces, friction forces are developed in a direction that is tangent to the target plane.

3.3.4 Friction in Interface problems

Frictional phenomena may need to be considered when the tangential part of a motion is important in the response of two or more bodies becoming separated or coming into contact. Because of its microscopic nature, friction cannot be modelled adequately in numerical analysis of macroscopic model arch testing process. The frictional resistance to sliding is therefore simulated by assuming mathematical relationships between stresses and other variables, which describe contact of friction conditions. These

relationships can be derived from the micro-mechanical models of friction and then incorporated into an appropriate constitutive theory. Generally, the following two models are used to simulate the effects of friction (an extensive overview was given by Oden et al., in 1985):-

- Rigid friction model: Once sliding force exceeds the limit, the contact interfaces are continuously sliding relative to one another, in which the resisting force against sliding is equal to the limit, and the direction of the force always opposes the motion. In this case, neither 'stuck' nor 'non-sliding configuration' is allowed;
- Flexible friction model: This model allows both sticking and sliding conditions. The sticking zone is treated as an elastic zone with tangent sticking stiffness. The contact interfaces will deform tangentially if there is a sliding force applied. If the sliding force is less than the limit, then this motion is elastic and when the force is removed, the contact interfaces will return to their original tangential location. When the sliding force exceeds the limit, the surfaces will slide.

For the flexible friction model (Coulomb friction law), the tangential displacement of the contact node relative to the target is decomposed into elastic (or sticking) and sliding (inelastic) components. It may be noted that the nature of the friction forces developed during contact is complex and is affected by a number of factors; the characteristics of the interface, the response of the interface to normal forces, roughness of the contact surfaces, history of loading, and general failure of the interface materials, and so on.

For Mohr-Coulomb type failure, a simplified failure criterion, which ignores the initial bond strength, is generally used. As discussed in chapter two, the results of the shear tests of brickwork masonry showed the existence of such initial bonds between bricks and mortar. Therefore, a full failure criterion including the effects of initial bond strength was adopted in the present analysis.

It should be noted that, by the classical assumptions of the frictional law, a body slides when the maximum shear force is reached. In reality, however, bodies show tangential microdisplacements with the contact area before the sliding process starts (Wriggers, 1990). It has been found that the relation between the tangential force and the micro-

displacement is slightly nonlinear in the presliding phase (Woo et al., 1980), linear when sticking, and nonlinear (plastic) when initial sliding. This is similar to those discussed in the theory of elasto-plasticity. Inspired by the resemblance that exists between plastic and frictional phenomena, a number of plasticity theories of friction have been proposed (Fredriksson, 1976; Michalowski et al., 1978; Rodic et al., 1989). By analogy with plasticity, these theories generally rest upon four basic principles: (a) decomposition of the contact distance into adherence and slip (cf. decomposition of the strain into elastic and plastic parts); (b) laws of adherence; (c) slip criterion (cf. yield criterion); and (d) slip rules (cf. flow rules)

3.3.5 Initial Bond Simulation

All the contact elements of ANSYS5.3 are unable to take any tension. That is, if there is any tension developed within the interfaces, the connected bodies would fly away, and the analysis would immediately stop due to excessive displacements. This may be acceptable in the case of single arch alone, in which a reasonable high ultimate load may be predicted based on no tension allowed. However, to accurately model the open spandrel brickwork masonry arch, the tension within the masonry must be taken into account. This is partly because the real existence of bond strength between bricks and mortar, and more importantly, partly because the tension would inevitable develop within spandrel arches at a low level of loads. If the bond strength within brickwork masonry is not accounted for, the model will be likely to fail at a fictitious low load.

ANSYS5.3 does not provide any elements that are explicitly used to model the phenomenon of initial bonds. However, by adjusting the input parameters associated with the nonlinear spring element COMBIN40, it could be used to model the initial bond strength of brickwork masonry both in normal and in tangential directions. Fig. 3.9 shows the application of element COMBIN40 in the modelling of initial bonds. The element is assumed composed of a master spring (1) and a slave spring (2), and a gap (maybe closed initially).

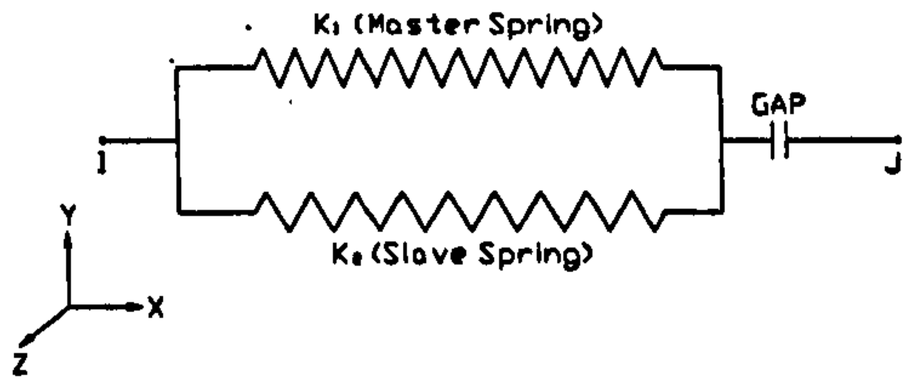

Fig. 3.9 Nonlinear Spring Element

The element itself is essentially one-dimensional. The combination of three such elements, however, may be used to model the three-dimensional effects. Once the tensile or frictional force exceeds the prescribed limit, i.e., the initial bond strength of the brickwork masonry in the direction concerned, the reaction force within the master spring will drop to zero. This indicates that the cohesion between the adjacent bodies (more clearly, between brick and mortar) is broken down, or the initial bond strength between the fill and the arch is lost. To maintain the numerical stability of the analysis after the failure of the master spring, the slave spring of arbitrary low stiffness parallel to the master spring is employed as a 'construct' element.

The element stiffness matrix is:

$$[Ke] = k\begin{bmatrix} 1 & -1 \\ -1 & 1 \end{bmatrix}$$

Where, $k = \begin{cases} k_1 + k_2 & \text{if the force limit was not exceeded in previous iteration;} \\ k_2 & \text{if the force limit was exceeded in previous iteration.} \end{cases}$

The load vector is:

$$\{F_e\} = (F_1 + F_2)\begin{Bmatrix} -1 \\ 1 \end{Bmatrix}$$

The forces of F_1 and F_2 are defined as follows:

(a) If the gap is open,

$F_1 + F_2 = 0.0$

If no sliding has taken place (or if the force limit has not exceeded), $F_1 = F_2 = 0.0$.

However, if sliding has taken place during unidirectional motion,

$F_1 = \dfrac{u_s k_1 k_2}{k_1 + k_2}$ where u_s = amount of sliding;

and thus, $F_1 = - F_2$

(b) If the gap is closed and the slider is sliding

$F_1 = \pm F_s$, and

$F_2 = K_2 u_2$

where $u_2 = u_J - u_I + u_{gap}$;

(c) If the gap is closed and the slider is not sliding, but had slid before,

$F_1 = \pm F_1 u_1$

And $F_2 = K_2 u_2$

Where, $u_1 = u_2 - u_s$

F_1 = force in spring 1;

F_2 = force in spring 2;

k_1 = stiffness of spring 1;

k_2 = stiffness of spring 2;

u_{gap} = initial gap size;

u_I = displacement at node I;

u_J = displacement at node J;

Fs = force required in spring 1 to cause sliding.

The force-deflection relationship under initial loading is as shown in Fig. 3.10. It may be noted that a positive or negative infinitesimal gap may be initially given in an analysis.

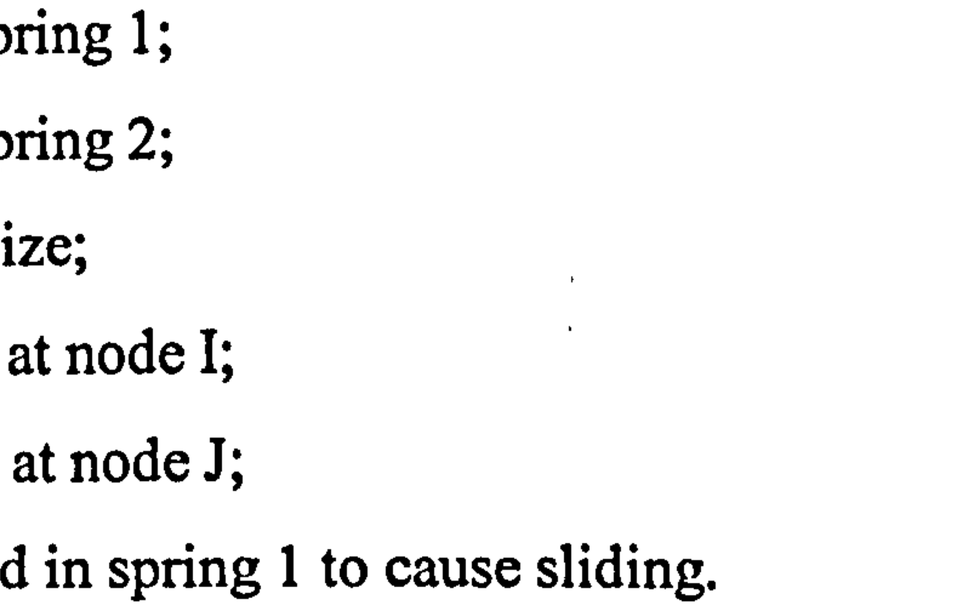

Fig. 3.10 Force-Deflection Relationship In Spring Elements

3.3.6 Discrete Modelling Of The OSBMAB

To develop a discrete finite element model of an arch, one has to prescribe discrete bodies and potential interfaces to capture the behaviour of the arch under various loading conditions. Ideally, interfaces may be placed at any locations where failure may occur. That is, for an open spandrel brickwork masonry arch, the interface elements may be placed at all brick-mortar joints in order to capture any failures at those locations. However, since there are a large number of brick-mortar joints within the open spandrel arch, it will be difficult to locate interfaces at all the joints, and the resources required to solve the problem will be significantly increased. Thus, it is sensible to prescribe the interfaces at the locations where the behaviour of the arch can be simulated at the loading conditions concerned.

To demonstrate the application of the discrete finite element modelling techniques in the analysis of the open spandrel brickwork masonry model arches tested, two of the five model arches (OSMA3 and OSMA4) were modelled and analysed.

The first model is a single arch (OSMA4). The interface elements (combination of contact and nonlinear spring elements) were used to simulate the behaviour up to failure. Depending on the accuracy required, potential failure sections might be modelled in the following two ways: masonry – mortar - masonry or masonry – masonry. The former assumed that an arch consists of a series of masonry units connected by mortar joints of certain thickness. Interface elements were prescribed at both sides of mortar joints as shown in Fig. 3.11. One of the advantages using this modelling method is that the effects of the properties of mortar such as thickness and strength on the behaviour of the arch may be studied. The latter assumes that an arch consists of a series of masonry units connected by joints without thickness as shown in Fig. 3.11(c).

The second model is an open spandrel arch without fill (OSMA3). The locations of the potential failure sections were determined largely based on those occurred during the model test. Since possible shear failure may take place at the interfaces between the bottom of the arch and the main arch, interface elements were also used in these areas. As Fig. 3.12 shows, a total of twenty-nine interfaces are assumed.

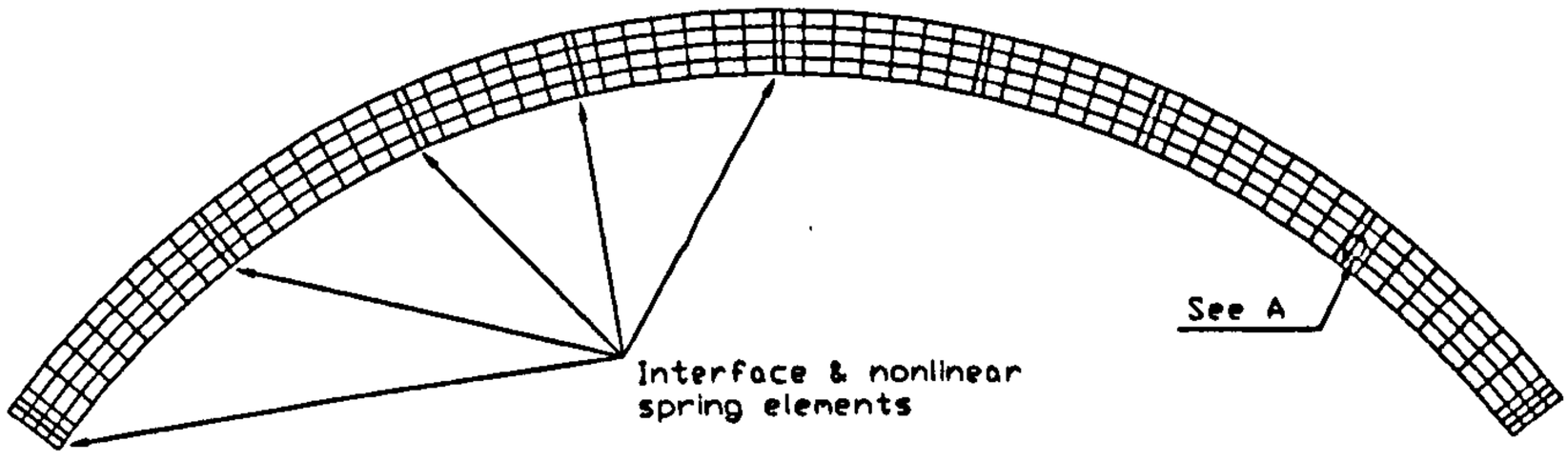

(a) Overview Of Discrete FE Model of OSMA4

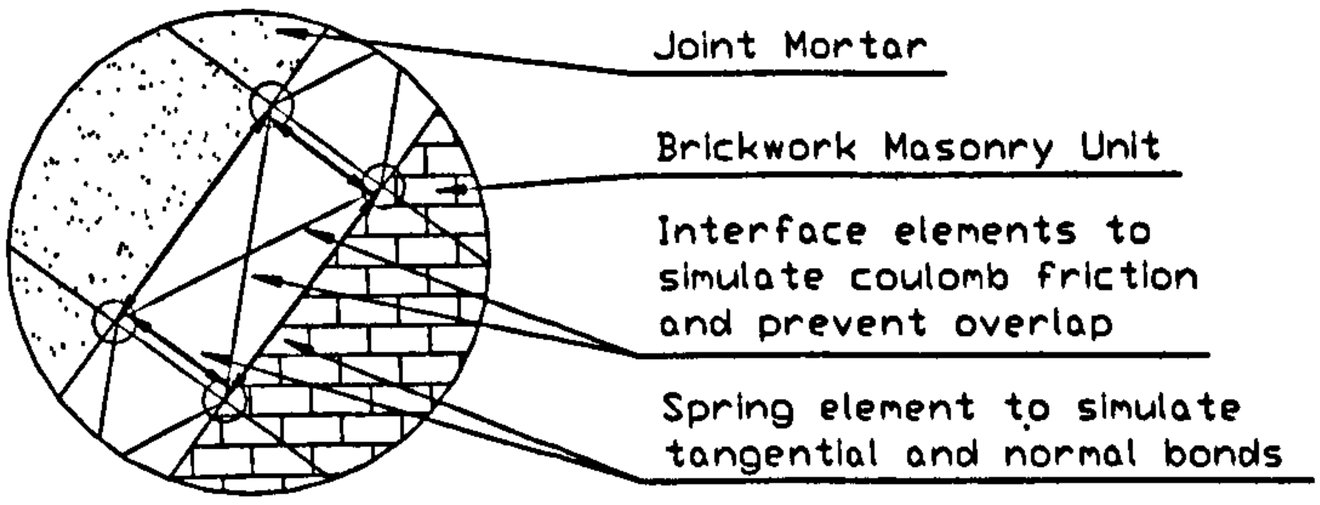

(b) Detailed A

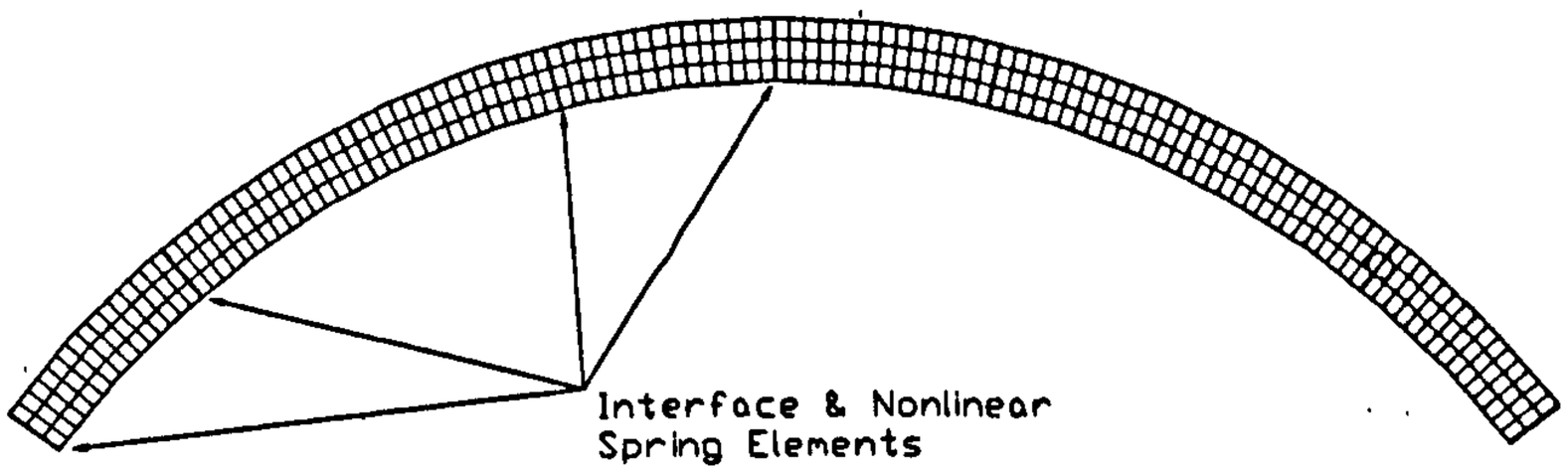

(c) Simplified Discrete FE Model of OSMA4

Fig. 3.11 Discrete FE Model of OSMA4

In the model, both the local failure and the global failure may be predicted. For the superstructures, three interfaces were prescribed within each spandrel arch, and one was prescribed within the spandrel pier. For the main arch, a total of thirteen interfaces were placed along the arch ring.

On the other hand, eight of the interfaces might be considered to act as 'control interfaces'. By changing their location, additional information (such as the effects on the load capacity or the mode of failure) on the structure could be obtained. These control interfaces, as Fig. 3.12 shows, were placed near the springings of both the main arch and

the end spandrel arches, near the bottom of the spandrel piers, and near the crown of the main arch. One of the other benefits from placing the interfaces near the springings was to prevent the solution from possible divergence caused by the boundary conditions where if either flexible-flexible or flexible-rigid interface elements were used. The model was numerically created, where the change in the value of one parameter would cause other related parameters to be changed accordingly.

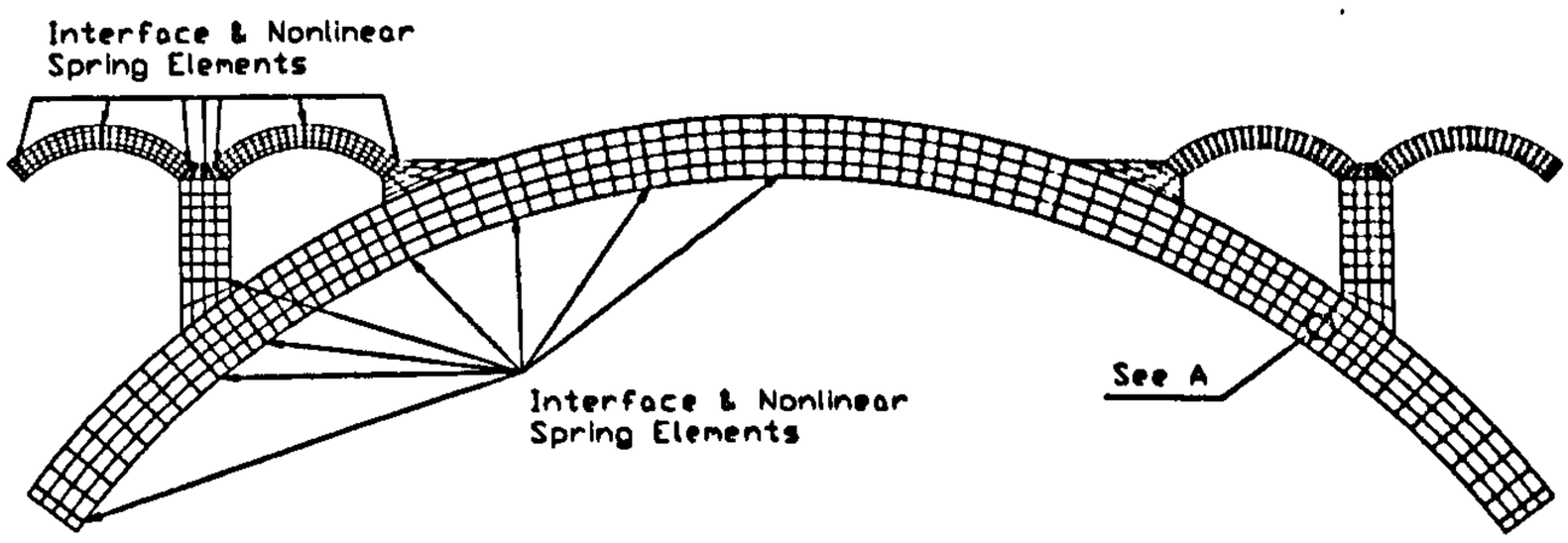

(a) Overview Of Discrete FE Model of OSMA3

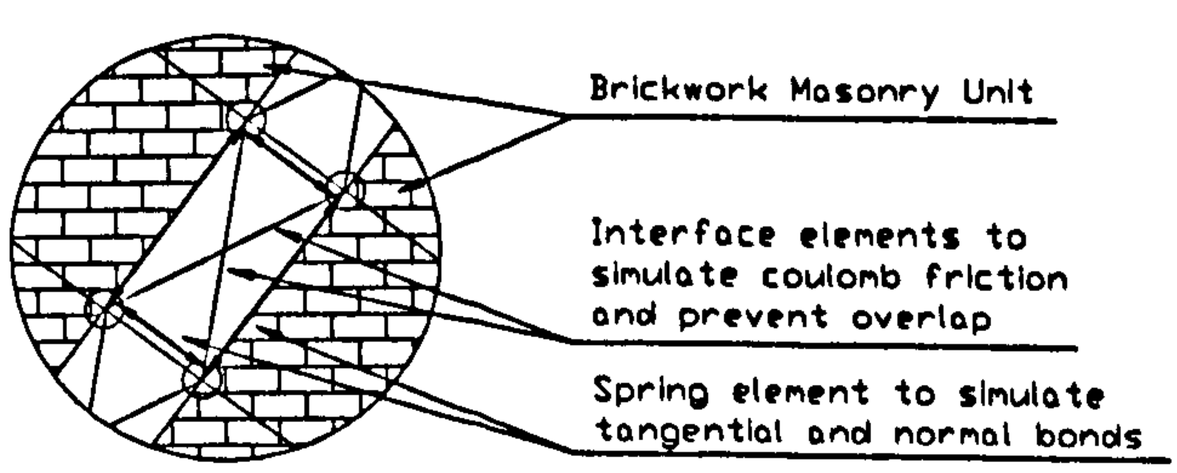

(b) Detailed A

Fig. 3.12 Discrete FE Model of OSMA3

Similar to the modelling of the model OSMA4, four-node quadrilateral elements were used to model the arch, and node-to-segment and nonlinear spring interface elements were used to simulate the cracking and/or sliding effects. The nonlinearity of the arch was modelled through the interface elements.

3.4 Mixed Modelling of OSBMAB

3.4.1 General

The smeared modelling approach is efficient and reasonably accurate for the modelling and the analyses of the open spandrel brickwork masonry model arches without fill, in which brickwork masonry is considered as a homogeneous continuum, and initially isotropic brittle-type material. When fill is considered, different modelling schemes may need to be considered for the interface between the fill and arch as well as the fill itself.

For the interface between the fill and arch, one of the modelling schemes may be to use SOLID65 to simulate interface materials. The thickness of the layer of the interface materials could be assumed reasonably small, and their material properties such as the tensile and compressive strengths, etc., may be assumed as those obtained from the material tests. The failure modes of the interface materials could be modelled through the smeared cracking and/or crushing. However, one of the limitations using this modelling approach is that the thickness of the interface materials has to be assumed. If it is too thick, the characteristics of the interfaces may not be realistically simulated, and if it is too thin, the number of elements may have to be significantly increased in order to avoid large number of irregular elements. The other modelling scheme is to use interface elements to model the connection between the fill and the arches as those used in the discrete modelling of the models OSMA3/4. The interfaces could be modelled using the combinations of contact and nonlinear spring elements. The material properties associated with the interfaces such as the bond strengths and the coefficients of friction may be assumed as those obtained from the corresponding material tests.

For the fill, depending on the types of fill, the following three modelling approaches may be used. Drucker-Prager failure criterion may be used to model the failure of the fill if soil/sand types of materials are used. The failure criterion used for the modelling of brittle types of materials may be used if the fill is made of the weak mortars or concrete. If fill is made of solid materials, interface elements may be used. The limitation of using interface elements to model the fill is that large number of prescribed interfaces has to be predefined within the fill to capture the possible failure modes along the paths. It may be difficult since, unlike brickwork masonry where the locations of the potential failure paths could be assumed beforehand (if the unit strength is far greater than that of the mortar), the failure paths within the fill largely remains uncertain.

A mixed smeared and discrete modelling approach has been developed for the modelling and analyses of the model arch with fill OSMA5. By adopting this mixed modelling approach, the smeared modelling approach was used for the modelling of the main arch and spandrel arches/piers and the fill while the discrete modelling approach was used to simulate the interaction between the fill and arch, and between the fill and the boundary supports. It is believed that this modelling approach could not only take into account of various behaviour of arch/fill and the interface between them, but also could improve the solution efficiency.

3.4.2 Interfaces Between Fill And Arch

In order to simulate the interaction between the fill and the main arch, spandrel arches, the top of the spandrel piers and the arch seats, attempts have been made to take both the initial bond strength and the friction along the interfaces into account. The bond strength was modelled using non-linear springs (COMBIN40) and the friction was modelled using three dimensional contact elements (CONTAC52 or CONTAC49). For clarity, the contact elements are briefly introduced.

For the interface between the fill and the arches, once the initial bond strength is exceeded, the main functions of the nonlinear spring elements will be disabled. In other words, the nodes, which were originally connected together by the springs, would move freely. Obviously, this was not the case in reality. Thus, contact elements were introduced to model the effects of friction along the interfaces, and to prevent the two coincident interfaces from overlapping.

Fig. 3.13 shows one type of the contact elements (CONTAC52). The element is defined by two nodes I and J, and works at its own local coordinate system with its origin at node I, and the positive direction is from node I toward node J. The orientation angles of the element coordinate systems (α and β) are calculated based on the locations of the nodes I and J.

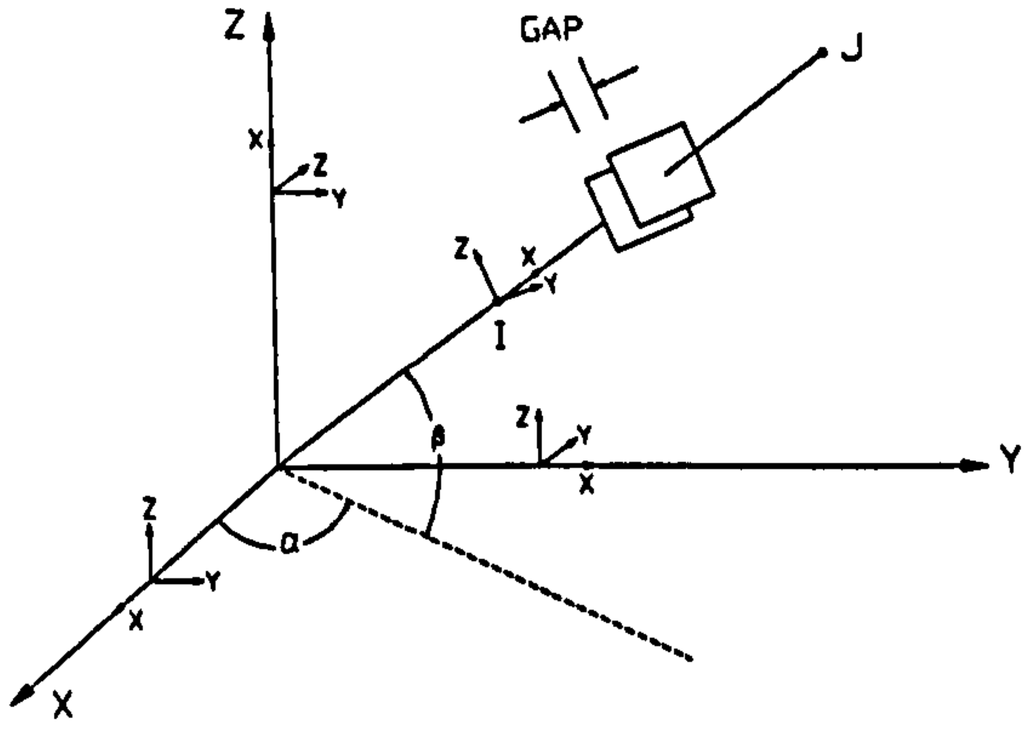

Fig. 3.13 Three-Dimensional Node-Node Contact Element

There are three possible conditions that the element may simulate. (a) Open condition:- when there is a gap between the node pair, it is said to be open condition. There are no reaction forces at these nodes; and the displacement of the corresponding nodes are independent of each other; (b) Sticking contact condition:- when there is no gap between the node pair, and the ratio of the tangential to the normal reaction at the contact interface is less than the local static friction coefficient, it is said to be sticking contact condition. Both the normal and tangential reactions at corresponding nodes are equal and opposite; (c) Slipping contact condition:- when there is no gap between the node pair, and the ratio of the tangential to the normal reaction at the contact interface is greater than or equal to the local static friction coefficient, it is said to be slipping contact condition. The normal reactions are equal and opposite.

The force-deflection relationships are separated into the normal and tangential (sliding) directions as shown in Fig. 3.14. The element condition at the beginning of the first step is determined from the input parameter. If the interface is closed and sticking, Kn is used in the gap resistance and Ks is used for sticking resistance. If the interface is closed but sliding, Kn is used in the gap resistance and the constant friction force μFn is used for the sliding resistance.

In the normal direction, when the normal force (Fn) is negative, the interface remains in contact and responds as a linear spring. As the normal force becomes positive, contact is broken and no force is transmitted.

In the tangential direction, for Fn < 0 and the absolute value of the tangential force (Fs) is less than $\mu|Fn|$, the interface sticks and responds as a linear spring. For Fn < 0 and Fs = $\mu|Fn|$, sliding occurs in the element y and/or x directions, and another parameter is introduced to represent the principal angle of the friction force in the element y-z plane. If contact is broken, Fs = 0.

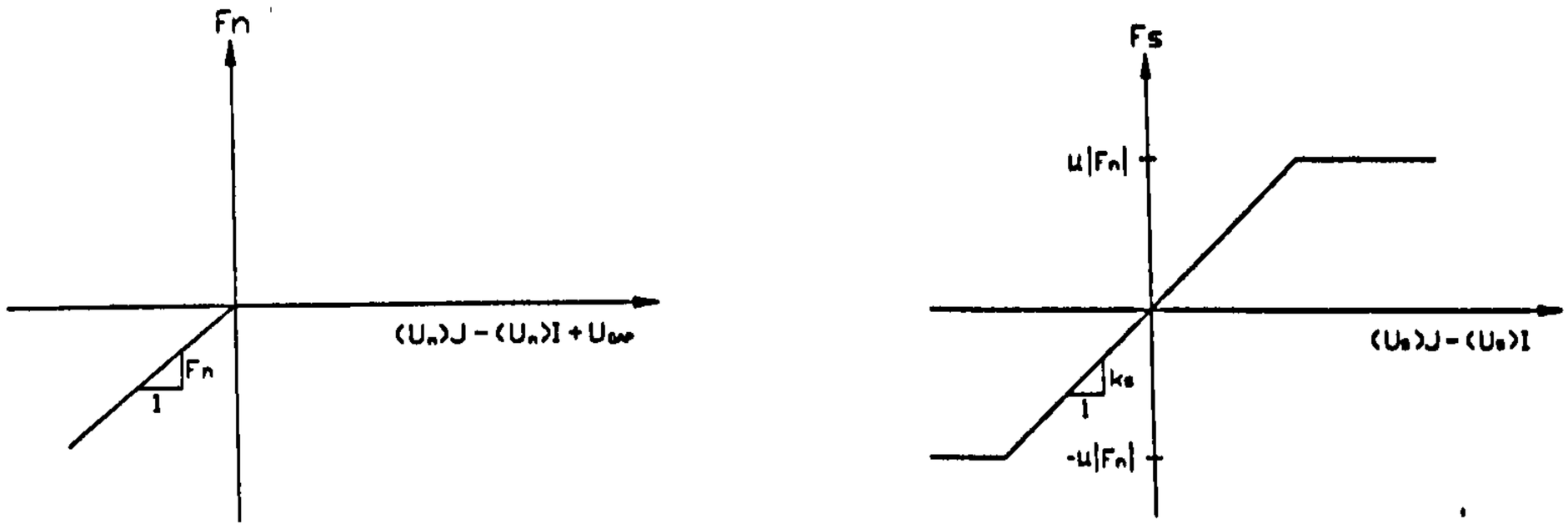

(a) In The Normal Direction **(b) In The Tangential Direction**

Fig. 3.14 Force-Deflection relationship In The Interface Element of CONTAC52

3.4.3 Main arch, Spandrel Arches/Piers

The smeared modelling approach was used for the modelling of the main arch, spandrel arches and spandrel piers. Different material properties may be used for the spandrel piers as they were constructed of the Raewell brickwork masonry instead of the Engineering brickwork masonry. Since the interface elements are to be defined between the fill and the arch, the number of elements along the extrados of the spandrel arches, the top of spandrel piers and the extrados of the main arch within the crown between the two arch seats should be well controlled. It should be great enough to capture of any responses within the interfaces under the loading conditions being concerned, but not too great in case an unnecessary number of interface elements are created.

3.4.4 Fill

Fill may be provided by a variety of materials, which can be lower-class concrete or mortar; granular materials such as limestone, sandstone, rubber masonry, gravel or hoggin; loose earth, ashlar masonry, or a mixture of clay and stones of a wide range of sizes, etc. These different fill materials may not be modelled by the same criterion. In

other words, different models need to be created to account for the different types of fills.

Weak mortar was used in the model arch test (OSMA5). The material test on the weak mortar showed that one of the main failure modes was tensile cracking and compressive crushing (Melbourne and Tao, 1997b). Therefore, Similar failure criterion to that of the arch was used to model the behaviour of the fill.

During the model test of OSMA5, the fill was restrained by the timber block at the boundary. There was little resistance to tension, but great resistance to compression between the timber block and the fill. To model the interface between the fill and its support, compression-only-elements may be used as adopted by Crisfield (1984 and 1985) and Choo et al. (1991 and 1992). That is, the elements are only mobilised as the fill moves towards the timber block. However, this modelling method may not be able to take the friction between the timber block and the support into account. The effects of the friction could be significant, as the fill would generally move in both normal and tangential directions towards the supports. Thus, a new modelling scheme is developed.

The boundary conditions are modelled by the combination of two types of elements. One is interface element as discussed above, and the other is a linear three-dimensional tension-compression element. The former element is used to model the effects of friction and to prevent the overlapping between the fill and the supports, and the latter is used to simulate the condition in tension.

This linear three-dimensional element, as shown in Fig. 3.15, has longitudinal spring capability, which is a uniaxial tension-compression element with up to three degrees of freedom at each node.

By assigning a low value to the stiffness of spring element, the element would carry little loads when in compression or in tension. In other words, the contact elements would carry most of the loads when in compression, and small tensile strength can be maintained when in tension to avoid possible numerical instability. The 'no tension' condition of the interface can be simulated at the same time.

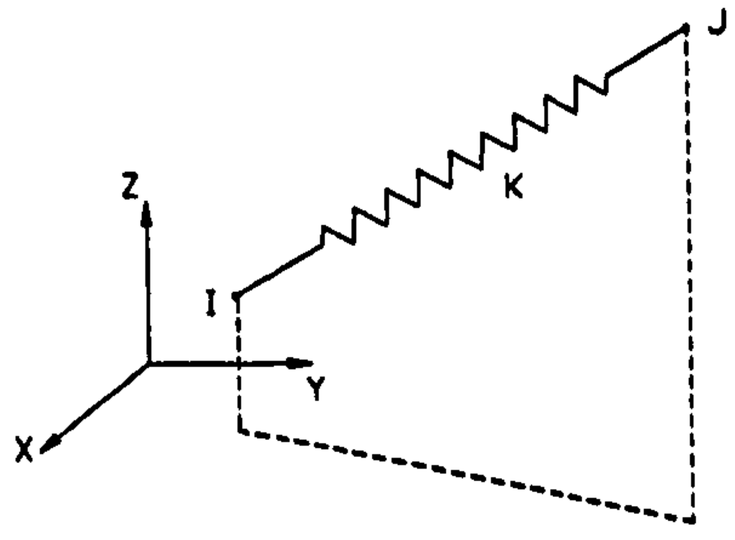

Fig. 3.15 Three-Dimensional Linear Spring Element

3.4.5 Mixed Modelling Of The OSBMAB

The mixed smeared-discrete modelling approach was used to simulate the behaviour of the open spandrel brickwork masonry arch bridge with fill (OSMA5) as shown in Fig. 3.16. For the main arch, spandrel arches, spandrel piers and arch seats, the smeared modelling technique was used; for the interfaces between the fill and the arch, the discrete modelling technique was used.

As Fig. 3.16a shows, for each pair of two nodes (one node is within the fill and the other is within the main arch. The pair in the model may be defined as coincident nodes, but is shown apart in the model for clarity), a total of four elements are defined. That is, in y axis (vertical), one nonlinear spring element was used to model the initial tensile bond between the arch and the fill, and one three-dimensional interface element was used to simulate the Coulomb friction along the two interfaces and to prevent the fill and the arch from overlapping each other after the failure of the spring element; in x and z axes, nonlinear spring elements were used to model the initial shear bond between the arch and the fill in these two directions, respectively. It should be noted that the 'x', 'y' and 'z' axes refer to the Cartesian coordinate system if the interfaces are located between the fill and the top of the spandrel piers, and between the fill and the arch seats; and that they refer to the corresponding local cylindrical coordinate systems if the interfaces are between the fill and the spandrel arches, and between the fill and the main arch.

For the purpose of visual verification, shell elements were used to model the 'cracking effect' along the boundary of the fill, i.e., between the fill and the supports. When cracks occur at the boundary, the fill move away from the support, the shell would act as a reference plane. It may be noted that in order to create the shell elements, the fill was

first meshed, and the nodes within the boundary of the fill were mirrored to generate the other set of nodes of the similar pattern, which were then used to form the shell elements.

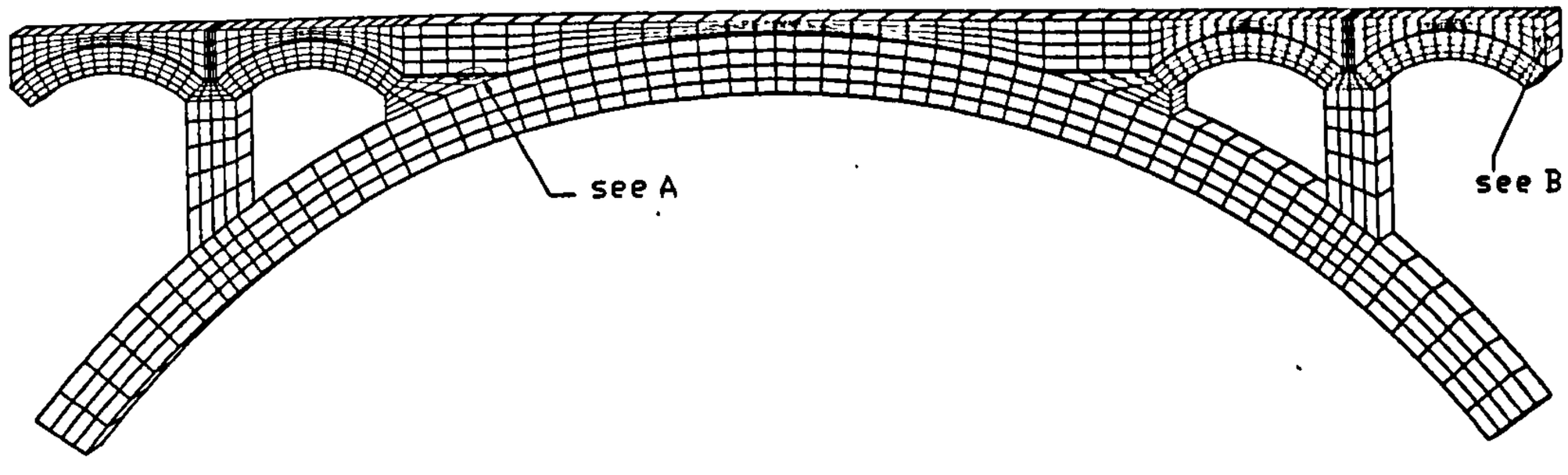

(a) Overview Of Mixed Smeared-Discrete Model

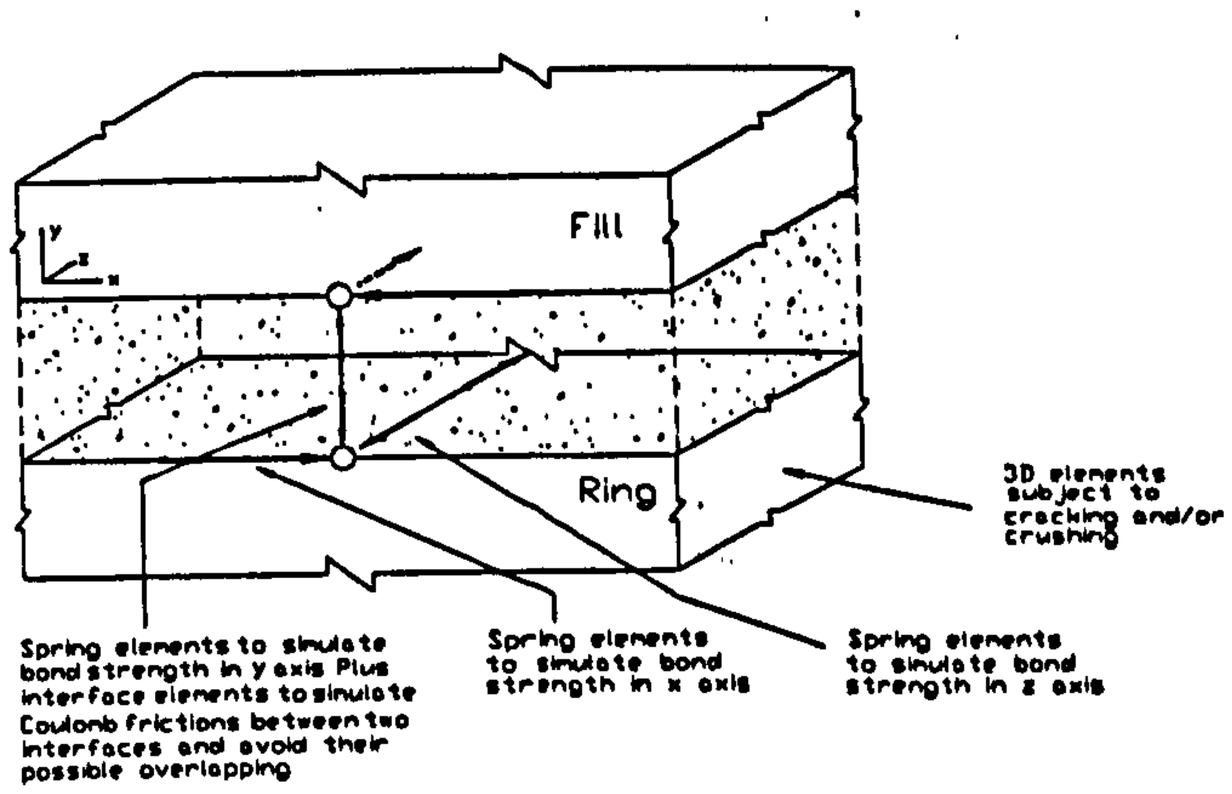

(b) Detailed A

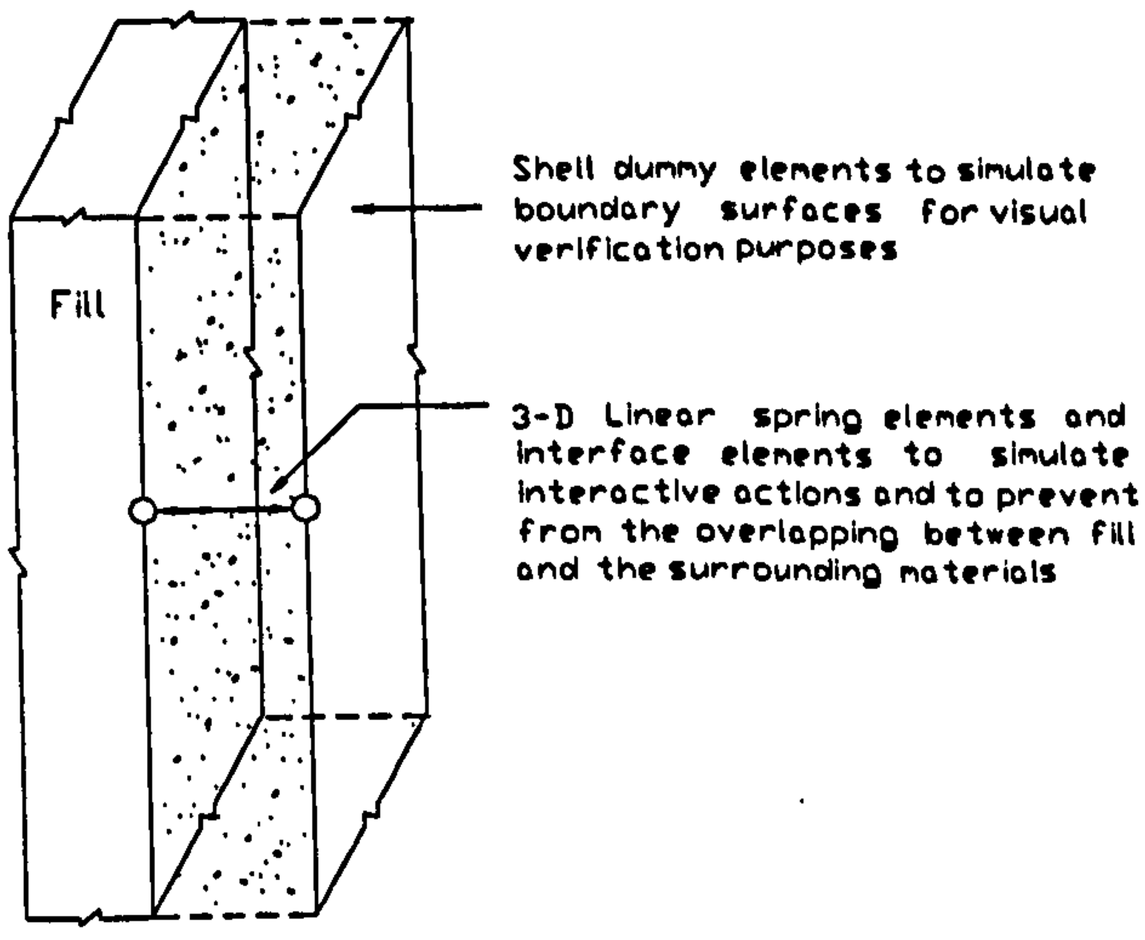

(c) Detailed B

Fig. 3.16 Mixed FE Model of OSMA5

CHAPTER 4 FE ANALYSES AND VERIFICATIONS

4.1 General

In Chapter 3, the smeared, the discrete and the smeared-discrete mixed FE modelling methods were presented in order to model open spandrel brickwork masonry arches. In this Chapter, these methods will be used to simulate the tests of the arch models described in Chapter 2. The FE simulation of the first model test of spandrel arches and piers only (OSMA1) was not carried out as there were few measurements recorded during the test, which would make it difficult to verify the results of the simulation.

For the FE analysis of each of the model arches, actual material properties, which were obtained from the material tests of the corresponding model arch, were adopted. For other parameters such as Poisson's ratio, and shear transfer coefficients along either open or close cracks, etc., which were not readily available, were assumed, and the justifications are given in Chapter 5.

The results of each of the FE analyses were then compared with the data obtained from the corresponding test of the model arches. For the models OSMA3 and OSMA4, the results of the FE analyses based on both the smeared and the discrete modelling methods were compared. Reasonable agreement has been achieved in terms of the modes of failure and ultimate loads, and the causes of the differences between some of the results of FE simulations and the model arch tests are discussed in detail.

The incremental Newton-Raphson techniques were adopted for the solution of nonlinear iterations, and process stops only on account of divergence of residual forces and/or displacements since the system of equations could not be solved due to the degradation of the stiffness matrix of the FE models caused by extensive cracking and/or displacements. As a consequence, all ultimate loads predicted by the FE simulations refer to the maximum sustained loads in the analyses, which correspond to the last converged load step.

During the model arch tests, the displacements caused by the self-weights of the models were not recorded. Only those caused by the applied loads were recorded, and were in

the radial direction for those along the intrados of main arches. In order to effectively compare the FE results with the data recorded during the corresponding model tests, the displacements obtained from the FE analyses were transferred to the polar coordinate system, and those caused by the self - weight were deducted from the total values. In other words, all displacements were converged to zero before the external loads were applied.

4.2 Three-Metre Span OSBMAB Without Fill (OSMA2)

The geometry and typical FE mesh of OSMA2 were given in Table 2.2 and Fig. 3.4. As discussed in Chapter 3, fixed boundary conditions were applied at both the end spandrel arches and the main arches. To simulate the destructive test of OSMA2, loads were applied at the top of the internal spandrel pier on the left hand side as that applied during the model test.

The Young's Modulus, density, and uniaxial compressive strength used in the FE model are the mean values directly from the corresponding material tests of the model arch OSMA2.

Since the tensile strength of the Raewell brickwork (σ_t) obtained from the tests was small, the FE analysis would unrealistically fail at a very low load if it were directly used. As discussed in Chapter 2, such low strength might not represent the true tensile strength of the brickwork units within the model arch. It was decided to use a value of 0.25 N/mm^2 tensile strength, i.e., 3.3% of the compressive strength for the preliminary analyses. It should be noted that such a value was used as a result of "lack" of reliable test data, and was only for discussion purposes. The true tensile strength is likely to be higher as it is shown in the analyses below.

The material properties used in the FE analysis of the model arch OSMA2 are given in Table 4.1.

Material Properties For The Analyses Of SM OSMA2 Table 4.1

Density	1800 (kg/m^3)
Poisson's Ratio	0.20
Young's Modulus	3500 (N/mm^2)
Uniaxial Crushing Strength (σ_c)	7.50 (N/mm^2)
Uniaxial Tensile Cracking Strength (σ_t)	0.25 (N/mm^2)
Shear Transfer Coefficient For Open Cracks (β_1)	0.01
Shear Transfer Coefficient For Close Cracks (β_2)	0.10

As described in Chapter 3, the coefficients β_1 and β_2 are used to account for the deduction of shear transfer capacity for open and closed cracks, respectively. Their typical values range from 0.0 to 1.0, with 0.0 representing a smooth crack, i.e., complete loss of shear transfer and 1.0 representing a rough crack, i.e., no loss of shear transfer. It

has been found that change in either coefficient hardly affects the behaviour of the model arches being considered though their effects are slightly different. Detailed discussions of the effects of these two coefficients are given in Chapter 5.

Figs.4.1 to 4.3 show the comparisons of the results between the FE analysis and the model test at three locations along the intrados of the main arch (see Section 2.3.2 for the locations P2, P4 and P6).

It is shown that the FE results are different from those obtained from the model tests in two aspects: (a) stiffer responses of displacements vs. applied loads at initial stage, and (b) lower ultimate loads.

For the former, it is partly caused by the high Young's Modulus, and partly by the assumption of homogeneous continuum, and initially isotropic material adopted in the smeared modelling method. For Young's Modulus of brickwork masonry, it is normally obtained from material test of brickwork prisms. The conditions of the prisms themselves and the loading in the material tests are largely different from those within the real model arches. The brickwork prisms used in the material tests are normally of constant thickness of mortar joints, and tested under the uniaxial loading condition while the brickwork masonry units within the real arches are largely of wedge mortar joints and subject to eccentric loading. As a result, the E values obtained from normal prism tests tend to be overestimated. Also, brickwork masonry is essentially an anisotropic material, and its E values vary in different directions. The E values from the normal prism test are likely to be the greatest. Though the anisotropic property of brickwork masonry is considered in the smeared model by assuming weak planes normal to the direction of the first principle stresses once cracks take place, such consideration is only limited to the cracked zones. In other words, the intact masonry units always maintain their initial stiffness. In a real masonry arch, however, the stiffness of masonry units tends to be weakened as soon as eccentric loading conditions are formed.

For the latter, it could be due to the relative low tensile strength used. In the FE model, 0.25 N/mm^2 of tensile strength is adopted, and it results in 10.72 kN of an ultimate load compared with 13.50 kN during the model test (note that 13.50 kN was the collapse load

with the removal of most of the instruments, and 12.12 kN was the last load with all instruments attached to the model arch). As discussed in Section 3.2, the failure criteria of brickwork masonry adopted in the smeared modelling method is governed by the

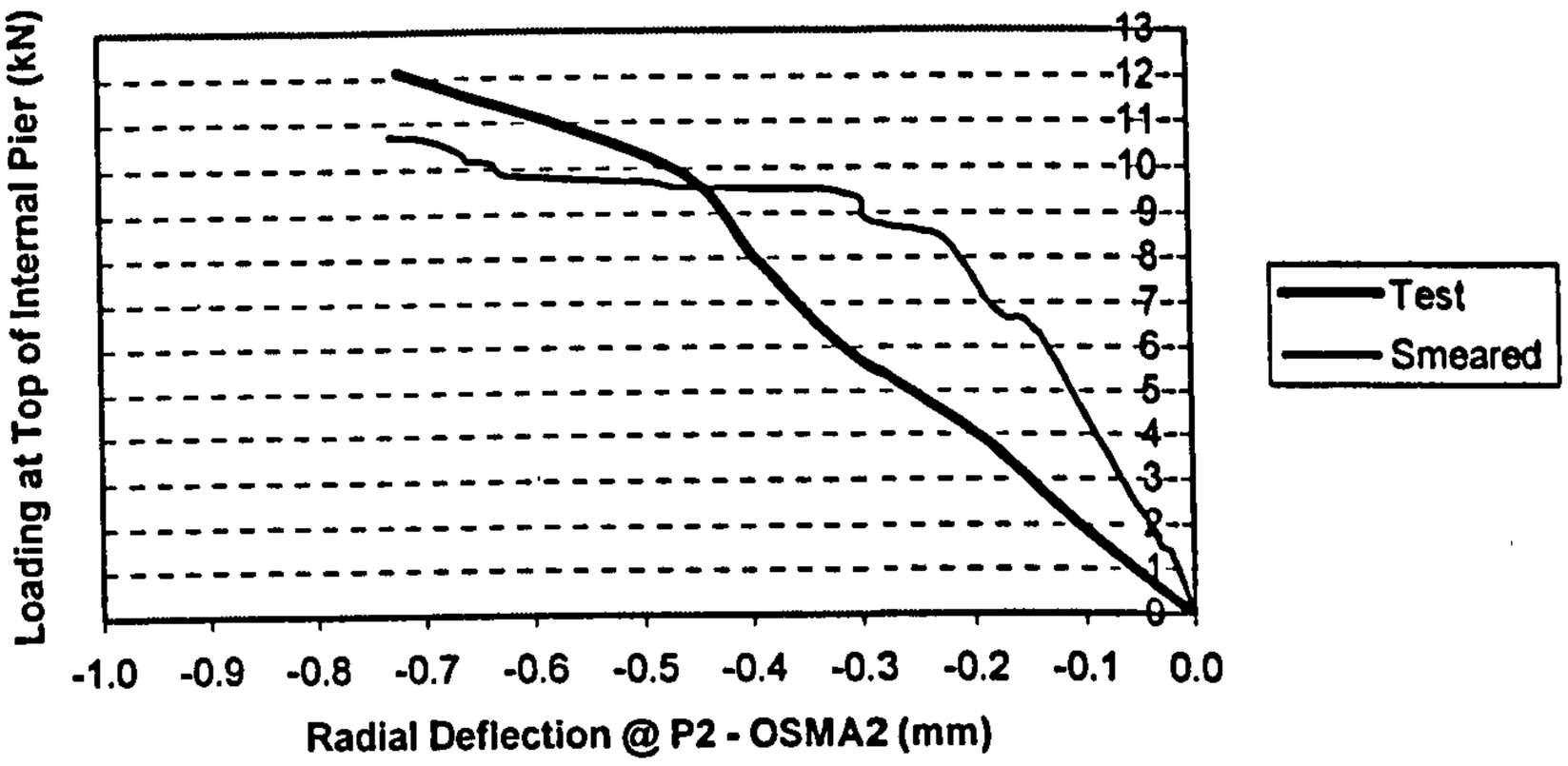

Fig. 4.1 Load-Deflection Curves At P2 Of OSMA2 Using Smeared Model

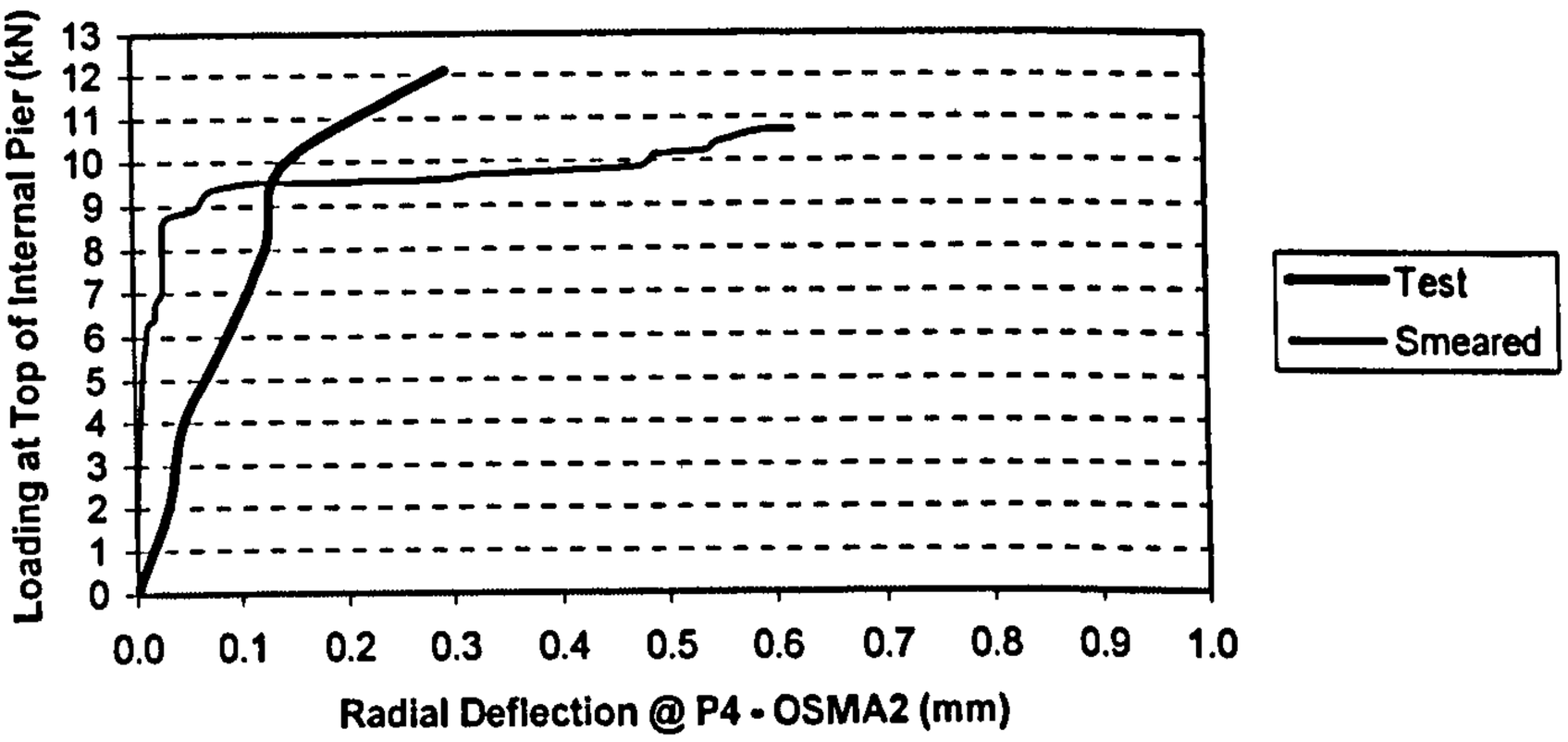

Fig. 4.2 Load-Deflection Curves At P4 Of OSMA2 Using Smeared Model

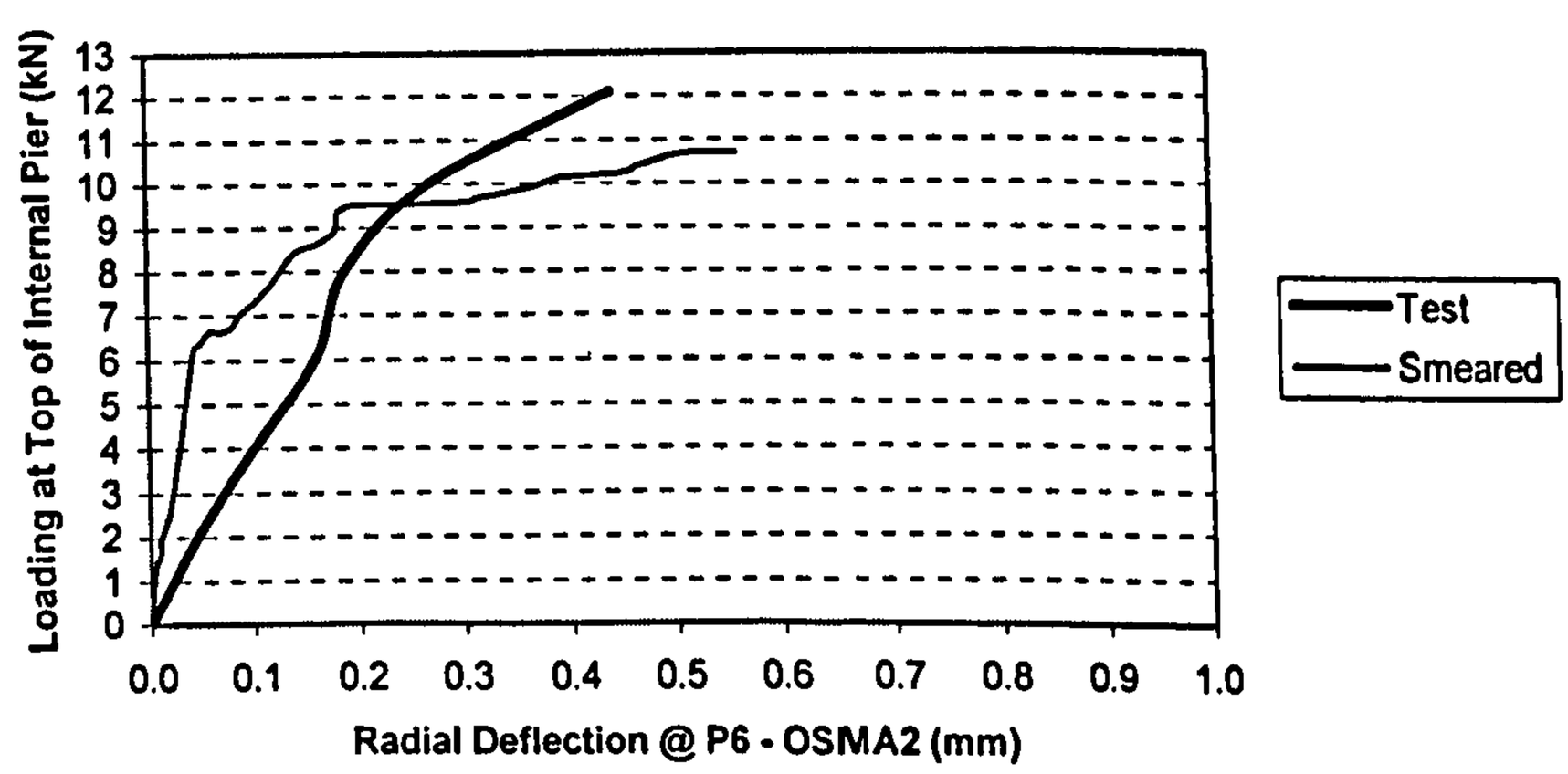

Fig. 4.3 Load-Deflection Curves At P6 Of OSMA2 Using Smeared Model

tensile strength of the material. The higher the tensile strength is, the greater the load level at which cracks occur. Consequently, the ultimate load is greater. It is known from Section 2.1.3.2 that the tensile (or bond) strength of brickwork masonry obtained from the tensile tests tend to be underestimated, and a multiplication factor may be required.

Fig.4.4 shows the sequences of the development of the cracks simulated by the FE analysis of the model OSMA2 using the smeared modelling method. As discussed in Section 3.2, cracking conditions are evaluated in the integration points of the elements. The cracked zones in the model generally refer to the condition where cracks have occurred at all eight integration points of an element.

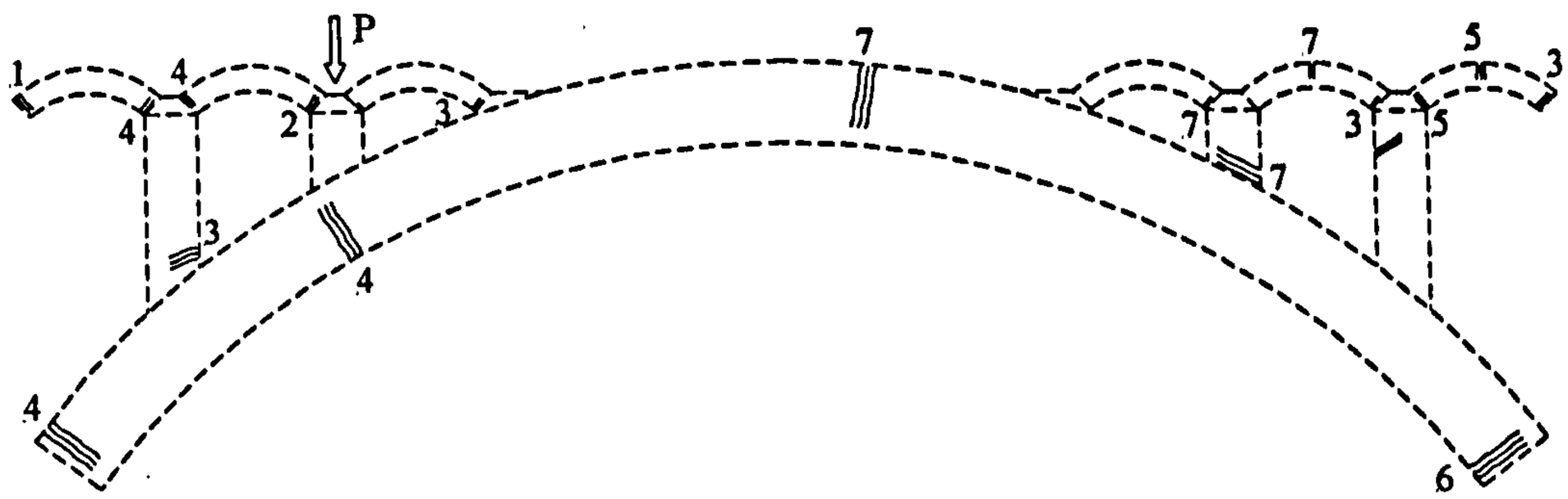

Fig. 4.4 Simulated Cracking Sequences of OSMA2 Using Smeared Model

Detailed descriptions at each major stage are given in Table 4.2.

Cracking Development and Discussion of OSMA2 **Table 4.2**

(1) At 1.8 kN	The first crack occurs at the extrados of the springing of the end spandrel arch SA1 on the left-hand side (note: the model arch was under its own weight before the application of the external loads). This crack continues to propagate towards the intrados of the spring, and spreads approximately within the region of the width of single Raewell brick. When the load reached about 12 kN, this crack extends across the whole cross section of the arch barrel of SA1.
(2) At 6.2 kN	The second crack occurs at the intrados of the springing of SA2 on the right-hand side. This crack continues to propagate towards the extrados of the

	spring, and eventually extends across the whole cross section of the arch barrel of SA2.
(3) At 7.7 kN	Four cracks occur at (a) the bottom of the pier 1 on right-hand side; (b) the intrados of the springing of SA3 on the right-hand side; (c) the intrados of the springing of SA5 on the right-hand side; and (d) the intrados of the springing of SA6 on the right-hand side. The cracks (a) and (d) continue to develop at later stages across the whole section while the cracks (b) and (c) hardly further propagate.
(4) At 8.6 kN	Four cracks occur at (a) the intrados of the springing of SA1 on the right-hand side; (b) the extrados of the springing of SA2 on the left-hand side; (c) the extrados of the springing of the main arch on the left-hand side; and (d) the intrados of the main arch under the loaded pier 2. These four cracks continue to propagate as the load increased. Especially, the cracks (c) and (d) eventually become two 'hinges'. It may be noted that, as the cracks develop within the main arch, the stiffness of the whole model arch is significantly reduced, which is reflected by the sudden propagation of all cracks within the spandrel arches.
(5) At 8.9 kN	Two cracks occur at (a) the intrados of the springing of SA6 on the left-hand side; and (b) the crown of SA6 at extrados. It clearly shows that, as the two existing cracks within the main arch develop, the main arch moves upwards. The development of the cracks within the end spandrel arch SA6 is primarily caused by the movement of the end that is supported upon the main arch. These two cracks together with the existing one are diffused across the sections as the load increases.
(6) At 9.1kN	One crack occurs at the intrados of the spring of the main arch. As it appears, the three cracks within SA6 rapidly spread.
(7) At 10.7 kN	Five cracks develop simultaneously, two of which are major cracks at (a) the extrados of the main arch near the crown on the unloaded side and (b) the bottom of the spandrel pier 3; and two are minor cracks at (a) the intrados of the springing of SA4 on the right-hand side and (b) the extrados of the crown of SA5 at extrados; and one diffused crack near the top of spandrel pier 4. As this crack appears, all the existing cracks within both the main arch and the spandrel arches/piers further propagate and are diffused, which indicated the general loss of the stiffness within the whole model arch.

It may be noted that, during the model arch test, one crack occurred at the bottom of the spandrel pier 4 instead of the pier 3 on the unloaded side (see Fig. 2.29). It was believed that this deviation was caused by the relatively random distribution of the material properties of the model arch tested. As the fourth crack near the crown of the main arch develops in the FE model, the unloaded half of the model tends to rotate. Since SA6 has severely deteriorated due to the extensive cracks, it could provide little support against the rotation of the unloaded part. As one crack develops at the extrados of the crown of SA5, another crack develops at the bottom of the pier 3, and diffused cracks occur near the top of the spandrel pier 4.

4.3 Five-Metre Span Main Arch Only (OSMA4)

4.3.1 Smeared Modelling And Analysis

The geometry and typical FE mesh of OSMA4 using the smeared modelling method were given in Table 2.2 and Fig. 3.5 As discussed in Chapter 3, fixed boundary conditions were applied at the ends of the main arch. To simulate the destructive test of OSMA4, loading was applied at the same location as that during the model test.

The Young's Modulus, density and uniaxial compressive strength used in the FE model are the mean values from the corresponding material tests of the model arch OSMA3.

The material properties used in the analyses are given in Table 4.3.

Material Properties For The Analyses Of SM OSMA4 Table 4.3

Density	2300 (kg/m^3)
Poisson's Ratio	0.20
Young's Modulus	10000 (N/mm^2)
Uniaxial Crushing Strength (σ_c)	18.00 (N/mm^2)
Uniaxial Tensile Cracking Strength (σ_t)	0.28 (N/mm^2)
Shear Transfer Coefficient For Open Cracks (β_1)	0.01
Shear Transfer Coefficient For Close Cracks (β_2)	0.10

Figs.4.5 to 4.7 show the comparisons of the results between the FE analysis and the model test at three locations along the intrados of the main arch (see Section 2.3.4 for the locations P2, P4 and P6).

Compared with the test results of the model OSMA4, the responses of load - deflection from the FE simulations appear stiffer. The causes were as discussed in Section 4.2.

In general, the curves of the load - deflection may be divided into four segments:- (a) the load is from 0 to 10.439 kN. At this stage, the model arch basically behaves linearly, which indicates that there may not be any cracks developed within the arch, nor the occurrence of micro-cracks affects the integrity of the structure. It may be concluded that the model behaves linearly up to about 77% of the ultimate load); (b) the load is equal to 10.400 kN. At this point, the model experiences sudden loss of the stiffness. It indicates that there is significant cracking developed within the arch, but not significant

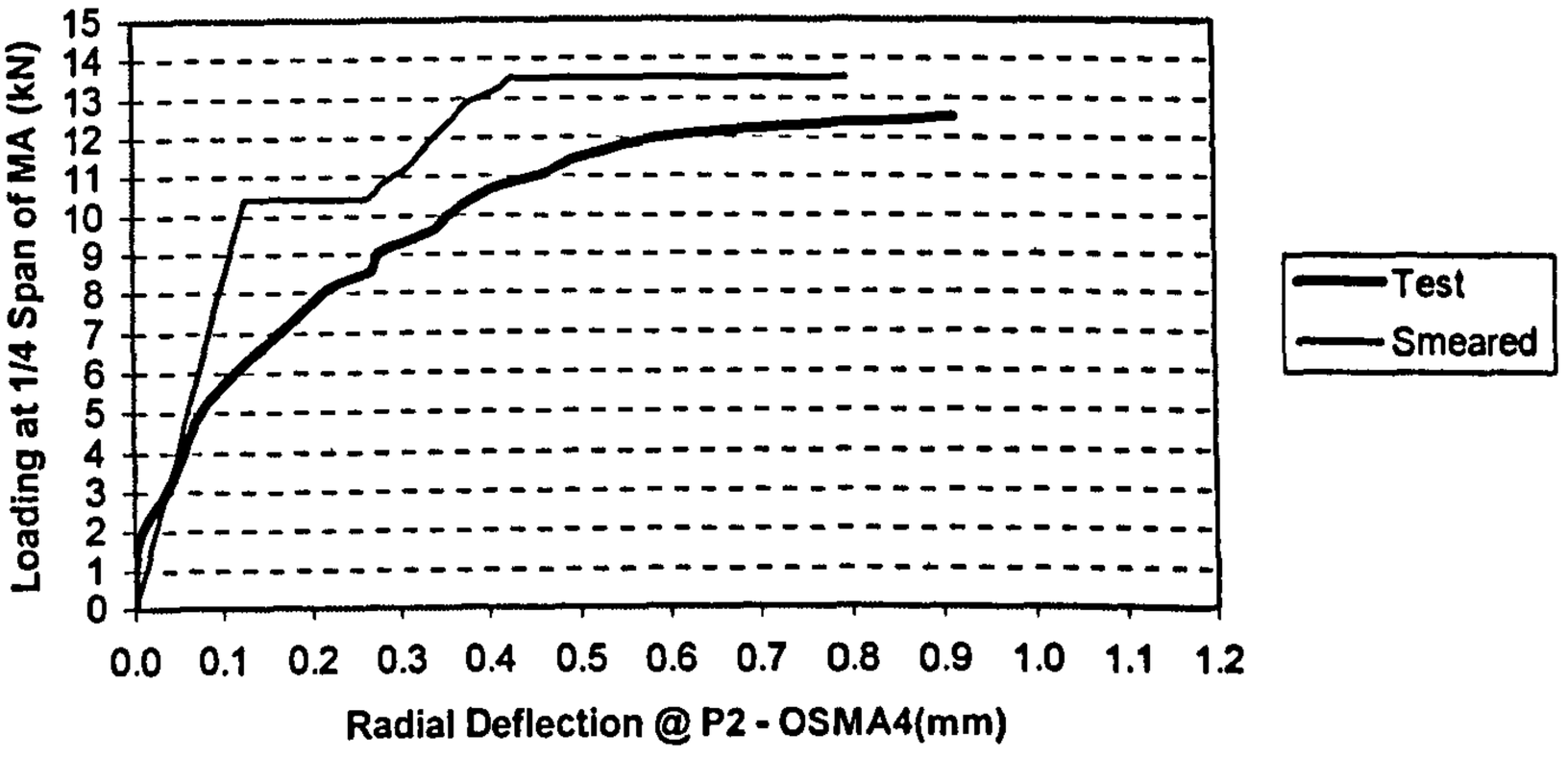

Fig. 4.5 Load-Deflection Curves At P2 Of OSMA4 Using Smeared Model

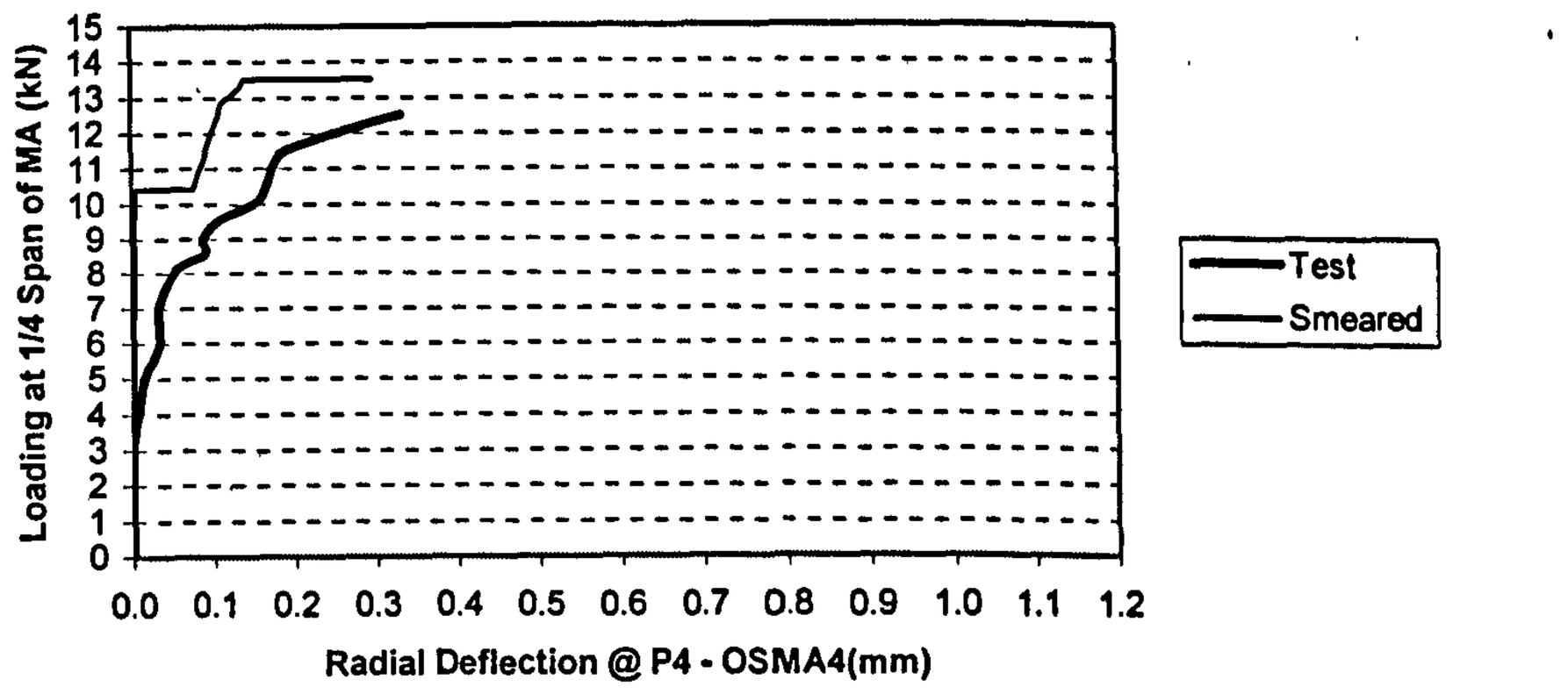

Fig. 4.6 Load-Deflection Curves At P4 Of OSMA4 Using Smeared Model

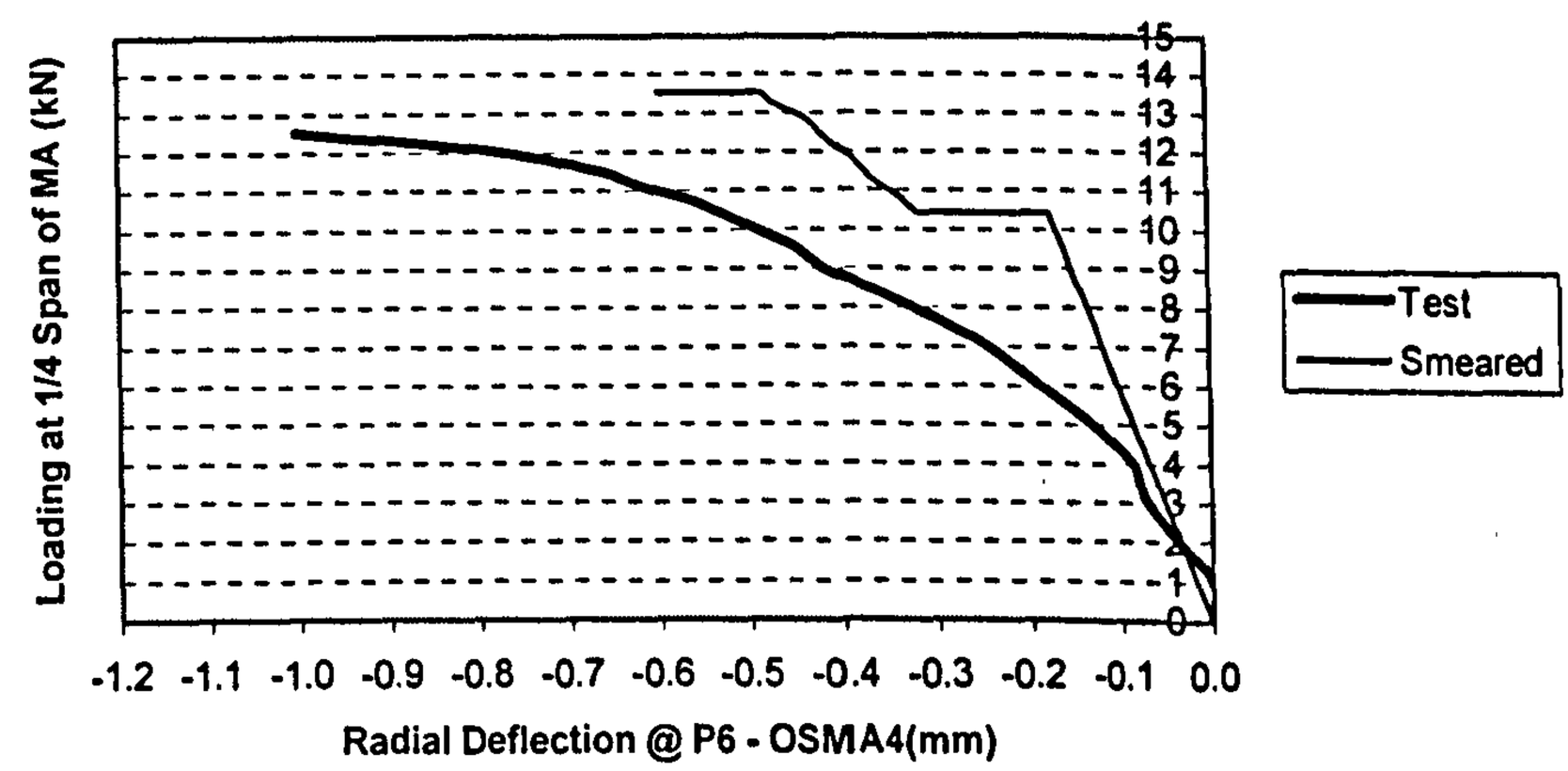

Fig. 4.7 Load-Deflection Curves At P6 Of OSMA4 Using Smeared Model

to cause the failure of the arch yet (note that it is a typical brittle-type of failure of components); (c) the load is from 10.440 to 13.499 kN. The model continues to behave linearly, but the stiffness is reduced to about one third of that at initial stage. Unlike during the initial stage, it can be seen that there are local variations in stiffness along the curves at this stage. Each of the variations indicates the occurrence of new cracks or the further development of the existing ones. This phenomenon is also evident in the curves obtained from the model test, and discussed previously (Section 2.5); and (d) the load is equal to 13.500 kN. The model fails. This was reflected in the FE analysis through the excessive residual forces generated within the model. As discussed in Section 3.2, this means that significant cracking suddenly develops within the model, and the model has so deteriorated that it cannot redistribute the forces associated with the cracked zones to the adjacent regions. This could be verified by the following review of the cracking pattern of the model. It is noted that the simulated responses between loads and deflections may largely represent the various stages of the deterioration of the model, and the ultimate load. However, unlike the nonlinear load-deflection response obtained from the model test, the simulated one is nearly perfect brittle type.

Fig.4.8 shows the sequences of the development of cracks simulated by the FE analysis of the model OSMA4, and detailed descriptions at the major stages of loading are given in Table 4.4.

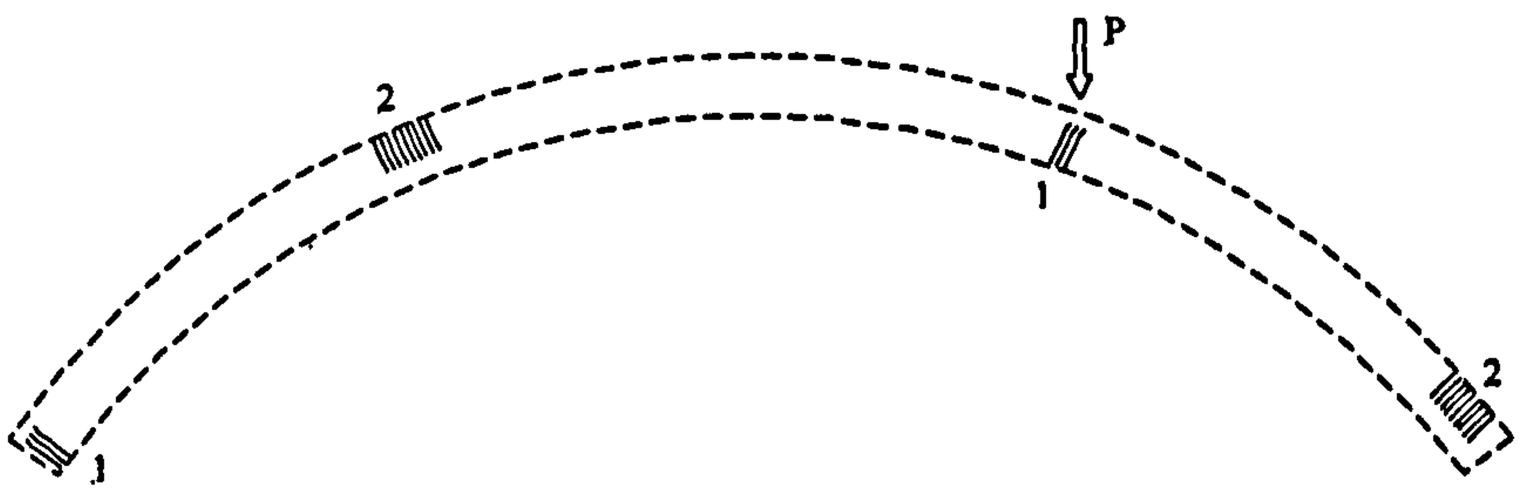

Fig. 4.8 Simulated Cracking Sequences of OSMA4 Using Smeared Model

(a) First Cracking

Immediately prior to the occurrence of the first cracking under the loading location, the first principal stresses at the nodes along the intrados of about 250 mm in length at the same location are within the range between 0.25 and 0.30 N/mm^2 (it may be noted that

nodal stresses and strains are extrapolated from those at the integration points of the elements. This may produce stress values above cracking stresses at the nodes. The actual stresses or strains at a node are generally somewhat lower). As the load increases (about 0.01 kN), the cracks rapidly propagate radially through four of the five elements along the arch barrel from the intrados towards the extrados within the region of one element width. The stresses within the cracked zones suddenly drop down to 0.001 N/mm^2. The rate of change in deflection at point P6 increases dramatically. This cracks smear through the entire thickness of the arch barrel at a load of 13.25 kN slightly before the failure of the model arch.

Cracking Development and Corresponding Loads of OSMA4 **Table 4.4**

(1) At 10.4 kN	No cracks occur until the load reaches 10.4 kN, at which two cracks occur at the intrados under the loading position and at the intrados adjacent to the support at the unloaded side, respectively.
(3) At 13.5 kN	Two cracks occur simultaneously along the extrados over the quarter span at the unloaded side, and near the springing at the loaded side.

For the cracks at the springing of the left – hand side, the change in stresses is similar to that under the loading location. As the load increases, it suddenly propagates radially through three of the five elements along the arch barrel from the intrados towards the extrados within one element width. This crack further propagates through the thickness of the fourth element at a load of 10.85 kN, and smears through the entire thickness of the arch barrel at a load of 13.5 kN when the model fails.

It may be noted that the cracks under the loading location could occur a bit earlier than the one at the springing of the left – hand side (or the unloaded side) if sufficient small load increments (0.01 kN or so) were used at this stage of loading.

(b) Second Cracking

Immediately prior to the occurrence of the cracks at a load of 13.49 kN around the quarter span at the unloaded side, the first principal stresses at the nodes along the extrados between 0.17L and 0.42L (note L is span) of about 1250 mm in length are within the range between 0.25 and 0.30 N/mm^2. As the load increases (about 0.01 kN), the cracks smears through the arch barrel within the region between 0.24L and 0.32L.

The stresses within the cracked zones suddenly drop down to 0.001 N/mm^2. The rate of change in deflection at point P6 increases significantly. It may be noted that the last converged results were obtained at a load of 13.49 kN. The details of final cracking patterns and deflections after the occurrence of the cracks at the quarter-span of the unloaded side may be slightly different from those recorded in the model test.

For the cracks at the springing over the loaded side, immediately prior to their occurrence, the first principal stresses of the nodes along the extrados between the springing and 0.08L of about 400 mm in length are within a range between 0.25 and 0.30 N/mm^2. As the load increases (about 0.01 kN), the cracks smears through the arch barrel within the above range.

Compared with that observed during the model arch test (Fig. 2.39), the cracking pattern is well simulated.

From the responses of the load - deflection and the patterns of the cracks of the model arch, it can be seen that the smeared modelling method may be used to realistically simulate the behaviour of the model arch at individual loading points, where sudden change in stiffness (or sudden development of cracks) is likely to take place. It may not realistically reproduce behaviour along the entire loading history since the constitutive relationships adopted in the smeared model are elastic - brittle type, and the behaviour of the real model arch is nonlinear - brittle. As a result, the responses of load - deflection is likely to be stiffer at each of its linear stages even if a more realistic Young's modulus (, which could lead to an overall agreement between FE results and test ones) is used in the smeared model. As ultimate loads are mainly affected by tensile strength in the smeared FE models, it will always be possible to achieve the true ultimate strength if there is one. If an ultimate load of arch is unknown beforehand, it may be predicted by using a value of tensile strength between 0.28 to 0.32 N/mm^2.

During the model tests of open spandrel masonry arches, it was noted that the failure of spandrel arches was mainly caused by the movements of the ends, which were supported upon the main arch. Further analyses were carried out to study the effects of the movements of the ends of an arch in different directions in order to identify the most vulnerable direction of movements. In an open spandrel arch, the ends of the spandrel

arches, at either loaded or unloaded sides, may move in any of the following directions: vertically down and/or up (ver-dn/ver-up), horizontally in and/or out (hor-in/hor-ot), circumferentially clockwise and/or counter clockwise (cir-clk/cir-ctc), and radially (tangentially) down and/or up.

By assuming that one end of the arch is fixed, and the other is free to move, Fig.4.9 shows the maximum relative movements in different directions that would cause the failure of the unloaded arch.

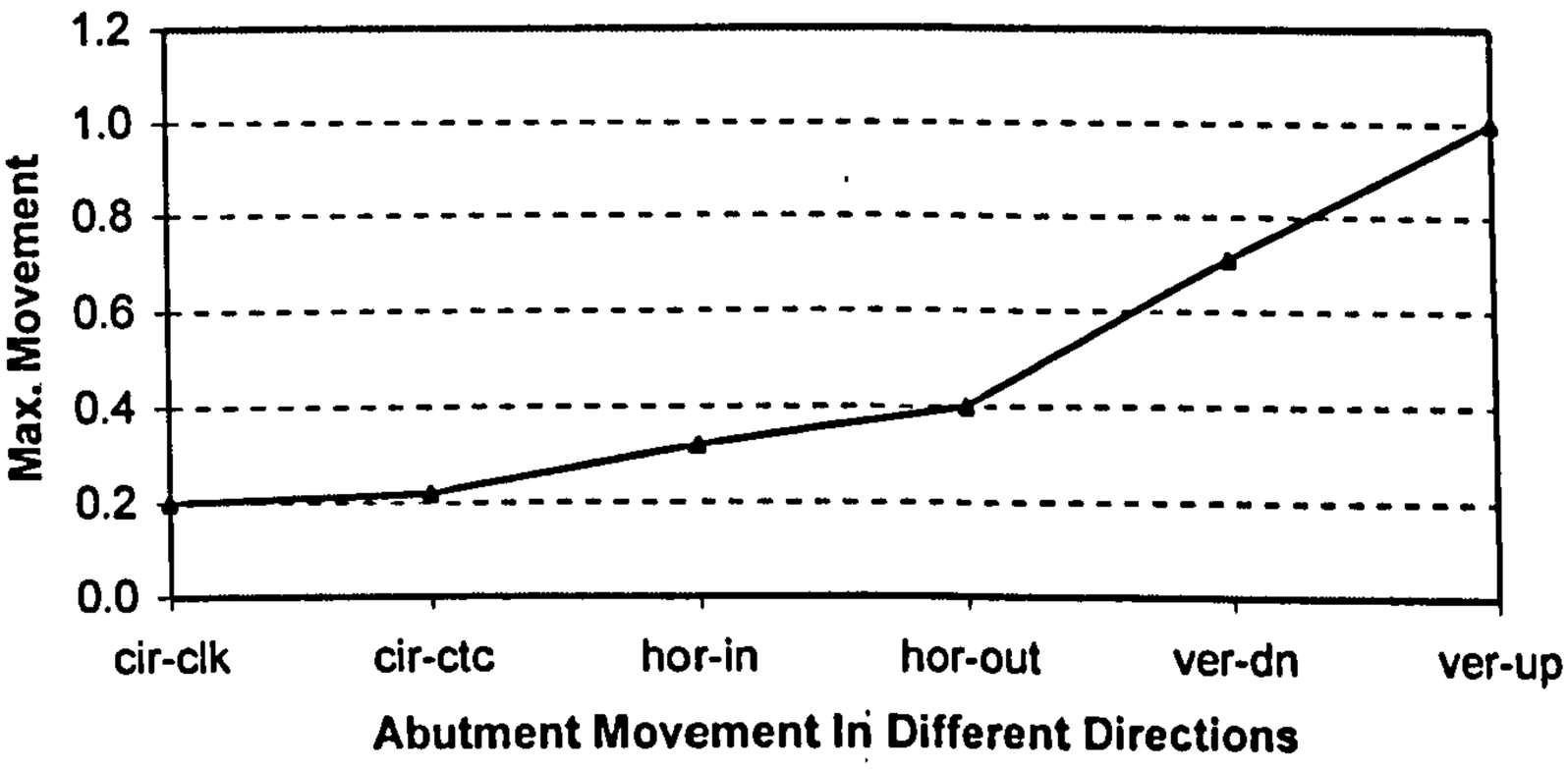

Fig. 4.9 Max. Movement Along Different Directions

It can be seen that the most vulnerable direction of the movements of the ends is along the circumference, especially towards the crown.

4.3.2 Discrete Modelling And Analysis

The geometry and typical FE mesh of OSMA4 using the discrete modelling method were given in Table 2.2 and Fig. 3.11. A total of thirty-three interfaces are defined along the arch ring. The interfaces between the arch supports and the ends of the arch were defined by two sets of coincident nodes. For those nodes that were attached to the supports, fixed boundary conditions were assumed. To simulate the destructive test of OSMA4, a load was applied at the same location as that during the model test.

The Young's Modulus and density used in the FE model were the mean values from the corresponding material tests of the model arch OSMA3.

Sensitivity studies were carried out for the determination of the values of the elements related parameters (See Chapter 5 for details). As the smeared models were unable to predict the behaviour of the arch with very low tensile strength, attempts have been made to use low tensile and shear bond strengths for all nonlinear spring elements COMBIN40. To simulate the shear effects along the interfaces, the nonlinear spring elements in the tangential directions would be disabled once the tangential stresses are over 0.001 N/mm^2, i.e., the friction is mainly taken by the contact elements. For the tensions at the direction normal to the interfaces, the nonlinear spring elements in these directions would be disabled once the normal stresses are over 0.001 N/mm^2.

The element CONTAC48 basically requires three input data, i.e., coefficient of friction, normal and tangential stiffness. For the coefficient of friction, 0.8 was used as obtained from the material tests (Section 2.1.3.3). Special care should be taken when the values of the stiffness are determined for masonry arches. It is known from the model tests that the model arches fail by the formation of hinges, and loads at the hinges are highly concentrated. If the stiffness is too small, the amount of penetration of contact nodes into target lines may be too great and/or the two surfaces of an interface may slide apart, which could affect the computations of the solutions. On the other hand, if the stiffness is too big, the determination of true contact status normally requires more iterations, and in some cases, convergence difficulties are inevitable. It has been found that the values of the normal stiffness (10000 N/mm) and tangential stiffness (1000 N/mm) could not only prevented overlapping between interfaces, but also leads to efficient solutions in terms of number of iterations.

For contact problems, it is generally believed that an efficient modelling method is to define all the contact nodes being on one surface, and all the target faces being on another surface, and one set of contact elements being generated between these two surfaces (i.e., asymmetric method). This practice may not be suitable for the modelling of a masonry arch such as the model osma4 since it is not easy to distinguish between the contact and target surfaces. Consequently, two sets of contact elements are defined in each interface, i.e., each surface is considered as both contact face and target face at the same time. This symmetric way to define contact elements are not only to stabilize the entire running process, but also overcome one of the (most) modelling difficulties associated with masonry arches – hinges, by allowing two targets.to be in contact with each other. As a hinge is being developed, the contact nodes could be passed back and forth between the adjacent elements on the target surface, and lead to convergence difficulties if the asymmetric modelling method is used.

The material properties used in the analyses are given in Table 4.5.

Material Properties For The Analyses Of DM OSMA4 Table 4.5

Density	2300 (kg/m^3)
Poisson's Ratio	0.20
Young's Modulus	10000 (N/mm^2)
For CONTAC48	
Coefficient of friction	0.80
Normal stiffness	10000 (N/mm)
Tangential stiffness	1000 (N/mm)
For COMBIN40 elements in radial direction	
Bond strength	0.0001 (N/mm^2)
Stiffness of master spring	0.01 (N/mm)
Stiffness of slave spring	0.001 (N/mm)
For COMBIN40 elements in tangential direction	
Bond strength	0.0001 (N/mm^2)
Stiffness of master spring	0.01 (N/mm)
Stiffness of slave spring	0.001 (N/mm)

Figs.4.10 to 4.12 show the comparisons of the results between the FE analysis and the model test at three locations along the intrados of the main arch (see Section 2.3.4 for the locations P2, P4 and P6). It may be noted that the absolute maximum scale of the X-

axis in the Figures is set to 6 mm in order to visibly compare the FE results with those obtained from the model test. As a result, the last three load increment results are not included in Figs. 4.10 (P2) and 4.12 (P6).

It is normally less straightforward to run and to achieve the true ultimate load when many contact elements are used. The change in status of contact elements could result in sudden change in the stiffness of models. The convergence difficulty may be experienced if the changes in status of large number of contact elements take place at the same load increment. To overcome this potential problem, the Program provide three methods:- (a) CTAT only; (b) CTAT and contact predictions to the predicted loading point; and (c) CTAT and contact predictions down to the minimum load increment specified before the status changes. The method (b) has generally been proved efficient in the analyses of the model OSMA4. Large load increments were applied until the load was up to 11.89 kN. As more contact elements separate, the load increments were automatically reduced to 1.65, and to 0.003 kN until the model fails at a load of 12.27 kN. The relatively large load increments at the initial stages indicate that the reduction of the stiffness of the arch model are relatively less due to the changes in the status of the contact elements, and thus the changes in the status take places at similar rates. Once most of the changes in the contact elements are complete, the gaps caused by the changes in contact status gradually increase. The effect on the change in the stiffness of the model due to the progressive development of the initial gaps is not as significant as that due to the initial changes in contact status. Therefore, the load increment increases. However, as the gaps develop to a certain extent, the stiffness of the model is greatly affected by the change in the geometry of the model (i.e., geometry nonlinearity). The load increment significantly decreases as the arch becomes "weaker and weaker". The whole loading process can clearly be seen from the deflections vs. loads curves in Figs. 4.10 – 4.12.

From Fig. 4.12, it can be seen that the deflection vs. load responses from the model test are correctly reproduced within the range from 0 to 4.5 kN. It is noted that the stiffness of the arch almost linearly decreases (suddenly) as the load increases from 10.24 kN to 12.045 kN, rather than non-linearly decreases (gradually) as expected. It is believed that

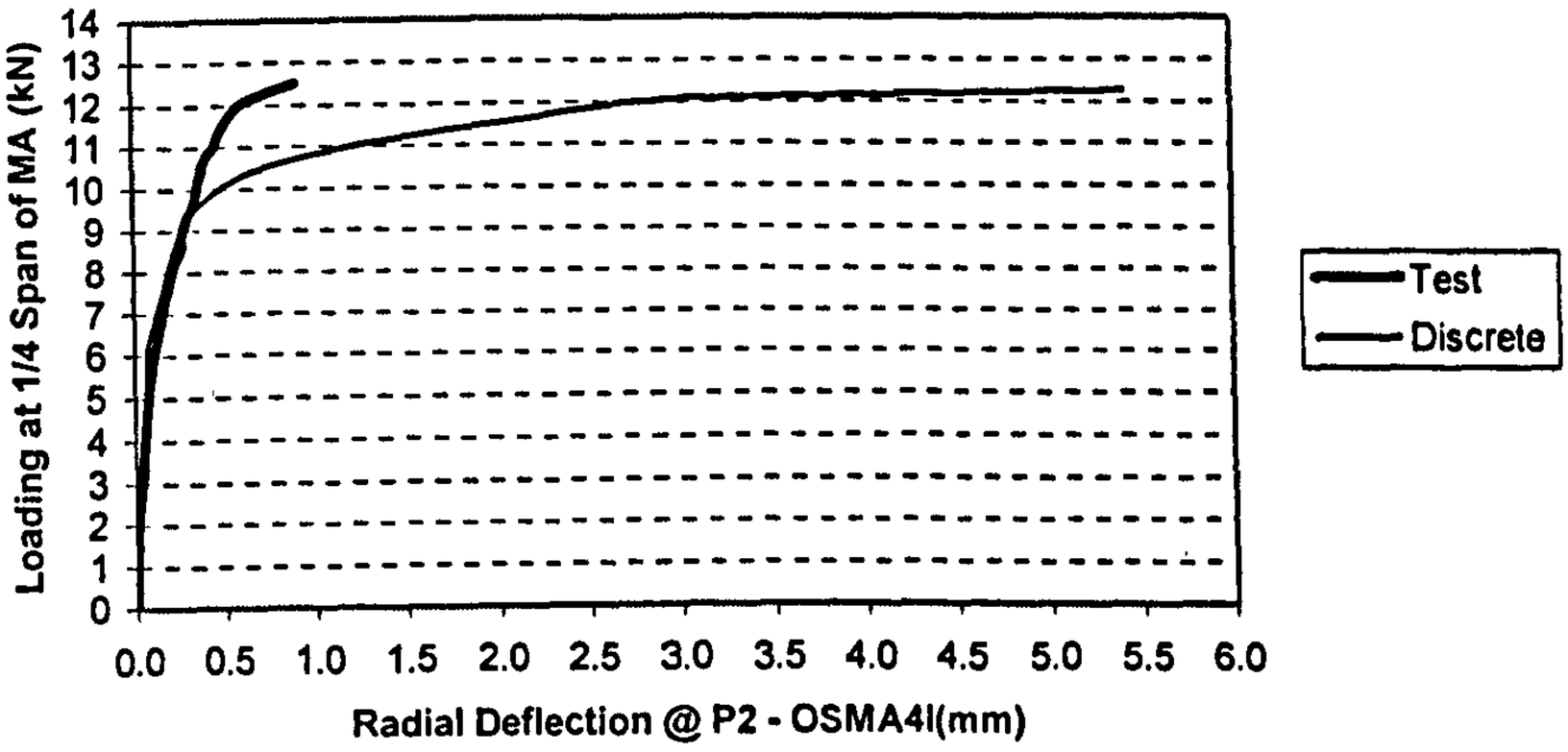

Fig. 4.10 Load-Deflection Curves At P2 Of OSMA4 Using Discrete Model

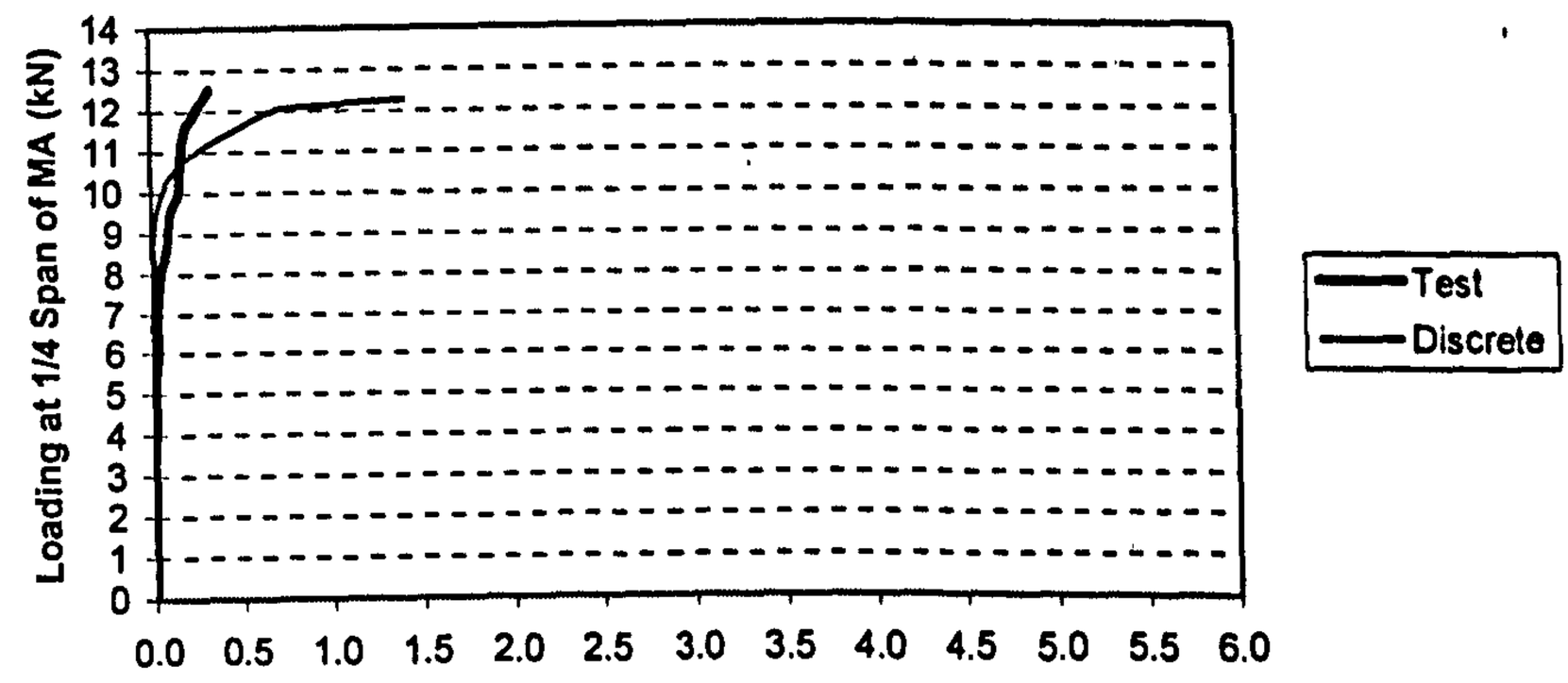

Fig. 4.11 Load-Deflection Curves At P4 Of OSMA4 Using Discrete Model

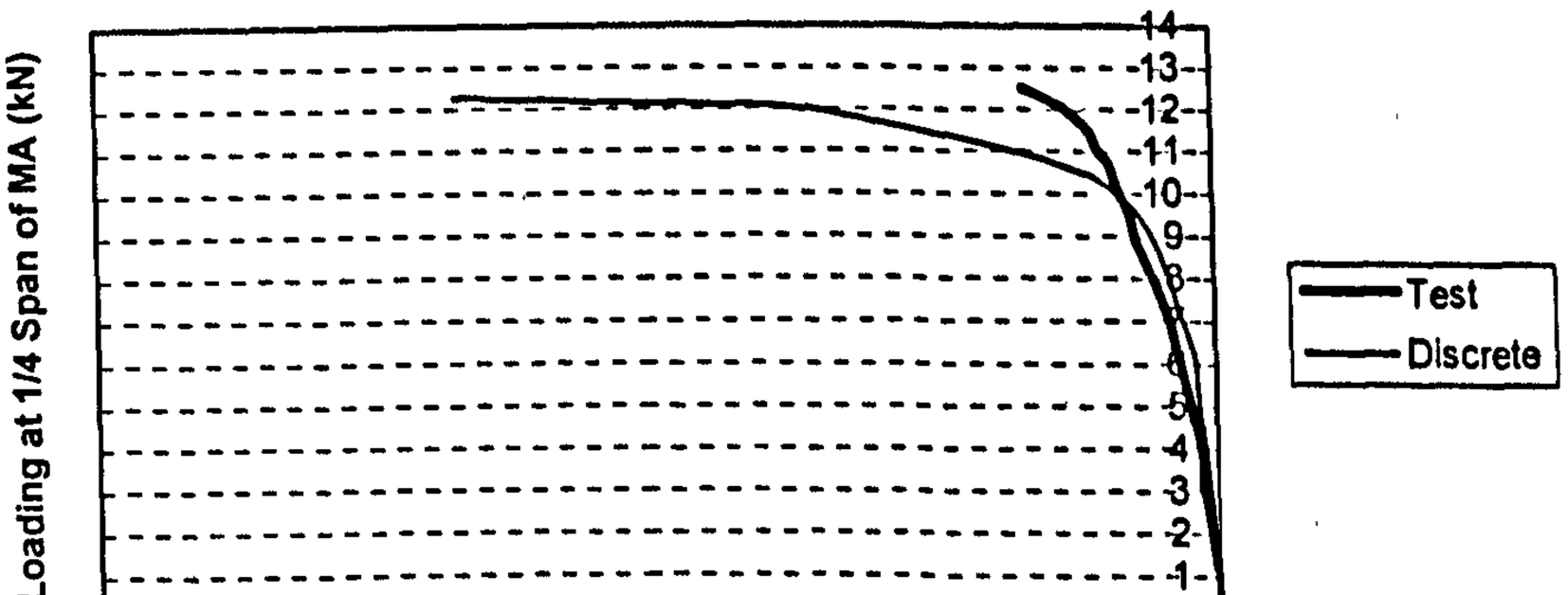

Fig. 4.12 Load-Deflection Curves At P6 Of OSMA4 Using Discrete Model

it is mainly caused by three factors:- (a) relatively large load increment; (b) relatively small number of interfaces along the arch ring; and (c) relatively small number of nodes along the arch barrel. Also, the occurrence of the simulated major loss of the stiffness of the arch (10.24 kN) is earlier than that from the test (11.50 kN). It could be because the negligible tensile capacity was assumed within the interfaces in the FE model. In other words, the tensile capacity within the model arch could not only delay the major loss of the overall stiffness, but also make the model arch stiffer. The detailed simulated relationships between the loads and deflections are given in Table 4.6, from which it can be seen that the stiffness of the model arch decreases as the load increases. It may be concluded that, for the load – deflection responses, the discrete modelling method results in good agreement with the test results within the initial phase, but tends to become softer at later phase if the effects of tensile strength of interfaces are ignored.

Load-Deflection Relationship At P6 Of OSMA4I **Table 4.6**

No.	Loads (kN)	Deflections At P6 (mm)	Load Increments (kN)	Deflection Increments (mm)	Stiffness (kN/mm)
1	0.000	0.000			
2	2.980	-0.039	2.980	0.039	76.410
3	4.960	-0.087	1.980	0.048	41.250
4	6.940	-0.167	1.980	0.080	24.750
5	10.240	-0.577	3.300	0.410	8.049
6	11.890	-2.009	1.650	1.432	1.152
7	11.993	-2.190	0.103	0.181	0.569
8	12.045	-2.280	0.052	0.090	0.578
9	12.071	-2.396	0.026	0.116	0.224
10	12.096	-2.567	0.025	0.171	0.146
11	12.148	-2.954	0.052	0.387	0.134
12	12.251	-3.827	0.103	0.873	0.118
13	12.264	-3.957	0.013	0.130	0.100
14	12.270	-4.024	0.006	0.067	0.090
15	12.274	-4.080	0.004	0.056	0.071

It is noted that the last recorded load was 12.50 kN during the model test of OSMA4. The analyses based on the discrete model show 12.27 kN of the ultimate load. The reduction of the ultimate load may be caused by the different loading pattern applied in the model test of the model OSMA4 and FE simulation. As discussed in Chapter 2, the knife load, which was effectively transformed into the uniform distributed load, was applied in the model while the point load (or true knife load) was used in the FE simulation. The reduction may also be caused by the different tensile strength used in

the FE simulation from that of the actual arch model. However, both effects are not significant. Thus, it may be reasonable to conclude that the analyses have well simulated the behaviour of the tested model arch in terms of the ultimate load.

The application of the self-weight of the model arch did not cause any separations of the contact elements along the interfaces. When the applied load reached 4.96 kN, the separations of the interfaces at the intrados took place at the intrados of the arch under the loading location and the springing at the unloaded side. As the load increased, the thrust line gradually moves away from the axis of the arch ring. As in Fig. 4.13 shows, the first hinge is formed at a load of 10.24 kN under the loading location (between blocks 23 and 24); and the second is at 11.89 kN at the springing of the unloaded side (between the support and block 1); and the third is at 12.05 kN around the quarter span of the unloaded side (between blocks 10 and 11); and the fourth is at 12.27 kN near the springing of the loaded side (between blocks 30 and 31).

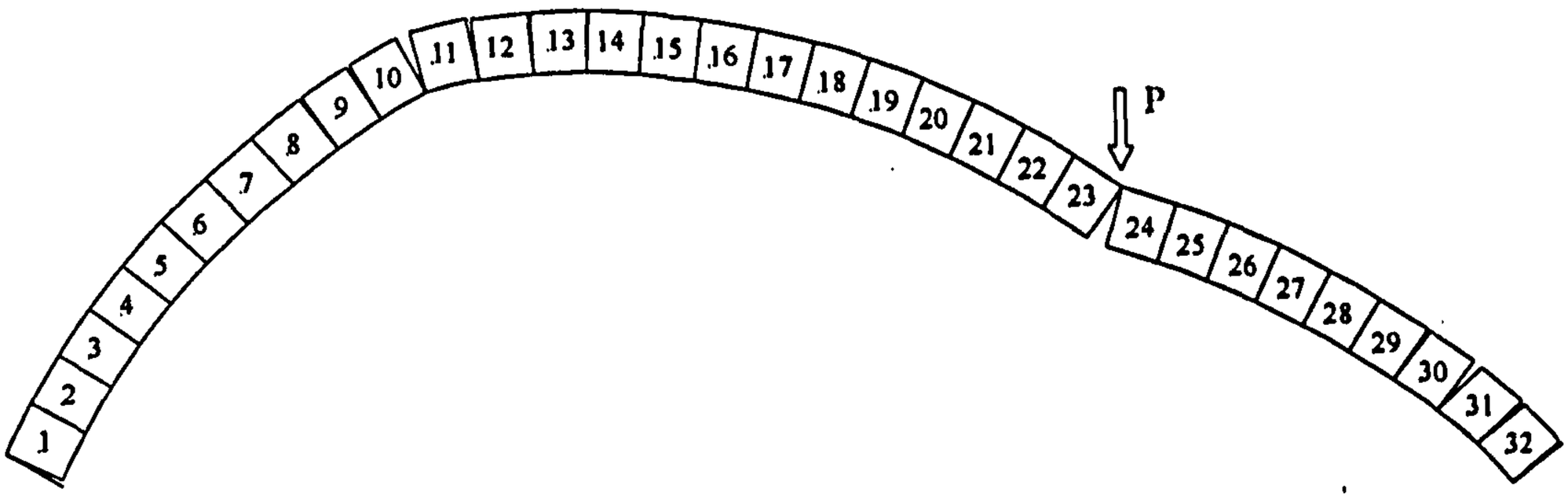

Fig. 4.13 Simulated Mode of Failure of OSMA4 Using Discrete Model

The first and the second hinges are formed at single interfaces. Though the third true hinge is developed at the interface between blocks 10 and 11, other four "quasi-" hinges (two at each side of the true hinge) are also formed. The fourth true hinge is formed between blocks 30 and 31 instead of the expected location between block 32 and the support. It may be noted that, once the first hinge is formed, the locations of the rest of the hinges are essentially determined by statics though their precise locations may be dependent on one another.

When the first hinge is formed at 10.240 kN (F), the horizontal force of the system (H) is 19.250 kN, and the upwards reaction at the loading location of block 23 (V) is 3.923

kN. As we know, the second hinge will take place at the extrados near the springing at the unloaded side. Its precise location will be where the maximum bending moment occurs within the deformed arch under the force F + ΔF and the self weight between the first hinge and the second one. In the case of the model OSMA4, the second hinge is formed at the springing on the unloaded side under the load increment 1.65 kN of ΔF. H is increased to 20.305 kN, and V is decreased to 3.665 kN. The fact that V becomes smaller indicates that the rate of the loss of the stiffness on the left hand side of the arch (relative to the load) is greater than that on the right hand side. As another 0.155 kN of ΔF is added, one of the "quasi-" hinges within the quarter span at the unloaded side becomes the third hinge. At this stage, H is increased to 20.403 kN, and V is decreased to 3.636 kN. The effect of the locations of the second and the third hinges on the location of the fourth hinge could be reflected by the final values of H and V. As another 0.228 kN of ΔF is added, one of the "quasi-" hinges near the springing at the loaded side becomes the fourth hinge. At this stage, H is increased to 20.409 kN, and V is decreased to 3.635 kN.

4.4 Five-Metre Span OSBMAB Without Fill (OSMA3)

4.4.1 Smeared Modelling And Analysis

The geometry and typical FE mesh of OSMA3 using the smeared modelling method were given in Table 2.2 and Fig. 3.6. Fixed boundary conditions were applied at the ends of the main arch and the end spandrel arches. To simulate the destructive test of OSMA3, a load was applied at the arch seat as that during the model test.

For the main arch and spandrel arches, the material properties and other elements related parameters are the same as those used for the smeared modelling and analysis of the model OSMA4 (Section 4.3.1) except that 0.30 N/mm^2 of tensile strength is used. This is because that the mean tensile strength obtained from the brickwork prisms of the model OSMA3 is higher than that from the brickwork prisms of the model OSMA4 (see Section 2.1.3.2); for the spandrel piers, they are the same as those used for the model OSMA2 (Section 4.2).

The material properties used in the analyses are given in Table 4.7.

Material Properties For The Analyses Of SM OSMA3 Table 4.7

Poisson's Ratio	0.20
Shear Transfer Coefficient For Open Cracks (β1)	0.01
Shear Transfer Coefficient For Close Cracks (β2)	0.10
For Main Arch and Spandrel Arches	
Density	2300 (kg/m^3)
Young's Modulus	10000 (N/mm^2)
Uniaxial Crushing Strength (σc)	18.00 (N/mm^2)
Uniaxial Tensile Cracking Strength (σt)	0.30 (N/mm^2)
For Spandrel Piers	
Density	1800 (kg/m^3)
Young's Modulus	3500 (N/mm^2)
Uniaxial Crushing Strength (σc)	7.50 (N/mm^2)
Uniaxial Tensile Cracking Strength (σt)	0.25 (N/mm^2)

Figs.4.14 to 4.16 show the comparisons of the results between the FE analysis and the model test at three locations along the intrados of the main arch (see Section 2.3.3 for the locations P2, P4 and P6).

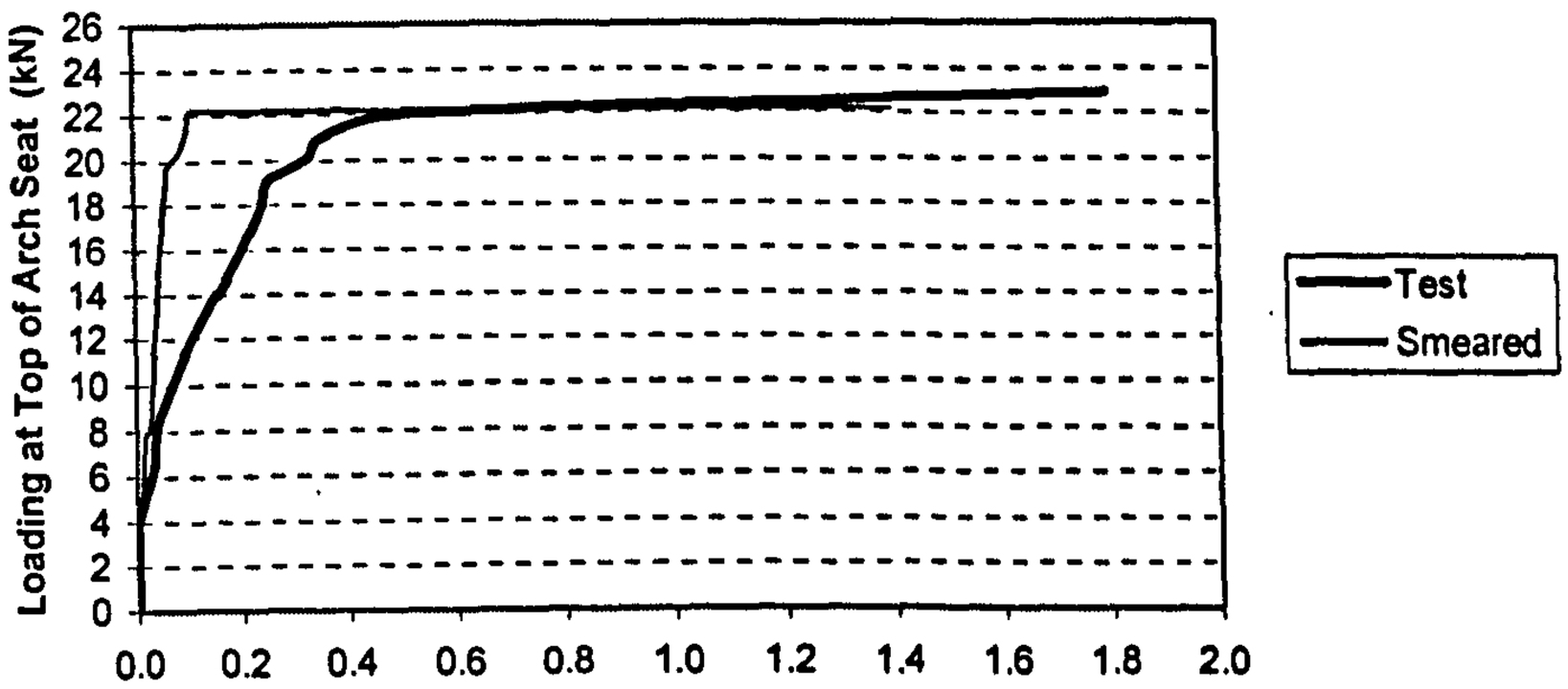

Fig. 4.14 Load-Deflection Curves At P2 Of OSMA3 Using Smeared Model

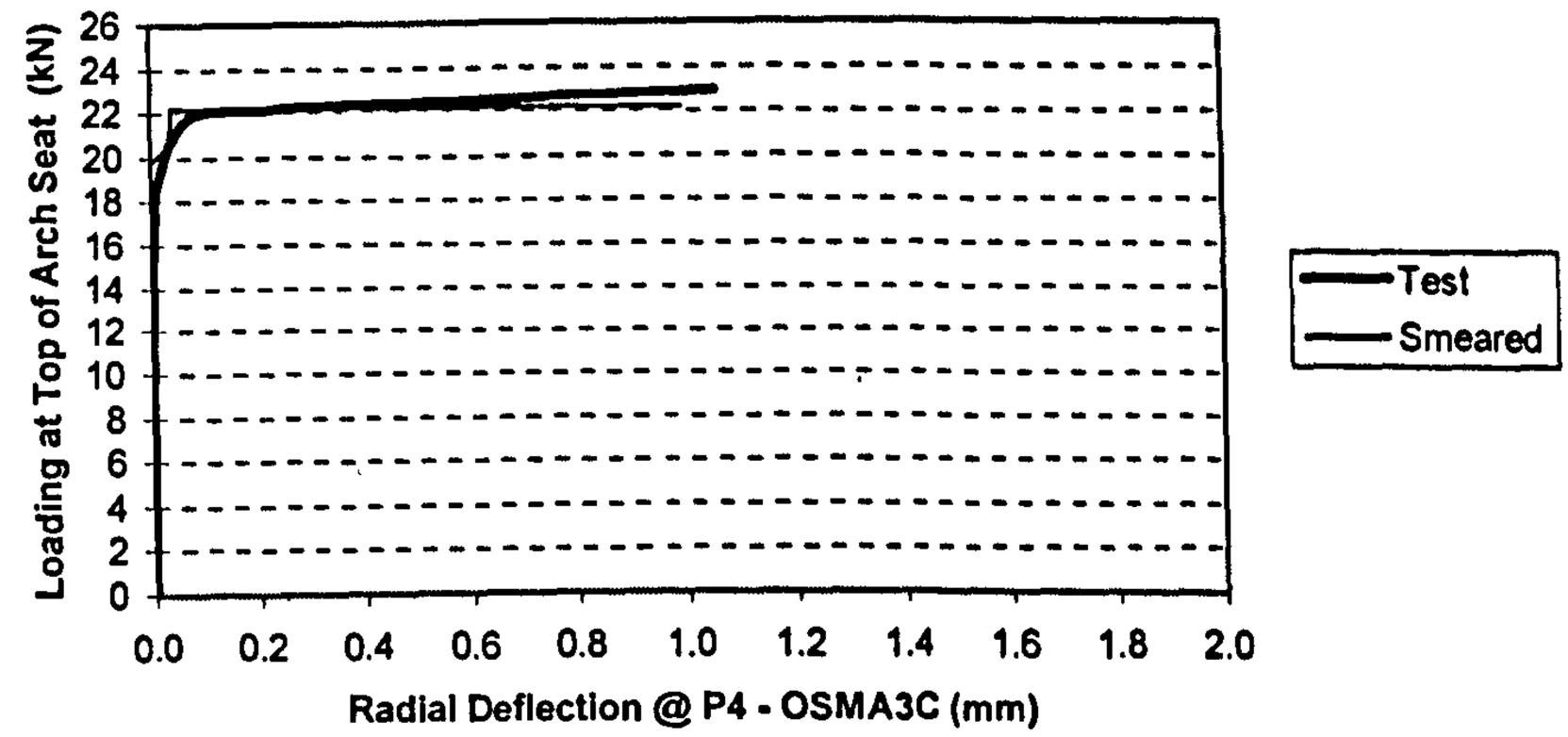

Fig. 4.15 Load-Deflection Curves At P4 Of OSMA3 Using Smeared Model

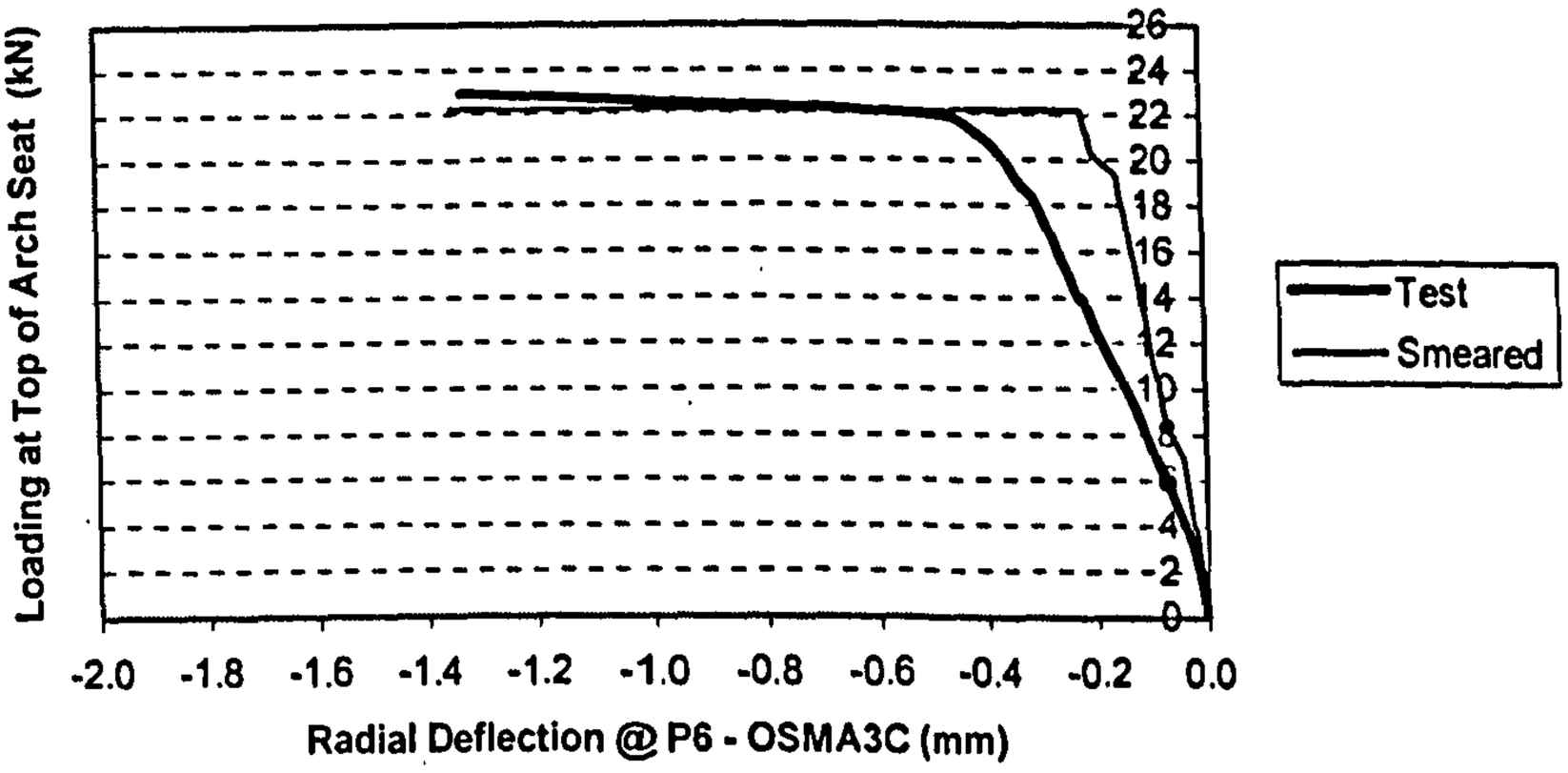

Fig. 4.16 Load-Deflection Curves At P6 Of OSMA3 Using Smeared Model

From Figs. 4.14 to 4.16, it can be seen that the responses of load - deflection recorded during the model tests are reasonably well reproduced in the FE simulations. The two curves are virtually coincident when the load is between 0 and 6 kN, and between 8 and 10 kN. Compared with the responses for the model OSMA4, the nonlinearity associated with the model OSMA3 is less severe. Since the interaction between the spandrel structures and the main arch postponed the occurrence of large amount of cracks within the main arch during the intermediate stages (it may be noted that the overall stiffness of the arch structure was hardly affected by the substantial cracking developed within the spandrel arches during these stages). Thus, a better overall agreement could be achieved.

It appears that there are more "steps" along the simulated curves than those along the tested ones. As discussed above, each of the steps are related the occurrence of the new cracks and/or the further development of the existing ones, and results in the sudden changes in stiffness of the model. As shown in Fig. 4.16, after the first major step at a load between 6 kN and 8 kN (equivalent stiffness at P6 changed from 0.01 mm/kN to 0.03 mm/kN), the model continue to behave almost linearly up to the second step at a load between 19 kN and 20 kN (the stiffness changed from 0.013 mm/kN to 0.060 mm/kN), and then to the third step at a load between 20 kN and 22 kN (the stiffness changed from 0.09 mm/kN to 700 mm/kN). The large load increment between the first and second steps indicates that the occurrence of the cracks immediately before the first step hardly affect the overall behaviour. The small load increment between the second and third steps indicates that the significant loss of the stiffness of the model was caused by the cracks within these two steps. That is, the existence of the spandrel arches and piers may limit the sudden change in overall stiffness of the model arch.

Fig.4.17 shows the sequences of the development of cracks simulated by FE analysis of the model OSMA3, and detailed descriptions at each stage are given in Table 4.8.

From the development of cracks within the open spandrel arch, it can be seen that the spandrel arches/piers postpone the occurrence of the cracks within the main arch. The arch fails due to the extensive cracks at four locations within the main arch (a) and (b) both springings; (c) under loading location; (d) between the arch seat and the crown of the main arch. Compared with the cracking pattern of single arch, the cracks around quarter span at the unloaded side move towards the crown of the main arch as the result

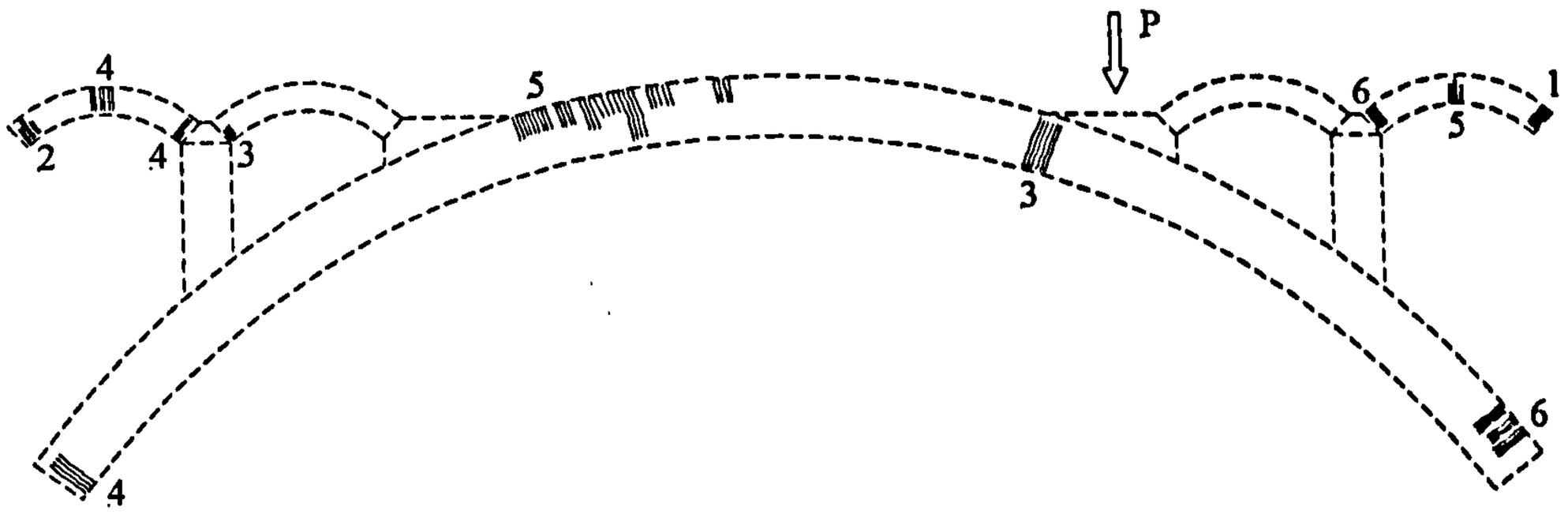

Fig. 4.17 Simulated Cracking Sequences of OSMA3 Using Smeared Model

Cracking Development and Corresponding Loads of OSMA3 **Table 4.8**

(1) At 5.420 kN	The first cracking appeared at the extrados of the springing of the end spandrel arch SA4 at the loaded side. The cracks were caused by the high tensile stresses that were resulted from the downward & inwards deformation of the main arch at the loaded side. As the load increases, these cracks gradually spread through the arch barrel at the springing, and rapidly smeared towards the crown of SA4 along the intrados when the load reached 22.219 kN. It may be noted that, in reality, these cracks would occur much earlier since there was little tensile capacity between the end of the end spandrel arch SA4 and the support frame. It will be seen that the ultimate load of an open spandrel arch under the loading location being considered largely depends on the load capacity of the main arch. These relatively late cracks only have local effects on cracking distribution within the spandrel structures, and have little effects on the load capacity of the structure.
(2) At 18.130 kN	Cracks occurred at the intrados of the springing of the end spandrel arch SA1 on the unloaded side. They were caused by the high tensile stresses, which was resulted from the upward & outwards deformation of the main arch at the unloaded side. The cracks rapidly propagate through the thickness of the arch barrel at the springing at a load of 20.000 kN as a result of the sudden displacement of the main arch due to the cracks that developed at the intrados of the main arch under the loading location.
(3) At 20.000 kN	Cracks occur at two locations. One is at the intrados of the main arch under the loading location, and the other is at the intrados of the left springing of the

	spandrel arch SA2. The crack at SA2 was caused by the upward & outward movement of the main arch, and the rotation of the spandrel pier 1. The occurrence of the first cracking at the main arch causes significant loss of the overall stiffness of the model (it can also be seen in Fig. 4.16). The cracks at the main arch propagates through the thickness of the arch barrel at a load of 22.219 kN.
(4) 22.219 kN	Cracks develop at three locations at the unloaded side. One is at the intrados of the springing of the main arch at the unloaded side; and the other two are at the extrados of the crown and the intrados of the left springing of the spandrel arch SA2. As cracks occur within the main arch, both new and existing cracks generally also develop within the spandrel arches. It may be noted that the cracks within the spandrel arch SA1 smear across the thickness of arch barrel, which indicates that the structural functions of the SA1 have been lost.
(5) At 22.220 kN	Cracks occur at two locations. One is at the extrados of the main arch between the arch seat and the crown of the main arch at the unloaded side, and the other is at the intrados of the crown of the spandrel arch SA4. As these cracks occur, the existing two cracks at the main arch and the one at the crown of the spandrel arch SA2 propagate rapidly. It should be noted the new cracks smear along the extrados between the arch seat and the crown of the main arch.
(6) At 22.225 kN	Smeared cracks develop around the extrados of the main arch near the springing at the loaded side. As these cracks occur, all the existing cracks within both the main arch and the spandrel arches propagate rapidly. The cracks develop at the extrados of the left springing of the spandrel arch SA4. This crack occurs as the result of the extension of the existing cracks around the crown of SA4. At the same time, the cracks under the load extend significantly around the arch seat, and the cracks between the arch seat and the crown of the main arch on the unloaded sided progress rapidly, which leads to the failure of the model arch.

of the interaction between the main arch and spandrel arches/piers. The sequences of the occurrence of the crack within spandrel arches/piers may not be realistically reproduced due to the difference in the tensile strengths adopted in the smeared model. However,

this only has local effects on the cracking patterns with spandrel arches/pier, and has little effects on the overall load capacity of the model arch.

4.4.2 Discrete Modelling And Analysis

The geometry and typical FE mesh of OSMA3 using the discrete modelling method were given in Table 2.2 and Fig. 3.12. Fixed boundary conditions were assumed for the main arch and the spandrel arches.

As discussed in Section 3.3.6, the locations of potential failure sections were prescribed largely based on the results of the observations during the model test (OSMA3) and the simulations using the smeared modelling method. Four parameters were used to locate the potential failure sections near the springings of the main arch & the end spandrel arches, and near the bottoms of the spandrel piers. By altering the values of these four parameters, different failure loads and modes of failure could be obtained, and the ultimate load would be the least one.

The advantages of using prescribed locations of failure sections are not only to reduce the number of highly nonlinear interface elements to be used, but also to effectively determine the sequences of the occurrence of failure sections. In other words, a failure section might be forced to occur at one particular location, and the development of failure sections within an arch could clearly be traced. Otherwise, many "quasi-" failure sections could be concentrated within small regions, and it could become difficult to identify the sequences of the occurrence of failure sections, which was experienced during the simulation of the model OSMA4 (Section 4.3.2). However, the limitations of using prescribed locations of failure sections are that a number of analyses must be carried out by assuming different values of these four prescribed parameters in order to achieve to determine the ultimate load and the modes of failure of the model arch.

The convergence difficulty due to the change in status of contact elements was generally overcome by using the method (b) (Section 4.3.2). However, direct use of this method could not lead to an efficient solution, and in some cases, convergence solution might not be achieved due to the highly nonlinearity of the model OSMA3. The nonlinearity was mainly due to the large number of contact elements used. Unlike that in the model

OSMA4, the change in contact status was by-and-large "one way", i.e., either progressively closing or progressively opening. For the OSMA3, the change in contact status could be "two ways", i.e., the status of interface elements could vary from "close" to "open" to "close" as the load increased, especially within the spandrel arches. Also, even at initial loading stages, moderate changes in contact status within the main arch would inevitably result in the sudden changes in contact status within spandrel arches. Therefore, if the method (b) were used, the load increment would automatically be reduced down to a very small value as soon as an initial load applies. This small load increment could generally be maintained for a few load steps, and then further decreased as the gaps of the contact elements within the main arch and the spandrel arches develop which could practically prevent achieving the final convergence solution.

It is known from the model tests that the model arch could still carry significant loads even when local cracks took place within the spandrel arches. In other words, the stiffness of the entire model arch was hardly be affected by the occurrence of these initial cracks within the spandrel arches. Thus, a small load increment was initially specified without using the convergence tool of automatic timing (CTAT) until convergence difficulty was encountered. Then, the run was resumed with the function of the CTAT. This procedure might need to be repeated a few times until the ultimate load was achieved.

The mean value 10000 N/mm2 of the Young's Modulus obtained from the material test was adopted. For other elements related parameters, the values were used as those in the analyses of OSMA4 (Section 4.3.2). The material properties used in the analyses are given in Table 4.9.

Figs.4.18 to 4.20 show the comparisons of the results between the FE analysis and the model test at three locations along the intrados of the main arch (see Section 2.3.3 for the locations P2, P4 and P6). It may be noted that the absolute maximum scale of the X-axis in the Figures is set to 2 mm in order to visibly compare the FE results with those obtained from the model test. As a result, the last three or four load increment results are not included in Figs. 4.18 (P2) and 4.20 (P6).

Material Properties For The Analyses Of DM OSMA3 Table 4.9

For Main Arch And Spandrel Arches	
Density	2300 (kg/m^3)
Poisson's Ratio	0.20
Young's Modulus	10000 (N/mm^2)
For Spandrel Piers	
Density	1800 (kg/m^3)
Poisson Ratio	0.20
Young's Modulus	3500 (N/mm^2)
For CONTAC48	
Coefficient Of Friction	0.80
Normal Stiffness	10000 (N/mm)
Tangential Stiffness	1000 (N/mm)
For COMBIN40 Elements In Radial Direction	
Bond Strength	0.0001 (N/mm^2)
Stiffness Of Master Spring	0.01 (N/mm)
Stiffness Of Slave Spring	0.001 (N/mm)
For COMBIN40 Elements In Tangential Direction	
Bond Strength	0.0001 (N/mm^2)
Stiffness Of Master Spring	0.01 (N/mm)
Stiffness Of Slave Spring	0.001 (N/mm)
Locations Of Potential Failure Sections	
To The Springing Of Main Arch	30 (mm)
To The Bottom Of Spandrel Piers	90 (mm)
To The Springing Of End Spandrel Arches	20 (mm)
To The Crown Of Main Arch (Unloaded Side)	600 (mm)

It can be noted that the loads vs. displacements obtained from the model test are correctly reproduced along the ring of the main arch, especially with the applied load up to 16 kN (about 70% of the ultimate load). The simulated softer behaviour of the model is caused by the factors discussed in Section 4.3.2. Since a small load increment maintains throughout the analysis, the simulated responses appear relatively smooth (no sudden change in stiffness of the model is involved).

Fig. 4.21 shows the mode of failure and the sequences of the development of the hinges, and the locations of the hinges and the corresponding loads are given in Table 4.10.

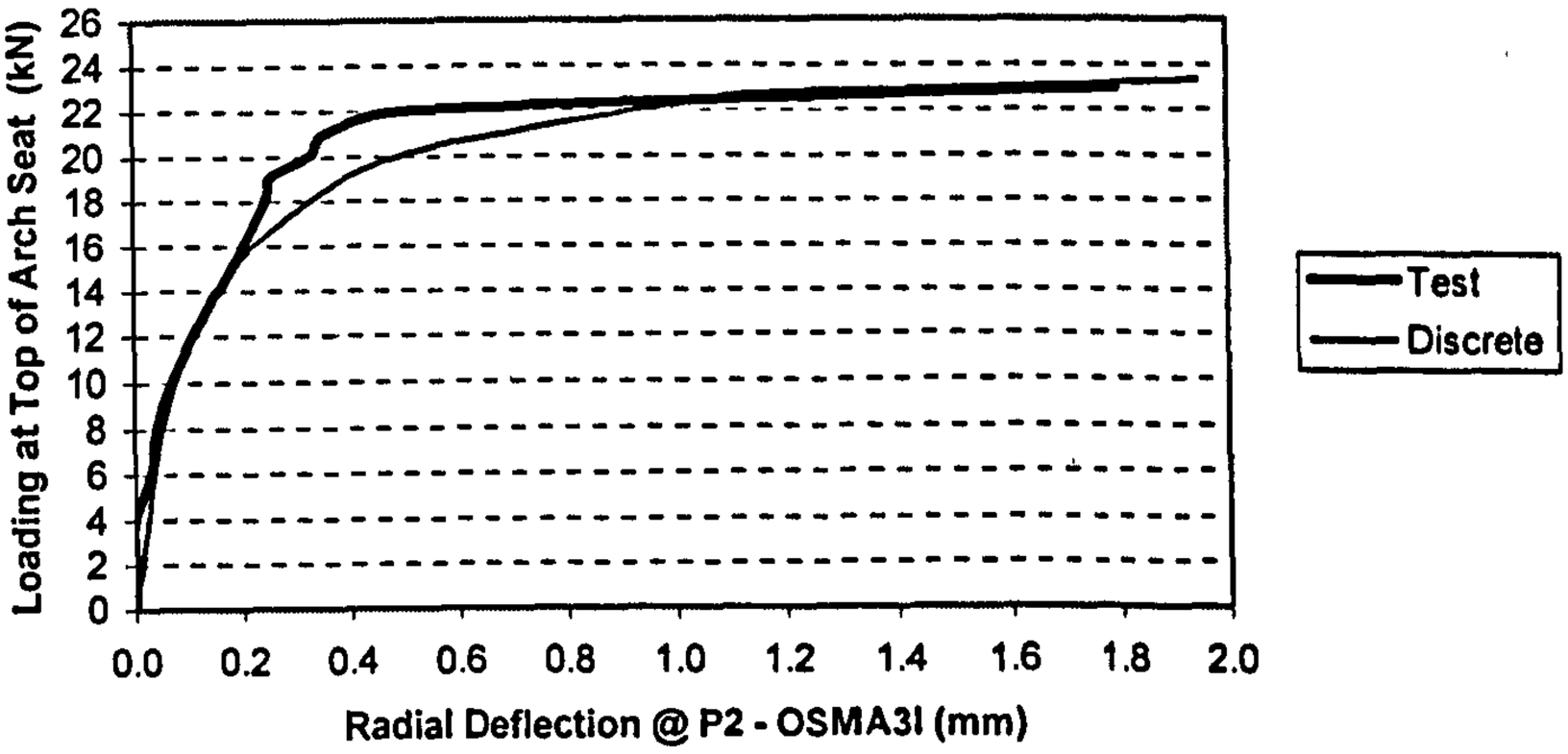

Fig. 4.18 Load-Deflection Curves At P2 Of OSMA3 Using Discrete Model

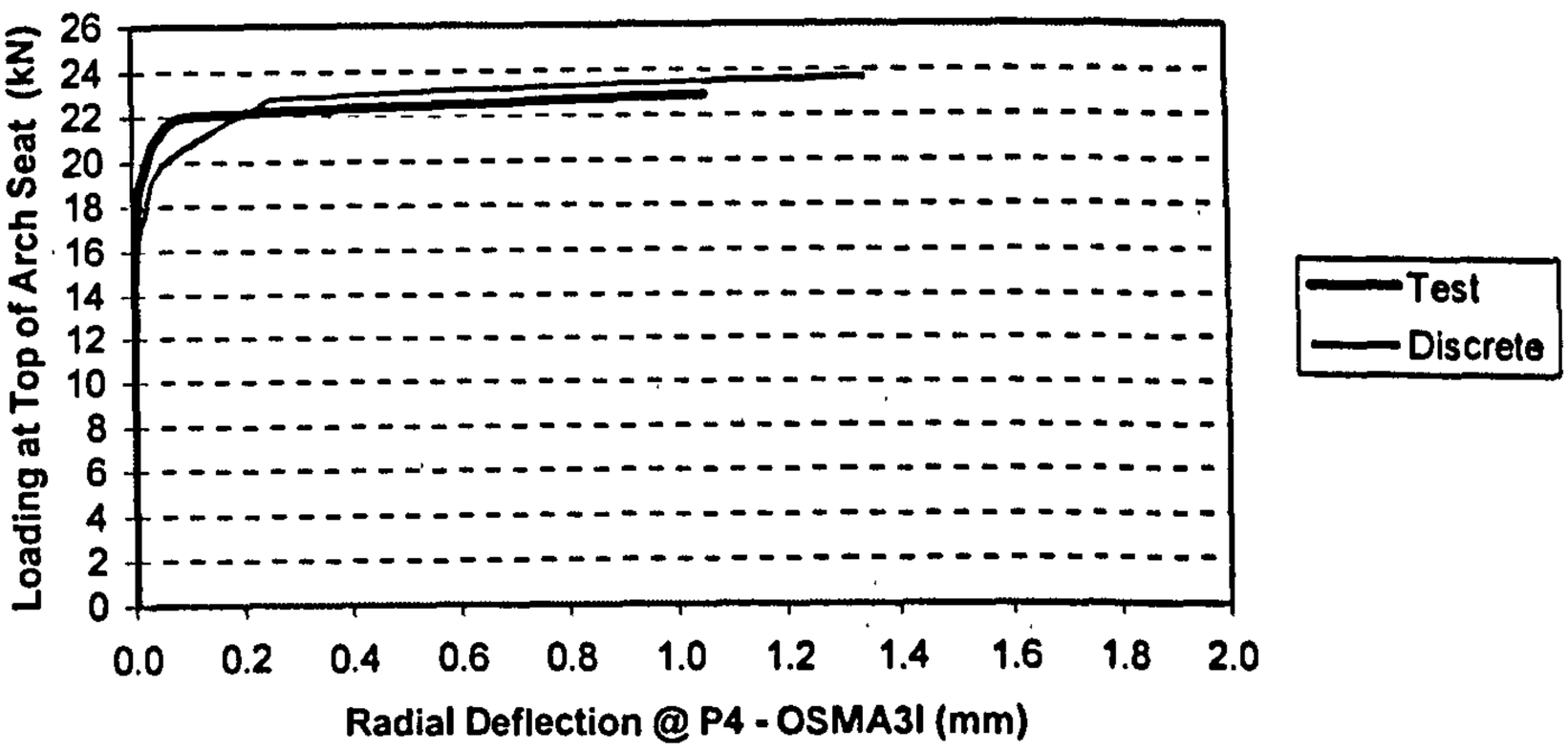

Fig. 4.19 Load-Deflection Curves At P4 Of OSMA3 Using Discrete Model

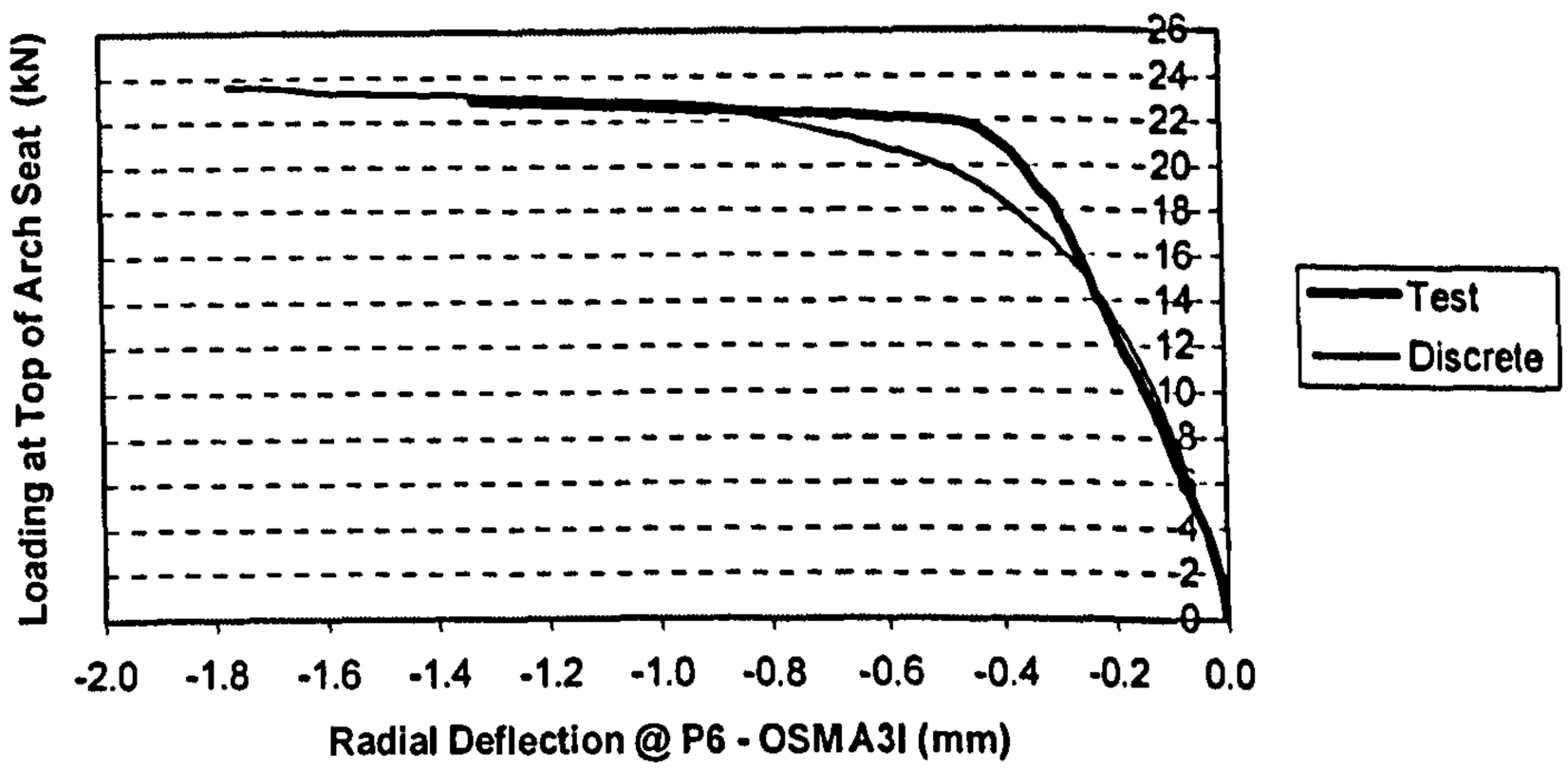

Fig. 4.20 Load-Deflection Curves At P6 Of OSMA3 Using Discrete Model

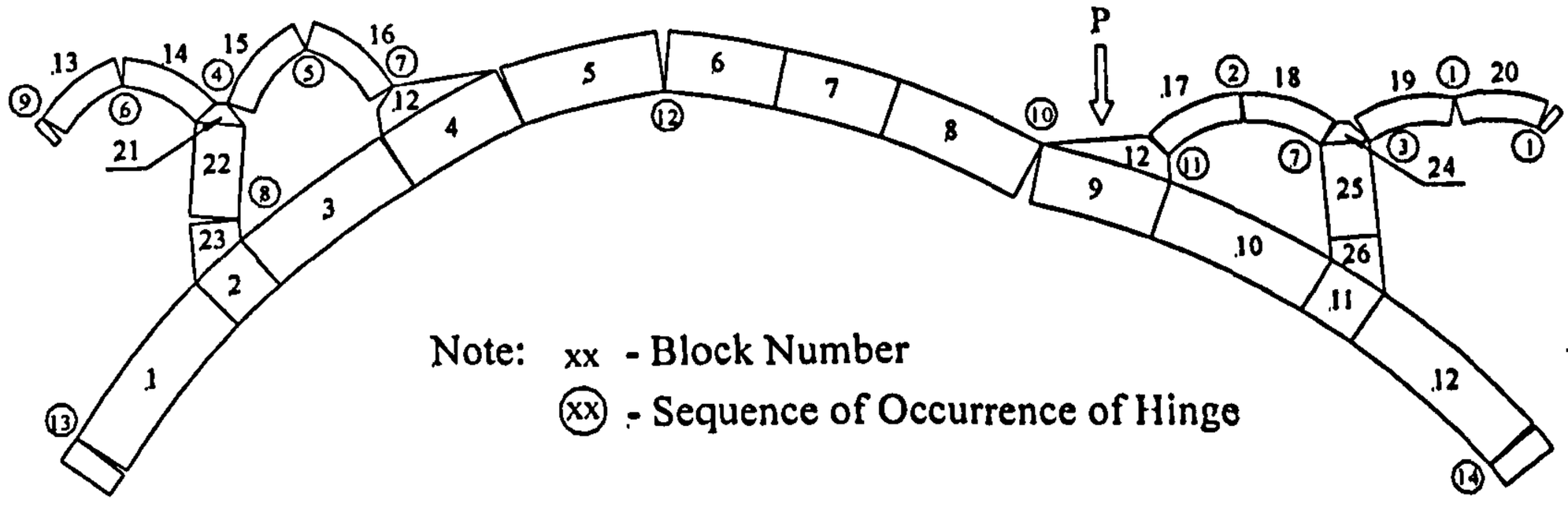

Fig. 4.21 Simulated Mode of Failure of OSMA3 Using Discrete Model

Sequence of Hinge Development and Corresponding Load Table 4.10

Hinge No	Loads (kN)	Locations
1	Self-weight	SA4 (Crown & Right End)
2	0.795	SA3 (Crown)
3	4.139	SA4 (Left End)
4	6.946	SA2 (Left End)
5	9.097	SA2 (Crown)
6	9.559	SA1 (Crown)
7	10.196	SA2 & SA3 (Left Ends)
8	10.446	Pier1
9	10.951	SA1 (Left End)
10	19.902	MA (Under load)
11	21.622	SA3 (Left End)
12	22.790	MA (Near Crown)
13	23.147	MA (Left End)
14	23.646	MA (Right End)

As the self-weight of the model is applied, the entire model deforms downwards and inwards with its maximum values at the intrados of the crown of the main arch, and at the intrados of the crowns of the end spandrel arches (SA1 & SA4), respectively. Since the interfaces can carry little tensile stresses, the hinges are immediately formed at the intrados of the outer springings of the end spandrel arches (SA1 and SA4), and at the extrados of the crowns of all four spandrel arches. The detailed responses of the spandrel arches and piers are discussed below.

(1) At the loaded side

For the end spandrel arch SA4, it continues to deform downwards and inwards as the applied load (P) increases. The third hinge is formed at the intrados of the left springing when P reaches 4.139 kN. It may be noted that, once the third hinge is formed, the

spandrel arch SA4 has little structural significance apart from providing a constant reaction upon the top of the pier at the point where the third hinge is located. This reaction is equal to the thrust within SA4, and its value is 0.787 kN with Fx = -0.324 kN, and Fy = -0.710 kN. The value of the vertical component (Fy) is approximately equal to the weight of half spandrel arch (SA4). Since only three hinges are formed within the spandrel arch SA4, it may not fail unless the movement at its left end is excessive. In this case, this type of failure will be one of the typical failure modes for a "perfect" arch (Melbourne, 1995).

For the spandrel arch SA3, since a hinge was formed at the extrados of the crown under the self-weight of the model, the reaction associated with the hinge acts upon two halves of SA3. The direction of this reaction is virtually horizontal, and its value remains about 0.353 kN. The second hinge occurs at the intrados of the right springing as P reaches 10.196 kN. The occurrence of the second hinge within SA3 causes the redistribution of the loads (or internal forces) along the arch barrels at its both ends. That is, at the left end, the increasing reaction at the intrados (potential location of the third hinge) drops (Fx drops from 0.3 to 0.172 kN, and Fy drops from 0.531 to 0.499 kN); and at the right end, the reaction at the intrados increases (Fx increases from 0.309 to 0.353 kN, and Fy increases from 0.495 to 0.731 kN). Once the second hinge occurs, the right half of SA3 hardly has any structural functions apart from providing nearly constant reactions upon the top of the pier (Fx = 0.335 kN, and Fy = 0.730 kN) and the crown of SA3 (Fx = 0.335 kN, and Fy = 0.000) at the points where the first and the second hinges are located, respectively. As the third hinge occurs at the intrados of the left springing when P reaches 21.622 kN, the function of SA3 is equivalent to two forces acting on the arch seat and the top of the pier at the locations where the second and third hinges are formed (Fx = 0.336 kN and Fy = 0.727 kN).

For the spandrel pier, there are not any hinges developed within it. The function spandrel pier is to transfer the loads from spandrel arches to the main arch. Prior to the development of the three hinges with SA3, the forces acting upon the interfaces between the spandrel pier and the main arch include (a) weight of the spandrel pier (2.104 kN); (b) weight of half SA4 (0.728 kN); (c) the vertical component of the interaction between spandrel pier and SA3 (varies from 0.168 to 1.376 kN depending on the stiffness of SA3); and (d) unbalanced horizontal forces at the top of the pier between SA3 and SA4.

Once the three hinges are developed within SA3, the spandrel pier simple transfers its own weight, and halves of the weights of SA3 and SA4 to the main arch (3.700 kN in total).

(2) At the unloaded side

For the spandrel arch SA2, one hinge was virtually developed at the extrados of the crown under self-weight only. As the load P increases, the unloaded side of the model moves upwards and outwards. The interfaces at the crown where the hinge is located gradually come into contact, and a new hinge starts to be developed at the intrados. As a result of the movement of the main arch and the rotation of the pier 1, the first hinge is formed at the extrados of the left end when P reaches 6.946 kN. Once the first hinge is formed, the relative movement within SA increases. The second hinge is formed at the intrados of the crown at 9.097 kN, and the third one is formed at the extrados of the right end at 10.196 kN. Once three hinges are developed, SA2 loses its structural capability, and it may be replaced by two forces, one of which acts on the top of the spandrel pier, and the other acts on the arch seat (the two forces are equal in magnitude and opposite in direction with Fx =2.923 kN & Fy = 0.727 kN). It is noted that, though both the spandrel arches SA2 and SA3/SA4 lose their structural functions due to the movements of the ends, the resultant horizontal forces are not the same, i.e., 2.923 kN for SA2 and 0.336 kN for SA3/SA4, which again indicates the most vulnerable direction of the end movement is along the circumference towards the crown (see Section 4.3.1).

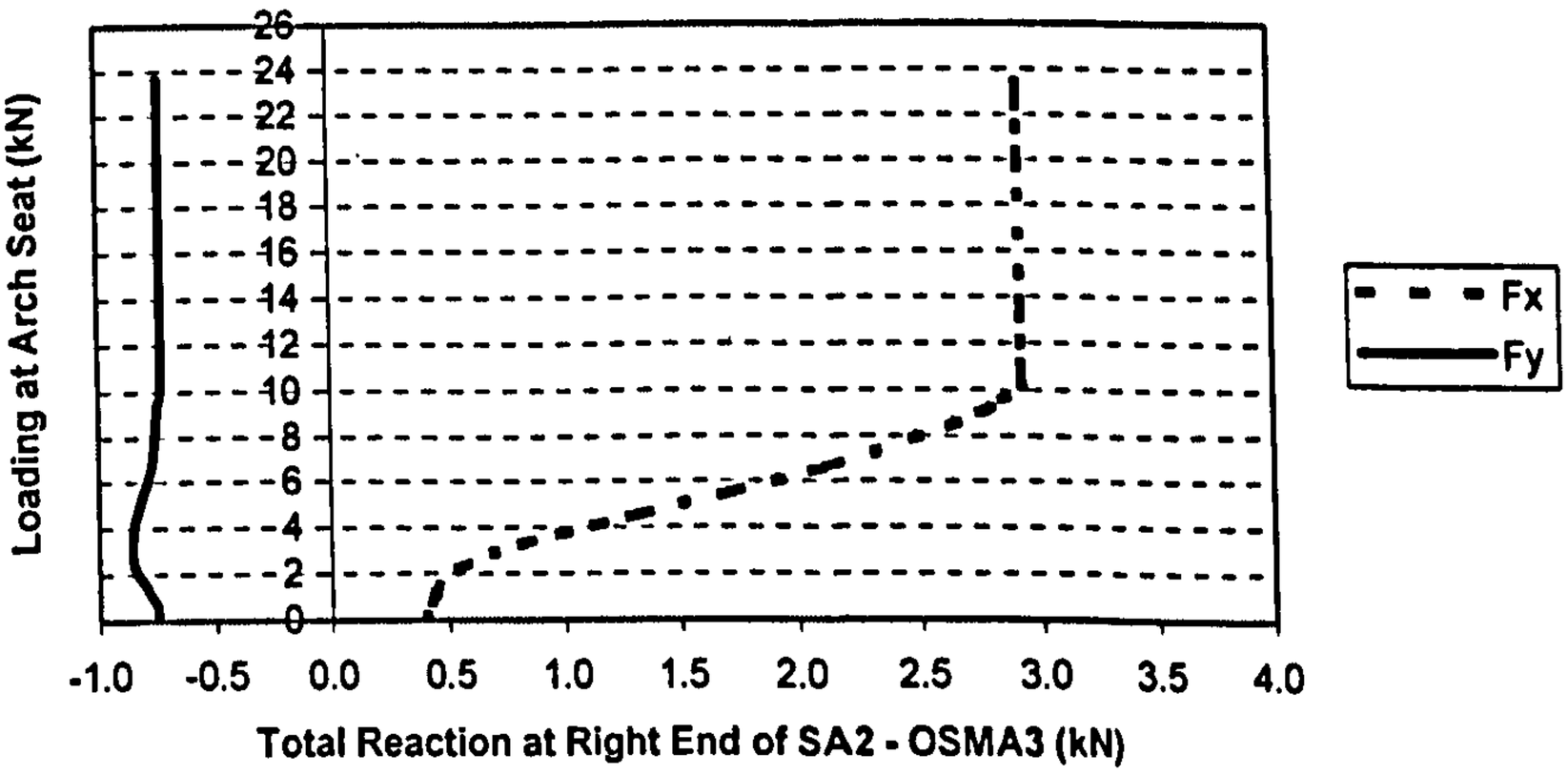

Fig. 4.22 Load – Reaction Curves at Right End of SA2 of OSMA3

For the spandrel arch SA1, two hinges were formed at the extrados of the crown and at the intrados of the left end under self-weight only. As the load P increases, the unloaded

side of the model moves upwards and outwards. Both interfaces where the hinges are located come into contact, and the hinges start to develop at the opposite direction. That is, one is formed at the intrados of the crown when P reaches 9.332 kN, and the other is formed at the extrados of the left end. The hinge is not fully developed at the right end. As a result, the horizontal components of SA1 (3.363 kN) and SA2 (2.923) are not balanced (+0.713 kN) at the top of the pier.

For the spandrel pier, a hinge is formed at the bottom half when P reaches 10.446 kN. The occurrence of this hinge is mainly due to the upward movement of the main arch within the region of the bottom the pier, and the unbalanced horizontal component at the top of the pier. Once this hinge is formed, the force transferred through the pier is constant, i.e. Fx = 0.713 kN and Fy = 3.208 kN (including the weight of part of the spandrel pier 1.607 kN, weight of half SA2 0.727, and the vertical reaction between SA1 and the spandrel pier).

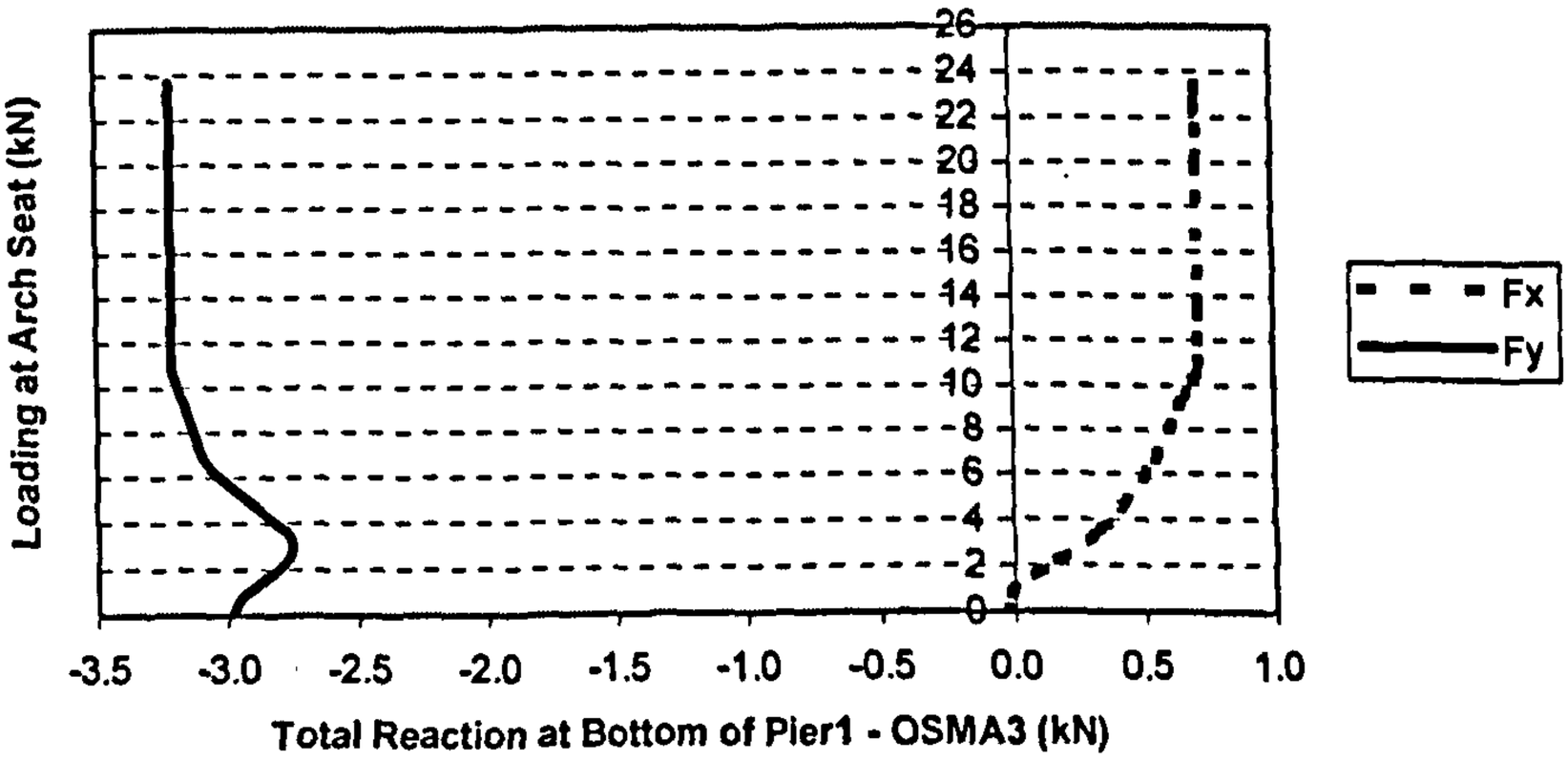

Fig. 4.23 Load – Reaction Curves at Bottom of Pier 1 of OSMA3

(3) Main Arch

Compared with that of main arch itself, the development of hinges within the main arch of the open spandrel arch is delayed as a result of the interaction with the spandrel arches and piers, especially at the unloaded side. The first hinge does not occur until the load reaches 19.902 kN. Due to the reaction transferred from the spandrel pier 1 to the main arch, the second hinge is developed between the arch seat and the crown instead of being developed at the springing at the unloaded side. Compare with the quarter-span hinge in the case of arch itself, this hinge moves up towards the crown of the main arch (about 600 mm horizontal distance between the crown and the hinge) due to the reaction

transferred from SA2. The third hinge is formed at the extrados of the springing at the unloaded side at 23.147 kN, and finally the fourth hinge appears at the intrados of the springing at the loaded side when P is up to 23.646 kN. It may be noted the fourth hinge moves downwards towards the springing (instead of near the springing in the case of arch itself) due to the combined reactions of the horizontal component in the main arch system and the spandrel pier 2.

As the reactions between the main arch and the spandrel arch 2 and pier 1 become constant when the load reaches 10.446 kN, the model may be simplified as shown in Fig, 4.24. That is, the spandrel arches and pier are replaced by two reactions at the unloaded side. The similar simplification may not be assumed at the loaded side since the third hinge at the spandrel arch SA3 occurs after the development of the first hinge under loading location.

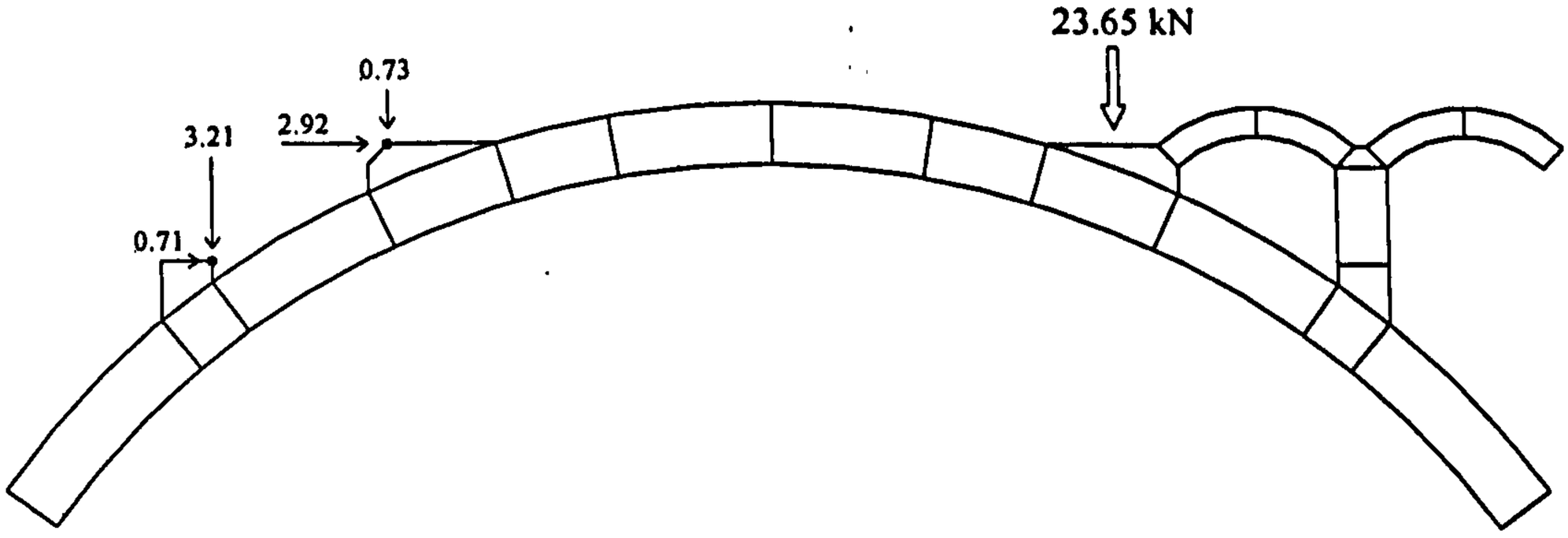

Fig. 4.24 Equivalent Model OSMA3

4.5 Five-Metre Span OSBMAB With Fill (OSMA5)

The geometry and typical FE mesh of the model OSMA5 using the mixed modelling method were given in Table2.2 and Fig. 3.16. Fixed boundary conditions were applied at the ends of the main arch and the end spandrel arches, and the nodes of the shell elements at both the ends of the fill. To simulate the destructive test of the model OSMA5, a load (or pressure) was applied at the arch seat as that during the model test.

For the main arch and spandrel arches, the material properties and other elements related parameters are the same as those used for the smeared modelling of the model OSMA4 (Section 4.3.1); For the spandrel piers, they are the same as those used for the model OSMA2 (Section 4.2) except the uniaxial tensile cracking stress whose value is 0.10 N/mm^2 instead of 0.28 $/mm^2$.

There are two reasons for using a low value. The first reason is due to relatively low tensile strengths of Raewell brickwork recorded during the prism test. The tensile resistance of the piers could be overestimated if the higher of 0.28 $/mm^2$ were used. The second reason is, as discussed in the analyses of the model OSMA3, one of the spandrel piers' functions is to support the spandrel arches and transfer the interactions between the spandrel arches and the piers, and their self weights to the main arch. This function could be replaced by the equivalent forces acting upon the interfaces between the bottoms of the spandrel arches and the main arch once sufficient amount of cracks are developed within the piers and the spandrel arches at the same side of the model. The application of the low tensile strength (or true value) could realistically simulate the effects of cracks within the piers on the behaviour of the model caused.

For the fill, the results obtained from the material tests (Section 2.1.2) are used. As discussed in the discrete modelling and analysis of the model OSMA4 (Section 4.3.2), low tensile and shear bond strengths for nonlinear spring elements COMBIN40 in three directions are assumed. Arbitrary values were assumed for the parameters of both elements SHELL63 and COMBIN14, as they had little structural significance.

The solution strategy for the model OSMA5 was more complex than those used in the above ones. Highly nonlinearity of the model is not only due to large potential regions of cracks within the arch, but also due to the possible separation and contact of large

number of interface/contact elements along the interface between the arch and the fill. An efficient solving process has been established as follows: -

(a) Run the model only with boundary conditions applied to stabilize the model;

(b) Run the model under self-weight only with NRF and CTAT;

(c) Use relatively small load increment (say, 100 N) and large maximum number of equilibrium iterations (say, 70), and run the model under applied loads with CTLS but without CTAT until non-convergent solutions are found;

(d) Use a large number of maximum number of substeps (or small number of load increments) with CTAT, and rerun the model until non-convergent solutions are found;

(e) Same as '4', but use NRM instead of NRF, and rerun the model until non-convergent solutions are found; Repeat '4' and '5' until the model becomes a mechanism, which can generally be identified by checking the cracking pattern of the model.

Step (a) is necessary not only for checking the correctness of the FE model, but also establishing initial states of the model. For step (b), since potential changes in the status of contact elements along the interface between the arch and the fill, it is unlikely to have the analysis converged with one step under self-weight of the model arch. CTAT is used to automatically control the incremental loading process. At post-process stage, the later analysis result data will be deducted by the results from this step in order to compare them with the test results as the initial states under self-weight were not recorded during the model arch tests. For step (c), CTAT was not used as the non-linearity of the model may not be severe, and convergent solutions may be found by using small load increments. Otherwise, if CTAT were used, it would predict the possible changes in status of the contact elements, and the load increment would be automatically reduced if any changes were predicted. As these changes in status of contact elements would occur almost at every single load increment, consequently, the load increment would be reduced to a very small value, and the run time would be significantly increased. At this stage, both force and displacement convergence criteria should be used throughout otherwise true convergent solution may not be found. For step (d), the step (c) fails when the response of the model becomes highly non-linear, which generally indicate the occurrence of many cracks and/or the changes in status of

many contact elements. If the model arch has not become a mechanism, CTAT is used to automatically reduced load increments until the solution converged. Depending on the states of contact elements, it may be necessary to reduce the normal and/or tangential stiffness to improve the convergence rates of contact elements provided that amount of penetration are controlled within the acceptable limits. As we know from the test results, there are several 'steps' along the load-deflection curves of the model arch. As discussed in Chapter 2, these 'steps' were associated with the occurrence of new cracks or the further development of the existing ones within the model arch. The failure of the analysis in Step (c) may not represent the true last step of the load-deflection curves. Therefore, it may be necessary to repeat step (c) and step (d), until last step is found. For step (e), the Newton-Raphson Iteration Method has significant effect on the success of the nonlinear analysis. The NRF is proved robust for the present analysis while the use of NRM could lead to further load increments. Step (e) and (d) may be repeated until true last convergent solution is found.

The material properties used in the analyses are given in Table 4.11.

Material Properties For The Analyses Of DM OSMA5 Table 4.11

For Main Arch And Spandrel Arches	
Density	2300 (kg/m^3)
Poisson Ratio	0.20
Modified Young's Modulus	6000 (N/mm^2)
Uniaxial Crushing Stress (σ_c)	18.00 (N/mm^2)
Uniaxial Tensile Cracking Stress (σ_t)	0.28 (N/mm^2)
Shear Transfer Coefficient For Open Cracks (β_1)	0.01
Shear Transfer Coefficient For Close Cracks (β_2)	0.10
For Spandrel Piers	
Density	1800 (kg/m^3)
Poisson Ratio	0.20
Modified Young's Modulus	3500 (N/mm^2)
Uniaxial Crushing Stress (σ_c)	7.50 (N/mm^2)
Uniaxial Tensile Cracking Stress (σ_t)	0.10 (N/mm^2)
Shear Transfer Coefficient For Open Cracks (β_1)	0.01
Shear Transfer Coefficient For Close Cracks (β_2)	0.10
For Fill	
Density	1540 (kg/m^3)
Poisson Ratio	0.30
Young's Modulus	2200 (N/mm^2)
Dilatancy angle	0

Cohesion (N/mm^2)	0.10
Angle of internal friction	39°
For CONTAC49	
Coefficient Of Friction	0.80
Normal Stiffness	1.0E+5 (N/mm)
Tangential Stiffness	5.0E+3 (N/mm)
For COMBIN40 Elements In X, Y and Z Directions	
Bond Strength	0.001 (N/mm^2)
Stiffness Of Master Spring	0.1 (N/mm)
Stiffness Of Slave Spring	0.01 (N/mm)
For COMBIN14 Elements	
Stiffness	0.10 (N/mm)
Coefficient Of Friction	0.30
For SHELL63	
Thickness	1 (mm)
Poisson Ratio	0.30
Young's Modulus	21000 (N/mm^2)

Figs.4.25 to 4.27 show the comparisons of the results between the FE analysis and the model test at three locations along the intrados of the main arch (see Section 2.3.5 for the locations P2, P4 and P6).

It can be seen that the simulated responses of loads and deflections along the intrados of the main arch are almost linearly throughout the loading history. The model arch does not experience sudden loss of the stiffness. However, minor change in stiffness can be seen at loads around 7 kN, 18.5 kN, and between 26 kN and the ultimate load 32.8 kN. As discussed above, this change in stiffness along the curves indicates that new cracks and/or the further development of the existing ones have taken place, but have little effects on the integrity (or the overall stiffness) of the model until the model fails. A typical brittle failure mode was thus simulated. The occurrence of the cracks within the main arch (or the loss of overall stiffness) was postponed due to the interaction between the main arch and the spandrel arches/piers and fill.

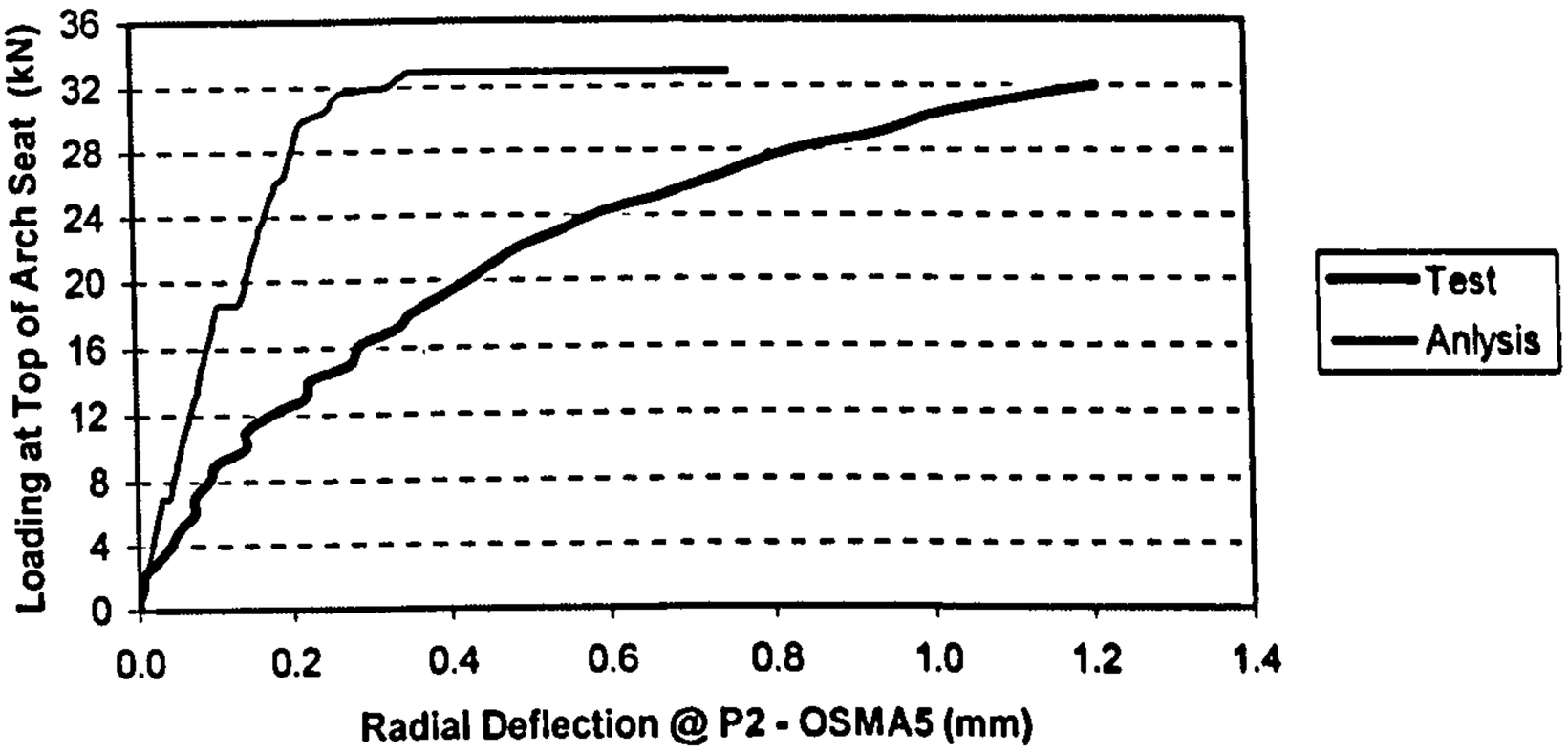

Fig. 4.25 Load-Deflection Curves At P2 Of OSMA5 Using Mixed Model

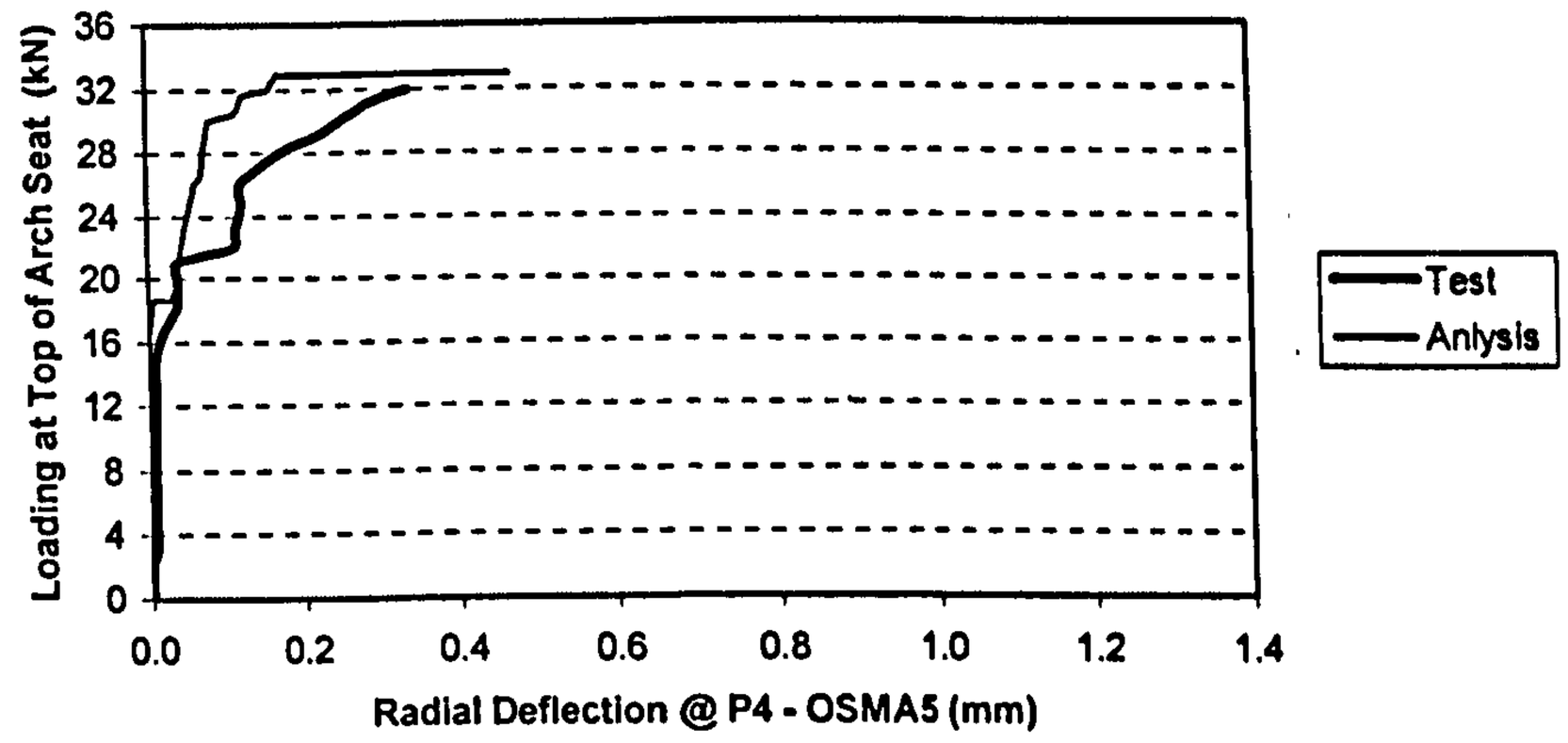

Fig. 4.26 Load-Deflection Curves At P4 Of OSMA5 Using Mixed Model

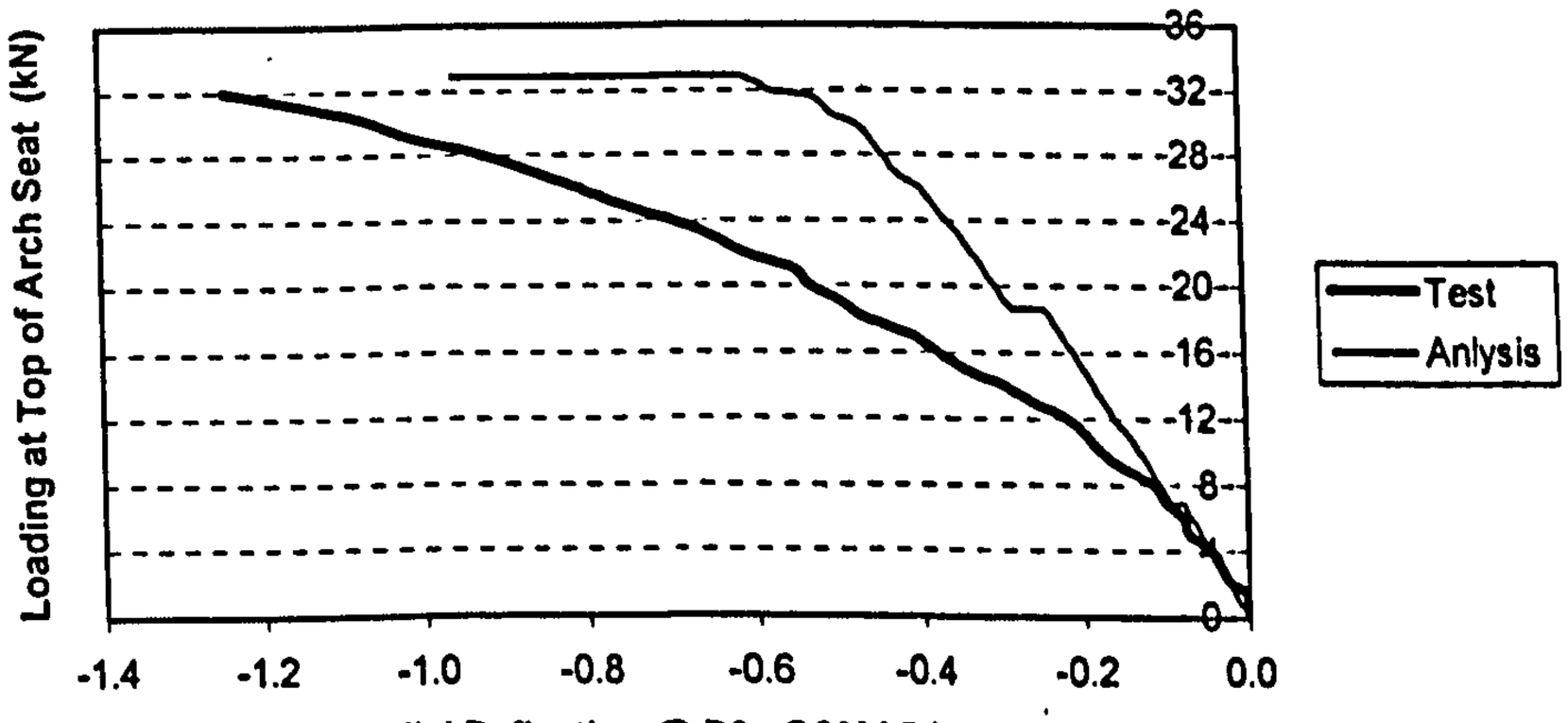

Fig. 4.27 Load-Deflection Curves At P6 Of OSMA5 Using Mixed Model

Fig.4.28 shows the sequences of the development of cracks simulated by the FE analysis of the model OSMA5 using the mixed modeling method, and the detailed descriptions at each major stage are given in Table 4.12.

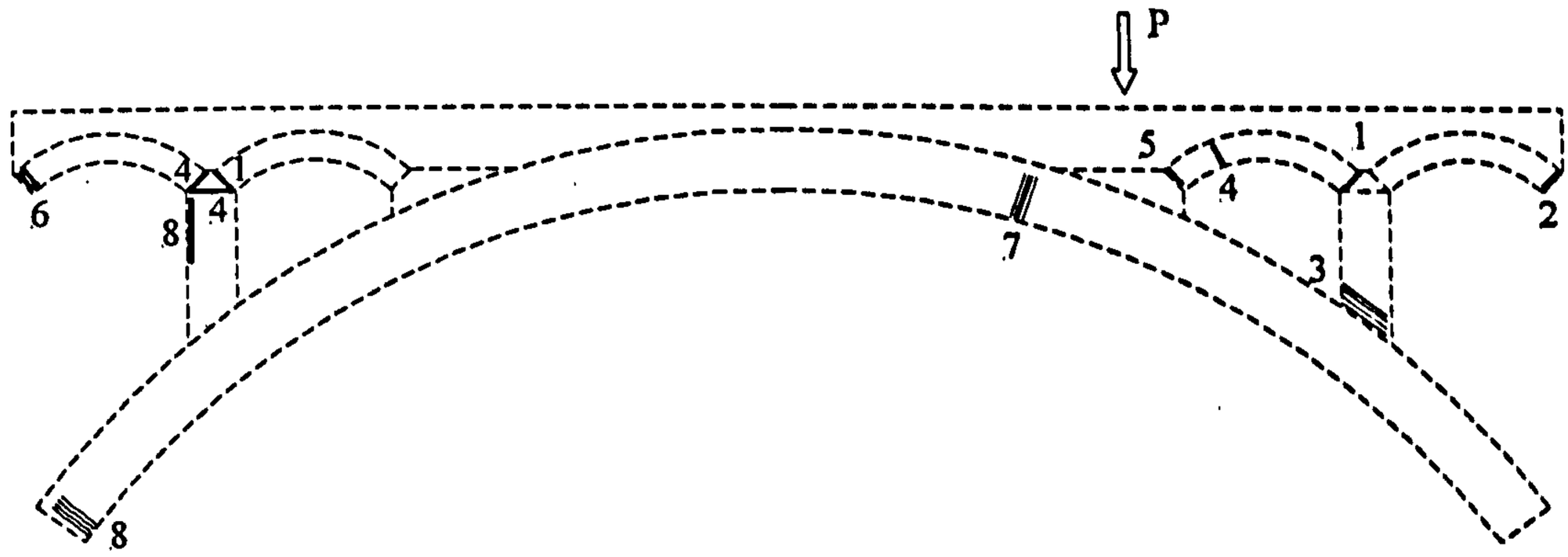

Fig. 4.28 Simulated Failure Pattern of OSMA5 Using Mixed Model

Cracking Development and Corresponding Loads of OSMA5 **Table 4.12**

Under Self-weight	Two minor cracks symmetrically developed within the top of the piers. One is around the extrados of the right springing of the spandrel arch SA3, and the other is around the extrados of the left springing of the spandrel arch SA2. The first cracks propagated through the half of the thickness of the arch ring at a load of 13.298 kN, and through the thickness at a load of 18.640 kN. The second crack smeared within the top of the pier 1 at a load of 18.640 kN.
6.942 kN	One crack developed at the extrados of the right springing of the spandrel arch SA4, and rapidly smeared through the thickness of the ring at a load of 6.956 kN. This crack was caused by the combined downward and inward movement of the main arch. Unlike the occurrence of the first cracking that had little effect on the overall stiffness of the model, the effect of this crack, despite of its insignificance, was still reflected at the load - deflection curves (the stiffness reduced from 90.909 kN/mm to 0.066 kN/mm as shown in Fig. 4.16).
11.698 kN	One crack occurred at the bottom of the spandrel pier 2 at the loaded side, and suddenly smeared through the thickness of the pier at a load of 18.640 kN.
18.640 kN	One new crack occurred at the intrados between the left springing and the

	crown of the spandrel arch SA3. Existing cracks at the top of the spandrel pier 1 and at the bottom the spandrel pier 2 extensively developed. The effect of the development of these cracks on the overall stiffness of the model was clearly reflected at the load - deflection curves (the stiffness reduced from 6.024 kN/mm to 0.031 kN/mm as shown in Fig. 4.16).
26.400 kN	One crack suddenly occurred at the left springing of the spandrel arch SA3 near the load.
30.000 kN	One crack occurred at the intrados of the left springing of the spandrel arch SA1.
30.400 kN	One crack occurred at the intrados of the main arch near the left side of the arch seat under the loading location, and radially propagated towards the extrados as the load increased.
32.000 kN	Cracks smeared along the left edge of the spandrel pier 1 at the top half. To some extent, the occurrence of these cracks indicated that the interaction between the main arch and the spandrel arches/piers and fill had become nearly constant.
32.01 kN	Cracking occurred at the intrados of the left springing of the main arch over the unloaded side, and the existing cracks at the top of the pier 1 smeared downwards. As the load increased, the existing cracks further smeared, and the model suddenly failed at a load of 32.847 kN without occurrence of significant new cracks.

It can be seen that the ultimate load and overall stiffness are further enhanced by the fill. As the loads increased, the fill separated along the boundary from the support at the loaded side due to the tensions induced by the downward displacements of the main arch. Also, the fill separated from the spandrel arch SA4 on the left half. The development of the tensile stresses at the extrados of the spandrel arch SA4 was postponed by the interactions between SA4 and the surrounding fill. At the unloaded side, the fill and the spandrel arch SA1 acted together, which enabled greater reactions to be transferred to the main arch. It was noted that a large part of the reactions were transferred through the spandrel pier 1 to the main arch since the other part that was transferred through the spandrel arch SA2 and the fill to the main arch was limited by the occurrence of the extensive cracks (or hinges) at the crown of SA2 and vertically

through the fill. The fill above the middle areas of the main arch played a significant role in restraining the upward displacement of the main arch, and postponing the occurrence of cracks within these areas. As results, the cracks both at the loading location and at the unloaded side were delayed.

CHAPTER 5 PARAMETRIC STUDIES

5.1 General

In the previous chapters, the behaviour of the open spandrel brickwork masonry arches was demonstrated by the model tests, and analyzed using nonlinear finite element methods. Three FE modelling techniques were developed for the modelling and analyses of the open spandrel model arches. The FE results were compared with those obtained from the corresponding model tests. Reasonable good correlation between the theoretical results and the test results has been achieved in terms of the modes of failure and ultimate loads. During the modelling of each model arch, however, various assumptions were made in order to create an idealised finite element model of its prototype. As discussed in Chapter 4, it is not always guaranteed to achieve realistic simulations of model tests using the parameters such as Young's modulus, etc., which were directly obtained from the material tests of the corresponding model arches. Also, the values of the parameters that the ANSYS elements required, such as the shear transfer capacity for cracked material in the smeared models, and the stiffness of the interfaces in the discrete models, etc., had to be assumed in order to model various phenomena associated with brickwork masonry arches. These alternations and assumptions would affect the simulated results in various ways. Therefore, it may be necessary to investigate the robustness of the methods of the FE simulations that were developed and used in the previous chapters, i.e., to study the effects of changes in materials and/or elements related parameters on the behaviour of the model arches.

Clearly, a complete study of all the parameters and their combinations may not be achieved owing to time and resource limitations. Attempts have only been made to investigate some of the parameters, which may not be accurately or readily obtained by normal material tests such as Young's modulus, tensile strength, etc., and those associated with the smeared and discrete models developed. It may be noted that most of the parametric studies were carried out using the model OSMA4, and other models were only used where appropriate.

5.2 Material Related Parameters

5.2.1 Young's Modulus

Accurate Young's modulus of brickwork masonry may not be easily obtained through prism tests. As discussed in Section 2.1.3, the test data could be influenced by various factors, one of which is the configuration of prisms. In order to obtain more representative Young's modulus (E) of the model arches, the brickwork prisms used in the material tests are of similar cross section of that of the main arch. The average value of 10000 N/mm^2 was obtained from the brickwork prism tests corresponding to the models OSMA3, 4 and 5, which appears smaller than those commonly reported for the Engineering brickwork masonry. However, the results of the FE simulations in Chapter 4 indicates that such E value still seems higher when compared with the responses of the load – deflection obtained from the model tests under similar loading conditions. The reason why the E values calculated from normal prism tests tend to be overestimated has been discussed in Section 4.2.

The effects of Young's Modulus have been previously discussed by Towler (1981), Crisfield (1985a), and Bridle and Hughes (1990). Various conclusions have been drawn on the effects of change in the modulus on the ultimate loads and the responses of loads vs. displacements. It appears that it has widely been accepted that lower E value in theoretical models generally results in a more realistic response of loads vs. displacements. For the ultimate loads, however, Crisfield (1985a) found that the reduction in the ultimate load caused by the reduction in E value is quite small but becomes more significant as the load moves from the quarter point towards the crown of arch. For shallow arches the collapse load can be reached before all hinges have fully penetrated. Bridle and Hughes (1990) found the failure live load increased from 282 to 354 kN/m as the E value changed from 5000 to 20000 N/mm^2.

No attempts have been made to investigate full range of the effects of changes in E values on the behaviour of the arches either with various configurations or under different loading locations. Parametric studies were only carried out on the models OSMA3 and OSMA4 under the loading location being concerned. However, the present results may appear to conflict with some of the previous findings, especially the ultimate load.

In simple terms, the occurrence of hinges may only depend on the geometry in the case of OSMA4. Since no tension (or negligible) was assumed with an interface between adjacent blocks, the separation of the blocks would take place either at the intrados or at the extrados once the first principal stress at a point is over zero. This stress may be simply determined by the axial forces and the bending moment at the point and the moment of inertia of the interface (the effects of the deformed geometry is trivial, thus it may be ignored), and the material properties may not need to be involved. This was confirmed by the FE results of the model smeared OSMA4. The stresses and strains due to different Young's modulus are listed in Table 5.1 As the E values increases from 1000 to 10000 N/mm^2, the stresses hardly changed, and the strains virtually decreases linearly.

Stresses and Strains For Different E Values **Table 5.1**

For Stresses (N/mm^2)

	σ_x	σ_y	σ_z	τ_{xy}
E=1000 (1)	0.133	-1.686	-0.311	0.284
E=6000 (2)	0.133	-1.683	-0.311	0.283
E=10000 (3)	0.133	-1.685	-0.310	0.283
Ratio of (2)/(1)	1.00	1.00	1.00	1.00
Ratio of (3)/(1)	1.00	1.00	1.00	1.00

For Strains

	ε_x	ε_y	ε_{xy}
E=1000 (1)	5.322E-04	-1.651E-03	6.806E-04
E=6000 (2)	8.869E-05	-2.750E-04	1.134E-04
E=10000 (3)	5.321E-05	-1.650E-04	6.799E-05
Ratio of (2)/(1)	0.17	0.17	0.17
Ratio of (3)/(1)	0.10	0.10	0.10

It may be noted that, for discrete models, the data are extracted from the node directly under the loading location when the first hinge is formed. Since two coincident nodes are initially defined under the loading location, and they may separate when the first hinge is formed, the selected node is the one that is attached to the block on the right hand side. All data are in polar coordinate system.

As expected, the greater the Young's modulus, the smaller the deflections (see Table 5.2, the reference point is P6 of the model OSMA4). It is interesting to note that the

sequences of the development of the four hinges and their corresponding loads are virtually unchanged as the E values increase from 1000 to 6000, and to 10000 N/mm^2.

Deflections Due to Different E Values Table 5.2

No.	Load (kN)	Deflections (mm)		
		E=1000	E=6000	E=10000
1	0.000	0.000	0.000	0.000
2	2.980	-0.338	-0.061	-0.039
3	4.960	-0.760	-0.137	-0.087
4	6.940	-1.454	-0.263	-0.167
5	10.240	-5.121	-0.914	-0.577
6	11.890	-17.962	-3.191	-2.009
7	11.993	-19.567	-3.477	-2.190
8	12.045	-20.372	-3.620	-2.280
9	12.058	-20.918	---	---
10	12.071	-21.669	-3.824	-2.396
11	12.096	-23.171	-4.093	-2.567
12	12.148	-26.638	-4.707	-2.954
13	12.251	-34.483	-6.091	-3.827
14	12.264	-35.614	-6.295	-3.957
15	12.270	-36.181	-6.399	-4.024
16	12.27*	-36.356	-6.451	-4.057

(*Note: - the ultimate load is 12.2723 kN when E is 1000 N/ mm^2, and 12.2735 kN when E is either 6000 or 10000 N/ mm^2).

The effects of different Young's Modulus can also be clearly seen from the load – deflection curves of the model OSMA4 obtained through either the smeared or the discrete modelling approaches. For the smeared models (Fig. 5.1), the first major crack occurs at a load of 10.4 kN when the E values are either 6000, 10000 or 15000 N/mm^2, and the model fails at a load of 13.5 kN for all three cases. For the discrete models (Fig.5.2), despite the large deflections involved, the development of the hinges also takes place at the same loading levels, and fails at the load 12.3 kN for the above E values.

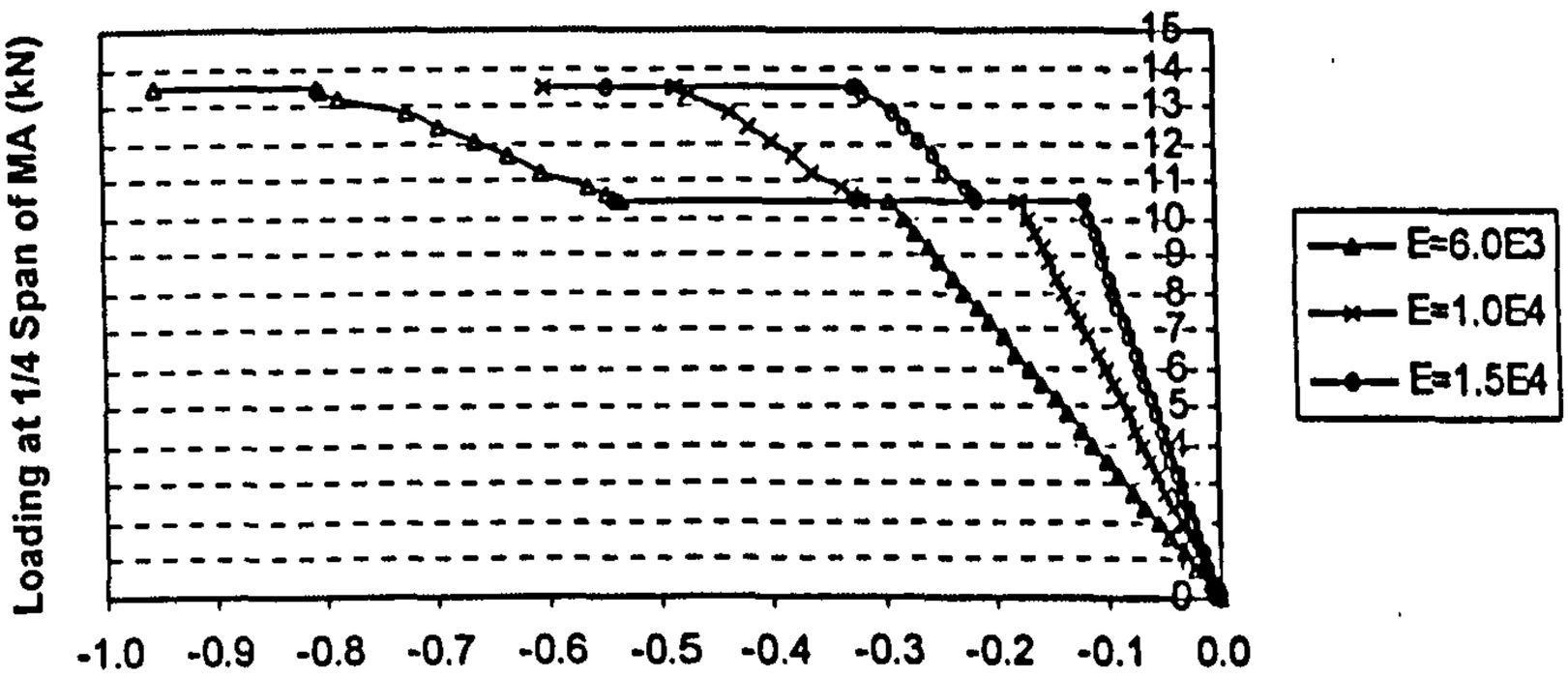

Fig. 5.1 Effects of Young's Modulus For the Smeared Models

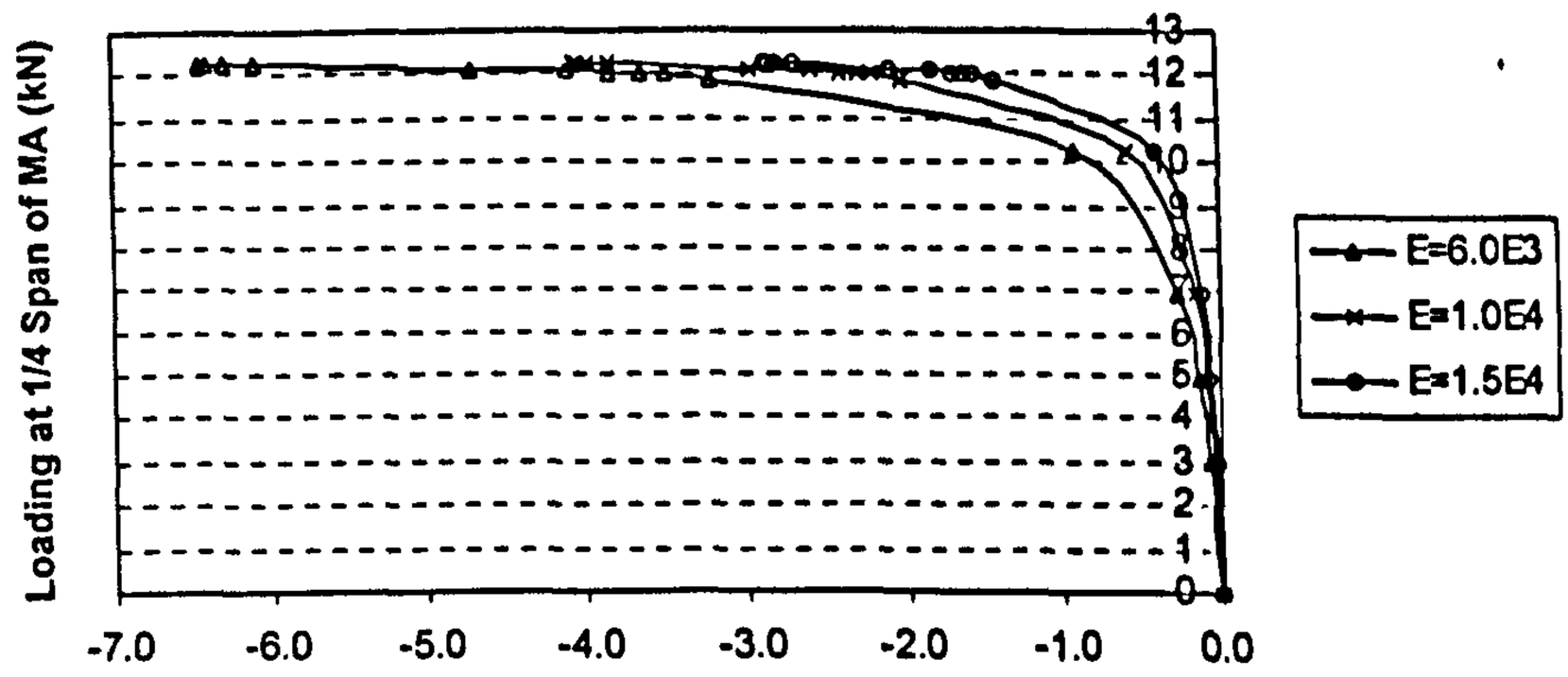

Fig. 5.2 Effects of Young's Modulus For the Discrete Models

In summary, a different Young's modulus may only affect the levels of the displacements and the strains within an arch, and hardly affect the levels of stresses, the ultimate loads, and the modes of failure. It may be the reason why so many different materials (see Section 1.3) could be used to study the behaviour of masonry arches, and similar results could be achieved (such as the hinge-typed modes of failure of an arch, and the order of the development of hinges). It may be noted that the above conclusions were drawn based on the limited cases of the loading and the configurations of arches, and further studies may be needed if general conclusions can be drawn.

5.2.2 Tensile Strength

In Chapter 4, it was shown that the load capacity of an arch would be increased if greater tensile strength were used in the smeared models. It would appear contrary to the common sense that the tensile capability at mortar joints of masonry arches only delay the occurrence of hinges rather than increase their load capacity. In this Section, why and how the tensile strength affects the load capacity of masonry arches will be discussed.

The effects of different tensile strength were first studied through the model OSMA4 of arch itself. Apart from the tensile strength, the same parameters for both the material and elements were used as those in the smeared models presented in the previous Chapter. The loading location was approximately at the quarter-span, and the load - deflection responses at the point P6 were plotted. As the tensile strength (σ_t) increases from 0.2 to 0.5 N/mm^2, the following points can be clearly identified from Fig. 5.3: -

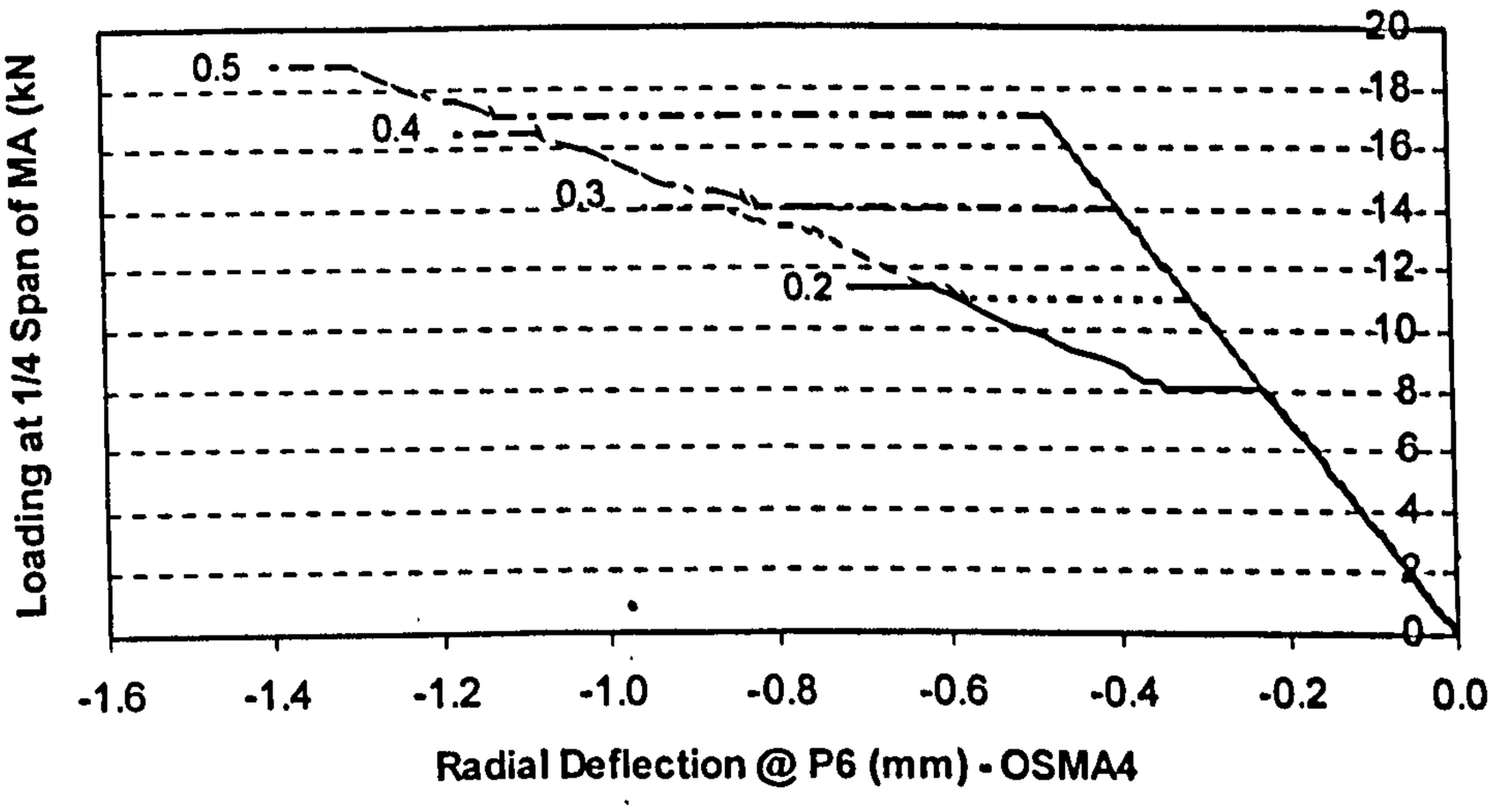

Fig. 5.3 Effects of Tensile Strength on Load Capacity – OSMA4

(a) The occurrence of the first crack was postponed. When σ_t is 0.2 N/mm^2, the crack initiated at load 8 kN, and when σ_t is 0.5 N/mm^2, the crack did not occur until the load reached 17 kN. For all cases, the first crack developed at the intrados of the arch under the loading locations with or without the cracks at the intrados of the springing of the unloaded side. The first crack tended to smear within a relatively large region with low σ_t, and as σ_t becomes greater, the first

crack either under loading location or at the springing of the unloaded side generally spread with one-width of elements along the thickness of arch ring;

(b) The behaviour of the model was the same before development of any cracks. For all cases, the load increments (0.4 kN) and the corresponding deflections were the same until the loads reached 8 kN, when cracks occurred in the case of 0.2 N/mm^2 tensile strength;

(c) The rate of the loss of stiffness due to the first crack was about the same. Before any cracking took place, the equivalent stiffness at the point P6 is about 35.5 kN/mm for all cases. The stiffness dropped to the range between 11 and 14 kN/mm after the development of the first crack;

(d) The greater the tensile strength, the larger the displacements due to the first crack. It is interesting to note that, for different tensile strength used, almost identical cracking patterns were followed although the cracks developed at different levels of loading;

(e) The modes of failure were identical. For all cases, the models failed by development of cracks through the arch ring at (1) the loading location, (2) the springings of the unloaded side, (3) the quarter-span of the unloaded side, and (4) the springings of the loaded side. When σ_t is 0.2 N/mm^2, the order of the cracks of (1), (2), (3) & (4), and the propagation of the cracks of (1) could clearly be identified. As σ_t increases, the cracks developed mainly at two stages (1) & (2) and (3) & (4);

(f) Typical brittle-type of failure. When σ_t is between 0.2 and 0.5 N/mm^2, the model behaved alternatively in elastic and brittle ways. Accumulated elastic deformation and local brittle failure led to the collapse of the model arch. As σ_t increased from 0.2, to 0.3, to 0.4 and to 0.5 N/mm^2, the percentage of the loads that could be carried within the first elastic range increased from 70%, to 79%, to 85% and to 91%. In other words, pure brittle failure would take place if the value of tensile strength was assumed too high, in which the response of load – deflection would be reflected as a straight line without any "steps" within the whole loading history.

It may be noted that, in order to make the results of different cases more comparable, the following solving strategy was adopted. First, CTAT and CTP were used. It was essential to use both CTAT and CTP. Depending on the characteristics of the

nonlinearity experienced in the model at various loading stages, the use of both CTAT and CTP could ensure the automatic reduction or multiplication of load increments. If the scales of the nonlinearity of models (or development of cracks) were similar, the load increments would be similar. By checking the load increments of the solution history of different cases, the characteristics of the model throughout the loading history could be identified (see the above (b)); second, the same total loads were specified. A maximum load of 20 kN was specified for all analyses of the model OSMA4. That is, after self-weight was applied, the applied load would gradually increase starting from zero, until unconverged solutions were encountered. The last convergence load (normally less than 20 kN) was then defined as the load capacity of the case being concerned. By specifying the same total loads for all cases, the rates of increase or decrease of load increments would be the same if the nonlinearity of the models were identical (see the above (c)); third, small minimum load increment should be specified. The load increments would generally change if the nonlinearity of the model changed. If solutions could not be converged at the minimum load increment specified, it is normally assumed that the model fails. However, whether it is a failure of the models due to overloaded or an artificial failure due to inappropriate solution procedures may not be easily identified. It was found that the load increments could be as low as one millionth of the above total load specified in order to achieve true failure conditions of the models.

Although brittle type of failure criterion was used in the smeared modelling approach, general nonlinearity that the model arches experienced during the tests may be simulated by assuming small tensile strength. As Fig. 5.4 shows, the response of the load-deflection is similar to the scaled one obtained from the model tests when σ_t is 0.05 N/mm^2.

Since lower tensile strength was assumed, the cracks tended to smear with relatively large zones around the four locations where "hinges" may develop, i.e., under the loading location, quarter-span of the unloaded side, and the two springings. The detailed development of the cracks was listed in Table 5.3. It was noted that the propagation of the cracks was clearer than that when higher σ_t was assumed.

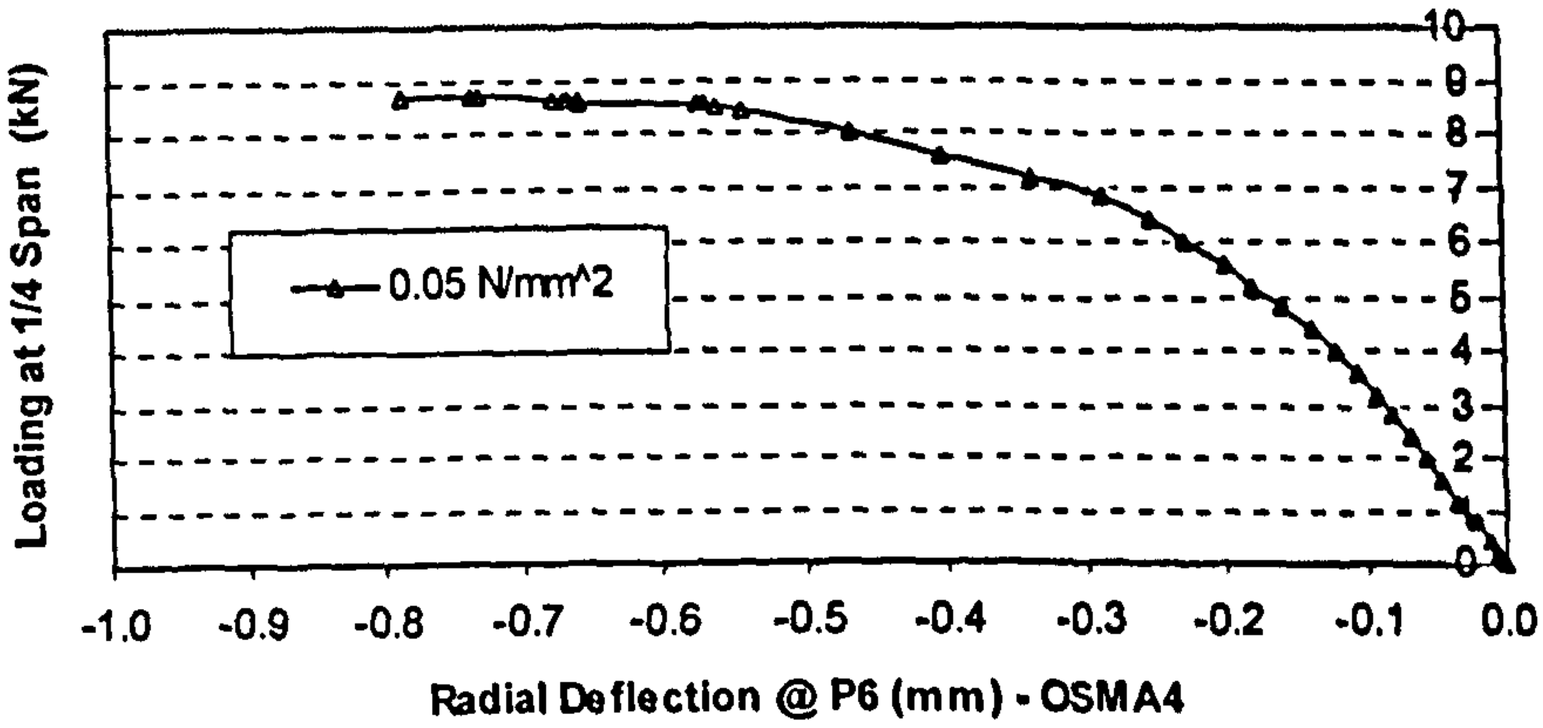

Fig. 5.4 Effects of Lower Tensile Strength – OSMA4

Cracking Developments With $\sigma_t = 0.05$ (N/mm^2) – OSMA4 Table 5. 3

Load (kN)	Cracking Sequences
3.6	Cracks initiated at the intrados of the arch under the loading location;
4.0	Cracks occurred at the intrados of the left springing, and the existing cracking under the load smeared radially;
6.8	More cracks developed around the loading location, and the existing cracks at the springing smeared radially;
7.0	Cracks occurred around the extrados of the quarter-span of the unloaded side, and the extrados near the springing at the loaded side;
8.4	More cracks developed at the extrados around quarter-span areas of the unloaded side, and at the extrados near the springing at the loaded side;
8.7	All existing cracks suddenly propagated, and the cracks under the loading location smeared towards the crown. Then the model failed.

The deterioration of the stiffness gradually took place instead of sudden brittle failure at the local areas. The models generally failed due to the extensive cracks within the model, in which the "four failure zones" may not clearly be identified. It appears that the use of lower tensile strength tends to result in a better simulation of the tested model apart from the load capacity that is normally underestimated. This might be caused by the limitations of the smeared modelling approach (SMA). The SMA assume that the

material is a homogeneous continuum, and initially isotropic. That is, if the first principal stress reaches the tensile strength at any integration points, cracks will take place in the plane normal to the above stresses, and the forces previously associated with the cracked zones are redistributed. This process repeats until sufficient cracks are developed within the model, and the forces can no longer be redistributed (or the model can no longer carry the forces that were previously taken by the cracked zones). In reality, due to the relatively lower tensile strength of the mortar, the cracks initiate in the mortar, and the propagation of the cracks is generally confined within the mortar joints. The flows of stresses would not be as smooth as those experienced in the smeared models. In other words, further development of the existing cracks is likely to be delayed, and the load capacity is consequently increased.

For the model OSMA3, the effects of the different tensile strength on the behaviour of the arch are similar to those for the model OSMA4, but complicated by the presence of the spandrel arches and piers.

Prior to the occurrence of any cracks, the model behaved linearly up to certain loads depending on the tensile strength, and the equivalent stiffness at the point P6 was about 127 kN/mm for all cases (note that the loads before the first crack appeared: - 1.8 kN when σ_t was 0.2 N/mm^2; 4.2 kN when σ_t was 0.3 N/mm^2; 7.4 kN when σ_t was 0.4 N/mm^2; 10.2 kN when σ_t was 0.5 N/mm^2). As the loads increased, the cracks tended to propagate before the next cracks took place when the tensile strength was small; and the cracks generally suddenly occurred with little propagation while the tensile strength was great. Consequently, the stiffness of the models dropped relatively sharply if the tensile strength was small. For instance, the stiffness dropped to about 75 kN/mm upon the occurrence of the cracks at the extrados of the right springing of the spandrel arch SA4 with a load of 2.4 kN applied when σ_t was 0.2 N/mm^2. When σ_t was 0.5 N/mm^2, however, the stiffness did not drop to the similar value until the cracks developed at the intrados of the left springing of the spandrel arch SA1 with a load of 23.1 kN applied.

It can be seen from Fig. 5.5 and Table 5.3 that, if the tensile strength was equal to 0.4 or 0.5 N/mm^2, the models could hardly carry any loads once cracks developed within the main arch. When σ_t was either 0.2 or 0.3 N/mm^2, the models could further carry about 10% of the ultimate loads after occurrence of the cracks in within the main arch. This

indicated that global sudden brittle failures were likely to be dominant if a higher tensile strength was assumed.

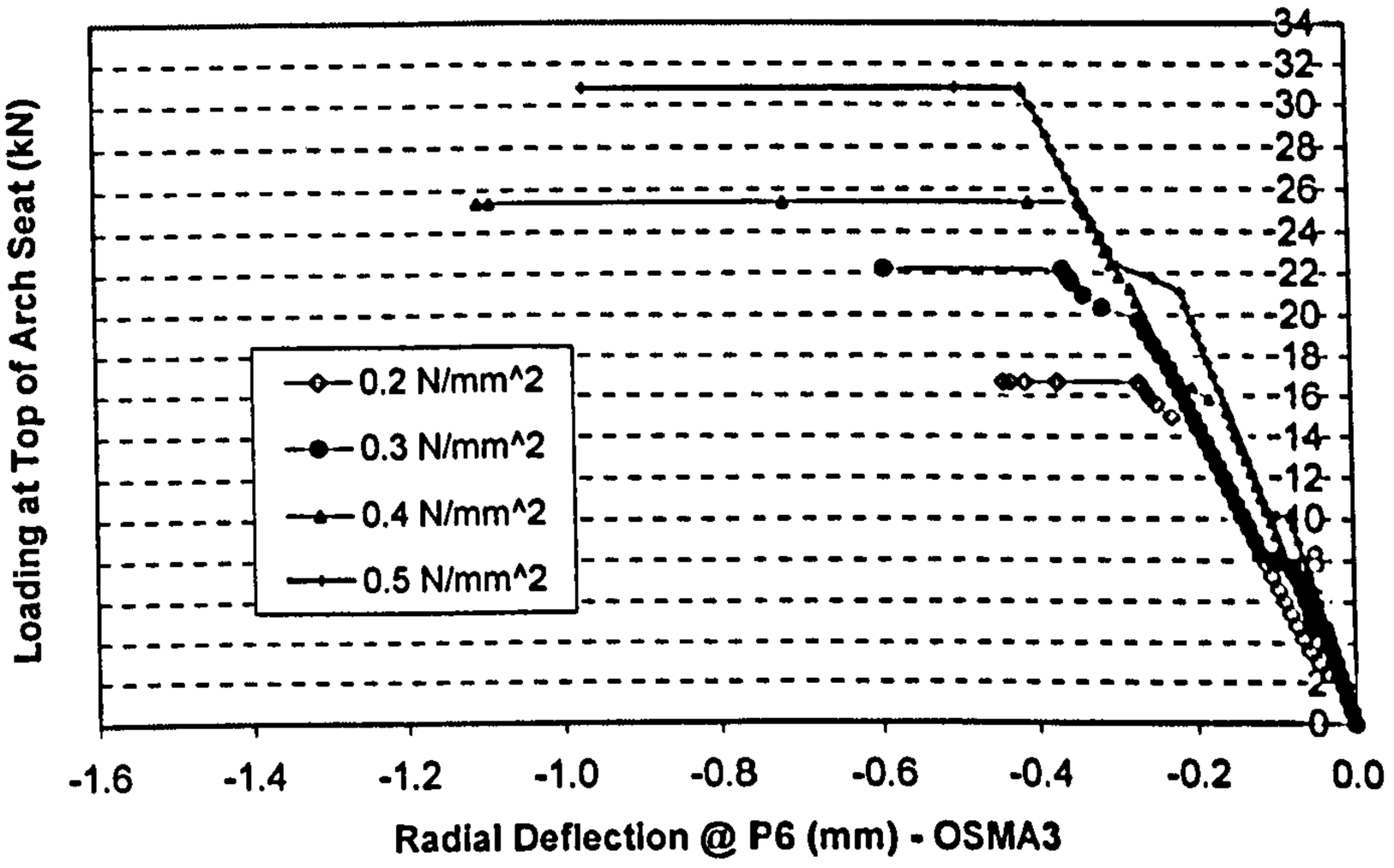

Fig. 5.5 Effects of Tensile Strength on Load Capacity – OSMA3

Cracking Loads VS. Tensile Strength σ_t (N/mm^2) **Table 5. 4**

Cracking Locations	Cracking Loads (kN)			
	σ_t = 0.2	σ_t = 0.3	σ_t = 0.4	σ_t = 0.5
Top of the Spandrel Pier 2 (minor cracks)	1.800	4.200	7.430	10.164
Extrados of the right springing of the SA4	2.400	5.420	15.848	21.740
Intrados of the left springing of the SA1	14.400	18.130	23.640	23.100
Intrados of the MA under the load	15.000	20.000	25.400	30.800
Smeared cracks within the SA1	16.687	22.219	25.400	30.801
Intrados of the left springing of the MA at the unloaded side	16.688	22.219	25.403	30.803
Extrados of the MA at the quarter-span of the unloaded side	16.689	22.220	25.404	--
Extrados of the right springing of the MA at the loaded side	--	22.225	25.404	--

Furthermore, for the single arch itself (OSMA4), after the first crack occurred within the arch (at the intrados of the arch under the load), the models could further carry about 30%, 21%, 15% and 9% of the ultimate loads for the tensile strength 0.2, 0.3, 0.4 and 0.5 N/mm^2, respectively. In other words, the spandrel arches and piers of open spandrel arches not only increased the load capacity, but also changed the modes of failure to certain extent, i.e., became more "brittle" type of failure. Fig. 5.6 shows the relationship between tensile strength and load capacities. The greater the tensile strength, the greater load capacities.

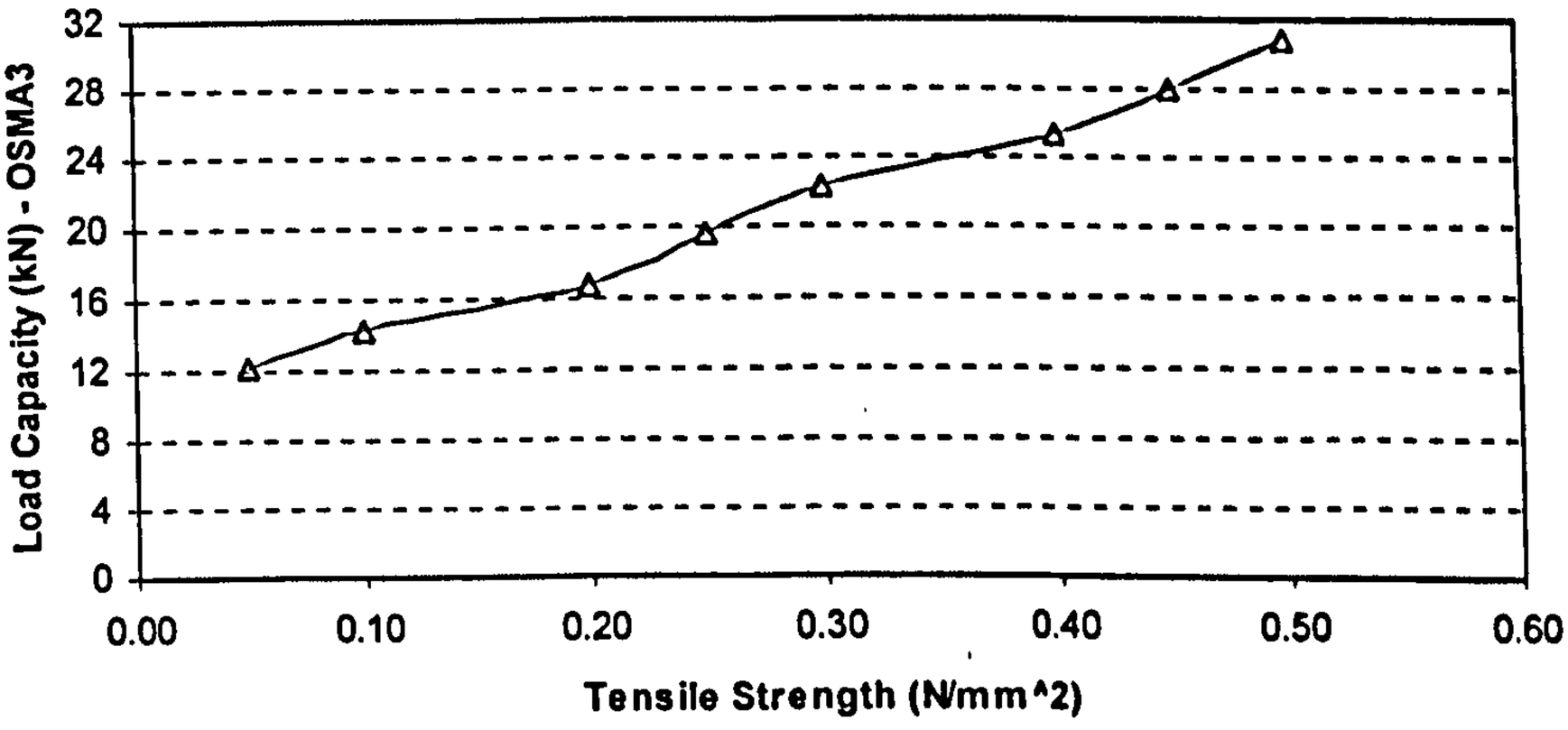

Fig. 5.6 Relationship Between Tensile Strength and Load Capacity – OSMA3

When a lower tensile strength 0.05 N/mm^2 was used, the response of the open spandrel arch (OSMA3) was also different from that of arch itself (OSMA4). From Fig. 5.6 and Table 5.5, it can be seen that cracks occurred earlier due to the lower tensile strength, but these cracks were only limited within the end spandrel arches. Their effects were reflected in the load – deflection curve by a series of local variations of the stiffness along the initial part of the curves. The first major change in the overall stiffness of the model took place at a load of 6 kN when cracks developed within the main arch. Unlike that in the model OSMA4, in which a substantial amount of new cracks developed within the arch upon the occurrence of the cracks under the loading location before failure, either occurrence of new cracks or further propagation of the existing cracks were by-and-large within the spandrel structures before cracks developed at other locations and the model failed. This difference in the development of cracks within the main arch was clearly due to the stiffening effect of the spandrel arches and piers. It can also be seen that, for the model OSMA3, the subsequent deterioration of the overall

stiffness upon the occurrence of the first crack within the main arch was not as rapidly as for the model OSMA4, and brittle type of failure was dominant.

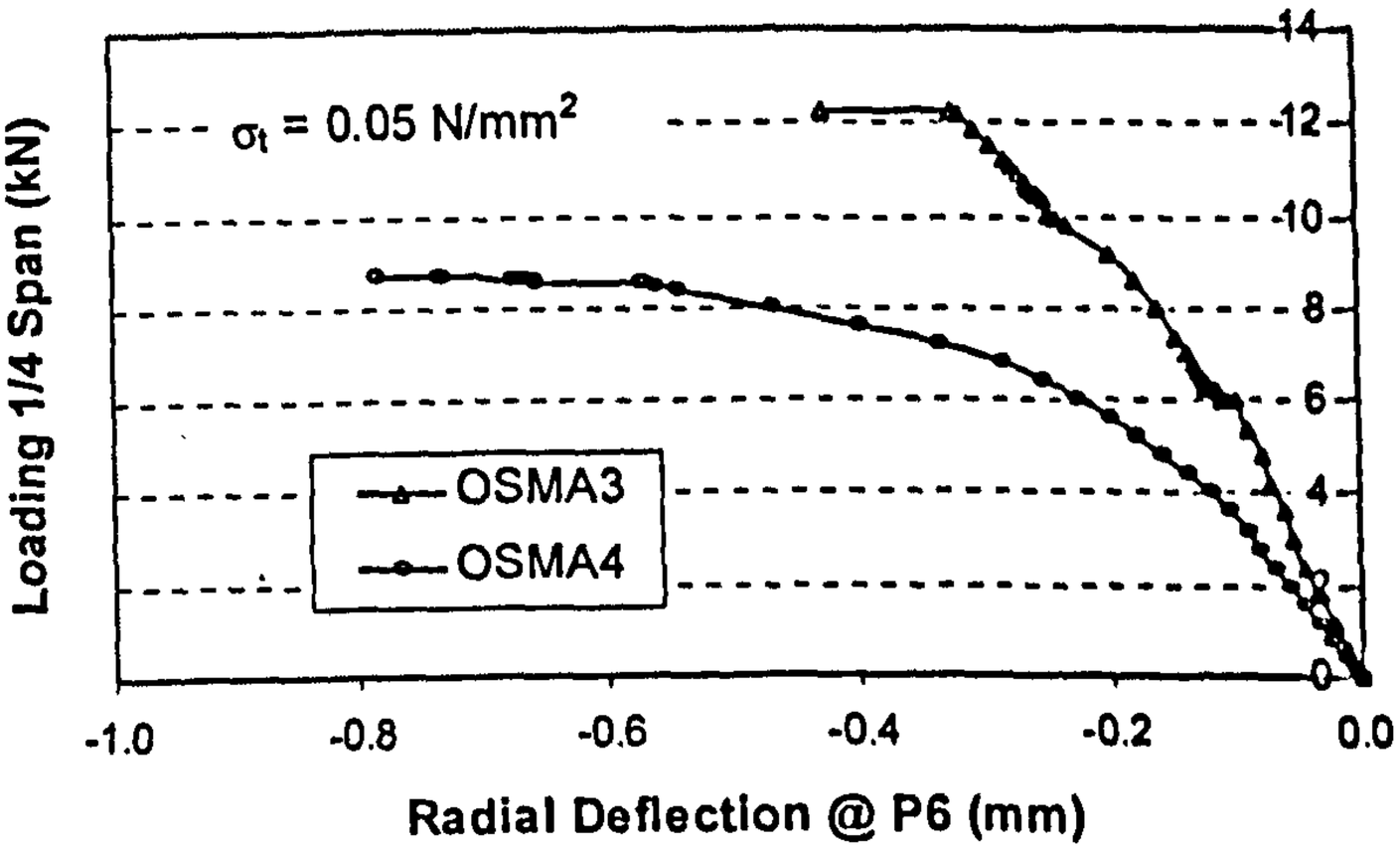

Fig. 5.7 Comparison of Lower σ_t Between OSMA3 And OSMA4

Cracking Developments With $\sigma_t = 0.05$ (N/mm^2) - OSMA3 Table 5. 5

Load (kN)	Cracking Sequences
Self Weight	As the self-weight of model was applied, cracks first occurred at the intrados of the springings of the spandrel arches SA1 & SA4 near the supports, and subsequently new cracks developed at the intrados of the crowns of both spandrel arches;
2.4	Cracks developed at the Intrados of the left springing of SA3 and at the extrados of the left springing of SA4 simultaneously;
6.0	Cracks developed at the intrados of main arch under the loading location;
9.2	Cracks occurred at the extrados of the crown of SA2, and at the bottom of pier 1 simultaneously;
11.1	Cracks developed at the bottom of the pier 2
12.2	Cracks developed at the intrados of the left springing of the main arch at the unloaded side, and the existing cracks, especially those under the loading areas smeared extensively through the arch seat. Then, the model failed.

These different responses between the models OSMA3 and OSMA4 of the same lower tensile strength suggested that the spandrel arches and piers increased the overall stiffness, delayed or prevented the occurrence of cracks within the main arch, enhanced the load capacity, but also changed the modes of failure of the main arch.

5.2.3 Density

An accurate measurement of the density of a brickwork masonry unit may not be difficult. But, to accurately choose a representative density for the entire arch structure may not be straightforward due to the variations of the test data from samples to samples. It is known that considerable contributions could be made by the self-weight to the overall stability of an arch. Thus, it is necessary to know that how the density affects the behaviour of a masonry arch.

Parametric studies were carried out on the models OSMA3 and OSMA4 using the smeared model. Apart from varying the density, the same parameters for both the material and elements were used as those presented in the previous Chapter.

For the model OSMA4, it can be seen from Fig. 5.8 that the same paths were followed at initial stages for different densities. The greater the density is, the later the occurrence of the first crack will be. Once the first crack developed, the loss of the stiffness appears more rapid for the low density than the great one. The load capacity increased if greater density were assumed. The modes of failure were hardly affected by different densities used.

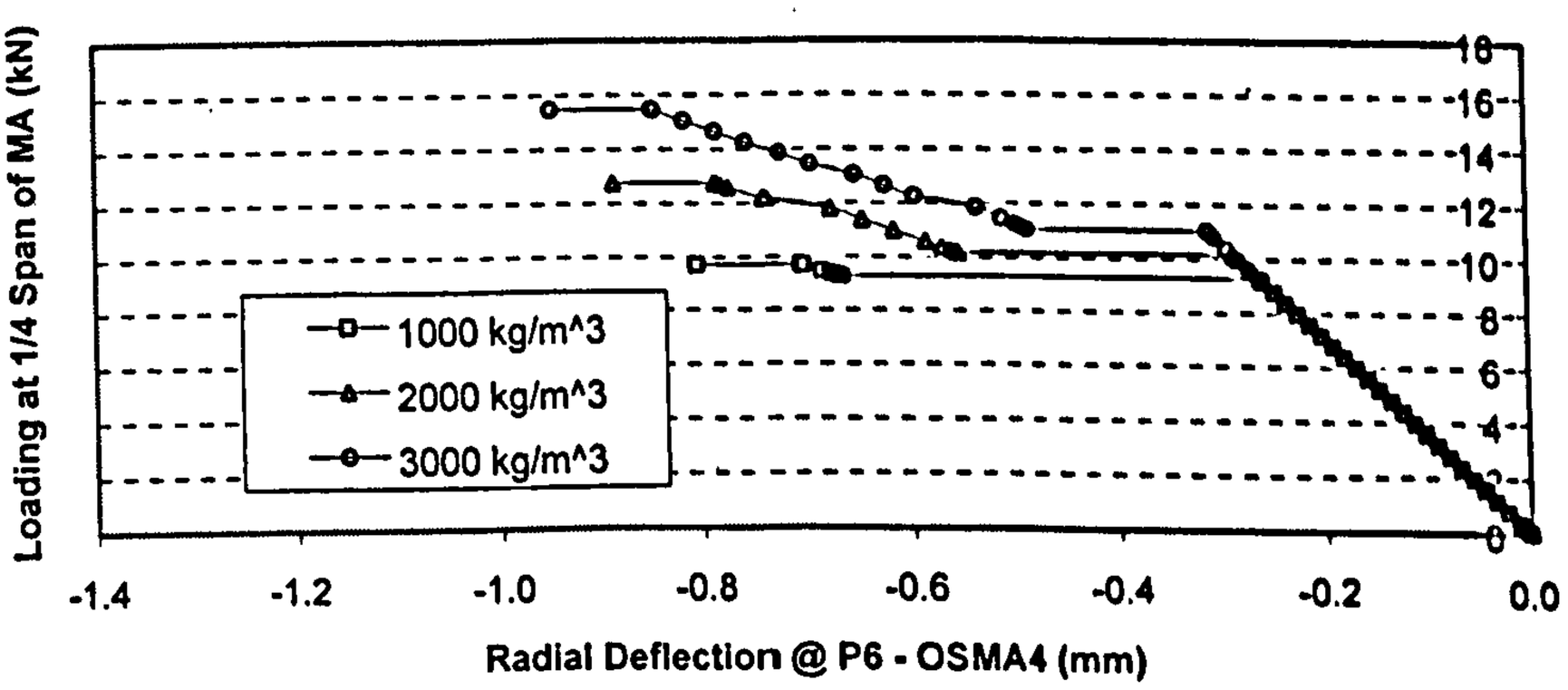

Fig. 5.8 Effects of Density on Load Capacity – OSMA4

For the model OSMA3, the effects of the variations in material density of the main arch on the behaviour of the open spandrel arch are more significant. From Fig. 5.9, it can be seen that the initial stiffness of the model of lower density is greater than that of great one until the occurrence of the cracks at the intrados of the spandrel arch 1 near the support. As the values of density increased, the first crack occurred earlier at the

extrados of the spandrel arch near the support due to the fact that higher stresses were induced within the spandrel arch 4 by relatively large displacement of the main arch under self-weight. The rest of the cracks occurred relatively late for the model OSMA3, and the load capacity was also greater. The relationship between density and load capacities is as shown in Fig. 5.10.

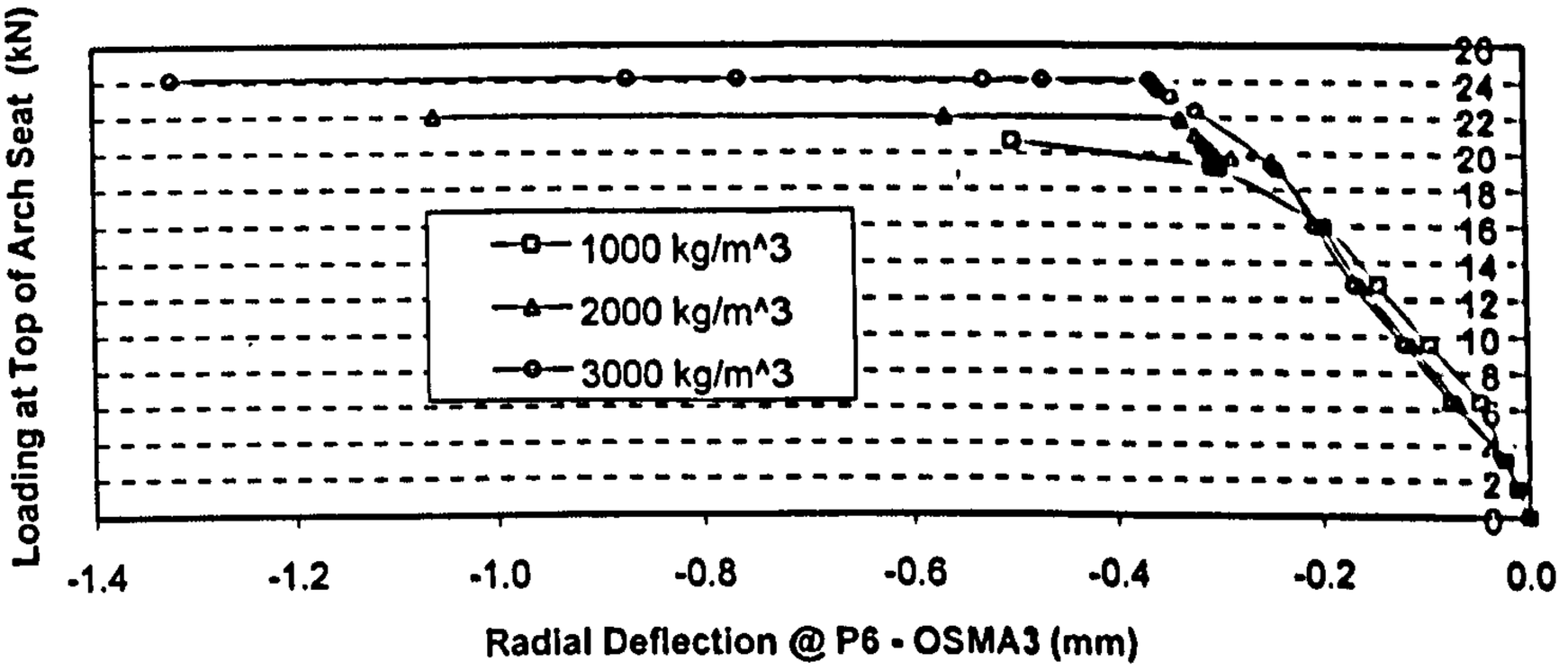

Fig. 5.9 Effects of Density on Load Capacity – OSMA3

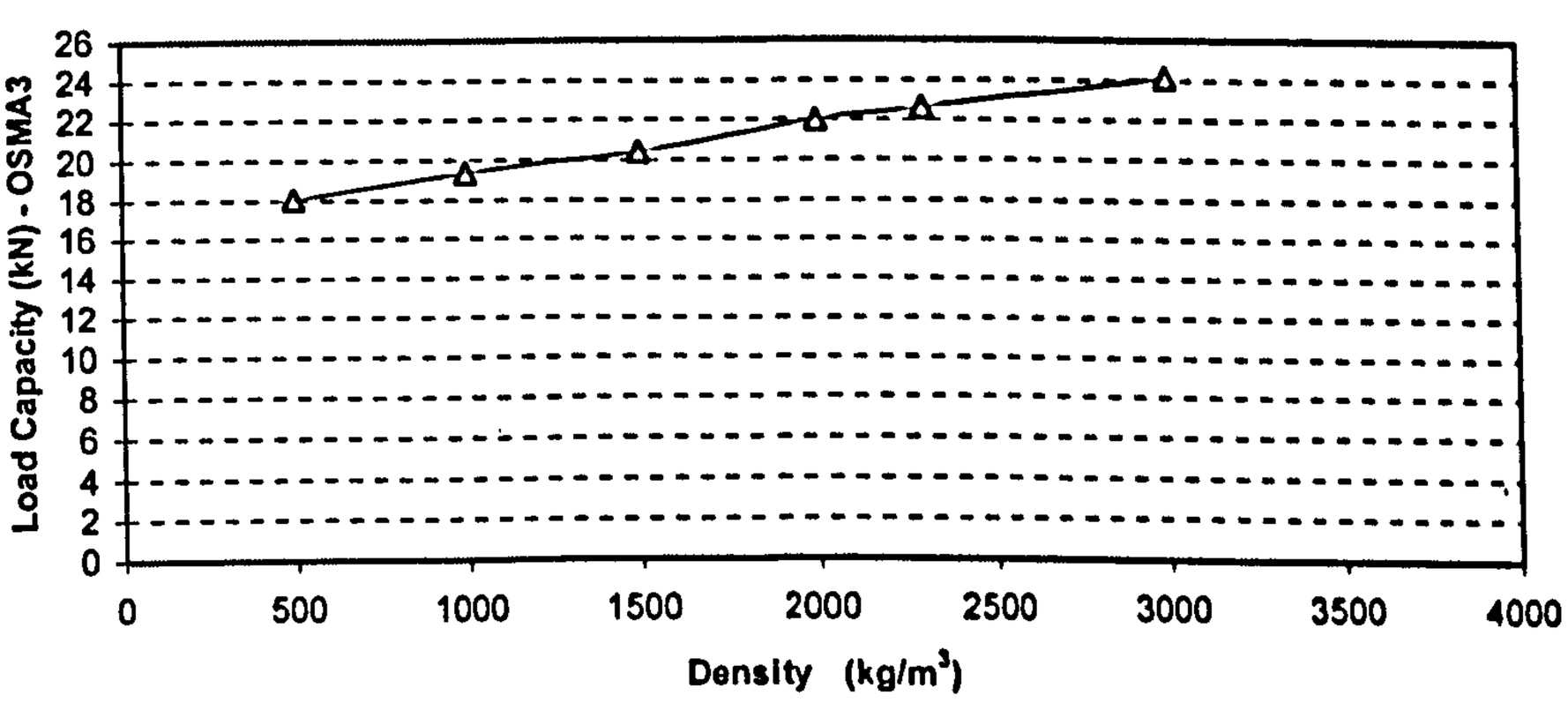

Fig. 5.10 Relationship Between Density and Load Capacity – OSMA3

The effects of different densities are further illustrated in Fig. 5.11, in which the first principal stresses of a node at the intrados of arch radially under the loading location are plotted against the self-weight and the applied loads for different densities. Under its own weight, the node is in compressive states. The greater the density, the greater the compressive stresses are. As the applied loads increased, the model behaves almost linearly until the first principal stresses reached the specified tensile strength 0.3 N/mm^2 at the integration points of the element (note: the nodal stresses are extrapolated from the integration point values, and they may be greater than those at the integration points

or the tensile strength), and the first crack took place within the elements being considered. The stresses associated with the nodes dropped substantially where new equilibrium conditions were formed. As a result, the greater density, the greater the load capacities are.

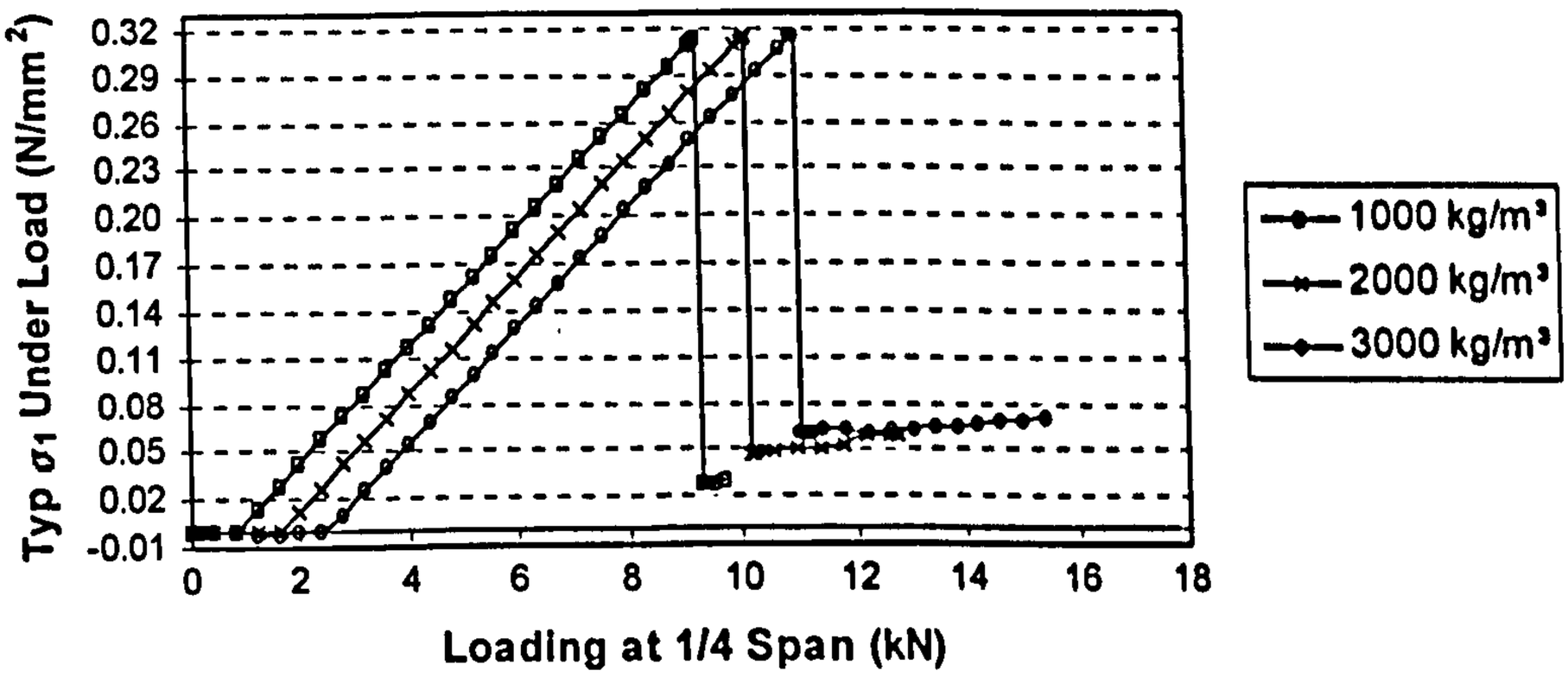

Fig. 5.11 Effects of Density on The First Principal Stresses

5.3 Element Related Parameters

5.3.1 Shear Transfer Coefficients

In the smeared modelling approach, several parameters were required in order to use the element SOLID65, two of which were shear transfer coefficients for an open crack (β_1) and shear transfer coefficients for a closed crack (β_2). Since the constitutive relationships of the element SOLID65 were established mainly based on the test results of concrete, these coefficients were adopted to account for the reductions of the shear modulus across the plane of the cracks by multiplying their un-cracked values by β_1 or β_2. As discussed in Chapter 3, they were closely related to the properties of the aggregate interlock and the dowel action of reinforced bars in reinforced concrete. The coefficients could range from 0.0 to 1.0, with 0.0 representing a smooth crack (complete loss of shear transfer) and 1.0 representing a rough crack (no loss of shear transfer). It may be noted that only one shear-retention factor is generally used to account for the reduction of shear transfer capacity due to the material cracking in most finite element packages. Two coefficients introduced in the element SOLID65 could provide greater flexibility in the modelling of the shear effects once cracks are formed.

In brickwork masonry, as discussed in the material tests in Chapter 2, shear transfer capacity was considerably different between bricks and mortar joints. Even within the joints themselves, it could be influenced by a number of factors, such as workmanship, mortar joint, joint shapes and orientation, absorption, etc. It could be difficult to determine representative coefficients for shear transfer capacities for the masonry arches. However, if the effects of different values of β_1 and β_2 on the behaviour of the masonry arches are known, the values may empirically be determined.

For the model OSMA4, based on the model presented in Chapter 3, other two values of β_1, 0.0 and 0.9 were used to compare its effect on the behaviour of the model arch. It was found that the model behaved in the same way until the first crack occurred. Then, the load increments became greater in the case of higher β_1, which indicated that the nonlinearity of the model of higher β_1 was relative moderate since the same nonlinear control settings were used in both cases. The ultimate loads were 13.48 kN and 13.49 kN respectively for $\beta_1 = 0.0$ and $\beta_1 = 0.9$. However, it could not simply draw a conclusion that a higher value of β_1 would result a higher ultimate load due to the fact that the behaviour of the model was found to be dependent on the loading path. In other

words, if two different load increments (note both were small enough to result in the true failure loads of a model using the smeared modelling approach) were used, the failure loads could be different even if all other material, geometry and model related parameters were the same.

The reasons of the different responses and similar ultimate loads obtained for $\beta_1 = 0.0$ and $\beta_1 = 0.9$ may be explained as follows: for the arch model and loading conditions being considered, once cracks occurs, they will continue to be opened until a "hinge" is formed at opposite of the arch ring. During this process, the shear stresses may be transferred either through the whole section of the ring (including the cracked and intact parts) if $\beta_1 = 0.9$ or through the intact parts only if $\beta_1 = 0.0$. In either case, the shear deformation and its effect on the behaviour of the model are not significant. Therefore, the final failure loads will be similar. If β_1 is assumed 0.0, however, the sudden removal of the shear stiffness from the system (within the local cracked areas) will generally cause numeric convergence difficulties. The more cracks occur, the severer the nonlinearity will be. Consequently, the run time will be increased. A value of 0.01 was used in the analyses in Chapter 3, which not only assumed low shear transfer capacity for an open crack, but also overcame possible convergence difficulties.

It was interesting to note that the values of β_2 hardly had any effects on the behaviour of the model OSMA4 in terms of variations in nonlinearities, deflections and ultimate loads. This might be because the cracks within the arch, once occurred, would continue to be open. β_2 (shear transfer coefficient for a closed crack) was rarely applicable to the arch under the configuration and loading conditions being considered.

For the model OSMA3, it appeared the effects of different values of β_1 were more significant than those for the model OSMA4. Compared the results of the model of 0.0 of β_1 with those of 0.5, the occurrence of the first crack at the extrados of the springing of the spandrel arch SA4 near the support were slightly earlier, but the first crack within the main arch occurred at the same loads. Upon the first crack within the main arch, the path of the propagation of the cracks within the spandrel arches, especially within SA1 and SA2 could be clearly identified for the model of zero of β_1. This could be because that, if shear transfer capacity for an open crack was considered, the occurrence of the new cracks or the further development of the existing cracks was delayed, i.e., the first

principal stresses were reduced. Consequently, the ultimate load of the model of 0.5 of β_1 was about 3% more than that of the model of 0.0 of β_1. It should be noted that the final cracking patterns were identical for different values of β_1 used. It was found that the use of a value of β_1 between 0.0 and 0.7 did not result in significant deviations of the ultimate loads and cracking patterns. However, if an unrealistic value (>0.7) was used, the corresponding results could be unrealistic (generally, the model encountered convergence difficulties at very low loads). It was believed to be one of the limitations of the element SOLID65.

The similar effects were found for different values of β_2 used except that the ultimate load of the model of 0.5 of β_2 was about 0.4% more than that of the model of 0.0 of β_2.

In summary, the effects of β_1 and β_2 on the behaviour of an arch are slightly different. For an arch itself such as the model OSMA4, different values of β_1 will hardly affect the responses of the model until the first crack occurs. With or without considering loss of the full shear transfer capacity, the arch behaves in a similar way. For an open spandrel arch such as the model OSMA3, different values of β_1 will affect the load levels at which the first crack occurs within the spandrel arches, but hardly affect the load levels at which the first crack occurs within the main arch. The variations of β_1 between 0.0 and 0.7 rarely affect the cracking patterns, but may affect the sequences of the occurrence of new cracks and the further development of the existing ones. The differences of the ultimate loads caused by the different values of β_1 in the above range may be limited to 5% only. If a value of β_1 greater than 0.7 is used, the model may behave unrealistically.

Different values of β_2 hardly affect the behaviour of both single arch (OSMA4) and open spandrel arch (OSMA3), except that ultimate loads of the open spandrel arch may be affected, but generally the differences are limited to 1% only. The usage of very low values of either β_1 or β_2 (such zero) generally result in convergence difficulties, and thus small load increments is required.

5.3.2 Normal & Tangential Stiffness

In the discrete and mixed modelling approaches, contact elements were used to model

the behaviour of the interfaces between individual blocks or between the fill and arch. Among the parameters required defining the contact elements adopted (CONTAC48 for the model OSMA3 and OSMA4 and CONTAC49 for the model OSMA5), the determination of the normal contact stiffness (KN) and the tangential contact stiffness (KS) may need special attention as they could affect both the local behaviour at the point of contact and the overall response of the arches.

Normal contact stiffness is used to enforce compatibility between the contact surfaces. The higher the values are used, the better this enforcement is. If low values of KN are used, the convergence difficulties could be overcome, but penetration will generally be too much, which would result in fictitious soft arches. Ideally, the stiffness should be high, but not so high that they adversely affect the convergence or need excessive number of iterations. A value of 10,000 N/mm of KN was found suitably for the modelling of the models OSMA3 and OSMA4 in terms of both amount of penetration and the rate of convergences.

KS is used to define the size of sticking zones. If KS is too large, the sticking zones could be too small, and convergence difficulties may be encountered since some of the points in contact oscillate between sliding and sticking (or the direction of sliding tendency alters). As discussed in Chapter 3, when the tangential forces between interfaces are "small", the two contacting bodies will stick together. When the forces are "large", the two bodies will slide relative to each other. This frictional effect could be modelled through either the elastic Coulomb or the rigid Coulomb law provided by the Program ANSYS5.3. The former is used to model both sticking and sliding behaviour, in which the tangential displacement is assumed to occur in sticking (or elastic) zone if $Fs < uFn$. The latter is used to model sliding behaviour only, i.e., the tangential displacement does not take place when $Fs < uFn$. In the analyses of both the single arch (OSMA4) and the open spandrel arch (OSMA3), an error of excessive displacements might appear if the elastic Coulomb law was used as soon as the self-weight of the model applied. It could be caused by the uncontrolled elastic tangential movements at the interfaces (or numerical noise) before the true Fn was fully established. This difficulty might be overcome by using additional linear springs with stiffness of 6 or 8 orders of magnitude weaker than the contact stiffness to provide some stiffness to the arch structure. As the stiffness of the additional springs is negligible compared with the

material stiffness, its effect on the final solution is negligible. Alternatively, the rigid Coulomb law might be used if the effect of the sticking behaviour is not concerned. The first method was used in the modelling of the models OSMA3 and OSMA5, and the second was used in the model OSMA4.

For the model OSMA5, it was found that convergence difficulty could be encountered at the early stages of loading if high normal contact stiffness was used. In order to overcome this, it was necessary to initially set KN a low value (say 1000 N/mm), and then gradually increase between load steps and/or restart until the penetration of the fill between the fill and arch was small enough. Since ANSYS5.3, by default, assumes that the tangent contact stiffness is one percent of the normal stiffness, the tangent stiffness need to be explicitly defined every time when the normal contact stiffness was changed, to maintain a consistent value for the tangent stiffness throughout the analyses.

5.4 Model Related Parameters

5.4.1 Number of Interfaces Along Arch Ring

In the discrete modelling approach, potential failure interfaces must be pre-defined within an arch model in order to simulate the behaviour during loading history. Clearly, the more the number of interfaces are pre-defined, the more detailed responses can be traced. Ideally, the number of the predefined interfaces should be large enough to capture the responses of a model being concerned, but should be kept small if possible. As the number of the interfaces increases, the solving time will normally be increased since more contact/interface elements must be used, which generally require small load increments. The model OSMA4 was used for the parametric studies of the effects of different number of interfaces along the arch ring on the behaviour of the model. The finite element model of OSMA4 and the related parameters were the same as those presented in Chapter 3 except the loading location.

Previously, the loading location of the model OSMA4 was assumed the same as that for the models OSMA3 and OSMA5. In other words, the loading location was at the middle of the underside of the arch seat of the corresponding models OSMA3 or OSMA5 in order to make the results comparable. In the parametric studies below, the loading locations were assumed at the quarter-span location to ensure that loads were automatically located at the same node even if a different number of predefined interfaces and elements were used.

The arch model was equally divided into eight basic segments along the span, in which 9 interfaces were defined. Each segment was then equally divided into 2, 3, 4, 5, and 8 subsegments, in which 17, 25, 33,41 and 65 interfaces were defined (note that a total of 72 bricks were used for constructing the main arch of the models OSMA3, OSMA4 and OSMA5). For the different number of the predefined interfaces along the ring, Fig. 5.12 shows the ultimate loads.

It was noted that, for the model OSMA4, the ultimate loads were not very sensitive to the number of the predefined interfaces (NPI) within the range being studied. For the NPI 9, 17, 25, 33, 41 and 65, the ultimate loads were 13.044, 12.762, 12.665, 12.623, 12.622 and 12.621kN, respectively. The difference in the ultimate loads was about 3% as the NPI increased from 9 to 65, and only 1% as the NPI increased from 17 to 65.

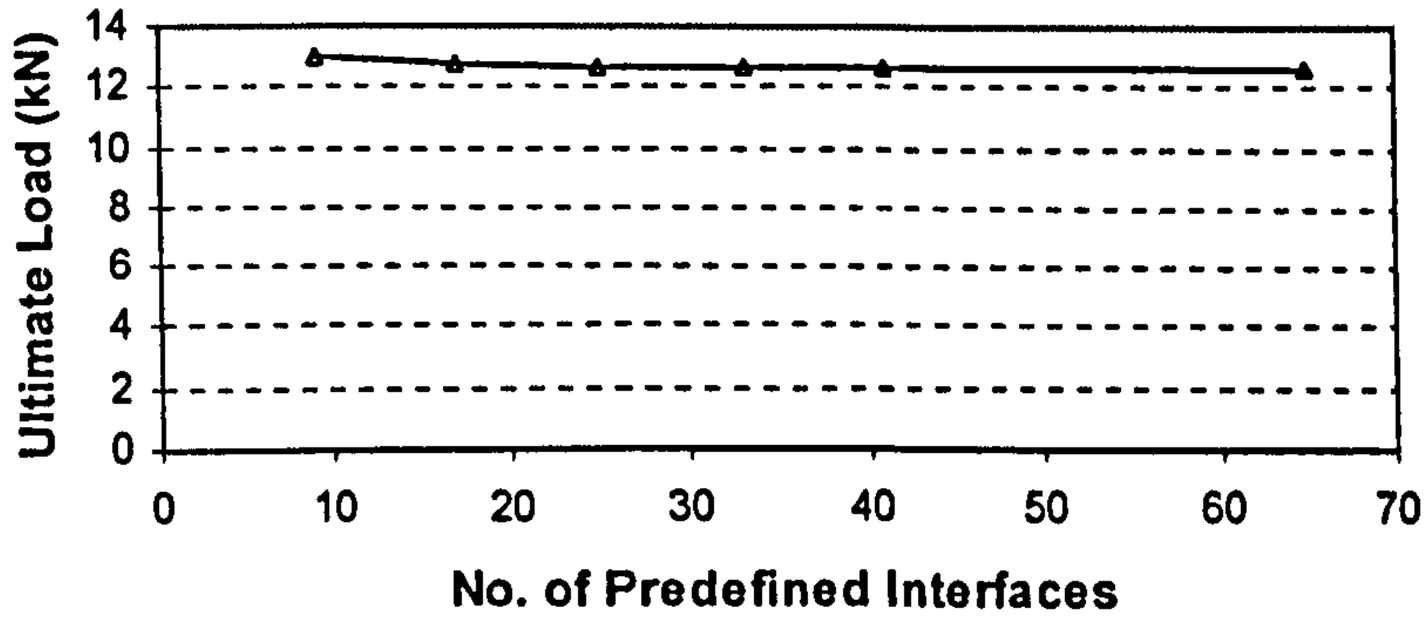

Fig. 5.12 Relationship Between Interfaces No. And Load Capacity

The variations of the ultimate loads were caused by the distributions of the hinges and semi-hinges around the quarter-span of the unloaded side and the springing of the loaded side as shown in Fig. 5.13. For all cases, two hinges were generally located at the extrados of the arch directly under the load and at the extrados of the springing of the unload side; one hinge was around the quarter-span of the unloaded side; and the fourth hinge or quasi-hinge was at/near the intrados of the springing of the loaded side.

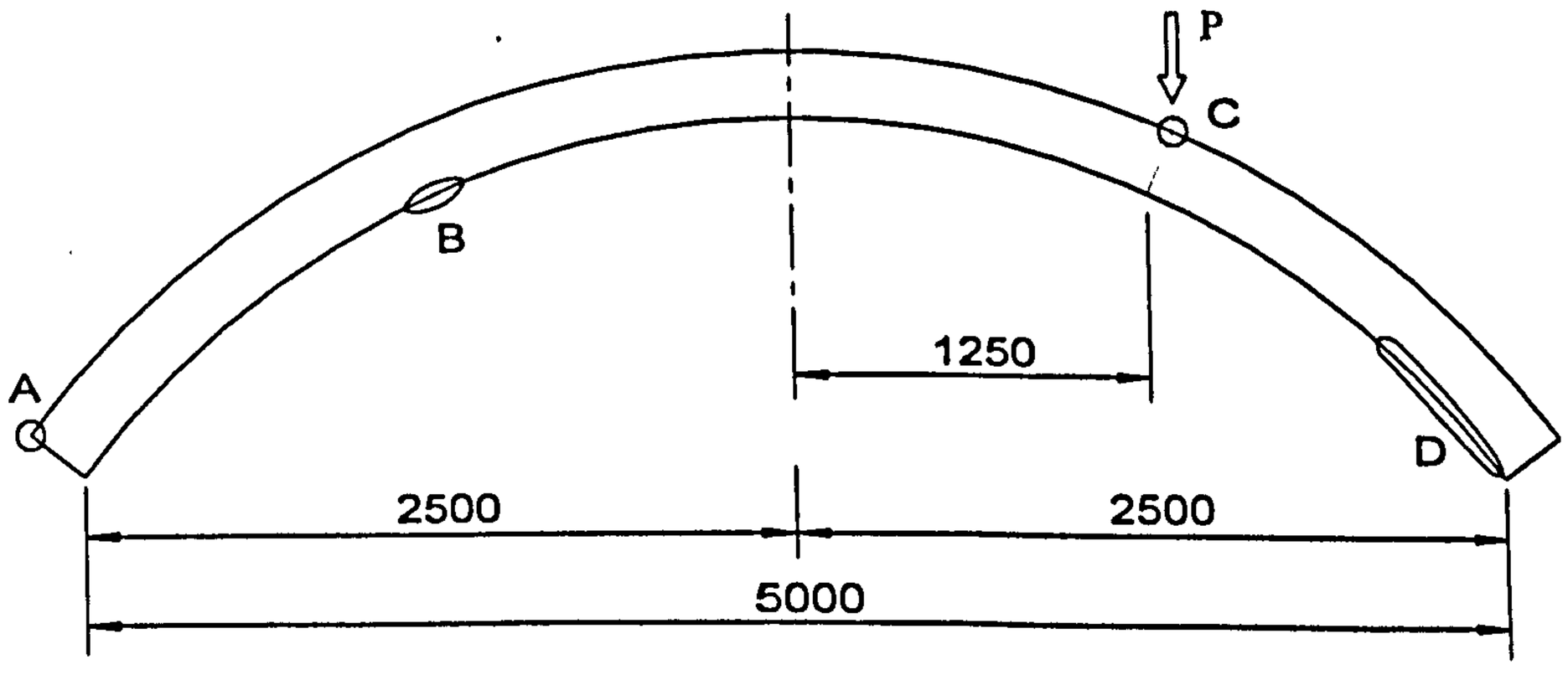

Fig. 5.13 Locations of Load and Hinges

When nine NPI were used, the distance between the hinge at the quarter-span of the unload side and the central line of the arch (m) was 1250 mm, and the distance between the hinge at the springing of the loaded side and the intrados of the springing (n) was about zero. As the NPI increased, value of m varied within the range between 940 and

1000 mm, and value of n varied within the range between 0 and 250 mm. The hinge at the location where m was 1250 mm was not necessary a natural location. In other words, the hinge could be developed somewhere at a reduced ultimate load (note, the location was more likely to move towards the crown) if more interfaces would have defined, as indicated by the results of the model with more NPI. For the model of nine NPI, the four hinges were nearly fully developed, and the horizontal component at each hinge was at 20.08 kN; and for the model of thirty-three NPI, the hinge near the springing of the loaded side moved away from the springing, and was not fully formed before the failure of the model, and the horizontal component at each hinge was about 19.86 kN.

The displacements were checked at two locations of the model of thirty-three NPI: - one was at the intrados under the loading location – the point "1/4L LD" (or the maximum downwards movement), and the other was at the extrados of the hinge within the quarter-span of the unloaded side – the point "1/4L ULD" (or the maximum upwards movement). As the applied load increased, the displacements at the point 1/4L LD were greater than those at the point 1/4L ULD in both X and Y directions prior to the development of the third hinge around the point 1/4L ULD (it may be noted that the second hinge was at the extrados of the springing of the unloaded side). As soon as the third hinge occurred, the displacements in Y direction at the point 1/4L ULD, and in X direction at the point 1/4L LD increased relatively due to the effects of rotations of the segments. As a result, the total displacements at the point 1/4L LD were less than those at the point 1/4L ULD until the model failed. Fig.5.14 shows the radial deflections at the points 1/4LD and 1/4ULD during the loading history.

It may be noted that care was taken when the animation tool of ANSYS5.3 was used to interpret the displacements of the model as its colour mapping system of contour plots were based on the largest value. In this case, the extreme colours in the displacement contour plots were based on the values of the last converged results, and then linearly changed for the plots of other load steps. It would falsely show that the displacements at the point 1/4L ULD were greater than those at the point 1/4L LD as soon as loads applied.

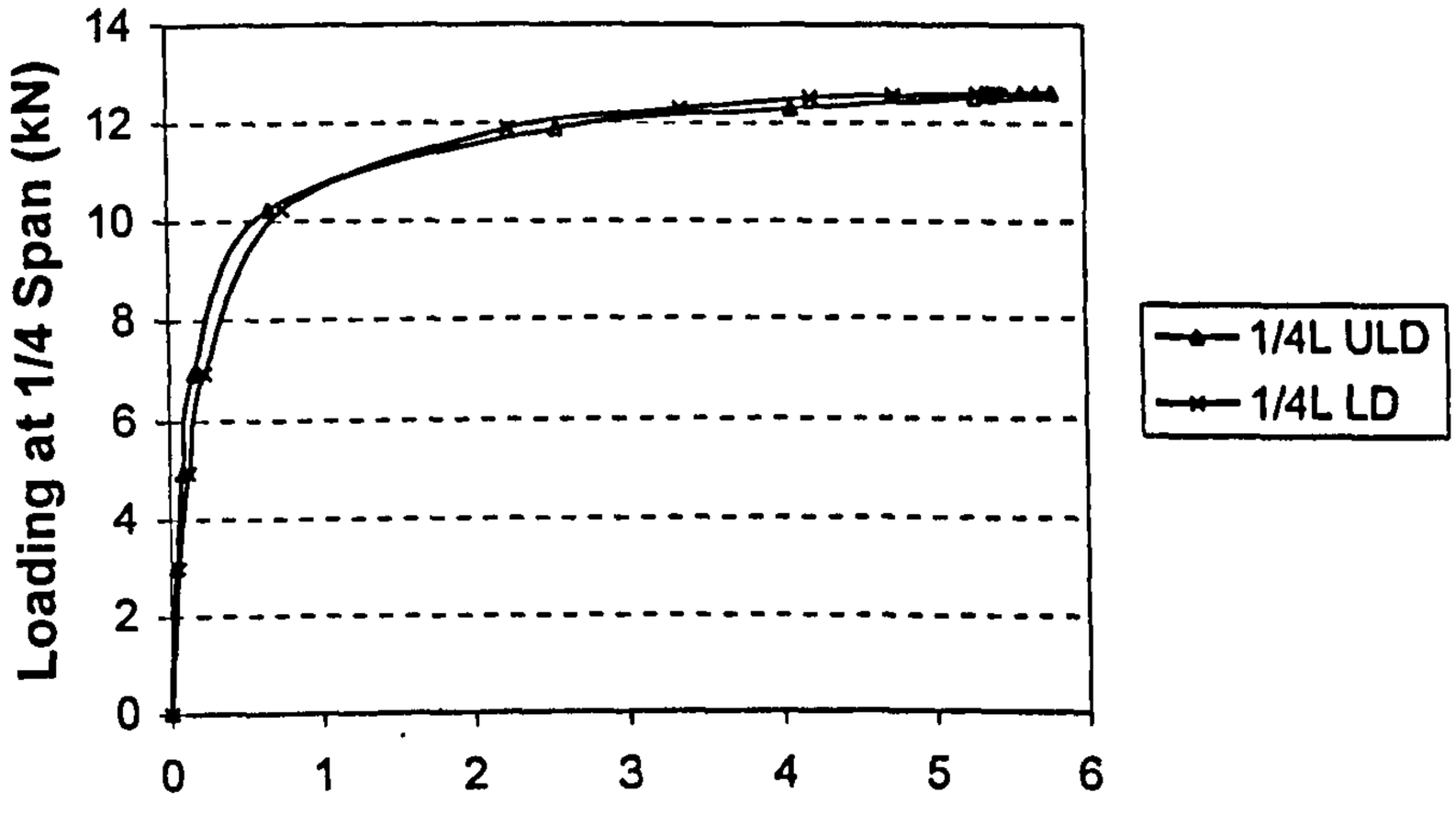

Fig. 5.14 Radial Deflections at ¼ L of Both Loaded (LD) and Unload Sides (ULD)

Considering that the restraint effects of spandrel arches and piers on the main arch of an open spandrel arch, and the above results, twelve NPI were adopted along the arch ring of the model OSMA3, and the results were as expected as presented in Chapter 4.

5.4.2 Miscellaneous

The effects of mesh sizes on the behaviour of the arches were studied for both the smeared models and the discrete models. For the model OSMA4, provided that sufficient elements (between 80 and 100) are defined along the ring of the arch, ultimate loads were 14.05 kN, 13.51 kN and 13.18 kN, respectively for three, five and seven rows of elements along the thickness of the arch barrel. For the models OSMA2, OSMA3 and OSMA4, the changes in mesh sizes within spandrel arches and piers are less sensitive to the overall behaviour of the models. However, if too small mesh sizes are used within the spandrel arches (especially within the end spandrel arches), convergence difficulties could be experienced at the early stages of analyses. In general, in order to simulate the propagation of cracks, minimum three rows of elements should be used through the thickness of the barrel of spandrel arches and the width of spandrel piers. As the integrity of the main arch has great influences on the overall behaviour of an open spandrel arch, more rows of elements should be used through the thickness of the barrel. Otherwise, it could not only make it difficult to simulate the sequences of the

development of cracks, but also artificially predict stiffer responses. For the discrete models, mesh sizes are less sensitive along the rings of arches and the heights of spandrel piers. The behaviour of arches could greatly be affected by the mesh sizes along the thickness of arch barrels. Compared with the smeared models, more elements should be defined across the arch barrels in order to ensure the success of the analyses. This is because the separations of interfaces are likely to take place suddenly, and hinges tend to be formed earlier since there is little tensile capacity within the interfaces. Once the hinges are formed, the displacements within an arch will increase rapidly due to the rotations of the segments between adjacent interfaces, which general leads to an early failure of the arch. Therefore, the use of more elements across arch barrel could not only overcome possible convergence difficulties, but also ensure a true ultimate load.

The nonlinear controls, such as CTAT, CTLS, CTP and convergence tolerances provided by the Program, could affect the solution accuracy and efficiency, and in some (or many) cases, improper use could lead to a failure of analyses. The efficient uses of the first three controls for both smeared and discrete models have been discussed in Chapter 4. It has been found that the controls of convergence tolerances are critical factors to ensure the successful simulations of the behaviour of arches, especially for the smeared models. By default, convergence is achieved at each load step when the residual forces fall below 0.1% of the applied load. If the default force tolerance is used, convergence difficulties could be encountered at early stages since the residual forces (or disequilibria forces) due to the redistribution of the forces previously taken by the uncracked zones could exceed the tolerance (for the models OSMA3 and OSMA5) unless extremely small load increments are used. However, the use of too small load increments could also practically prevent achieving solutions in terms of CPU time. It was found that a relatively large force tolerance such as one percent of the applied load might need to be used to ensure the success of the analyses. In fact, since a successful smeared model generally fails when the residual forces of the model become divergent, the use of larger force convergence tolerance has little effects in terms of the ultimate load.

For the smeared and mixed models, three-dimensional models must be created in order to use the element SOLID65 despite the fact that the problems being concerned are essentially two-dimensional. In order to reduce the sizes of the models, only one layer of

elements was defined along the thickness of the arches in the analyses. In other words, the actual thickness of an arch was scaled down to a value. This value was determined in such a way that the optimal sizes and shapes of the elements could be ensured. For instance, 100 mm was used as the thickness of the model in case of the model OSMA4. This simplification may lead to the results without taking the transverse stiffening effects into account. However, the results of additional analyses by defining three or five layers of elements across the thickness of arch indicated that there were little differences in terms of the deflections and the ultimate loads.

Chapter 6 Summary And Conclusions

6.1 Summary

The behaviour of open spandrel brickwork masonry arches was studied through a series of model arch tests and finite element simulations. A total of five brickwork model arches were constructed and tested: (1) spandrel arches and spandrel piers only (OSMA1); (2) three-metre span of open spandrel arch of half-metre depth with three spandrel arches at each side without fill (OSMA2); (3) five-metre span of arch itself one-metre depth (OSMA3); (4) five-metre span of open spandrel arch of one-metre depth with two spandrel arches at each side without fill (OSMA4); and (5) five-metre span of open spandrel arch of one-metre depth with two spandrel arches at each side with fill (OSMA5). Three finite element modelling methods were developed: - (1) the smeared modelling method (SMM); (2) the discrete modelling method (DMM); and (3) the mixed modelling method (MMM). Detailed discussions and observations of the model tests were presented in Chapter 2, and the formations of finite element models, simulations and verifications were presented in Chapters 3, 4 and 5, respectively. Most of the material properties used in the FE models were obtained through various material tests of the corresponding model arches. The values of other parameters used in the FE models were justified through sensitivity studies. Both the observed and recorded behaviour of the model arches during the tests could be reproduced by the smeared and/or discrete models. Reasonably good correlations were achieved in terms of the ultimate loads, the patterns of cracks or hinges and load-displacement responses along the intrados of main arches between the test results and those simulated by the finite element models.

All the finite element models were developed using APDL (ANSYS Parametric Design Language). The FE models (including meshing) could automatically be generated once the materials-, geometry-, and elements-related parameters were input. Therefore, the models could be used for the analyses and assessment of general single arches and open spandrel arches of various configurations.

For the smeared models, the required materials-related parameters include Poisson's ratio, density, and Young's modulus; and the required elements-related parameters

include shear transfer coefficients for open and closed cracks; uniaxial crushing strength; and uniaxial tensile cracking strength. The change in the value of Poisson's ratio has little effects on the behaviour of arches, and a value between 0.15 and 0.3 may be assumed. Though the load capacity of a masonry arch can be affected by the material density used, it is reasonable to assume that a representative density could be obtained with sufficient accuracy through a few tests of brickwork masonry units. The Young's modulus of brickwork masonry varies from prisms to prisms. If an average of the Young's moduli obtained from the standard prism tests is used in FE analyses of a masonry arch, stiffer responses are likely to be predicted. It has been found from Chapter 5 that the Young's modulus used in the FE analyses has little effects on the ultimate loads predicted. Thus, it can be determined with certain confidence as far as the determination of the load capacity of a masonry arch is concerned. As discussed in Chapter 4, any values between 0 and 1 inclusive of shear transfer coefficients for closed cracks hardly have any effects on the behaviour of arches, and shear transfer coefficients for open cracks do have some effects on the development of cracks and ultimate loads if values over 0.7 are used. However, considering that brickwork masonry arches generally fails due to the formation of hinges and shear strengths between mortar joints are relatively low, small values between 0.01 and 0.1 may be used for shear transfer coefficients for closed and open cracks. The uniaxial crushing strength of brickwork masonry can be obtained through prism tests. As the stresses within masonry arches through loading history are generally less than the uniaxial crushing strength, the accuracy of the uniaxial crushing strength obtained from prism tests may not be critical. The last parameter required is the uniaxial tensile strength of masonry, which may need special attentions. The success of the analyses using the SMM largely depends on the tensile strength of brickwork masonry. If it is assumed too small, ultimate loads could be underestimated, and if it is assumed too great, the ultimate load could be overestimated and the true failure modes of the model are unlikely to be predicted. The tensile strength of brickwork masonry may be obtained through the tensile tests of brickwork prisms. Otherwise, it has been found that a value between 0.28 and 0.30 N/mm^2 is normally sufficient to realistically simulate the behaviour of brickwork masonry arches.

For the discrete models, the required materials-related parameters are the same as those for the smeared models, i.e., Poisson's ratio, density, and Young's modulus. The same

principles as those discussed for the smeared models may be used to determine their values. The required elements-related parameters mainly include coefficient of friction, normal stiffness and tangential stiffness. The coefficient of friction may be obtained from shear tests of two-course brickwork prism. However, since the results from tensile tests are likely to be scatter, a representative value may not be readily determined. It has been found that any value over 0.4 (note that the average of test results are normally well over 0.4) could normally ensure the success of the analyses. If too small coefficient of friction is assumed for the contact elements within interfaces, the model could unexpectedly fail at very low ultimate load due to excessive shear displacements. The normal stiffness of contact elements may be assumed the same as the Young's modulus obtained from the prism tests of the corresponding model arch, and the tangential stiffness may be assumed as 1/10 or 1/100 of the normal stiffness. For the mixed models, however, the normal stiffness may initially be set to a low value in order to facilitate the convergence of the analyses, and gradually modify it to limit the penetrations. It may be noted that as the tangential stiffness, by default, is equal to 1/100 of the normal stiffness, it must explicitly be revised whenever the normal stiffness is modified to ensure the consistent frictional characteristics.

Both the model tests and the finite element simulations show that, in an open spandrel brickwork masonry arch, the main arch generally fails due to the formation of four hinges (or extensive cracks within four areas). Due to the stiffening effects of the spandrel arches and piers, especially those at the unloaded sides, the hinge that normally occurs at the quarter-span areas for a single arch moves towards the crown of the main arch at some point between the arch seat of the unloaded side and the crown of the main arch.

The function of the end spandrel arch at the loaded side is mainly to transfer half of its own weight and part of fill weight to its end support. The functions of the spandrel pier at the loaded side may be described at two stages. At the first stage prior to the failure of the adjacent internal spandrel arch, the pier transfers its own weight, half of the weight of the end spandrel arch, and the interactions between itself and the internal spandrel arch to the main arch. At the second stage after the failure of the adjacent internal spandrel arch, the pier simply transfers its own weight and half of the weight of each adjacent spandrel arch to the main arch. At this stage, the function of the spandrel arches

and piers at the loaded side may simply be replaced by two point loads acting on the main arch at the interfaces between the arch seat and the end of the internal spandrel arch and between the end of the spandrel pier and the main arch. In summary, the existence of the spandrel arches and piers at the loaded side have no contributions to the increase in ultimate loads and overall stiffness. As a matter of fact, its presence has ultimate loads and overall stiffness reduced.

The function of the end spandrel arch at the unloaded side is mainly to transfer the reactions at its supports to the spandrel piers at the loaded side and to the adjacent internal spandrel arch. These forces are then acting on the main arch at the interfaces between the bottom of the spandrel pier and between the arch seat at the unloaded side and the internal spandrel arch. It is these interactions that provide additional stiffness to the main arch; enhance the ultimate load and postpone the occurrence of cracks of the main arch. The maximum forces acting on the interfaces between the internal spandrel arch and the main arch are the reactions of the internal arch at the end adjacent to the arch seat when three hinges are fully developed within the internal arch. The functions of the spandrel pier at the unload side may be described in three stages. At the first stage prior to the failure of the both internal and end spandrel arches, it transfers its own weight and the interactions with the spandrel arches to the main arch. At the second stage after the failure of the internal arch, it transfers its own weight, half of the weight of the internal spandrel arch and the interactions with the end spandrel arch to the main arch. At the third stage after the full development of the hinge within the bottom half of its own height. It transfers its own weight, half of the weight of the internal spandrel arch and the interactions with the end spandrel arch to the main arch. At this stage, the reactions acting on the main arch through the spandrel piers reach their maximum, and remain constant until the failure of the entire model (at this stage, three hinges may or may be fully formed within the end spandrel arch). In summary, the existence of the spandrel arches and piers at the unloaded side are essential to enhance ultimate loads, increase overall stiffness and postpone the occurrence of hinges (or cracks) of the main arch. The function of the spandrel arches and piers at the unloaded side may be replaced by two equivalent point loads acting on the main arch at the interfaces between the arch seat and the end of the internal spandrel arch and between the end of the spandrel pier and the main arch.

6.2 Conclusions

From the model tests and the finite element analyses, a number of conclusions can be drawn with regard to the behaviour of open spandrel brickwork masonry arches. It may be noted that these conclusions are drawn largely based on the results of the arch models with the configurations and loading conditions being concerned. Some of them are applicable to a wide range of (brickwork) masonry arches while further work may be needed should the others be used.

Conclusions that can be drawn from both observations during the tests and the finite element simulations of the model arches include: -

- ◊ OSBMA behave almost linearly up to 75 – 90 % of ultimate loads;

- ◊ OSBMA generally fail by the formation of both local and global hinged mechanisms. In general, there are four hinges within the main arch. Depending on the local characteristics and loading conditions, various combinations of local mechanisms may be developed within the spandrel arches and piers;

- ◊ The location of the third hinge within the main arch of OSBMA moves from the quarter-span areas of the unloaded side towards the crown of the main arch due to the interaction between the spandrel structures and the main arch. For the main arch itself (OSMA4), the open spandrel arch without fill (OSMA3) and with fill (OSMA5), the distance between the hinge and the crown of the main arch was about 970 mm, 560 mm and 400 mm, respectively;

- ◊ The overall stiffness and ultimate loads are enhanced due to the interactions between the spandrel arches/piers and the main arch. Compared with that of the main arch itself, the load capacity of OSBMA could be increased up to 80% without fill, and 150% with fill when loads are applied near quarter-span areas;

- ◊ Compared with those of the main arch itself, both the occurrence and the further development of hinges or cracks (note, separations of interfaces for the DMM or

propagations of cracks for the SMM) are postponed due to the interactions between the spandrel arches/piers and the main arch;

◊ The effects of the spandrel arches and piers on the behaviour of the main arch may be different when loads are applied at the locations away from the crown of the main arch. The spandrel arches and piers at the loaded sides have negative effects on the overall stiffness and load capacity, and in any structural idealization may be replaced by two equivalent forces acting on the interfaces between the internal spandrel arch and the adjacent arch seat and between the bottom of the pier and the main arch. The spandrel arches and piers at the unloaded sides play an essential role in enhancing the overall stiffness and ultimate loads of the main arch itself, and they can also be replaced by two equivalent forces acting on the interfaces between the internal spandrel arch and the adjacent arch seat and between the bottom of the pier and the main arch;

◊ The effects of fill on the behaviour of OSBMA are similar to those of the spandrel arches. When loads are applied at locations away from the crown of the main arch, the fill on the loaded side has negative effects on the overall stiffness and load capacity. The fill on the unloaded side, (which may be assumed as an additional part of the spandrel arches to some extent), transfers greater reactions (note, compared with those without fill) onto the main arch. Both the upward displacements at the unload side, and the downwards displacements at the loaded side of the main arch are further reduced, and ultimate loads are further enhanced;

◊ The smeared models can be used to efficiently simulate the behaviour of open spandrel brickwork masonry arches without fill. The sequences of the occurrence of cracks and their detailed propagations can be readily traced during the loading history. The simulated responses of masonry arches include a series of alternative linear behaviour and local brittle-type failure behaviour due to the constitutive relationship adopted. The simulated cracks can freely occur and propagate within the masonry arches if cracking conditions are met. In reality, cracks are more likely to follow the mortar joints. The effect of this difference in the cracking patterns could result in a relatively low ultimate load predicted.

◊ The discrete models can be used to effectively and realistically predict the behaviour of open spandrel brickwork masonry arches without fill in terms of load – displacement responses, ultimate loads and the movement of the thrust lines during the history of loading. Ultimate loads could slightly be underestimated without taking the tensile capacity of joint mortar into account;

◊ The mixed models can be used to predict the behaviour of open spandrel brickwork masonry arches with fill, in which the effects of the main arch, the spandrel arches and piers, and the fill can realistically be simulated;

◊ If Young's modulus obtained from normal brickwork prism tests is directly used in finite element analyses of brickwork masonry arches, the simulated responses between loads and deflections are likely to be stiffer than those obtained from the corresponding model tests. Reduced modulus may be used in finite element analyses. The percentage of reduction of the modulus depends on the methods by which the tests are carried out. For the present research, it has been found that 40% of reduction of the Young's modulus are acceptable in general;

◊ Changes in Young's modulus have little effects on the levels of stresses, modes of failure and ultimate loads of masonry arches. They affect the levels of displacements and strains within masonry arches. The lower the Young's modulus, the greater the displacements and strains will be;

◊ Changes in density in the finite element models will affect the ultimate loads predicted. The greater the density used, the greater the ultimate loads will be predicted. This is because greater density results in greater initial compressive stresses within masonry arches, which must be relieved before any cracks can take place;

◊ Tensile strength is a critical factor to govern the load capacity of OSBMA if the smeared models are used. As it increases, the ultimate load predicted will increase. Due to the fact that the smeared models may slightly underestimate the

ultimate load of a brickwork masonry arch, a factored tensile strength obtained from prism tests may be used in finite element analyses of OSBMA.

◊ The open spandrel masonry arches fail at relatively low compressive stresses. Crushing failure of masonry is not as critical as that in filled masonry arches.

◊ For the failure mode of OSBMA, there are four hinges within the main arch, and a series of local hinges and crackings within the spandrel arches and spandrel piers. Under normal test conditions, cracks/hinges are likely to occur simultaneously within the spandrel structures, which could cause difficulties in tracing the sequences of the occurrence of cracks;

◊ Local shear failures can take place at the interfaces between the internal spandrel arch and the adjacent arch seat, and the rest of the structure remains intact should loads be applied at the crown of the internal spandrel arch. This type of failure may be prevented by building "shear studs" within the contact areas between the spandrel structures and the main arch;

◊ The overall stiffness of OSBMA could be different from one to another even if similar materials and workmanship are used, but the corresponding load capacities are normally similar.

CHAPTER 7 FUTURE WORK

In the present research, both model arch tests and FE modelling and analyses were carried out in order to study the behaviour of open spandrel brickwork masonry arches. It has been shown that reasonably good correlations between the results obtained from these two approaches have been achieved in terms of the ultimate loads, the modes of failure and the load-deflection responses. However, further work is still needed either to improve some methods adopted in the present research or to investigate other factors, which may affect the behaviour of the open spandrel arches. Among many, the following three aspects, which are closely linked to the present research are discussed, i.e., material tests, arch models and tests, and FE modelling methods.

7.1 Material Tests

It has been shown in Chapter 5 that material properties such as Young's Modulus and tensile strength of masonry units greatly affect the accuracy of the results of FE analyses. In the present research, an average of 10000 N/mm^2 of the Young's Modulus of the brickwork masonry units, which was obtained from the material tests, was used in the FE modelling. The results from both the SMM and the DMM indicated that such value appeared too higher since the predicted load-deflection responses were stiffener than those obtained from the model tests. It should be noted that the Young's Modulus used is already mush less than those reported elsewhere (Crisfield 1985a and Hodgson 1996). The possible reason why relatively lower E values were obtained in the present research was given in Section 2.1.3.1. Therefore, it is believed that the current standard prism test method, from which the E values of brickwork masonry units are derived, may not be adequate should the brickwork masonry in the arches be concerned. Modified test method may need to be developed. The new method should take account of the anisotropic properties of brickwork masonry units either through adopting different E values in different directions or deriving a more representative one for each individual arch.

In the smeared FE models, it is essential to use a realistic tensile strength of brickwork masonry in order to ensure the accuracy of both the ultimate load and the mode of

failure of an arch being analysed. In the present research, it has been shown that a value between 0.28 and 0.32 N/mm^2 of the tensile strength of the brickwork units generally leads to an acceptable accurate result simulated. However, as discussed in Section 2.1.3.2, the results of the tensile tests of brickwork masonry units may be influenced by a number of factors. A difference of 0.1 N/mm^2 of the tensile strength used in the SMM could result in up to 20% of the difference of the ultimate loads predicted (Section 5.2.2). Thus, it is necessary to develop a procedure of conducting the tensile tests of brickwork masonry units, which should take account of the factors discussed in Section 2.1.3.2 and other factors such as the development of initial bond strength, workmanship and curing conditions.

It is also necessary to conduct tests on brickwork prisms with wedged mortar joints under eccentric loading conditions to enable better understanding of the behaviour of the brickwork masonry units in the masonry arches.

7.2 Model Arches and Tests

During the present research, four and "half" model arches were constructed and tested, through which various behaviour of the open spandrel brick masonry arches were observed and verified. However, other possible behaviour such as ring separation and crushing of masonry unit material, etc., may be "prevented" either due to the limitations of the above models or due to the way that the loading was applied. In addition, mortar was used as fill instead of other common used materials since the models were relatively small and spandrel walls were not constructed. Therefore, larger scale open spandrel brickwork masonry arches with spandrel walls need to be built and tested should the above factors be investigated.

The effects of the self-weight of the model arches were not directly measured in the present research. As described in Chapter 2, both strain and deflection gauges were installed after the removal of the centrings of both the main arch and the spandrel arches. The FE simulations have shown that great deformation and stresses can be produced under self-weight only condition, especially within the spandrel arches. It may be noted that the ultimate load was only about 50% of the self-weight in the case of the model OSMA3. Therefore, it is necessary to quantify the effects of the self-weight on

the behaviour of open spandrel brickwork masonry arches. This can be achieved by attaching both deflection and surface strain gauges to the model arches before the centrings of the main arch and spandrel arches are removed.

It was shown in Chapter 2 that fine cracks occurred within the spandrel arches prior to the application of external loading, and it was caused by the deformation of the main arch as shown in Fig. 7.1. It may suggest that different methods be used to construct open spandrel arches.

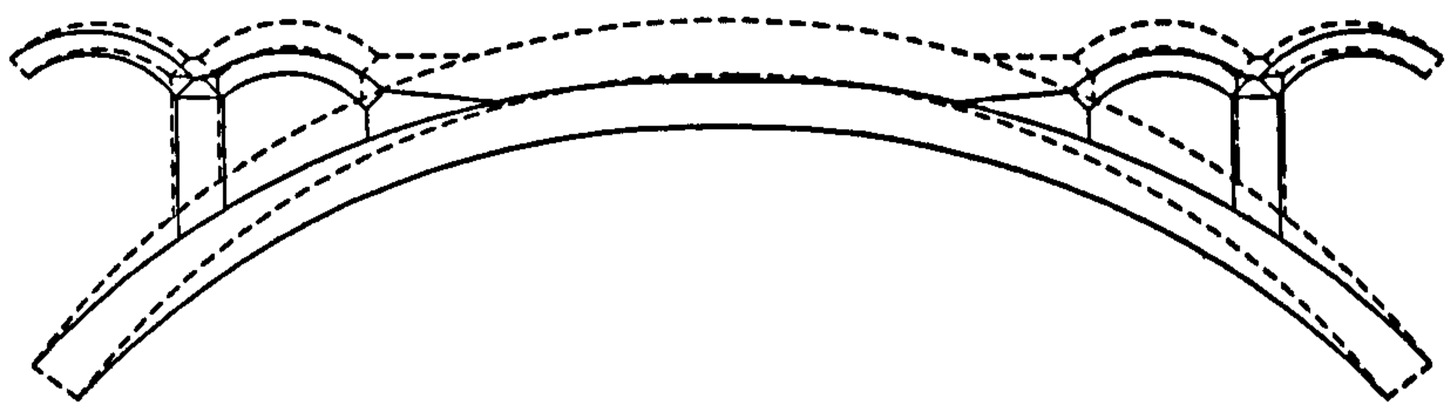

Fig. 7.1 Deformation of the OSMAB Under Self-weight

Figure 7.2 shows two methods of constructing an open spandrel arch. The method 1 was used in the present research, in which the main arch is first built on the centring of the main arch. Then the centrings of the spandrel arches are set up to build the spandrel

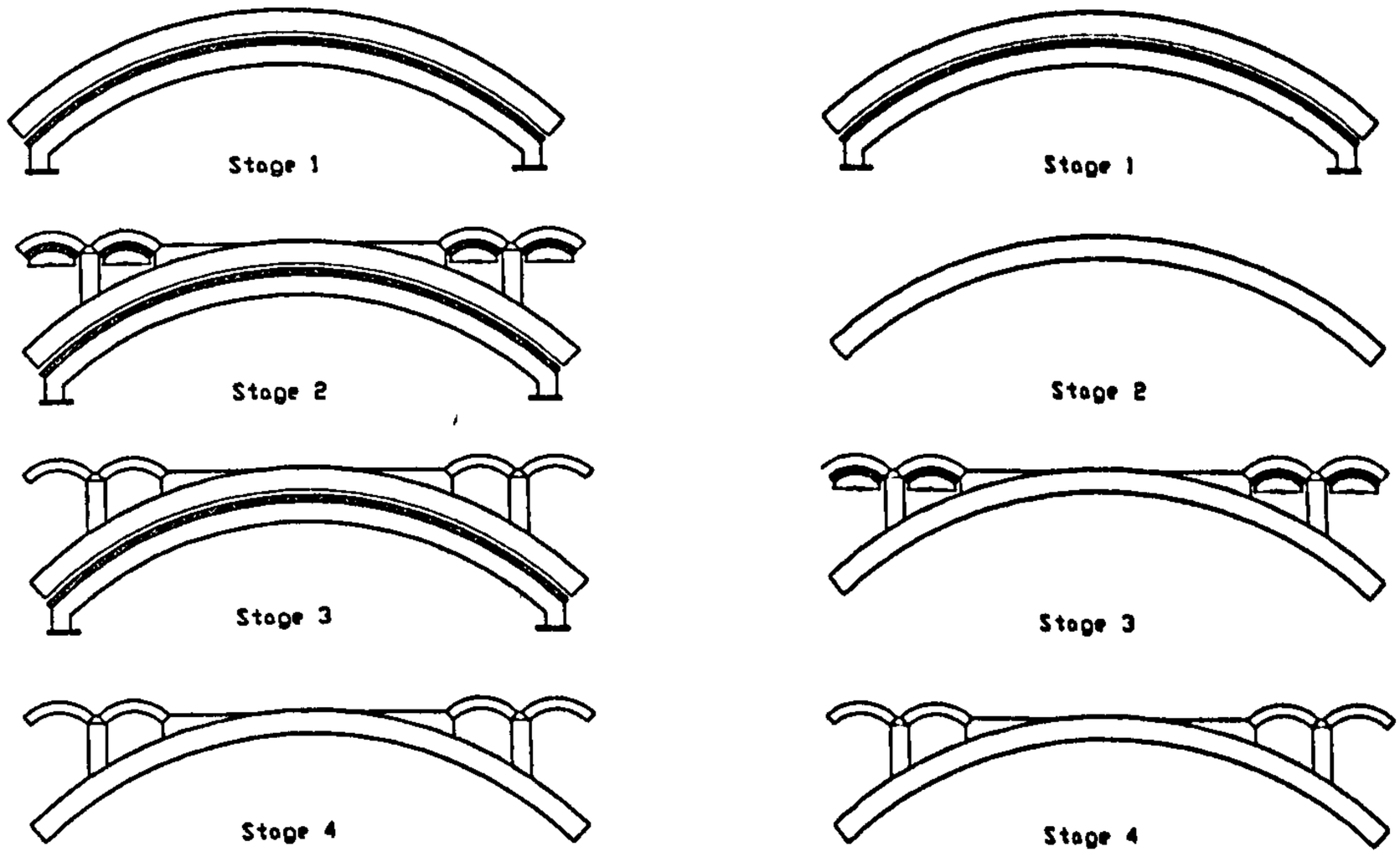

(a) Construction Method 1 **(b) Construction Method 2**

Fig. 7.2 Construction Methods of OSMAB

arches. For the removal of the centrings, the centrings of the spandrel arches are first removed, and followed by that of the main arch. In the method 2, the centring of the main arch is removed after the completion of the main arch. The centrings of the spandrel arches are supported on the main arch alone. For the former, the main arch and the spandrel structures acts together when the centring of the main arch is removed. The deformation of the main arch, although it is relatively small compared with that if the main arch and the spandrel arches act separately, could cause the cracks within spandrel arches. For the latter, the possible fine cracks could be minimized as the joint mortar within spandrel arches could take up much smaller deformation caused by the removal of the spandrel arch centrings.

7.3 FE Modelling

The smeared, discrete and mixed modelling methods were developed and used to analyse the model arches. As discussed in Chapter 4, these different modelling schemes made it possible to reveal the behaviour of the model arches from different aspects. However, the applications of these methods could be limited partly because of the assumptions made in each of the three modelling methods, and partly because of the complexity of the modelling and solution approaches adopted. Further work may be needed should the methods be widely used.

For the smeared modelling method, it has been shown that the FE results largely depend on the value of the tensile strength of brickwork masonry used. The greater the tensile strength is, the greater the predicted ultimate load will be, and vice versa. If a very small value of the tensile strength is used (say, 0.005 N/mm^2), the predicted ultimate load could be as low as 2 kN in the case the model OSMA4. It appears in conflict with the fact that a brickwork masonry arch is still capable of carry significant loads even when the tensile strength of the mortar is ignored. It is believed that the failure at the lower load could be caused by the assumptions of "homogeneous and initially isotropic continuum" adopted in the smeared modelling, and the limitations of the element SOLID65 used. These assumptions means that cracking can take place once the first principal stress reaches the tensile strength, whose locations are not necessarily confined within the mortar joints. In reality, due to the relatively lower tensile strength of the mortar, the cracks initiate in the mortar, and generally propagate within the mortar

joints. The effects of the "free" propagation of the cracks tend to modify the modes of the failure of the arch from the hinged mechanism to other forms of failure such as ring separation type. Also, the stiffness of the model decreases rapidly due to relatively large area of cracking, and large displacements develop within the model. But the element SOLID65 is incapable of coping with this geometry nonlinearity. The model thus fails at a relatively low load. One of the methods to overcome this difficulty may be to model the brick and the mortar separately, i.e., different material properties are assigned to the brick and the mortar. However, the drawback of such method is that small size of elements has to be defined within the mortar joints, which will lead to the significant increase in the total number of the elements. Alternatively, the element SOLID65 can be used to model the joint mortar only, and the rest of the structure are modelled using the element SOLID45 as shown in Figure 7.3. This can potentially model more realistic crack patterns within brickwork masonry arches, and minimized the possible convergence difficulties caused by a large number of the concrete type elements used.

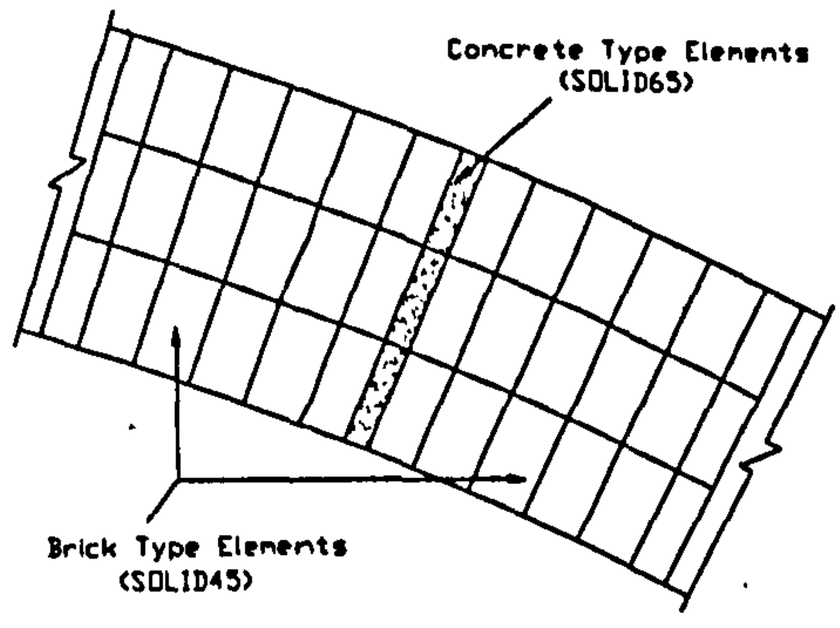

Fig. 7.3 Modified Smeared Modelling Method

For the discrete modelling method, the brickwork masonry is modelled as a series of elastic blocks connected along the common faces, and the effects of the material nonlinearity of the brickwork masonry and the possibility of the cracking at either side of the mortar joints are not considered. These factors are considered insignificant in the present research due to the relatively small sizes of the model arches and the low stress levels at failure. Further work may include the modelling of the mortar joints and interface elements at both sides of the joints, and the material nonlinearity is incorporated through the relevant failure criterion or through the adoption of the element SOLID65. Further, the initial bond strength of the brickwork masonry was modelled through the interface and nonlinear spring elements as described in Section 3.3.

However, the subsequent sensitivity analyses indicated that there were little differences in the predicted ultimate loads among the results using different initial bond strength. As a result a small value of 0.0001 N/mm^2 of the initial bond strength was used in all the cases, i.e., the tensile strength of the mortar was ignored. More work may be needed to further evaluate the effects of the initial bond strength on the behaviour of the brickwork masonry arches.

For the mixed modelling method, the "superelements" were created in order to model the arches and the fill, as well as their interfaces as described in Section 3.4. Due to the presence of a large number of the nonlinear elements of the SOLID65, CONTACT52 and COMBIN40, special attentions were paid to both the detailed modelling and solution schemes. Small load increments had to used to overcome the convergence difficulties. The further work may include the incorporation of the improvements of both the smeared and discrete modelling methods as discussed above, and development of the modelling schemes for different types of fill material.

REFERENCES

1. (ACI) Masonry Standards joint Committee, American Concrete Institute and American Society of Civil Engineers (1992) Building code requirements for masonry structures, ACI *530/ASCE5/TMS 402-92*, Detroit, New York.
2. (SRAT) Scientific Research Academy of Transport (1963) Design Theory of Brick & Stone Arch Bridges, Beijing, (in Chinese).
3. American Society for Testing and Materials (1986) 'Measurement of masonry Flexural Strength ', *ASTM C 1072-82*, ASTM, Philadelphia, PA.
4. American Society for Testing and Materials (1987) 'Test Method for Flexural Bond Stress of Masonry ', *ASTM E 518-80*, ASTM, Philadelphia, PA.
5. Anderegg, F. O. (1940) 'Some Properties of Mortars in Masonry ', *Proc. ASTM 40*, 1130-1142.
6. Andreaus, ugo (1988) 'A 3-D Finite Element For The Analysis of Masonry Structures', *Proc. 8th Int. Brick & Block Masonry Conference*, Dublin, 1405-1416.
7. ANSYS5.3 Element Reference, 000655, Seventh Edition, SAS IP, Inc.
8. ANSYS5.3 Theory Reference, 000656, Seventh Edition, SAS IP, Inc.
9. ASE (Austrian Society of Engineers) (1890), quoted from Pippard and Chitty (1951).
10. Atwood (1801) 'Dissertation on The Construction and Properties of Arches ', *W. Bulmer Co.*
11. Back, N., Burdekin, M. and Cowley, A. (1973) 'Review of The Research on Fixed And Sliding Joints ', *Proc. 13th Int. MTDR Conf*, Macmillan, London, 87-97.
12. Baker, I. O. (1920) A treatise on Masonry Construction, Wiley, New York.
13. Barlow, W. H (1846) 'The Existence (Practically) of The Line of Equal Horizontal Thrust in Arches, And The Mode of Determining it ', 728, *Proc. ICE*, pp162-182.
14. Bazant, Z. P. and Cedolin, L. (1979) 'Blunt Crack Band Propagation in Finite Element Analysis ', *J. Engrg. Mech. Div.*, ASCE 105(2), 297-315.
15. Belytschko, T. and Neal, M. O. (1991) 'Contact-Impact by The Pinball Algorithm With Penalty And Lagrangian Methods ', *Int. J. Numer. Methods Eng.*, 31, 547-572.
16. Böhm, J. (1987) 'A Comparison of Different Contact Algorithms With Applications', *Comput. Struct.*, 26, 207-221.

17. Boothby, T. E. (1994) 'Stability of Masonry Piers And Arches Including Sliding', *Journal of Engineering Mechanics*, Vol. 120, No. 2, ASCE, pp304319.
18. (BRE) Building Research Establishment (1991) Testing bond strength of masonry, BRE Digest 360.
19. Bridle, R. J. and Hughes, T. P. (1990) 'An Energy Method For Arch Bridge Analysis ', *Proc Instn Civ Engrs*, Part 2, 89, Sep, 375-385.
20. Bron, O. (1991) An investigation of a soil/masonry arch model using photoelastic methods, MSc thesis, University of Wales College of Cardiff.
21. Brown, D. J. (1993) Bridges, Michael Beazley ISBN 1 85732 163 4.
22. BS 5628 Part 1(1985) Code Of Practice For The Use Of Masonry. Part 1 Structural Use Of Unreinforced Masonry, Part 1: 1978. British Standards Institution, London.
23. Buyukozturk, O. and Shareef, S. S. (1985) 'Constitute Modelling of Concrete in Finite Element Analysis ', *Computers & Structures*, 21, 581-610.
24. Cescotto, S. and Charlier, R. (1993) 'Frictional Contact Finite Elements Based on Mixed Variational Principles ', *Int. J. Numer. Methods Eng.*, 36, 1681-1701.
25. Chand, R., Haug, E. J. and Rim, K. (1976) 'Analysis of Unbonded Contact Problems by Means of Quadratic Programming ', *Journal of Optimization Theory And Applications*, Vol. 20, No. 2, Oct., 171-189.
26. Chettoe, C. S. and Henderson, W. (1957) 'Masonry Arch Bridges ', *Proc Instn Civ Engrs*, Part 7, 723.
27. Choo, B. S., Coutie, M. G., and Gong, N. G. (1991) 'Finite Element Analysis Of Masonry Arch Bridge Using Tapered Beam Elements ', *Proc Instn Civ Engrs*, Part 2, Dec, 755-770.
28. Choo, B. S. and Gong, N. G. (1995) 'Effect of Skew on The Strength of Masonry Arch Bridges ', *Proceedings of The First International Conference on Arch Bridges*, Bolton, UK, 205-214.
29. Cooke, N. (1987) 'Instability Of Masonry Arches ', *Proc Instn Civ Engrs*, Part 2, 83, Sep, 497-515.
30. Cox, D. and Halsall, R. (1996) Brickwork Arch Bridges, The Brick Development Association, CI/SfB 182.
31. Coyne, P. (1989) 'China's Historic Bridges', Arts of Asia, May/June.
32. Crisfield, M. A. (1984) 'A Finite Element Computer Program For The Analysis Of Masonry Arches ', Department of Transport. TRRL Laboratory Report 1115, Transport Research Laboratory, Crowthorne.

33. Crisfield, M. A. (1985a) 'Finite Element And Mechanism Methods For The Analysis Of Masonry And Brickwork Arches ', Department of Transport. TRRL Research Report 19, Transport Research Laboratory, Crowthorne.
34. Crisfield, M. A. (1985b) 'Computer Methods For the Analysis of Masonry Arches ', *Proc. 2nd Int. Conf. on Civil and Struct. Eng. Computing*, Vol. 2, Edinburgh, 213-220.
35. Crisfield, M. A. and Page, J. (1990) 'Assessment of The Load Carrying Capacity of Arch Bridges ', The Maintenance of Brick And Stone Masonry Structures (Edited by Sowden, A. M.), 81-113.
36. Das, P. C. (1995) 'The Assessment of Masonry Arch Bridges', *Proceedings of The First International Conference on Arch Bridges*, Bolton, UK, 21-27.
37. Davey, N. (1953) Tests on Road Bridges, HMSO, London.
38. Davies, S. R. (1985) 'The Assessment Of Load Carrying Of Masonry Capacity Of Masonry Arch Bridges ', *Proc 2nd Int Conf on Civil and Structural Engineering Computing*, Dec. Edinburgh: Civil-Comp Press.
39. Davies, S. R. (1989) 'March - A Computer Program For The Assessment Of Masonry Arches ', *Conference: Structural faults and repair 89*, London, Jun, 1, Edinburgh, Engineering Technics Press, 277-287.
40. Dhanasekar, M., Page, A. W. and Kleeman, P. W. (1985) 'The Failure Of Brick Masonry Under Biaxial Stresses ', *Proc. Inst. Civ. Engrs*, Part 2, 79, June, 295-313.
41. Draper, R., Soar, K., Taylor, N., Pridmore, T. (1995) 'Computer Vision For Masonry Vault Testing', *Proceedings of The First International Conference on Arch Bridges*, Bolton, UK, 257-266.
42. Druck, D. C. (1954) 'Coulomb Friction, Plasticity And Limit Load ', *Journal of Applied Mechanics*, ASME, Vol. 21, 71-74.
43. Drysdale, R. G., Hamid, A. A. and Baker, L. R. (1994) Masonry Structures: Behaviour and Design, Prentice Hall, Inc., 0-13-562026-0.
44. Duddock, E. C. (1974) 'Hollow Spandrels In Arch Bridges: A Historical Study ', *The Structural Engineer*, 52, No 8, Aug, 281 - 293.
45. (EB) Encyclopedia Brittanica (1984a), Encyclopedia Brittanica, 15th Ed., Edinburgh, Vol. 3, 'Bridges, Construction and History of '.
46. (EB) Encyclopedia Brittanica (1984b), Encyclopedia Brittanica, 15th Ed., Edinburgh, Vol. 3, 'Building Construction '.

47. (EB) Encyclopedia Brittanica (1984c), Encyclopedia Brittanica, 15th Ed., Edinburgh, Vol. 11, 'Masonry Construction '.
48. (EE) The Edinburgh Encylopaedia (1804), Edinburgh, IV Part 2, 'Bridge'.
49. Eidsheim, O. M. (1980) 'Non-linear Analysis of Elastic-Plastic Shells Using Hybrid Stress Finite Element ', Report No. 80-1, *Div. of Struct. Mech.*, The Norwegian Inst. of Tech., Trondheim, Norway.
50. Ellingwood, M. and Tallin, A. (1985) 'Limit States Criteria For Masonry Construction ', *Journal of Structural Engineering*, 111, 1, January, 108-122.
51. Fordham, A. A. (1929) 'Masonry and concrete arches ', *Proc Instn Struct Engng.*
52. Francis, A. J., Horman, C. B. and Jerrems, L.E. (1970) 'The effect of joint thickness and other factors on the compressive strength of brickwork ', *Proceedings of the Second International Brick Masonry Conference*, Stoke-on-Trent, England, 31-37.
53. Gautier, H. (1714) Traite des Ponts, Paris, quoted from Ruddock (1974).
54. Gens, A., Carol, I. and Alonso, E. E. (1989) 'Elasto-Plastic Model For Joints And Interfaces ', *the Second International Conference on Computational Plasticity*, COMPLAS II, Part 2, Sept, Barcelona, 1151-1264.
55. Gilbert, M., Hobbs., B and Molyneaux, T. (1995) 'The Response of Masonry Parapets to Accidental Vehicle Impact ', *Proceedings of The First International Conference on Arch Bridges*, Bolton, 143-153.
56. Goodman, R. E., Taylor, R. L., and Brekke, T. L. (1968) 'A Model For The Mechanics Of Jointed Rock ', *J. Soil Mech. And Foundation. Div.*, ASCE, 94(3), 637-659.
57. Gu, M. Q. and Shi, S. F (1994) The Design Handbook of Highway Bridges and Tunnels (Vol.1), The People's Transport Publisher, Beijing, p129.
58. Hamid, A. A., Drysdale, R. G. and Heidebrecht, A. C. (1979) 'Shear Strength of Concrete Masonry Joints ', *Journal of The Structural Division, Proceedings of ASCE*, Vol. 105, ST7, July, 1227-1240.
59. Harvey, W. J. (1988) 'Application Of The Mechanism Analysis To Masonry Arches', *The Structural Engineer*, 66, 5, 1 Mar, 77-84.
60. Hayes, W. J. (1938) '*Strengthening & Reconstruction of Weak Bridges Under The Road & Rail Traffic Act, 1933* ', Students' Paper No. 953, Proc. ICE, Vol. 10, 15-40.

61. Hendry, A. W. et al. (1985) 'Test On Stone Masonry Arch At Bridgemill-Girvan ', Department of Transport. TRRL Contractor Report 7, Transport Research Laboratory, Crowthorne.
62. Hendry, A. W., Davies, S. R., Royles, R., Ponniah, D. A., Ford, M. C. and Komeyli-Birjandi, F. (1986) 'Load Test To Collapse On A Masonry Arch Bridge At Bargower, Strathclyde ', Department of Transport. TRRL Contractor Report 26, Transport Research Laboratory, Crowthorne.
63. Hendry, A. W. et al. (1990) 'Masonry Properties For Assessing Arch Bridges ', Department of Transport. TRRL Contractor Report 244, Transport Research Laboratory, Crowthorne.
64. Heuze, F. E. and Barbour, T. G. (1982) ' New Models For Rock Joints And Interfaces ', *J. Geotech. Engng. Div.*, ASCE, 108(5), 757-77 6.
65. Heyman, J. (1966) 'The Stone Skeleton', *Inter. J. Solids Struct.*, 2 249-279.
66. Heyman, J. (1969) 'The Safety Of Masonry Arches ', *Int J Mech Sci*, 11, 363-385.
67. Heyman, J. (1980) 'The Estimation Of The Strength Of Masonry Arches ', *Proc Inst Civ Engrs*, Part 2, 69, Dec, 921-937.
68. Heyman, J. (1982) The Masonry Arch. Chichester: Ellis Horwood Ltd.
69. Howe, M A. (1897) A Treatise On Arches. New York: John Wiley & Sons.
70. Huddleston, J. V. (1959) 'Finite Deflections And Snap-Through of High Circular Arches ', *J. of Appl. Mech.*, 35, 763-769.
71. Hodgson, J. A. (1996) The Behaviour Of Skewed Brickwork Masonry Arch Bridges, PhD Thesis, University of Salford.
72. Howe, M. A. (1897) A Treatise On Arches, New York: John Wiley & Sons.
73. Hu, G. Q., Xu, L. C., Shang, G. X., Cheng, S. S., Wang, B. H. and Chou, W. F. (1995) 'Lightweight Stone Arch Bridge in Hunan, China ', *Proceedings of The First International Conference on Arch Bridges*, Bolton, UK, 627-634.
74. Hughes, T. G. and Vilnay, O. (1988) 'The Analysis of Masonry Arches ', Proceedings 8th Int. Brick/Block Masonry Conf., Dublin, 1311-1318.
75. Hughes, T. J. R., Taylor, R. L., Sackman, J. L. Curnier, A. and Kanoknukulchai (1976) 'A Finite Element Method For a Class of Contact-Impact Problems ', *Comput. Meth. Appl. Mech. Engng*, 8, 249-276.
76. Hung, N. D. and Saxce, G. D. (1980) 'Frictionless Contact of Elastic Bodies by Finite Element Method And Mathematical Programming Technique ', *Comput. Struct.*, Vol. 11, 55-67.

77. (ICE) Institution of Civil Engineers (1828), MS Report of Sir John Rennie, Vol. 11-20.

78. Jervoise, E. (1936) Ancient Bridges of Wales And Western England.

79. Joo, J. W. and Kwak, B. M. (1986) 'Analysis and Application of Elastoplastic Contact Problems Considering Large Deformation ', *Comput. Struct.*, 24, 935-961.

80. Khoo, C. L. and Hendry, A. W. (1975) 'A Failure Criterion For Brickwork In Axial Compression ', Proceedings Of The Third International Brick Masonry Conference. Bundesverbande Deutschen Zeigelindustrie, Bonn.

81. Kikuchi, N. and Oden, J. T. (1984) 'Contact Problems in Elastostatics ', *Finite Element: Special Problems in Solid Mechanics* (Oden, J. T and Carey, Eds), Vol. IV, Prentice Hall, Englewood Cliff, NJ.

82. Klarbring, A. and Bjorkman, G. (1988) 'A Mathematical Programming Approach to Contact Problems With Friction And Varying Contact Surface ', *Comput. Struct.*, 30, 1185-1198.

83. Knapp, R. G. (1992) 'China's Bridges: Craft And Symbolism ', *Proc. Int. Historic Bridges Conference*, Columbus, Ohio, 91-132.

84. Koohariani, A. (1952) 'Limit Analysis of Voussoir (Segmental) And Concrete Arches', ACI, Vol. 24, No. 4, pp317-328.

85. Livesley R. K. (1978) 'Limit Analysis Of Structures Formed From Rigid Blocks ', *Int. J. Numerical Methods in Engineering*, Vol.12, 1853 - 1871.

86. Livesley R. K. (1992a) 'The Collapse Analysis of Masonry Arch Bridges', *Proc. Conf. Applied Solid Mechanics 4*, Elsevier, pp 261-274.

87. Livesley R. K. (1992b) 'A Computational Model For The Limit Analysis of Three-Dimensional Masonry Structures', Masonry Construction: *Structural Mechanics and Other Aspects* (Ed. Calladine, C. R.), Kluwer Academic Publishers, pp161-172.

88. Loo, Y. C., and Yang, Y. (1991) 'Cracking And Failure Analysis Of Masonry Arch Bridges ', *Journal of Structural Engineering*, 117 No 6, Paper 25878, 1641-1659.

89. Lou, Z. H., Lou, Y. Y and Li, Y. (1993a) 'Evaluation Methods of Bearing Capacity of Existing Two-Way Curved Arch Bridge Superstructure', *Science And Technology of Highway Transport*, No. 1, pp25-31 (In Chinese).

90. Lourenco, P. B., Rots, J. G. (1993) 'On The Use of Micro-Models For The Analysis Of Masonry Shear Walls', *Proc. Second International Symposium On Computer Methods In Structural Masonry* (Eds. Pande, G. N. and Middleton J.), Swansea, UK, April.

91. Lourenco, P. B. and Rots, J.G. (1994) 'Understanding the behavior of shear walls: a numerical review ', *Proc. 10th Int. Brick/Block Masonry Conference* (Eds. Shrive, N.G. and Huizer, A.), University of Calgary, Alberta, July, Canada.
92. Lourenco, P. B. and Rots, J.G. (1997) 'On The Use Of Homogenisation Techniques For The Analysis Of Masonry Structures', *Masonry International*, Vol. 11, No. 1, pp.26-32.
93. Lu, D. Q. et al. (1992) Chinese Stone Bridges (Pictorial Volume), the People's Transport Publications, Beijing (In Chinese).
94. Luo, Y. (1959) Chinese Stone Bridges, the People's Transport Publications, Beijing (In Chinese).
95. Luo, Y. and Tang, H. C. (1993) The Study of Chinese Stone Arch Bridges, the People's Transport Publications, Beijing (In Chinese).
96. Mao, Y. S. (1978) 'Bridges in China: Old And New ', Foreign Language Publications, Beijing.
97. Mao, Y. S. and Tang, H. C. (1986) Technical History of Chinese Ancient Bridges, Bejing Publications, Beijing (In Chinese).
98. Mare, De (1975) Bridges of Britain, London, BT Batsford
99. Mehlhorn, G., Kollegger, J., Kesner, M. and Kolmar, W. (1985) 'Nonlinear Contact Problems - a Finite Element Approach Implemented in ADINA', *Comput. Struct.*, 21, 69-80.
100. Melbourne, C. (1986) 'Mass concrete voussoir arches', Concrete, Feb.
101. Melbourne, C., Quazzaz, A. and Walker, P. J. (1989a) 'Load Testing To Collapse Of Model And Full Scale Brickwork Masonry Arches', *Proceedings SERC Conference on repair, maintenance and operation in civil engineering*, Jun. Engineering Technics Press.
102. Melbourne, C., Quazzaz, A. and Walker, P. J. (1989b) 'Influence Of Ring Separation On The Load Carrying Capacity Of Brickwork Masonry Arch Bridges', *Proceedings SERC Conference on repair, maintenance and operation in civil engineering*, Jun. Engineering Technical Press.
103. Melbourne, C. (1990a) 'The Behaviour Of Brick Arch Bridges ', *British Masonry Society Proceedings*, 4, 54-57.
104. Melbourne, C. (1990b) 'The Behaviour Of Masonry Arch Bridges - The Effect Of Defects ', *Proceedings of the Fourth Rail Bridge Centenary Conference*, Edinburgh.

105.Melbourne, C. and Gilbert, M. (1992) 'The Behaviour Of Multi-Ring Brick Arch Bridges Containing Ring Separation ', 3rd *International Masonry Conference*, London.

106.Melbourne, C. and Wagstaff, M. (1992) 'The Behaviour Of Multi-span Masonry Arch Bridges ', *Third International Masonry Conference*, London.

107.Melbourne, C. and Gilbert, M. (1993) 'A study of the effects of ring separation on the load carrying capacity of masonry arch bridges ', 2nd International Conference on Bridge Management, University of Surrey.

108.Melbourne, C. and Wagstaff, M. (1993) 'Load Tests To Collapse Of Three Large Scale Multispan Brickwork Arch Bridges ', *2nd International Conference on Bridge Management*, University of Surrey.

109.Melbourne, C. (1995) Arch Bridges, ISBN: 0 7277 2048 1, Thomas Telford, London.

110.Melbourne, C. and Tao, H. Y. (1995a) "The Behaviour of Open Spandrel Masonry Arch Bridges", *Proceedings of The First International Conference on Arch Bridges*, Bolton, UK, pp239-244.

111.Melbourne, C. and Tao, H. Y. (1995b) Load Test To Collapse Of A 3 Metre Span Open Spandrel Brick Masonry Arch Bridge, Test Report, Bolton Institute.

112.Melbourne, C. and Tao, H. Y. (1995c) "The Behaviour of Open Spandrel Masonry Arch Bridges", *Proc. Brit. Masonry Soc.*, 7, pp 145-148.

113.Melbourne, C. and Tao, H. Y. (1996) Load Test To Collapse Of A 5 Metre Span Open Spandrel Brick Masonry Arch Bridge, Test Report, University of Salford.

114.Melbourne, C., Gilbert, M. and Wagstaff, M. (1997) 'The Collapse Behaviour of Multi-Span Brickwork Arch Bridges ', *The Structural Engineer*, Vol 75, No8, Sept., 297-305.

115.Melbourne, C. and Tao, H. Y. (1997a) Load Test To Failure Of A 5 Metre Span Brick Masonry Arch Bridge, Test Report, University of Salford.

116.Melbourne, C. and Tao, H. Y. (1997b) Load Test To Collapse Of A 5 Metre Span Open Spandrel Brick Masonry Arch Bridge With Fill, Test Report, University of Salford.

117.Melbourne, C. and Tao, H. Y. (1998) "The Behaviour of Open Spandrel Brickwork Arch Bridges", *Arch Bridges*, Ainopoli (ed.), Balkema, Rotterdam, ISBN 90 5809 0 12 4, pp263-269.

118. (MEXE) Military Engineering Experimental Establishment (1963) Military Load Classification of Civil Bridges by The Reconnaissance And Correlation Methods. SOLOG study B. 38. Military Engineering Experimental Establishment, Christchurch.

119. Michaloswki, R. and Mroz, Z. (1978) 'Associated And Non-associated Sliding Rules in Contact Friction Problems ', *Archives of Mechanics*, 30, pp259-276.

120. Morley, A. (1912) Theory of Structures, Ed. Longmans, Green & Co., 39 Paternoster Row, London.

121. (MoT) Ministry Of Chinese Transports (1974) Design Codes of Highway Brick, Stone And Concrete Bridges And Culverts, the People's Transport Publications, Beijing (In Chinese).

122. (MoT) Ministry Of Chinese Transports (1985) Design Codes of Highway Brick, Stone And Concrete Bridges And Culverts (JTJ 022-85), the People's Transport Publications, Beijing (In Chinese).

123. (MoT) Ministry Of Chinese Transports (1989) General Design Codes of Highway Bridges And Culverts (JTJ 021-89). The People's Transport Publications, Beijing (In Chinese).

124. Moseley (1835) 'Equilibrium of The Arch And Theory of Equilibrium of Bodies in Contact ', *Transactions of The Cambridge Philosophical Society*, No. 5/6.

125. Oden, J. T. and Pires, E. B. (1983) 'Numerical Analysis of Certain Contact Problems in Elasticity With Non-Classical Friction Laws ', *Comput. Struct.*, V16, No. 1-4, 481-485.

126. Okamoto, N. and Nakazawa, A. (1979) 'Finite Element Incremental Contact Analysis With Various Frictional Conditions ', *Int. J. Numer. Methods Eng.*, 14, 337-357.

127. Ostachowicz, W. (1984) 'Mixed Finite Element Method For Contact Problems ', *Comput. Struct.*, 18, 937-945.

128. Page, A. W. (1982) 'An Experimental Investigation Of The Biaxial Strength Of Brick Masonry ', *Proceedings of the Sixth International Brick Masonry Conference*, Rome, 3-15.

129. Page, J. (1987) 'Load Tests To Collapse On Two Arch Bridges At Preston, Shropshire And Prestwood, Staffordshire ', Department of Transport. TRRL Research Report 110, Transport Research Laboratory, Crowthorne.

130.Page, J. (1988) 'Load tests on two arch bridges at Torksey and Shinafoot ', Department of Transport. TRRL Research Report 159, Transport Research Laboratory, Crowthorne.

131.Page, J. (1989) ' Load tests to collapse on two arch bridges at Strathmashire and Barlae ', Department of Transport. TRRL Research Report 201, Transport Research Laboratory, Crowthorne.

132.Page, J. (1993) Masonry Arch Bridges, HMSO.

133.Pande, G. N. and Middleton, J. (1994) Development of A Constitute Model For Structural Masonry, Department of Civil Engineering, University College of Swansea, October, 1994.

134.Pearson, J. C. (1963) 'Measurement of bond between brick and mortar ', *Proc. ASTM*, 43, 857-867.

135.Pippard, A. J. S., Tranter, E. and Chitty, L. (1937) 'The Mechanics Of The Voussoir Arch ', *J Instn Civ Engrs*, 4 Dec, 281 - 306.

136.Pippard, A. J. S. and Chitty, L. (1942) 'Repeated Load Tests On A Voussoir Arch ', *J Instn Civ Engrs*, Paper 5268, 79-86.

137.Pippard, A. J. S. (1948) 'The Approximate Estimation of Safe Loads on Masonry Bridges ', *The Civil Engineer in War*, 1, 365, Institution of Civil Engineers, London.

138.Pippard, A. J. S. (1952) 'The Masonry Arch ', Studies in elastic structures. London: Edward Arnold & Co. Ch 11, 276 - 320.

139.Pippard, A. J. S. and Chitty, L. (1951) 'A Study of The Voussoir Arch', *Research Paper 11,* Building Research Station, London.

140.Pippard, A. J. S. and Baker, J. F. (1957) The Analysis of Engineering Structures, E Arnold Ltd., London.

141.Pippard, A. J. S. and Baker, J. F. (1962) 'The Voussoir Arch ', In: Pippard and Baker. The analysis of engineering structures. London:Edward Arnold & Co. Ch16, 385 - 403.

142.Pluijm, R. V. D. (1992) 'Material properties of masonry and its components under tension and shear ', *Proc. 6th Can. Mas. Symp.* Univ. of Saskaton, Canada, 675-686.

143.Pluijm, R. V. D. (1995) 'Numerical Evaluation of bond tests on masonry ', *Masonry International*, Vol. 9, No. 1, 16-24.

144.Powell, B. and Hodgkinson, H. R. (1976) '*Determination of Stress-Strain Relationship of Brickwork* ', TN249, British Ceramic Research Association, Stoke-on-Trent.

145.Riddington, J. R. and Jukes, P. (1994) 'Determination of Material Properties for Use in Masonry FE Analysis ', 314-319.

146.Royles, R and Hendry, A W. (1990) 'Model Tests On Masonry Arches ', *Proc Instn Civ Engrs.*, Part 2, June, 299 - 321.

147.Ruddock, E C. (1974a) 'Hollow spandrels in arch bridges: a historical study ', The *Structural Engineer*, 52, No 8, Aug, 281 - 293.

148.Ruddock, E C. (1974b) 'William Edwards' Bridge at Pontypridd ', *Industrial Archaeology*, 193-208.

149.Qian, L. X. (1987) 'The Analysis of The Load Capacity of *Zhao Zhou* Bridge ', *Civil Engineering Journal*, Vol. 20, No 4, 39-48 (In Chinese).

150.(SAA) Standards Association in Australia (1988) Masonry in Buildings, Australian Standard 3700-1988, SAA, North Sydney, N. S. W.

151.Sachdeva, T. D. and Ramakrishnan, C. V. (1981) 'A Finite Element Solution For The Two-Dimensional Elastic Contact Problems With Friction ', *Int. J. Numer. Methods Eng.*, 17, 1257-1271.

152.Sahlin, S. (1971) Structural Masonry, Prentice-Hall, Englewood Cliffs, NJ.

153.Sawko, F. and Towler, K. 'Structural Behaviour Of Brickwork Arches', *Seventh Int. Conf. On Loadbearing Brickwork*, British Ceramic Soc., London, Vol. 30, pp. 160-168.

154.Sawko, F. and Rouf, M. A. (1984) 'On The Stiffness Properties Of Masonry', *Proc. I. C.* E., Part 2, Vol. 77, PP 1-12.

155.Sawko, F. and Rouf, M. A. (1985) 'A Proposed Numerical Model For Structural Masonry', *Masonry International*, Vol. 5, pp. 22-27.

156.Sayegh, A. F. and Tso, F. K. (1986) ' Treatment of Frictionless Contact Boundaries by Direct Minimization ', *Comput. Struct.*, 23, 1, 39-49.

157.Selberg, A. (1953) 'On the Bearing Capacity of Voussoir Arches ', IABSE publication, Vol 13, 322-326.

158.Simo, J. C., Wriggers, P. and Taylor, R. L. (1985) 'A perturbed Lagrangian Formulation For The Finite Element Solution of Contact Problems ', *Comput. Meth. appl. Mech. Engng.*, 50, 163-180.

159.Smeaton, J. (1760) Mr. Smeaton's Answer to The Misrepresentations of His Plan For Black-Friars Bridge, quoted from Ruddock (1974).

160.Smith, F. W. and Harvey, W. J. (1989) 'Full Scale Test Of A Masonry Arch ', *Proceedings SERC Conference On Repair, Maintenance And Operation In Civil Engineering*, Jun. Engineering Technics Press.

161.Smith, F. W., Harvey, W. J. and Vardy, A. E. (1990) 'Three Hinge Analysis Of Masonry Arches ', *The Structural Engineer*, 68, No 11, Jun, 203 - 213.

162.Smith, N. A. F. (1993) 'The Roman Bridge-Builder: Some Aspects of His Work ', The Structural Engineers, Vol. 71, No 9/4, May, 160-165.

163.Stadter, J. T. and Weiss, R. O. (1979) 'Analysis of Contact Through Finite Element Gaps ', *Comput. Struct.*, 10, 867-873.

164.Stephenson (1846), On the discussion on the paper 'The Existence (Practically) of The Line of Equal Horizontal Thrust in Arches, And The Mode of Determining it ' (Barlow, 1846), Paper 728, *Proc. ICE*, pp162-182.

165.Tabor, D. (1981) 'Friction - The Present State of Our Understanding ', *J. Lubr. Technol.*, 103, 169-179.

166.Taylor, N. (1991) 'Moment-Thrust Limit State Properties of Masonry ', *Masonry International*, Vol. 5, No. 2, 55-58.

167.Taylor, N. and Mallinder, P. A. (1987) 'On the Limit State Properties Of Masonry ', *Proc Instn Civ Engrs*, 83, part 2, Mar, 33-41.

168.Tellett, J, (1982) A review of The Literature on Brickwork Arches, *British Ceramic Research Association*, Technical Note No 338.

169.Tellett, J. (1983) 'A Review Of The Literature On Brickwork Arches ', *Eighth International Symposium on Loadbearing Brickwork*, London, Nov.

170.Tocqueville, A. D. (1945) Democracy in America, Vol. II, quoted from Kranakis, E. (1997) Constructing a Bridge: An Exploration of Engineering Culture, Design, and Research in Nineteenth-Century France and America, The MIT Press, 0-262-11217-5.

171.Toi, Y. and Yoshid, S. (1991) 'Numerical Simulation of Nonlinear Behaviours of Two-Dimensional Block Structures ', *Computers & Structures*, Vol. 41, No. 4, 593-603.

172.Towler, K (1981) The Structural Behavior Of Brickwork Arches. Ph.D. Thesis, Liverpool, Sept.

173. Towler, K. and Sawko, F. (1982) 'Limit State Behaviour Of Brickwork Arches ', Proc *6th Int. Brick Masonry Conference*, Rome, May.

174. Turner, M. J., Dill, E.H., Martin, H.C. & Melosh, R. J. (1960) 'Large deflection of structures subject to heating and external load ', *J. Aero. Sci*, 27, 97-106.

175. Van Beek, G. W. (1987) 'Arches and Vaults in The Ancient Near East ', *Scientific American*, Vol. 256, 78-86.

176. Vijayakar, S. M., Busby, H. R. and Houser, D. R. (1988) 'Linearization of Multibody Frictional Contact Problems ', *Comput. Struct.*, 29, 4, 569-576.

177. Vilnay, O. (1988) 'Dynamical Behaviour Of Three-Voussoir Arch ', *J. Struct Eng*, 114, No 5, May, 1173-1186.

178. Walker, P. J., Qazzaz, A. N. and Melbourne, C. (1989) 'The Performance Of Masonry Arch Bridges With Ring Separation ', Armer, Clarke and Garas (eds). The Life Of Structures - Physical Testing, Butterworths, London.

179. Walklate, R. P. and Mann, J. W. (1983) 'A Method For Determining The Permissible Loading of Brick And Masonry Arches ', *Instn. Civ. Engrs.*, Part 2, 75, 585-597.

180. Williams, E. O. (1927) 'The Philosophy Of Masonry Arches ', *Instn Civ Engrs*, selected engineering papers No 56. London: ICE.

181. Willam, K. J., and Warnke, E. D. (1975) 'Constitutive Model for the triaxial Behaviour of Concrete ', *Proceedings, International Association for Bridge and Structural Engineering*, Vol. 19, ISMES, Bergama, Italy, p.174

182. Wriggers, P., and Simo, J. C. (1985) 'A Note on Tangential Stiffness For Fully Nonlinear Contact Problems ', *Communications in Applied Numerical Methods*, Vol. 1, 199-203.

183. Wriggers, P., Van, T. V. and Stein, E. (1990) 'Finite Element Formulation of Large Deformation Impact-Contact Problems With Friction ', *Comput. Struct.*, 37, 3, 319-331.

184. Xiang, G. H. (1993) 'The Development Of Highway Stone Arch Bridges In Hunan, China ', *Southern Highway Engineering*, Sept, (In Chinese).

185. Yu, Z. M. (1961) 'Stress Analysis of Chinese Circular Arches', Suzhou Construction Bureau, (In Chinese).

186. Zienkiewicz, O. C., Taylor, R. L. and Tao, J. M. (1971) 'Reduced Integration Technique in General Analysis of Plates And Shells ', *International Journal For Numerical Methods in Engineering*, Vol. 3, 1971, 275-290.

Appendix I Selected Work Relating To Masonry Arches

Time And Investigators	Events	Remarks
Antiquity	Arches/arch bridges are believed originating in either Egypt or Iraq or Italy or China.	In China, it is evident that arch forms were used in the tiled windows between 5000 - 4000BC.
595 - 606 Li	Built *Zhao Zhou* bridge, which is a single span stone arch bridge. For main arch, span 37.02m, rise 7.23m, thickness of arch barrel 1.0m; for spandrel arch, span 3.8m, rise 1.0m, span 3.1m, rise 1.3m; for spandrel piers, thickness 1.3 m, height 1.0m.	This bridge is the oldest OSMAB in the world. Modern survey shows that the geometrical factor of safety of this bridge is 3.703. The segmental arc, open spandrels and small abutments are the three main achievements in bridge construction.
1675 Hooke	Drew the analogy between the arch form and a loaded catenary. The solution to arch is: " As the continuous flexible hangs downward so will the contiguous rigid stand upward inverted. "	The first recorded insight into the structural performance of an arch. His findings were not published as an anagram until after his death in 1703.
1695 La Hire	Theoretically investigated into the structural action of voussoir semi-circular arches, and deduced that the weights of the voussoirs at the springings needed to be infinite, and concluded that an arch composed of smooth voussoirs could not stand.	The concept of the funicular polygon. The wedge theory. Proposed to make the joints of the voussoirs perpendicular to the line of thrust to ensure no sliding occurred, and to build arch with variable thickness.
1697 Gregory	Attempted to obtain the mathematical properties of the catenary; stated that an arch having a shape other than an inverted catenary could only stand if an inverted catenary could be within its thickness.	The idea of 'lower - bound theorem' of plasticity is invoked.
1717 Gautier	Gave numerical rules of proportion for bridges, relating thickness of abutments and internal piers (for multi-span bridges); First described the ' eyes of bridges', open spandrels multi-span arch bridges. The advantages of eyes are stated: ' they relieve the structure of much of its weight, save masonry, and make passages for floodwater '	Tests on wooden voussoirs; Proportional arch bridges; He also described several Roman bridges, the medieval Pont St. Esprit and the Renaissance Pont Neuf at Toulouse, all with an ' eye ', cylindrical through each spandrel over the middle of the intermediate piers. Picon suggests that Gautier's approach to bridge design was more architectural.
1729 - 1730 Couplet	Obtained a correct solution to the problem of arch design. Stated that the voussoirs interlock with each other, thereby prevent sliding or any failure due to sliding, but no resistance to separation between voussoirs, the pressure acted normal to the face of each voussoir	He developed a complete theory of masonry which could be applied to the analysis and design of arches. The concept of collapse mechanism Tested to verify that masonry was capable of sustaining infinite frictional forces.
1733 - 1802 Coulomb	Asserted the importance of the 'safe theorem' by concluding that it is only necessary to find one line of thrust contained within the arch boundaries that satisfies equilibrium to ensure stability under given loads, and believe that there were two causes of rupture: the first arising from the turning over of certain parts of one voussoir on the wedge of another; and the second, from the slipping or sliding of the voussoirs on each other.	He reinvented his own theory. The 'safe theorem' Two failure modes: hinged mechanism or sliding between voussoirs.
1736 Langley	Designed the *Westminster* Bridge, a multi-span opened arch, in which a large cylindrical	The designer of the first OSMAB in Britain was. He showed the concern of the stability

	void was located over the central line of each pier, and two further voids over the haunches of each arch.	of multi-span OSMAB '... making the cylinders ... free from the danger of uncqual pressure'.
1736 Muller	Analysed semi-circular and semi-elliptical arches and all others in which the curve is vertical at the springings , and showed that the top of the spandrel or the filling material over the arch should start parallel to the curve of the soffit at the crown, thus falling at first towards the haunches, but then rise steeply as the soffit approached the vertical.	He showed the concern of the reasonable distribution of filling based on the assumption of constant density of material in the arch and spandrel.
1708 - 1794 Perronet	Proposed to use a semi-ellipse arc to overcome the hump problem. Attempted to study the sizes of internal piers of multi-span arch bridges He developed very flat arches supported on slender piers.	He is called the father of modern bridge building. He served as director of the engineering school, *School of Bridge and Highways*, in the world. His works included the *Neuilly* Bridge over the Seine, the *Pont Sainte-Maxence* over the Oise, and the *Pont de la Concord* over the Seine in Paris. Semi-ellipse arc and sizes of internal piers.
1746 - 1756 William Edwards	Attempted to the bridge Taaf at Pontypridd for four times. Upon the failure of his multi-span and filled arch bridges, He finally built an open arch, which still stands.	The story of William Edwards' four attempts indicated that OSMAB might be the only solution for large single-span masonry arch bridges.
1746 - 1770 Smeaton	Related arch thickness, span, and degrees of arc to the width of pier, and promoted the design and construction of OSMAB.	Proportional arches Open spandrel arches
1748 Poleni	Used the idea of the 'lower-bound theorem' to study the cracked dome by slicing it into a series of 'arches'. Experimented with a suitably weighted string of beads to show that the meridional cracks appearing in it had caused some concern.	Tested to verify the 'lower-bound theorem'. His stated explicitly that stability would be assured if "our chain can be found to lie entirely within the thickness of the arch", and further, that if each individual arch were stable, so also would be the complete dome.
1758 Emerson	Suggested that the use of materials of varying density to release the weight of the filling and to achieve a ' horizontal ' roadway. Further concluded that suitable materials could not be found for the semi-circular arch.	He first proposed to adapt filling materials of varying density to achieve an arch bridge with good configuration.
1801 Atwood	Made experiments on two models of arches with polished metal voussoirs, in which he measured the pressure perpendicular to the face of certain voussoirs in order to prove formulas based on the wedge theory.	Model tests to prove the wedge theory.
1810 Boistard	Established minimum abutment requiring at collapse, and investigated the forces on the centring during construction.	The minimum abutment The forces on the centring Collapse modes.
1811 Rennie	Built the first Waterloo bridge, whose level-topped masonry arches were described by Canova as "the noblest bridge in the world".	He subsequently designed and built the New London Bridge of multiple masonry arches, which was completed in 1831.
1826 Navier	Showed that if the resultant pressure at the crown and joints at which the hinges form acts at one-third of the depth of the ring from the extrados and intrados respectively, then the joints will just be on the point of opening.	The beginning of the 'middle-third rule', or no-tension criterion. Established a straight-line law for the pressure distribution across the bearing surfaces of voussoirs. His work might be influenced by his uncle Gautier.
1835 Moseley	Theoretically showed that for an arch in which the mortar was unable to transmit tension the line of pressure must lie everywhere within the arch ring.	The first British scientist to make a major contribution to the understanding of the behaviour of the arch. For the stability of an arch, the mortar cannot transmit tension and

	(Actually, the line of pressure or thrust may fall outside the arch ring within a voussoir provided it lies within the ring at the mortar joint).	the line of pressure must lie everywhere within the arch. The masonry arch bridges might begin to be obsolescent by this time.
1845 RTA	Under the British Rail Traffic Act (RTA) 1845 the railway companies are only liable, as regards sufficiency of structure, to maintain the bridges to carry the weight of traffic as existing at the time the bridge was built.	The Act is certainly applied to masonry arch bridges. The British Locomotives Act of 1861 clearly stated: '... it was unreasonable for them (bridge authorities) to be expected to strengthen their own bridges in order that their road transport competitors should gain an advantage thereby.'
1846 Barlow	Pointed out that if the arch depth was more than sufficient to contain the thrust line then it was possible for the arch to contain many thrust curves and could therefore be supported on any one of these curves, and stated that an arch would exert more pressure and resist less than theory dictated because the assumed conditions of unyielding materials and perfect joints were incompatible with practice, and stated that the factor of safety against sliding is independent of the other failure modes and it is only dependent upon the direction of the voussoir joints	Compared with Moseley, he graphically showed the solution to arch, and demonstrated the thrust line by model tests. The effects of friction were considered in arch design neglecting the adhesive qualities of mortar. The rule is: ' If the angles between the line of thrust and the normal to the joints are less than the angle of friction then the arch is stable against collapse due to sliding'. Restated the 'safe theorem' Failure modes of arch Ring separations
1846 Snell	Questioned the possible failure of materials and its effect on modifying the position of the line of thrust.	Possible failure of materials. Stability of certain arches.
1846 Stephenson	Stated that The arch, per se, should always be considered as composed of separate masses, not set in a matrix; but combined in a certain form, the only adhesion being the friction of the surfaces.	Arches were considered discrete mass.
1846 Bidder	Stated that if the arch was well bonded together throughout its entire depth, having great adhesive properties, upon which it should be considered as a homogeneous mass as to arches turned in one entire bond, being stronger than those composed of separate rings.	Arches were considered homogeneous mass.
1854 Villarceau	Developed general procedures for calculating lines of thrust, which ensured that they lay at the mid-depth of the voussoirs. His results are given in the form of tables, which can be used immediately in standard calculations by the bridge designers.	Instead of finding out the position of the line of thrust, he required the centre line of the arch to coincide with one of the possible thrust lines for the given loading. Procedures to ensure the 'middle third rule'
1875 Fuller	Constructed the thrust line of two-hinged arches and graphically determined the position of the thrust line of an elastic arch at the inception of elastic theory.	The important feature of his construction method is the degeneration of the funicular polygon into two straight lines.
1879 Castigliano	If the line of thrust lay everywhere within the middle third the arch could be treated as a continuous rib provided that the abutments were rigid. If the thrust lay outside the middle third, the portion in tension was discarded and the structure was reanalyzed; this process was repeated until no tension existed in the remaining part of the arch and stresses were then calculated using elastic theory.	Demonstrated a trial-and-error method of locating the position of the line of thrust, and developed the concept of structural analysis by the strain energy method. The thrust line was first calculated for the complete arch by the method of minimum strain energy
1890	The Austrian Society of Engineers (ASE)	Tested to verify that voussoir arches behave

ASE	carried out a series of experiments to determine: a voussoir arch shows a linear relationship between load and displacement.	linearly.
1897 Howe	Proposed a graphical method to approximately determine the loading necessary to make the equilibrium polygon follow the axis of the arch for OSMAB.	Graphical method to solving OSMAB. Pointed out the problems regarding to the filling in filled arches.
1898 Rankine	' Semi-elliptical arches may be treated as approximately hydrostatic arches (arches built of a figure suited to fluid pressure - that is, pressure of equal intensity in all directions '.	The hydrostatic arches. The importance of the backing.
1920 Baker	Introduced a geometric factor of safety against rotation at any joint, based on the ratio of the eccentricity of the line of thrust from the centre of the joint to the depth of the joint.	Geometric factor of safety The 'middle-third rule' ensures a minimum factor of safety of 3 throughout arch.
1927 Williams	In the paper "The Philosophy of Masonry Arches", he gave the design formulas for various types of arches for spans up to 300 ft.; treatment of filled and open-arch construction and comparison of rules with various authorities; economics of masonry arches.	One of the distinctive features of his work may be his combination between philosophy and masonry arches. In a sense, it may not be easy to well understand the behaviour of masonry arches without sound philosophies.
1929 Fordham	Argued that small span filled arch bridges may safely be designed following some empirical rule. In the case of large span arches, the construction, if a filled arch was adopted, would cause an excessive dead load upon the arch.	Apart from the transverse openings, he also proposed the 'masked' openings along the longitudinal direction which certainly further reduce the weight of the superstructure.
1933 RRTA	The British Road and Rail Traffic Act (RRTA) 1933 indicated the concern of the maximum speed and axle weight, and the assessment of old masonry arch bridges.	The Act was in force before the railway and canal companies had fully investigated the condition of their bridges. Four years later 2,050 railway bridges were classified as weak, and half of them were proposed to reconstruct.
1937 - 1962 Pippard et al.	Steel and concrete voussoir model arch tests, concerning the effects of fill, different mortar strength, cycling loading, abutment movements, etc.	His results enabled the MEXE assessment method. Elastic methods, Collapse mechanism Experimental work, Assessment method.
1953 Davey	The brickwork arch bridge was found to be a very complex structure consisting of an arch ring greatly stiffened by the fill and the superstructure.	The effects of fill and the superstructure were considered. It was 2.5 times stiffer in the presence of the fill than in its absence under loading quarter point.
1963 MEXE	British Military Engineering Experimental Establishment (MEXE) rules: 'The real strength of an arch bridge is almost impossible to calculate, and recourse has therefore been made to an empirical formula based on the bridge dimensions. The bridge was first assumed to be soundly built in good-quality brickwork, with well-pointed joints, to be free from cracks, and to have adequate abutments. For such an idealised bridge, a provisional load class is obtained from a nomograph. This provisional load class is then modified by factors, which allow for the way in which the actual bridge differs from the idealised bridge assumed in calculating the class. '	MEXE assessment method, largely based on the work of Pippard et al. (1936) and Davey (1953), is considerable emphasis on the geometrical properties of the bridge, and that the arch is treated in a late-nineteenth century way, as an elastic redundant structure. The British Ministry of Transport, in 1963, adopted the MEXE approach, with some modification, issued its assessment method. Both methods are easy to use and have served well, but they are now considered to be conservative, particularly for long spans. It also has an additional shortcoming in that spans are limited to 18 m and distorted arches cannot be assessed.
1949 - 1975	The Chinese Ministry of Transport (MoT) and Ministry of Railways (MoR) Evaluated, tested,	MoT & MoR investigated the nation's old (ancient) arch bridges. Though some of

MoT & MoR	strengthened and repaired a large amount of masonry arch bridges.	arches were considered not to be used by theory (elastic), they still carried vehicles without any strengthening.
1966 - 1982 Heyman	Largely concerned with understanding the stability of masonry structures from the point view of plastic theory. In 1982, wrote the book *The Masonry Arch*, in which the work related to masonry arches/arch bridges, especially that before mid-nineteenth century, reviewed, discussed and evaluated. Argued that the assumption of zero tensile strength errs might be unrealistic for spandrel masonry if it interlocks with the voussoirs so that tensile stresses are transmitted locally.	He explicitly takes an masonry arch bridge into account based on modern plasticity theorems of limit analysis (lower - bound theory). He has illuminated much of the ground in the history of masonry arches, and concerned the geometric factor of safety and collapse mechanism.
1980 Shang et al.	Recognized the springing-cracking nature of masonry arch bridges, and suggested that the boundary conditions should be different from either ' fixed ' or ' hinged ' ones. The ' plane-hinged ' boundary conditions were thus adopted in the construction of such structures. Furthermore, the plane-hinge theory was proposed for masonry arch bridges.	The plane-hinge theory is remarkable in the history of the developments of masonry arch bridges. From then on, larger and larger span masonry arch bridges have been built with confidence throughout China.
1986 Mao et al.	Mao and Tang et al., a total of twenty-four authors wrote the book *Technical History of The Ancient Chinese Bridges* (up to 1881), with the help and co-operation from more than hundred investigators throughout the country. In this book, the development of masonry arch bridges is examined in great detail, and the achievements of such bridges in the ancient China are evaluated.	The book, with considerably original records and evidences, comprehensively reviewed the ancient Chinese masonry arch bridges, from which independent patterns of the development of masonry arch bridges in China can be seen just obviously.
1993 Luo and Tang	Wrote an excellent review and research book named *The Study of Chinese Stone Arch Bridges*. The book briefly reviews the history of masonry arch bridges, and the developments of different forms of arch bridges in both ancient and modern China, and introduces the work related to masonry arch bridges carried out by the investigators both inside and outside China.	The book also introduces a variety of new theories developed either by themselves or by other investigators in China. The different construction approaches, and the aesthetics of masonry arch bridges are also discussed. It may not be overestimated that to read the book is a must if interested in the understanding of masonry arches, especially of the 'power' of Chinese masonry arches.
1994 ISE	The informal study group of arch bridges was established in Institution of Structural Engineers (ISE).	This study group may represent a new stage of the development of masonry arch bridges in the UK and the worldwide.
1980 - 1994 TRL	The British Transport Research Laboratory (TRL) tested a number of masonry arch bridges, evaluated old assessment approaches, and proposed new assessment and analysis methods.	The laboratory and the field arch tests were largely carried out by Melbourne et al. (1986-1997); Hendry et al. (1985 -1990); Page (1987-1989).
1980 - 1994 MoT	The Chinese Ministry of Transport (MoT) tested a large amount of two-way curved masonry arch bridges, proposed new assessment methods and analysis models.	The laboratory and the field arch tests were mainly carried out by MoT through the China Academy of Transport Sciences, and the local bridge authorities.
1980 - Worldwide	Carrying out various analyses either to computerize the ancient approaches, or to find out a ready way to locate the thrust lines and identify the collapse modes, or to get a bit further into the inside of masonry arches and the materials.	So called elastic method, mechanism method and finite element method.

The history of masonry arches is continual discovery and rediscovery, invention and reinvention. It may be

interesting to question how further the modern investigators understand the behaviour of masonry arches than, say, Hooke, Gautier, or Barlow did. With the state-of-the-art technologies, how accurately one can interpret the behaviour of a masonry arch ?

Sources: Barlow, 1846; Howe, 1897; Morley, 1912; Williams, 1927; Fordham, 1929; Hayes, 1938; Pippard et al., 1951; MEXE, 1963; Ruddock, 1974; Mare, 1975; Irvine, 1981; Tellett, 1983; Heyman, 1982; EB, 1984; Crisfield, 1985; Mao et al., 1986; Van Beck, 1987; Knapp, 1992; Smith, 1993; Brown, 1993; Page, 1993; Luo and Tang, 1993; Melbourne, 1995; etc.

Appendix II Plates Of The Model Arch Tests

Plate 1. Data Logger

Plate 2. Deflection Gauges (LVDTs)

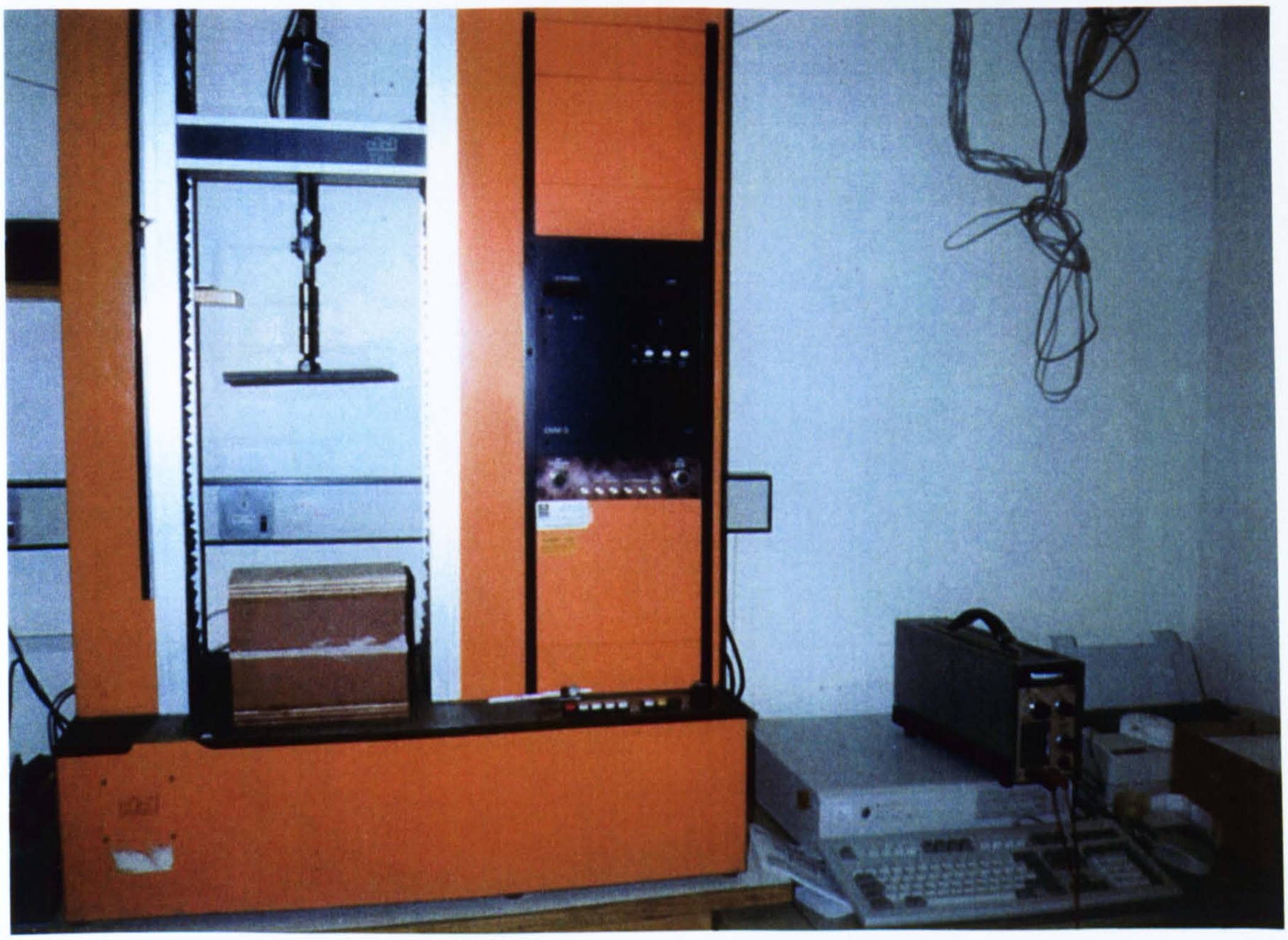

Plate 3. Set-up of Brickwork Tensile Test

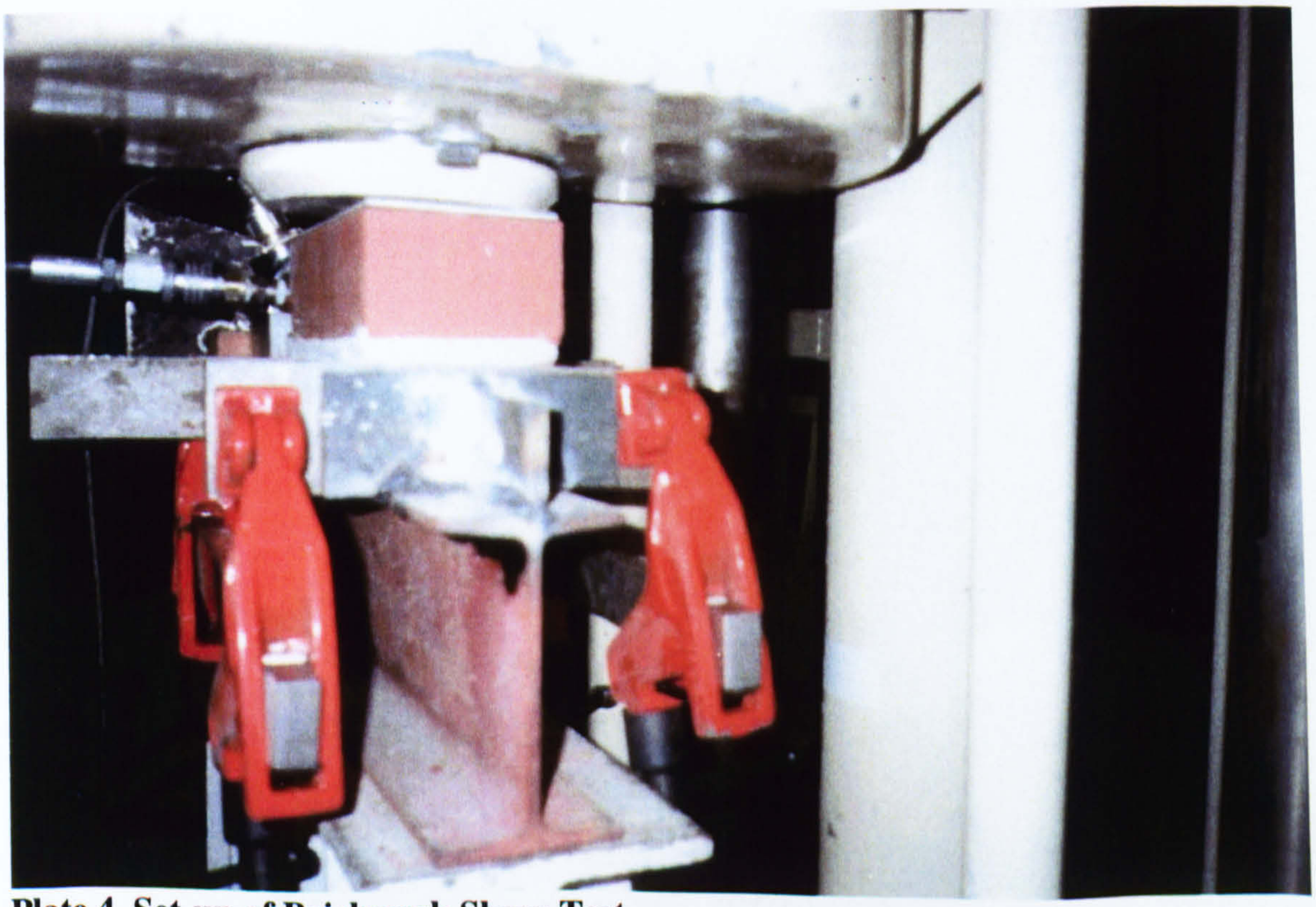

Plate 4. Set-up of Brickwork Shear Test

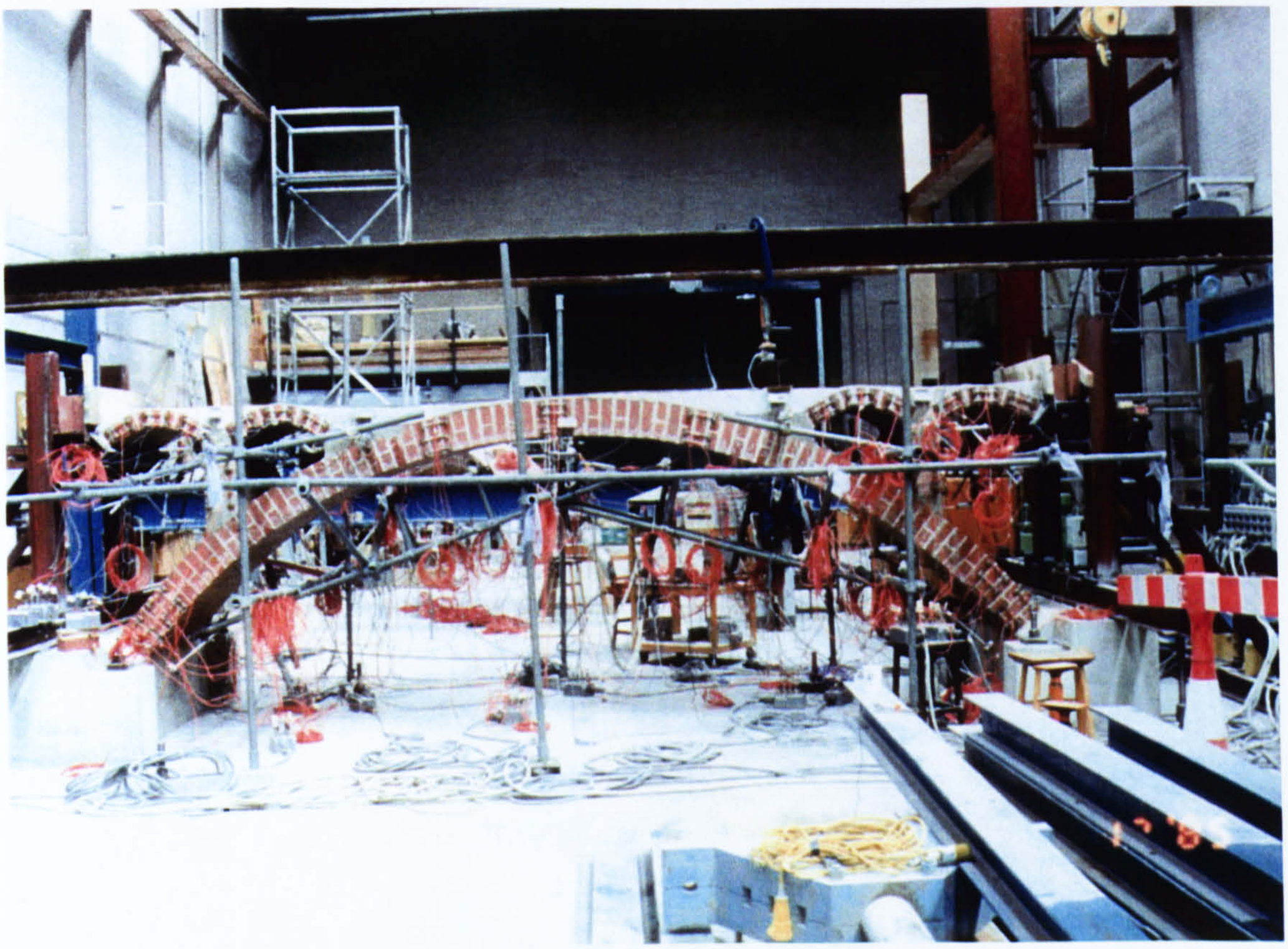

Plate 5. Typical Arrangements of Surface Strain Gauges

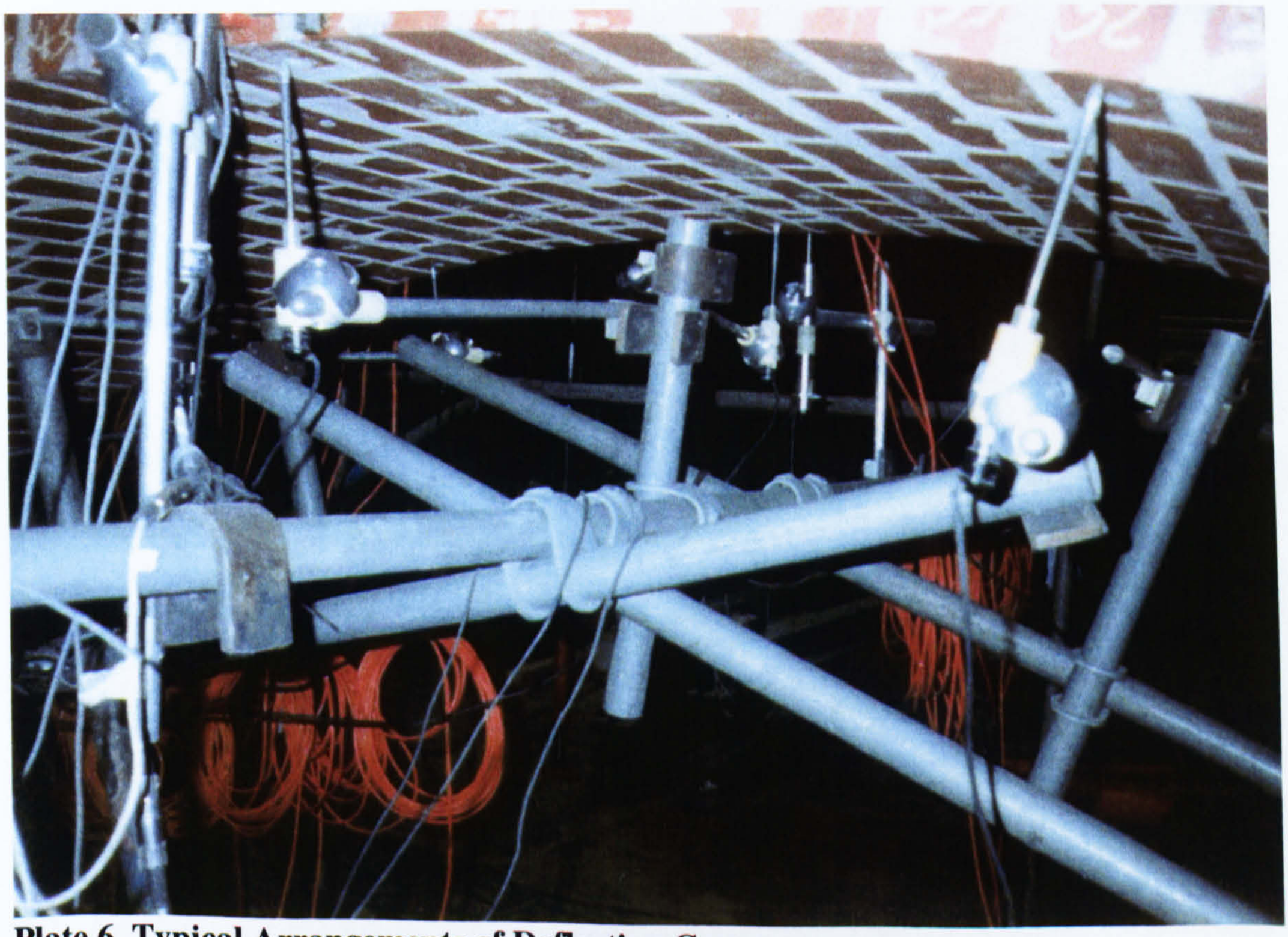

Plate 6. Typical Arrangements of Deflection Gauges

Plate 7. Failure Mechanism of The Model OSMA1

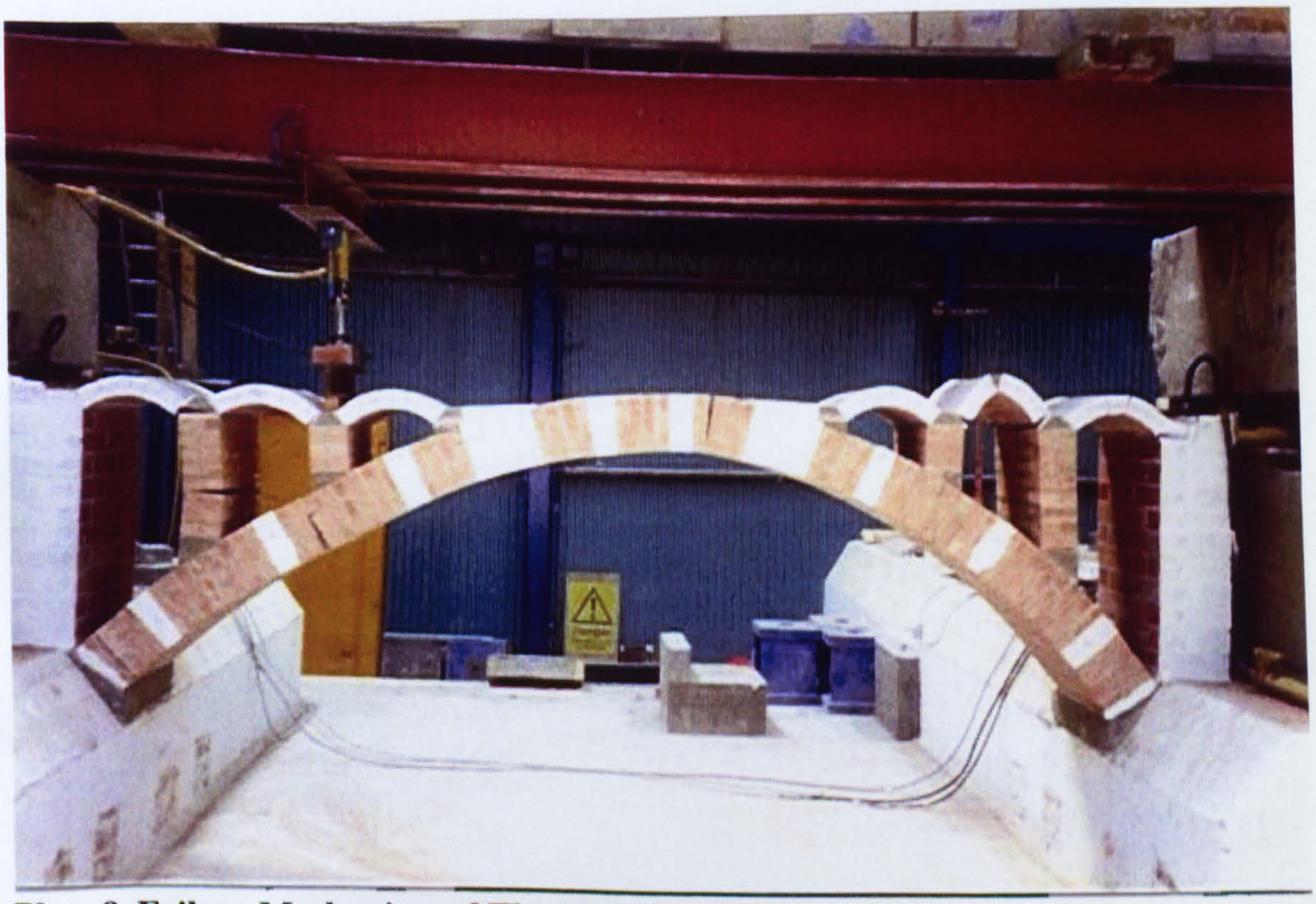

Plate 8. Failure Mechanism of The Model OSMA2

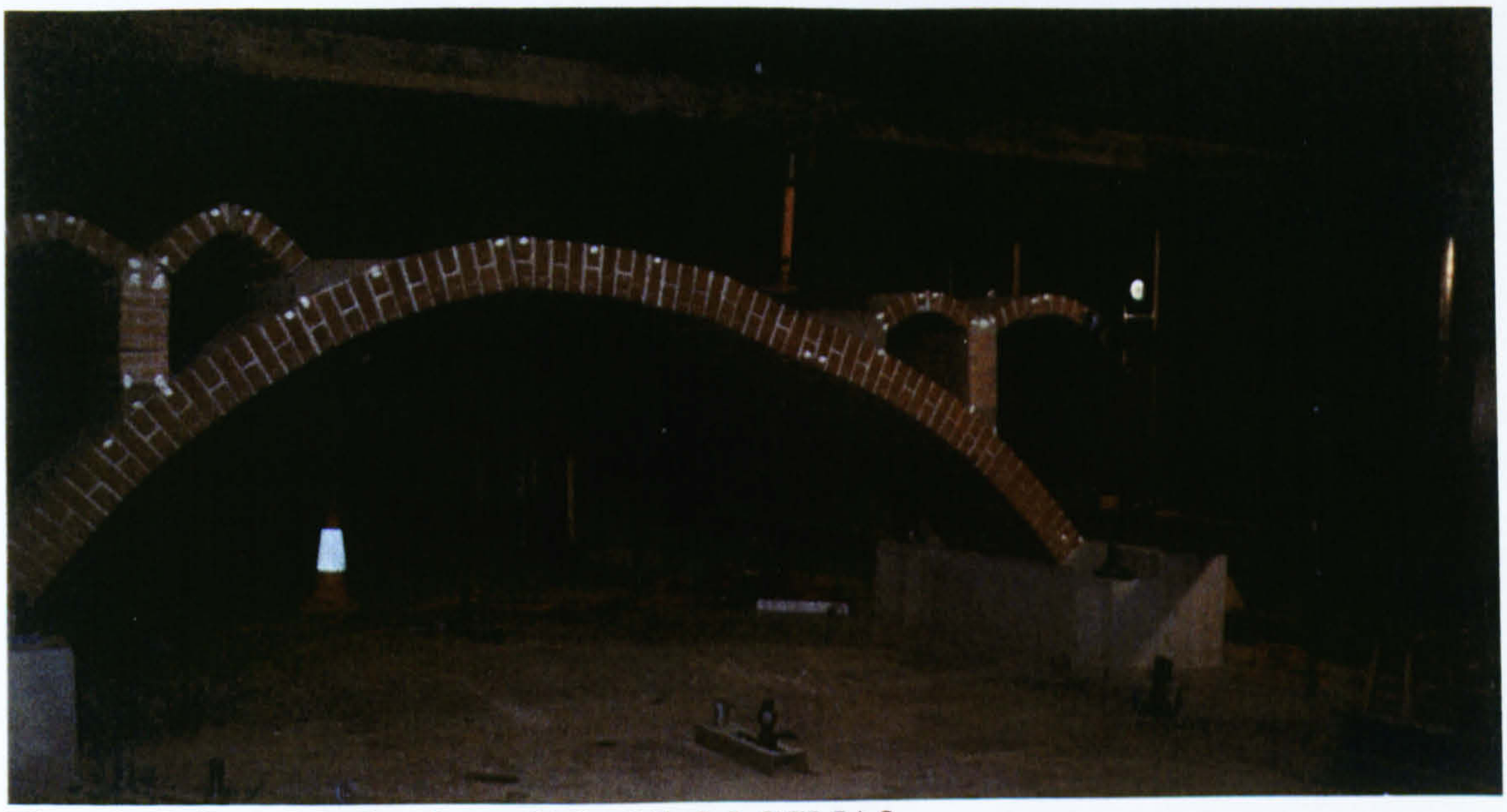

Plate 9. Failure Mechanism of The Model OSMA3

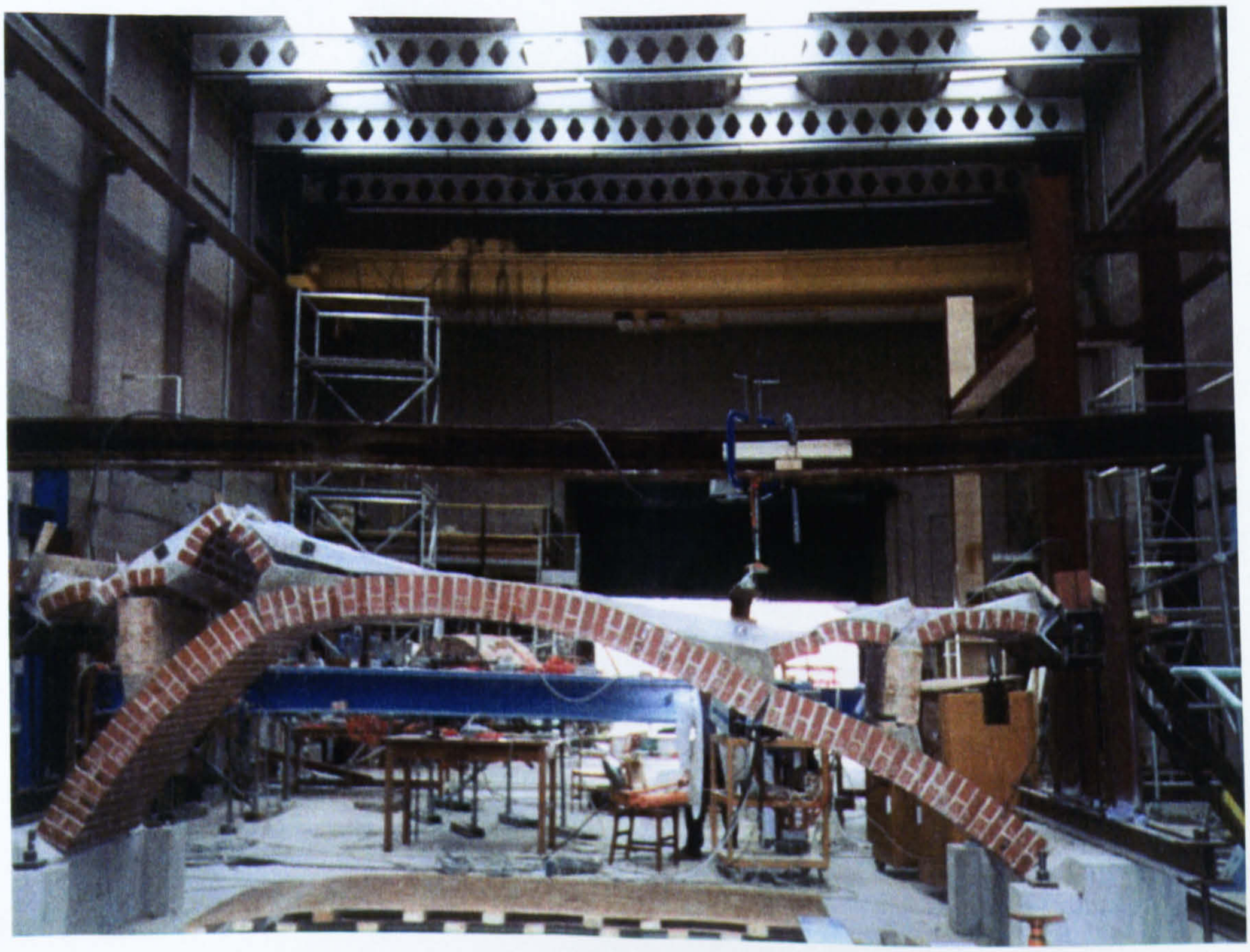

Plate 10. Failure Mechanism of The Model OSMA5